



PhD-FSTM-2024-084
Faculty of Science, Technology and Medicine

DISSERTATION

Defence held on 05/12/2024 in Belvaux

to obtain the degree of

DOCTEUR DE L'UNIVERSITÉ DU LUXEMBOURG

EN PHYSIQUE

by

Ingrid AZEVEDO GONÇALVES

Born on 19 August 1995 in Obidos, Brésil (Brazil)

Nanosecond Pulsed Plasma-Induced Free-Radical Polymerization of Liquid Methacrylate Monomers for the Synthesis of Hydrogel Films

Dissertation defence committee

Dr Roberto Quintana Vicente, dissertation supervisor
Doctor, Luxembourg Institute of Science and Technology

Dr Nicolas Boscher
Doctor, Luxembourg Institute of Science and Technology

Dr Jan Lagerwall, Chairman
Professor, Université du Luxembourg

Dr Elaine Armelin Diggroc
Professor, Universitat Politècnica de Catalunya, UPC, Spain

Dr Guillaume Nonglaton
Doctor, CEA-Leti, Grenoble, France

ABSTRACT

Hydrogels, as a class of soft materials, consist of hydrophilic three-dimensional polymer networks that swell upon immersion in liquid environments while retaining their structural integrity. Traditionally, these materials have well-established applications in biomedicine, including wound dressing and contact lenses. Nowadays, hydrogels in the form of thin films have found applications in advanced fields such as artificial skins, biosensors, and flexible electronics. As films, their performance and functionality are heavily influenced by the polymeric network structure and thickness.

In this context, plasma polymerization is a widely used method to deposit thin films due to its scalability, substrate independence, and being solventless and without the need of chemical initiator. However, several side reactions can yield the loss of the monomer's functionalities and regularity compared to polymers obtained via wet chemistry polymerization. Recent studies have demonstrated the use of nanosecond-pulsed plasma to minimize fragmentation and recombination reactions in plasma-state polymerization, promoting a conventional free-radical polymerization pathway for depositing functional polymer films. In this context, the plasma polymerization of monomers deposited as liquid layers is a relatively underexplored approach compared to vapor-phase methods and offers the possibility to use low vapor pressure monomers, high molecular weight oligomers, or even solid particles dispersed in a liquid medium to form composite films.

This thesis aims to understand the effect of plasma pulse frequency and liquid parameters on the chemistry, growth rate, and properties of hydrogel films. The research specifically examines the use of 2-hydroxyethyl methacrylate (HEMA) as a model hydrophilic monomer. The findings in this study highlight how adjusting the plasma pulse frequency and spray delivery rate influences the retention of monomer functionalities, polymeric growth, and growth rate of the films. Notably, using liquid layers demonstrates a higher chemical structure preservation and deposition rates when compared to the injection of HEMA in the vapor phase using the same reactor.

Hydrogel films were further synthesized by copolymerizing methacrylic acid (MAA) and ethylene glycol dimethacrylate (EGDMA) using the same setup. The research reported for the first time the influence of plasma pulse frequency to tune the swelling ratios and viscoelastic

modulus of the resulting hydrogels. Such hydrogel properties were accessed by quartz crystal microbalance with dissipation monitoring (QCM-D) coupled with spectroscopic ellipsometry (SE).

Taking advantage of the versatility of the studied apparatus, plasma-induced free-radical polymerization of a high molecular weight oligomer (polyethylene glycol dimethacrylate (PEGDMA₄₀₀)) was conducted onto several substrates. The resulting hydrogels exhibited thermo-responsive behavior, as evidenced by QCM-D coupled SE. In-depth characterization of the hydrogel properties through QCM-D and SE showed their suitability for providing insights into the hydrated layer, swelling ratio, and viscoelastic modulus of plasma-polymerized hydrogel films.

ACKNOWLEDGEMENTS

A doctoral dissertation is a collaborative endeavor that relies on the contributions of various individuals, whether through scientific support or emotional encouragement. I am deeply grateful to all those who have contributed directly or indirectly to this research.

I extend my gratitude to Dr. Guillaume Nonglaton from Leti-CET Tech and Prof. Elaine Armelin Diggroc from Universitat Politècnica de Catalunya for accepting to be external jury members for my defense and for reviewing my doctoral dissertation.

I am also grateful to Prof. Jan Lagerwall from the University of Luxembourg, Dr Nicolas Boscher, and Dr Roberto Quintana Vicente for kindly agreeing to contribute to this work as my CET committee and dissertation defense committee. Their expertise and invaluable feedback over the past four years have significantly contributed to the development of my PhD.

In particular, I am immensely thankful to my supervisor, Dr Roberto Quintana Vicente, for entrusting me with this life-changing opportunity. These years have been transformative, marked by substantial personal and professional growth. For all his patience in assisting me through every stage of my PhD. His guidance and perceptive analysis enabled me to grow immensely as a researcher and made this dissertation possible.

I am incredibly grateful for having the assistance of Jordi, as my QCM-D expert. His joyful attitude was a pleasure to be around for a coffee and fruitful scientific discussion

I would also like to express my appreciation to Dominique. I could learn a lot from her insightful feedback, advice, and assistance during our meetings and experimental work.

My deepest gratitude goes to François for his valuable contributions, including valuable discussions on my research and his continuous encouragement.

I am also thankful to the friends I met in LIST, with whom I could share scientific knowledge and good moments: Elisa, Emut, Hadi, Marta, Thiago, and Zahra. I would also like to acknowledge my colleagues for their academic discussions, advice, and coffee breaks: Edyta, Amine, Camilo, Rodolphe, Kamal, João Paulo, João Mallmann, Marko, Drialys, Anthony, Faezah, Awais, and many others.

À minha família, em especial, meus pais, Allan e Fátima, por serem sempre meu alicerce. Obrigada por todo amor, conselhos e apoio que sempre me deram. Foram eles que nunca me deixaram esquecer que somos do tamanho dos nossos sonhos. Ao meu irmãozinho, Yan, em que eu sempre tento ser minha melhor versão para server como espelho. Além disso, meus avós, com sua sabedoria e encorajamento, me deram motivação para eu conseguir caminhar nessa etapa da vida.

Finally, this dissertation and its outcomes have been made possible by the support provided by the Luxembourg National Research Fund (FNR) through COATIHN project (C19/MS/13641732), the Luxembourg Institute of Science and Technology (LIST) for the infrastructure and University of Luxembourg for its doctoral program.

LIST OF ABBREVIATIONS

AAc	Acrylic acid
AAm	Acrylamide
AFM	Atomic force microscopy
AP-DBD	Atmospheric pressure dielectric barrier discharge
AP-PECVD	Atmospheric-pressure plasma-enhanced chemical vapor deposition
BMA	Butyl methacrylate
BMAAB	4,4'-bis(methacryloylamino)azobenzene
CW	Continuous wave
D ₂ O	Deuterium oxide
DEAEMA	2-(diethylamino)ethyl methacrylate
DMAEMA	Dimethylaminoethyl
EGDMA	Ethylene glycol dimethacrylate
EMA	Ethyl methacrylate
ϵ -CL	ϵ -caprolactone
f_{pe}	Plasma pulse frequency
FRP	Free-radical polymerization
FTIR	Fourier-transform infrared spectroscopy
GMA	Glycidyl methacrylate
GPC-MS	Gel permeation chromatography coupled with high-resolution mass spectrometry
HEMA	2-hydroxyethyl methacrylate
iCVD	Initiated chemical vapor deposition
LA-PECVD	Liquid-assisted plasma enhanced chemical vapor deposition
LDPE	Low density polyethylene
MAA	Methacrylic acid
MALDI-HRMS	Matrix-assisted laser desorption/ionization high-resolution mass spectrometry
MBA	N,N'-methylenebisacrylamide
MMA	Methyl methacrylate
MMA	Methyl methacrylate

M_p	Peak molecular weight
M_w^*	Apparent weight average molar mass
NIPAAm	N-Isopropylacrylamide
NMR	Nuclear magnetic resonance spectroscopy
PEGDMA ₄₀₀	Polyethylene glycol dimethacrylate
PEG	Poly(ethylene glycol)
PES	Polyethersulfone
PP	Polypropylene
P_{sat}	Saturation vapor pressure
PVP	Polyvinylpyrrolidone
QCM-D	Quartz crystal microbalance with dissipation monitoring
RSGP	Rapid step-growth polymerization
SE	Spectroscopic ellipsometry
SEM	Scanning electron microscopy
T_e	Temperature of the electrons
T_i	Temperature of ions, neutrals, and metastable species
WCA	Water contact angle
XPS	X-ray photoelectron spectroscopy

Table of Contents

GENERAL INTRODUCTION	12
CHAPTER 1 : STATE OF ART	16
1.1 Hydrogel.....	17
1.2 Atmospheric-Pressure Plasma Polymerization	28
1.3 Hydrogel synthesized by plasma polymerization.....	38
CHAPTER 2 : DEPOSITION AND CHARACTERIZATION.....	43
2.1 AP-DBD set-up, electrodes and generator.....	44
2.2 Generator and nanopulsed-plasma electrical measurements.....	44
2.3 Monomers.....	45
2.4 Liquid layer formation.....	46
2.5 Substrates	47
2.6 Characterization.....	48
CHAPTER 3 : FREE-RADICAL POLYMERIZATION OF 2-(HYDROXYETHYL) METHACRYLATE FROM LIQUID ASSISTED THIN FILM DEPOSITION USING NANOSECOND PULSED ATMOSPHERIC PLASMA	55
3.1 Introduction.....	56
3.2 Results and discussion	57
3.3 Conclusion.....	71
CHAPTER 4 : HYDROGEL SYNTHESIS VIA NANOSECOND PULSED PLASMA INDUCED COPOLYMERIZATION OF MAA AND EGDMA FROM LIQUID LAYERS.....	73
4.1 Introduction.....	74
4.2 Results and discussion	77
4.3 Conclusion.....	98
CHAPTER 5 : SYNTHESIS OF THERMORESPONSIVE PP(PEGDMA₄₀₀) HYDROGEL FILMS VIA LIQUID-ASSISTED PLASMA-INDUCED FREE-RADICAL POLYMERIZATION FROM LIQUID LAYERS.....	101
5.1 Introduction.....	102
5.2 Results and discussion	103
5.3 Conclusion.....	109
CHAPTER 6 : CONCLUSION AND OUTLOOKS.....	112
PUBLICATION LIST.....	116
REFERENCES.....	117
ANNEX A.....	150
ANNEX B.....	173
ANNEX C.....	185
ANNEX D.....	189

General Introduction

Hydrogels are a class of soft materials consisting of a hydrophilic three-dimensional polymer network, which swells when immersed in liquid environments while maintaining its structure.¹⁻³ These materials have diverse applications in the biomedical field, commonly used in wound dressing, topical and drug delivery, cosmetics products, and contact lenses.⁴⁻⁹ As research and development have advanced, the application of hydrogels has expanded to more fields. Prominent fields nowadays for its application include tissue engineering,¹⁰⁻¹⁴ flexible electronics,¹⁵⁻¹⁷ (bio)sensors,^{18,19} and photonic devices.^{20,21}

The last 20 years were marked by the increase in research and development of hydrogels, where these materials were not only synthesized as bulk gels and gel particles but also have raised attention as hydrogel films.²²⁻²⁵ Hydrogel films are usually made of thin layers (ranging from nanometers to micrometers) of hydrophilic polymer networks and present the desired properties as bulk ones.^{26,22} The polymeric network structure of hydrogels plays a crucial role in their performance and functionality as thin films.^{27,28}

Several approaches have been developed to prepare hydrogel as films or coatings on substrates. The most common approaches include layer-by-layer assembly and precursor deposition through spin coating, followed by cross-linking, either physical or chemical.^{22,29,30} Additionally, triggering the polymerization, whether via addition or condensation processes, is a necessary step in both techniques.^{22,30}

Atmospheric-pressure plasma technology has gained attention for directly synthesizing and depositing functional polymeric thin films with controlled thickness.^{31,32} This deposition approach is particularly noteworthy due to its substrate-independent nature, scalability, and avoidance of solvents and chemical initiators.³³⁻³⁵ Plasma-induced polymerization methods aim to achieve polymer structures resembling those obtained through conventional free-radical polymerization, such as the polymers obtained in wet chemistry.³² While promising, plasma polymerization may lead to several side reactions, resulting in the loss of desired chemical functionalities and alterations in the monomer's original chemistry.^{33,36-38} Research efforts have been directed toward minimizing these detrimental reactions caused by exposure to plasma reactive species while enhancing control over the chemical structure of the plasma polymer.³⁹⁻⁴¹ A notable approach is pulsed plasma, which allows for the temporal control of monomer

exposure to plasma reactive species.^{33,40,41} Recent advancements in this field include the introduction of nanosecond pulsed plasma using ultrashort square pulse generators.⁴² This technique combines extremely short plasma discharges (approximately 100 ns per pulse) with longer off-times (in the range of hundreds of milliseconds), demonstrating excellent retention of the monomer's original structure and influencing polymer chain growth by tuning the plasma pulse frequency.⁴²⁻⁴⁴

Regarding the physical state of the monomers polymerized by plasma, they can be injected as vapor, solid, liquid, or aerosol.^{32,45} However, studies focusing on controlling the chemistry and mechanisms of plasma polymerization from liquid monomers remain scarce compared to vapor-phase approaches.⁴⁵⁻⁴⁹ Conveniently, liquid or aerosol monomer delivery offers significant advantages, such as utilizing monomers with low vapor pressure, high molecular weight, and even solids dispersed in a liquid medium to form composites films.⁵⁰⁻⁵⁴

Despite the advancements in plasma technology over the past few years for synthesizing hydrogels, studies investigating control over the network structure in hydrogel films obtained via plasma polymerization remain limited. Additionally, understanding the correlation between the polymeric network structure and the properties of plasma-formed hydrogel thin films poses characterization challenges due to the inherent cross-linked nature of these soft materials.

Thesis framework: Objectives and structure of the thesis

This thesis aims to deposit hydrogel thin films from liquid layers of monomers through atmospheric-pressure nanosecond-pulsed plasma-induced free-radical polymerization. The objective relies on elucidating the influence of plasma pulse frequency on the polymerization mechanisms governing the formation of the hydrogel film from the liquid layer. By detailed characterizations of the chemistry and properties (swelling, viscoelastic properties...) of the hydrogels, this study aims to provide a deeper understanding of their polymeric network structure.

Considering the stated aim, the Thesis is organized in the following chapters:

Chapter One offers an introduction and literature review for atmospheric-pressure nanosecond-pulsed plasma-induced free-radical polymerization to obtain hydrogel films.

Chapter Two summarizes equipment, techniques and monomers used during the study. The characterization methodologies described in this chapter are used in the subsequent chapters.

Chapter Three addressed atmospheric-pressure nanosecond-pulsed plasma-induced free-radical homopolymerization of 2-hydroxyethyl methacrylate (HEMA), a model methacrylate monomer for the synthesis of hydrophilic polymers. This chapter aimed to control the ratio between plasma-formed initiating species and monomer molecules available for polymerization by tuning the pulse frequency and spray rate of the liquid monomer, respectively. Growth rate, chemical structure, monomer conversion, and polymeric growth of the formed products are studied and characterized in depth. Moreover, a comparative study between HEMA deposited from the monomer in liquid and the vapor phase, using the same reactor and plasma generator, was carried out to evidence differences in the chemical structure of the films.

Chapter Four expands the study to the copolymerization of liquid layers of two methacrylates from the perspective of forming stable hydrogel thin films. The chosen monomers were methacrylic acid (MAA) and ethylene glycol dimethacrylate (EGDMA). The pulse frequency and the composition of the mixture of monomer(s) in the liquid layer are investigated to tune the network structure of the hydrogels. The swelling and the viscoelastic properties of the swollen hydrogel thin film were determined by coupling quartz crystal microbalance with dissipation monitoring (QCM-D) and spectroscopic ellipsometry techniques.

Chapter Five focus on the application of nanosecond-pulsed plasma-induced free-radical polymerization for the direct synthesis and deposition of polyethylene glycol dimethacrylate (PEGDMA₄₀₀) hydrogels. To showcase the potential applications of these thin film materials, water-stable hydrogel films were deposited onto several different surfaces (such as fabrics). The thermo-responsive properties of the thin films were also investigated.

Chapter 1 : State of art

1.1 Hydrogel

1.1.1 Definition

Hydrogels are 3D hydrophilic polymer networks able to absorb and retain large quantities of liquid in their swollen state (water or biological fluids).^{1,3} The stability of the hydrogel structure in its swollen state is achieved by chemical or physical cross-linking of the polymeric chains,⁸ see Figure 1.1a. In their swollen state (Figure 1.1b), the polymeric chains in the network are pulled away from each other, allowing the hydrogel to absorb significant volumes of liquid.¹ The network structure of hydrogels is defined by several parameters, including the polymer volume fraction in the swollen state (ϕ_s), the number of average molecular weight between cross-links (\bar{M}_c), and the network mesh size (ξ).^{2,55}

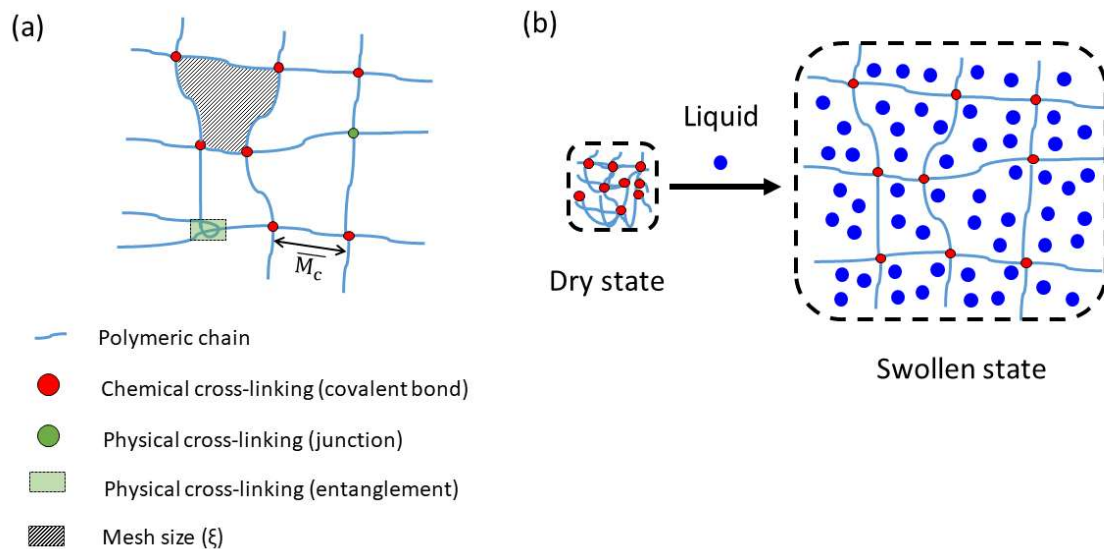


Figure 1.1: (a) Hydrogel network structure. (b) Schematic representation of hydrogels in a swollen and dry state by the incorporation of liquid. Adapted with permission from Richbourg.¹ Copyright 2020 Elsevier.

1.1.2 Classification

Hydrogels can be classified based on various criteria such as their physical properties, responsiveness to stimuli, preparation technique, source material, presence of ionic charges, degradability, and nature of cross-linking. Hydrogels' classification is based on their distinct

characteristics, defined by their response to different environments and their suitability to specific applications.⁵⁶ For instance, the classification of hydrogels based on their cross-linking methods can provide insights into their mechanical strength, swelling behavior, and biodegradability.⁵⁷ Based on these criteria, a specific hydrogel can often be classified by multiple parameters. For example, the hydrogel could be derived from a synthetic source, non-biodegradable, and prepared through copolymerization. Among the various classification criteria, two stand out for their significant impact on the choice of synthesis route, structure, and final properties of the hydrogel: cross-linking and source of the polymer.⁵

1.1.2.1 Cross-linking in hydrogels and its importance

The presence of cross-links provides a stable network structure while in the swollen state.⁸ In this context, cross-linking density refers to the concentration of cross-links within the hydrogel network. Additionally, several studies could find a relationship between the cross-linking density and the several hydrogel properties measured,⁵⁸⁻⁶⁰ as shown in the schematic in Figure 1.2. Hence, adjusting cross-linking density in hydrogels is a critical parameter that significantly influences important hydrogel properties, such as swelling behavior and mechanical properties. For instance, a higher cross-linking density generally results in an increase in the stiffness and mechanical strength of hydrogels, as the cross-links act as anchors holding the polymer chains together.⁵⁹ Therefore, hydrogels exhibiting high cross-linking density are suitable for applications requiring high strength and durability.^{61,62} However, this high cross-linking density can often be associated with a decrease in the swelling ratio.⁵⁹

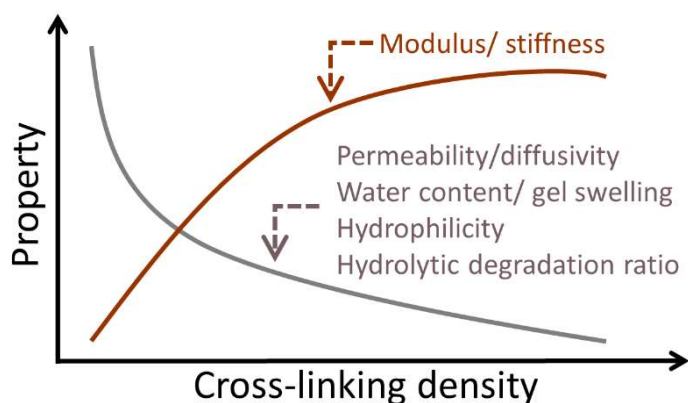


Figure 1.2: Important properties of hydrogels as a function of cross-linking density. Adapted with permission from Lin *et al.*⁵⁹ Copyright 2008, Chien-Chi Lin et al, Springer Nature.

Similar to the cross-linking density, the type of cross-links also plays a crucial role in determining the overall performance of hydrogels. Hydrogels can be classified based on the type of cross-linking, which is divided into two main methods: chemical or physical cross-linking (Figure 1.3a). Physically cross-linked hydrogels rely on reversible interactions to form the network structure, such as hydrogen bonding, ionic interactions, or hydrophobic interactions to hold the polymer chains together.⁶³ On the other hand, chemical cross-linking involves the formation of covalent bonds between polymer chains, leading to the creation of a stable and irreversible network structure. The mechanism for their formation typically involves free-radical polymerization induced cross-linking, cross-linked by enzymes, and chemical reactions between functional groups (such as, click chemistry, Schiff base formation, esterification, and Michael addition reaction).^{3,8,64} Current widely used strategies for the formation of hydrogels are summarized in Figure 1.3b.

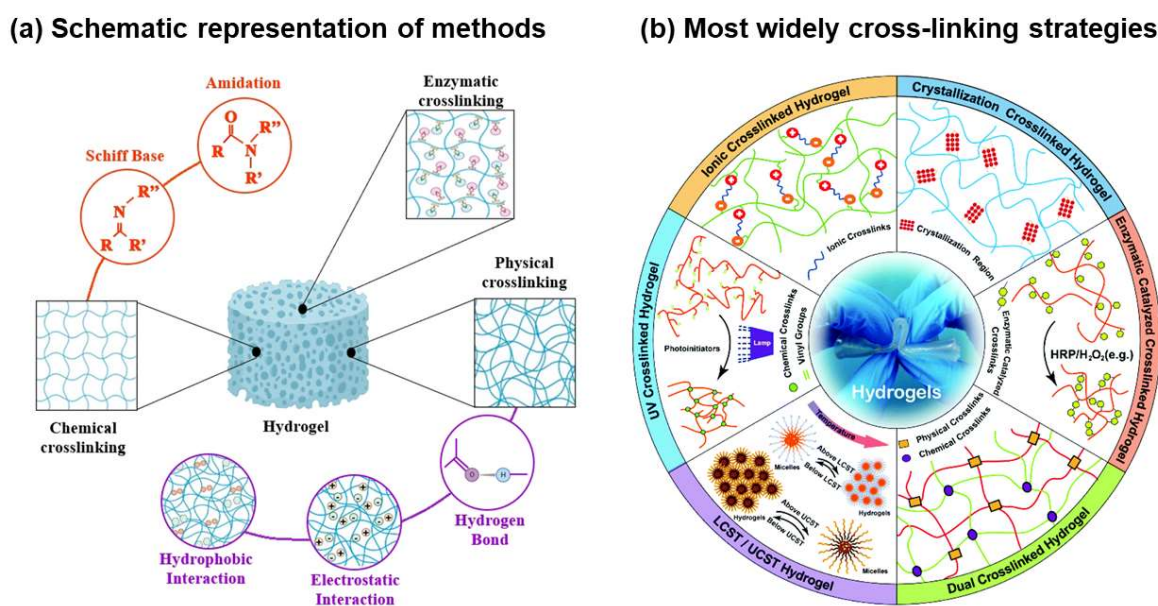


Figure 1.3: (a) Schematic representation of cross-linking methods and examples of the physical or chemical interactions. Reprinted with permission from Paiva *et al.*⁵⁹⁻⁶⁵ Copyright 2023, The Mayara T. P. Paiva et al, under exclusive licence to Springer Science Business Media, LLC (b) Most widely used cross-linking strategies to obtain hydrogel network structure. Reprinted with permission from Hu *et al.*⁶⁴ Copyright 2019, RSC.

Compared with physically cross-linked hydrogels, chemically ones exhibit enhanced stability under physiological conditions, more tuneable physicochemical properties, better

mechanical strength, and tunable degradation behavior.^{64,66} Thanks to the unique properties conferred by these properties, chemically cross-linked hydrogels find promising applications. For example, due to their stability and mechanical strength, chemically cross-linked are suitable for drug delivery systems, where maintaining the integrity of the hydrogel matrix is crucial for controlled release of bioactive molecules.^{67,68}

As previously mentioned (see Figure 1.2), important hydrogel characteristics, such as swellability, and elasticity, exhibit critical dependence on the cross-linking density. In this context, chemically cross-linked hydrogels can tailor such properties by varying the concentration of the cross-linking agent during the synthesis.^{69,70} For example, the work of Unger *et al.* discusses the synthesis of hydrogels poly(HEMA) using ethylene glycol dimethacrylate (EGDMA) as a cross-linking agent through initiated chemical vapor deposition.⁷⁰ As expected, by increasing the EGDMA fraction during polymerization, the swellability in water decreased (Figure 1.4).

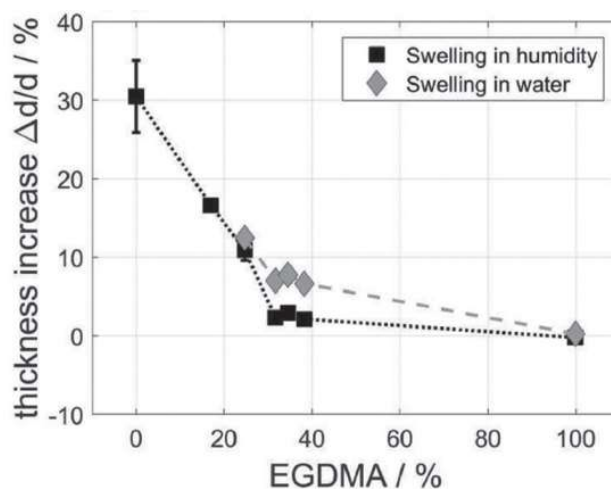


Figure 1.4: Thickness increase of hydrogels in water and in humid environments versus the EGDMA fraction. Reprinted with permission from Unger *et al.*⁷⁰ Copyright 2016 WILEY-VCH Verlag GmbH & Co. KGaA, Weinheim.

1.1.2.2 Source of the polymeric chains in hydrogels

Hydrogels can be categorized based on the source of their hydrophilic polymers: natural, synthetic, and hybrid. Natural hydrogels are often derived from biopolymers, such as polysaccharides, polypeptides, and other biocompatible substances found in nature.⁷¹

Conversely, synthetic hydrogels are created using organic chemistry principles, enabling control over their properties and functionalities.⁶³ Hybrid hydrogels, a third category, combine natural and synthetic precursors, which merge both sources.

Synthetic hydrogels have emerged as a prominent class due to several advantages over their natural counterparts. These advantages include greater control over impurities, high absorption capacity, well-defined structure and functionality, and tunable degradation and stability across various pH, temperature, pressure, and enzyme conditions.^{71,72} The ability to precisely engineer synthetic hydrogels makes them valuable in to be used for specific purposes, such as drug delivery or controlled release systems, and creating advanced materials for various industries, including pharmaceuticals and regenerative medicine.^{73,74}

Various types of synthetic monomers have been reported for the synthesis of hydrogels, such as acrylates, glycols and acrylamides, based on different mechanisms of polymerization and cross-linking types (Table 1.1).

Table 1.1: Examples of hydrogel synthesis based on different mechanisms for the formation of the polymeric network, synthetic monomer(s) used, and type of cross-linking promoted.

Mechanism	Monomer*	Cross-linking**	Proposed polymeric network structure	Ref.
Free-radical polymerization	AAc; MMA; EMA; BMA	Chemical: BMAAB	<p>X = R = CH₃; C₂H₅; C₄H₉</p>	75
	HEMA	Chemical: EGDMA		76

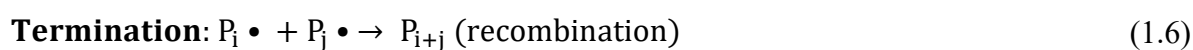
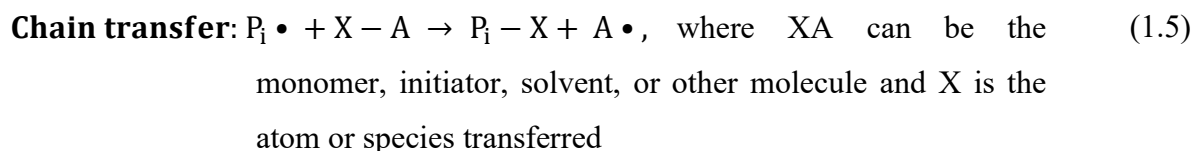
	NIPAAm	Chemical: MBA	$ \begin{array}{c} \text{---CH}_2\text{---CH---CH}_2\text{---CH---CH}_2\text{---CH---} \\ \quad \quad \quad \quad \\ \text{O=C} \quad \quad \text{C=O} \quad \quad \text{C=O} \\ \quad \quad \quad \quad \\ \text{NH} \quad \quad \text{NH} \quad \quad \text{NH} \\ \quad \quad \quad \quad \\ \text{H}_3\text{C---CH} \quad \quad \text{CH}_2 \quad \quad \text{HC---CH}_3 \\ \quad \quad \quad \quad \\ \text{CH}_3 \quad \quad \text{NH} \quad \quad \text{CH}_3 \\ \\ \text{C=O} \\ \\ \text{---CH}_2\text{---C---C---CH}_2\text{---CH---} \\ \quad \quad \\ \text{C=O} \quad \text{H} \quad \quad \text{C=O} \\ \quad \quad \\ \text{NH} \quad \quad \text{NH} \\ \quad \quad \\ \text{HC---CH}_3 \quad \quad \text{HC---CH}_3 \\ \quad \quad \\ \text{CH}_3 \quad \quad \text{CH}_3 \end{array} $	77
Step-growth	ϵ -CL; PEG	Physical	$ \text{CH}_3\text{---O---} \left[\text{---C}_2\text{H}_4\text{---O---} \right]_Y \left[\text{---C} \begin{array}{c} \text{CH}_2 \\ \end{array} \text{---C}_8\text{H}_{10}\text{---O---} \right]_X \text{OOCHN(CH}_2)_6\text{NHCOO---O---C}_8\text{H}_{10}\text{---C} \begin{array}{c} \text{CH}_2 \\ \end{array} \text{---} \right]_X $ <p style="text-align: center;"> PEG PCL </p>	78

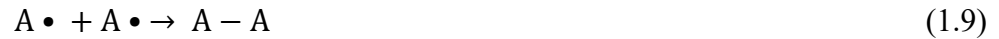
*AAc: Acrylic acid ; BMA: Butyl methacrylate; EMA: Ethyl methacrylate; MAA: Methacrylic acid; MMA: Methyl methacrylate; NIPAAm: N-Isopropylacrylamide; ϵ -CL: ϵ -caprolactone.

**BMAAB: 4'-bis(methacryloylamino)azobenzene; MBA: N,N'-methylenebisacrylamide.

1.1.3 Free-radical polymerization for synthesizing hydrogels - the strategy

Free-radical polymerization (FRP) is a commonly used mechanism to form hydrogel polymeric networks (Table 1.1). In FRP, vinyl monomers undergo well-defined reaction pathways to promote the polymeric chain growth and synthesize the polymer. The reaction mechanisms of FRP for a homopolymerization consists of the following reactions:





FRP is initiated by reactive species produced from the initiator (i.e., noted “I”, Eq 1.1). Free radicals in Eq 1.1 might be generated from chemical initiators by thermal or UV-light decomposition or redox process.^{3,79} Initiation of the polymerization will occur through the reaction between the free radical and monomer molecule by the π -bond to form a new radical center (Eq 1.2), and the former radical in Eq 1.1 will be the end group of the formed polymer.^{79,80} The propagation occurs via the gradual addition of the monomers successively to continuously propagate the reactive center (Eq 1.3 and Eq 1.4). An undesired chain-breaking reaction during FRP is chain transfer (Eq 1.5), which occurs between the growing macroradical by the transfer of hydrogen or other atoms or species to it from some molecules present in the system.⁷⁹ The occurrence of chain transfer results in producing a new radical ($A\bullet$) and termination of the propagating chain (P_i-X) by hydrogen abstraction, for example.⁷⁹ The new radical ($A\bullet$) can terminate the polymerization (Eq 1.8, Eq 1.9) or reinitiate it (Eq 1.10). Termination of the polymeric growth of FRP might occur through the recombination of two radicals (Eq 1.6) or through disproportionation (Eq 1.7).^{79,81} Finally, termination by disproportionation gives two terminated chains. In this case, one terminated chain will have an unsaturated carbon group while the other one is saturated.^{79,80}

Initiator concentration is a key parameter in determining the growth of polymeric chains, impacting molecular weight, polymerization kinetics, and structural properties of formed polymers. The free radicals from the initiator decomposition participate in two key competing reactions: propagation and termination. When the initiator concentration is high, a larger number of free radicals are generated. This can increase the number of reactive center growing chains, raising the probability of termination events.⁷⁹ Conversely, using a lower initiator concentration can yield a higher degree of polymerization, although at the cost of a slower polymerization rate and potentially incomplete monomer conversion.⁷⁹ Balancing these competing reactions is crucial for achieving the desired molecular weight distribution and reaction kinetics in free-radical polymerization, ultimately enhancing monomer conversion during the propagation reaction rather than the initiation phase.

Furthermore, the kinetic chain length (ν) in free-radical polymerization is a critical parameter that determines the average chain length of polymer chains and influences the overall kinetics of the polymerization process.^{79,82} It reflects the number of monomer units added to a growing polymer chain before termination or chain transfer reactions occur. This length is defined as the average number of molecules consumed/polymerized ($[M]$) per radical ($[M\bullet]$).^{79,83} Eq 1.11 demonstrates the relationship between ν and the ratio of monomer concentration to free radical concentration under steady-state assumptions.^{79,83}

$$\nu = \frac{k_p [M]}{2 k_t [M\bullet]} \text{ , where } k_p \text{ is the constant rate for propagation and } k_t \text{ is the rate constant for termination} \quad (1.11)$$

1.1.4 Hydrogel films

Hydrogel has been such a constant theme of research, as can be seen in Figure 1.5 (blue circles), where from 2000 there were about 1000 publications and its almost 11 times higher in 2020. These materials were synthesized as bulk gels and gel particles and have raised attention as hydrogel films. The field of hydrogel as thin films has growing research interest in the past 15 years (Figure 1.5-green circles).

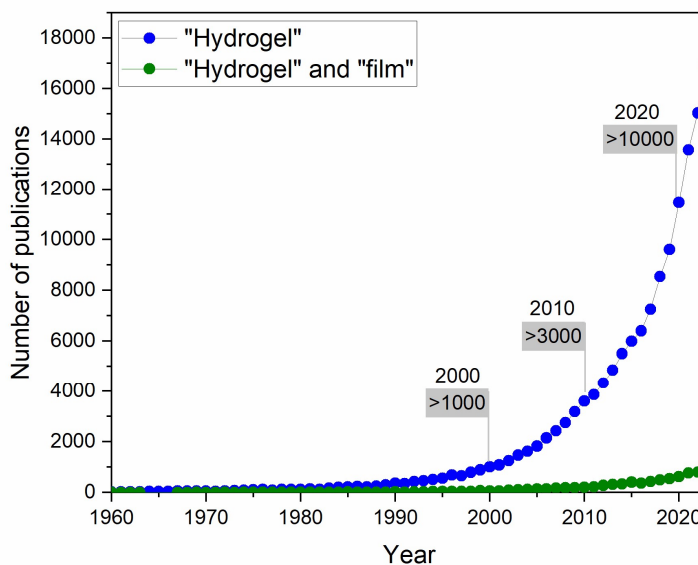


Figure 1.5: The number of references published (patents and articles) under the tag of “hydrogel” or the tag “hydrogel” and “film” as the abstract/keyword in SciFinder. The search was performed on April 12, 2024.

Hydrogel films are usually made of thin layers (ranging from few nanometers to few micrometers) of hydrophilic polymer networks and present the same desired properties as bulk ones.^{26,22} Interestingly, hydrogel films can show faster response to stimuli and higher flexibility compared to the bulk ones.^{26,84} Hydrogel films represent a promising material class due to their unique ability to combine the advantageous properties of hydrogels with the benefits of films. These materials are commonly investigated in promising applications, such as tissue engineering,^{10–13} flexible electronics,^{15–17} (bio)sensors,^{18,19} and in photonic devices.^{20,21}

1.1.4.1 Characterization of mechanical and swelling properties of hydrogel films

To measure the properties of hydrogels in film form, various techniques can be employed based on the specific characteristics of interest. However, to the best of our knowledge, the *in operando* measurement of the swelling behavior and mechanical properties of hydrogel films has not been fully established in the literature. This gap may be attributed to the increasing development of hydrogels as freestanding films or coatings on substrates has garnered significant attention in recent years (Figure 1.5). In this sense, Table 1.2 summarizes the main techniques currently being investigated for the *in operando* characterization of the swelling behavior and mechanical properties of hydrogel films.

Table 1.2: Characterization techniques for swelling behavior and mechanical properties of hydrogel films

Technique	Measurement conditions	Measured property	Ref.
Quartz-crystal microbalance with dissipation monitoring (QCM-D) coupled with spectroscopic ellipsometry (SE)	Working conditions	Thickness, viscoelastic properties, cross-link density	85,86
Spectroscopic ellipsometry SE	Wet media	Swelling (variation in thickness before and after exposure to liquid)	87
QCM	Dry conditions	Swelling (variation in thickness before and after exposure to liquid)	86

Gravimetric analysis	Specific conditions	Swelling (mass before and after exposure to liquid)	88
Atomic force microscopy	Dry condition or wet media	Swelling (variation in thickness before and after exposure to liquid), viscoelastic properties	89,90
Dynamic mechanical analysis	Specific conditions	Viscoelastic properties, cross-link density, stress/strain curves	91
Electron microscopy	Under vacuum	Thickness	92
Optical microscopy	Wet media	Thickness	93
Nuclear magnetic resonance spectroscopy	Specific conditions	Cross-link density	90

1.1.4.2 Synthesis and deposition techniques for hydrogel films

Hydrogels as thin films are mainly prepared as freestanding films or coatings deposited on substrates.²² The most common approaches to obtain hydrogel films are based on the deposition of the precursor (monomers or polymer solution) either by layer-by-layer method or by spin coating.^{22,29,30} Regarding the layer-by-layer assembly method, it allows precise control over thickness, interfacial properties, and functions.^{18,94} Moreover, this method permits the coating deposition on various substrates, facilitating the creation of freestanding hydrogel thin films with specific properties.¹⁸ However, its main drawback is the time-consuming nature of the process. The sequential assembly of multiple layers can be labor-intensive and time-consuming, especially when many layers are required to achieve the desired film thickness and properties.^{95,96} Alternatively, spin coating is a valuable technique for spreading hydrogel films on substrates at both laboratory and industrial scales.^{29,97} It is highly utilized due to its simplicity and cost-effectiveness in depositing smooth and uniform films, followed by necessary drying or annealing.^{29,97} However, its main disadvantages rely on the scalability and waste of material since excess must be applied on the surface beforehand, as well as the reproducibility of this method.⁹⁷⁻⁹⁹

In addition to the deposition of the precursor, polymerization reactions may be a required step for hydrogel film synthesis. The main approaches for synthesizing these materials are shown in Figure 1.6 and categorized by different techniques that can induce polymer network

formation by free-radical polymerization (FRP). The three methods shown are wet chemistry, initiated chemical vapor deposition (iCVD), and plasma-initiated FRP.

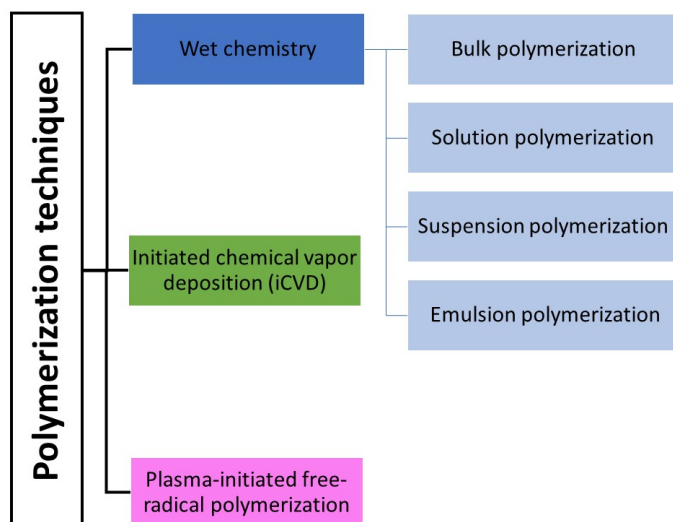


Figure 1.6: Widely used free-radical polymerization techniques for hydrogel film synthesis.

Wet chemistry is a widely and well-established method to obtain hydrogels.^{9,63,71,100} Briefly, it encompasses various polymerization mechanisms, including FRP, that utilize liquid-phase reactions to synthesize polymers. This method can be further divided into bulk, solution, suspension, and emulsion polymerization, based on the specific chemical substances added to the liquid mixture, such as solvent or surfactant.^{3,14,101,102} However, the main components are the liquid monomer and the initiator.³

Chemical vapor deposition (CVD) is a highly applied technique to synthesize polymeric thin films.^{70,103–105} Through initiated chemical vapor depositions (iCVD), polymeric chains grow through FRP via the mass transport of vapor vinylic monomers and initiators.¹⁰³ In this process, reactions are triggered in the gas-phase region, where the formation of the initiating species and intermediate reactions occur.^{103,106} These formed species will enable gas-solid reactions to occur at the substrate surface, leading to thin film growth, while volatile products and unreacted species then desorb from the surface and are removed.^{103,106}

Finally, there are studies highlighting the potential of plasma-initiated FRP in the polymerization of the polymeric chains of the hydrogel films or even playing a role in the cross-linking stage.^{51,54,107–109} The generation of reactive species due to exposure to plasma, without

solely relying on chemical substances (such as initiator), has made plasma polymerization an interesting approach for the elaboration of hydrogels.^{45,66}

1.2 Atmospheric-Pressure Plasma Polymerization

1.2.1 Plasma

Plasma, known as the fourth state of matter, is a partially or fully ionized gas containing a mixture of molecules, ions, electrons, photons, and excited species (Figure 1.7).^{32,110,111} Ionization of the gas to plasma state can occur when the gas molecules are exposed to high-energy radiation, electric fields, or high electrical potential and current.^{111,112}

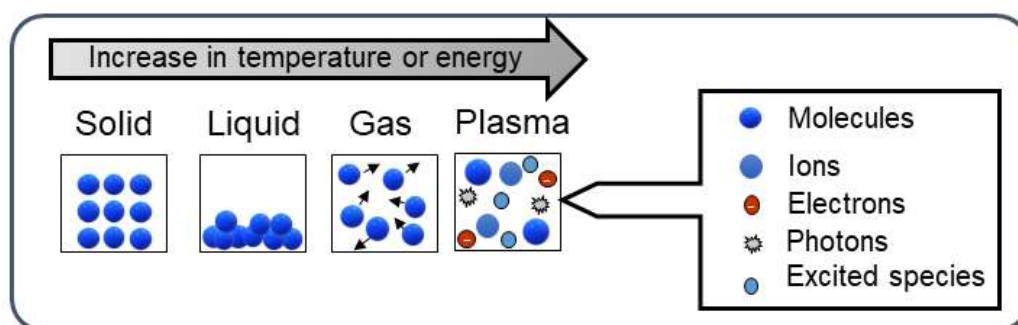


Figure 1.7: The four states of matter.

1.2.2 Classification of Plasmas

Depending on the temperature of the charged species present, i.e., temperature of the electrons (T_e) and temperature of ions, neutrals, and metastable species (T_i), plasma can be classified either by thermal or non-thermal plasma.^{32,113} Different nomenclatures, general properties, and examples of thermal and non-thermal plasma are summarized in Table 1.3.

Thermal plasma is characterized by the thermal equilibrium between the electrons' temperatures, T_e , and the ion's temperature, T_i , (ca. 10000 K).^{114,115} While non-thermal plasma is composed of low temperature T_i (ca. 300-1000 K) and relatively high temperature T_e (10,000-100,000 K).^{110,114,115}

Non-thermal plasmas, such as glow discharges and dielectric barrier discharges, are widely used in polymer science for both processing and surface modification.^{111,116,117} Compared to their counterparts, non-thermal plasma has low electron density.^{111,114} This means that even though the T_e is high, the surrounding surfaces remain at relatively low temperatures.^{33,34} This non-equilibrium feature allows plasma-phase chemistry reactions and minimizes thermal degradations of the polymer structure.³²⁻³⁴

Table 1.3: Characteristics of thermal and non-thermal plasmas.^{111,114}

	Thermal plasma	Non-thermal plasma
Nomenclatures	Thermal plasma, hot plasma, near-equilibrium plasma	Non-thermal plasma, cold plasma, low-temperature plasma, non-equilibrium plasma
Properties	<ul style="list-style-type: none"> - $T_e = T_i$ - High electron density - Inelastic collisions between electrons and heavy particles create the plasma-reactive species - Elastic collisions heat the heavy particles, leading to electron energy consumption 	<ul style="list-style-type: none"> - $T_e \gg T_i$ - Lower electron density - Inelastic collisions between electrons and heavy particles induce plasma chemistry - Few elastic collisions are slightly heating heavy particles, leading to electron energy remaining high
Example	Electrical arcs, thermonuclear reactions generated by plasma	Low-pressure direct current and radio frequency discharges, glow discharges, and corona discharges

1.2.3 Plasma polymerization

Plasma polymerization is a process that utilizes plasma induced chemical reactions to convert organic-based molecules into plasma polymers or plasma polymer film.^{33,35} These molecules are often referred as either precursors or monomers (containing polymerizable group). Plasma polymerization can be carried out using various types of non-thermal plasmas, such as glow discharges, dielectric barrier discharges, and plasma jets, offering versatility in tailoring the properties of the deposited films.^{33,113,118,119}

One of the key advantages of plasma polymerization is its ability to operate as a dry and solvent free process, resulting in an interesting eco-friendly approach. Furthermore, it can be

used to uniformly functionalize the surface properties of a wide variety of materials (ceramic, metals, etc.) as plasma polymer films.^{31,32} Additionally, plasma polymerization is known for producing coatings with high and tunable deposition rates, making it cost-efficient for industrial upscaling.^{120,121} These advantages have enabled its application in various applications, such as food packaging,^{122,123} corrosion-resistant coatings,^{124–126} drug release,¹²⁷ antibacterial coatings¹²⁸ and in biochip technologies.¹²⁹

However, even when synthesized from the same monomer, the structures of plasma polymers differ from the structures obtained by conventional polymer chemistry. While conventional polymers consist of well-defined repeating units, plasma polymers can exhibit a highly cross-linked and heterogeneous network structure.^{35,130} Another main difference from the ones obtained in conventional polymer chemistry is that plasma polymers can be obtained from precursors that do not undergo polymerization by conventional pathways, such as methane.^{33,35,130}

1.2.3.1 Mechanisms of plasma polymerization

The polymeric growth mechanism in plasma polymerization generally proposes several reactions, often involving fragmentation and poly-recombination of the exposed molecules, to form the plasma polymers.^{32,33,120,130,131} The fragmentation of organic molecules can occur upon collisions with plasma reactive species (electrons, photons, ions, etc.), forming free radicals from the non-specific bond dissociation of the molecules.^{32,33,35,111} Indeed, considering electron energy distribution in non-thermal plasmas (the majority are around 2–3 eV), almost all chemical bonds involved in organic molecules can be dissociated.^{35,111,125} These highly reactive free radicals can induce reactions through radical-radical and radical-molecule reactions.¹²⁵ The resulting products can undergo random recombination, rearrangement, and further fragmentation, ultimately leading to the reorganization of initial organic molecules into macromolecular structures – the plasma polymers.^{33,111}

The polymerization pathway, among other parameters, is also strongly dependent on the nature of the initial molecule. The presence of polymerizable bonds enables the plasma-induced free-radical chain-growth polymerization pathway, strongly resembling that described for conventional wet polymer chemistry.^{111,120,125,132} Furthermore, the plasma polymerization mechanism of monomers might include fragmentation, poly-recombination, formation of film-

forming intermediates, and even ion-molecule reactions and ionic chain-growth pathways.
32,33,35,111,120

Possible reaction pathways of the monomer in plasma polymerization were proposed by Yasuda in 1985 in the rapid step-growth polymerization (RSGP) model and are presented in Figure 1.8.^{133–135} Yasuda proposed RSGP to polymerize vapor-phase monomers under low-pressure and high-power continuous wave (CW) plasma.^{32,133}

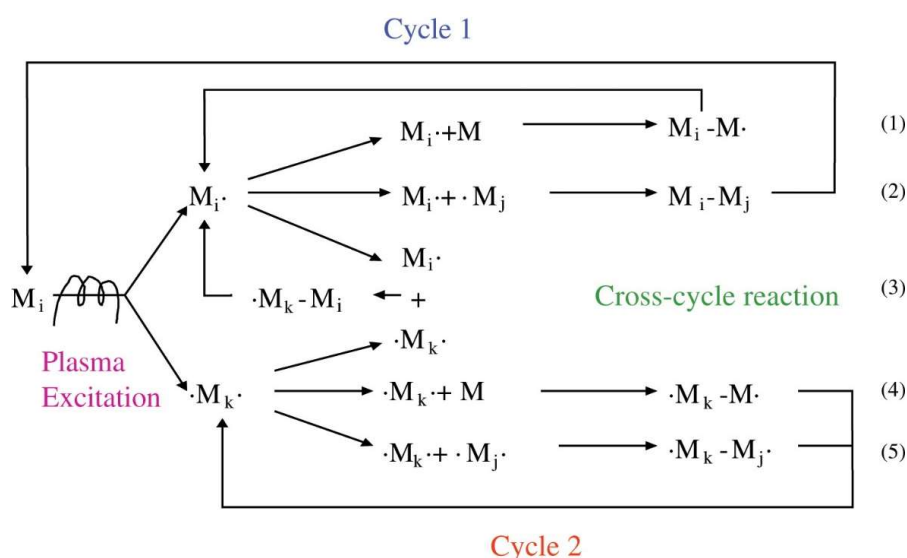


Figure 1.8: Growth mechanism of plasma polymers in rapid step growth polymerization (RSGP) model. Reprinted with permission from Yasuda.¹³⁴ Copyright 2003 Elsevier.

This model suggests the dissociation of the monomer as monoradicals (Cycle 1) or biradicals species (Cycle 2) plasma-formed radical fragments.¹³³ These fragments then contribute to the rapid, step-wise growth of the polymer films. The RSGP model considers the alteration of monomer chemistry by recombination/fragmentation reactions and reinitiation of the produced stable species.^{32,33,133} And, the growth of the plasma polymers exhibiting a highly cross-linked and heterogeneous network structure. Moreover, the model considers the influence of the reactivity of biradicals species formed from the fragmentation of unsaturated bonds (e.g., C=C, C=O...) upon exposure to plasma (Cycle 2 in Figure 1.8).¹³³ These plasma-formed reactive radicals depicted as “ $\cdot M_k \cdot$ ” (such as “ $\cdot O \cdot$ ”) can react with the other molecules and produce stable products, for example, CO₂ and CO.^{32,133} These stable products might be desorbed and removed from the plasma polymers afterward.^{32,133}

The formation of plasma polymers mainly occurs either on solid surfaces in contact with the plasma, leading to the growth of polymer films, or within the plasma volume, producing polymer powders or macroparticles.³⁵ The mechanism of plasma polymerization yielding to the deposition as solid films for vapor-phase monomers involves complex gas-phase and surface reactions.^{33,35} A schematic representation of steps involved in the deposition and plasma polymerization of vapor-phase monomers are shown in Figure 1.9. The deposition of the film occurs when the molecule fails to leave the surface of the substrate by loss of kinetic energy or by the formation of a chemical bond.^{33,35} Moreover, it is extremely important to note that plasma reactive species are able to simultaneously build and destroy (i.e. by etching) the forming polymeric film.

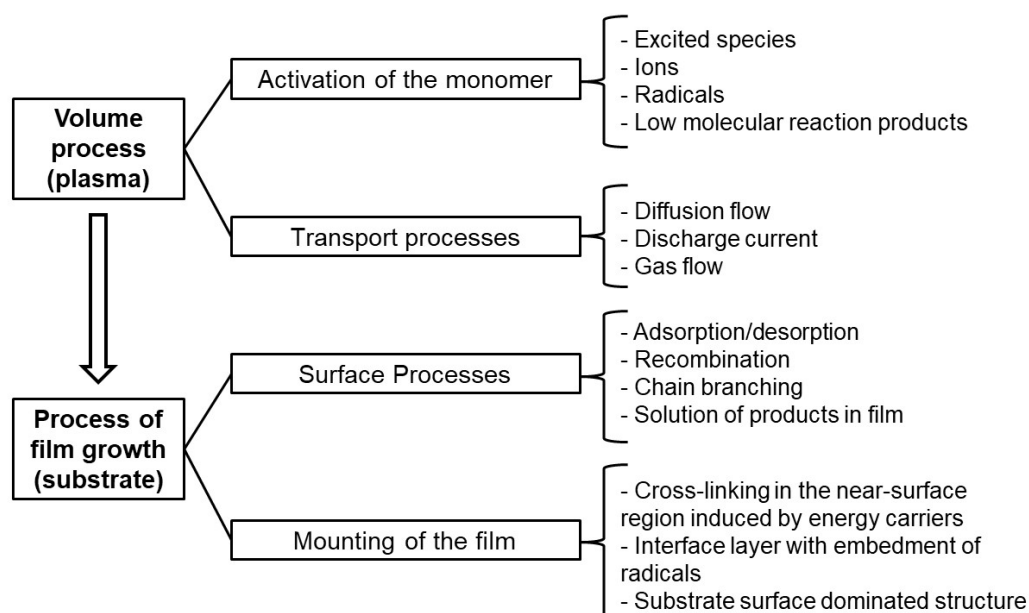


Figure 1.9: Schematic representation of plasma polymerization of monomer plasma polymerization yielding to the deposition as solid films for vapor-phase monomers in low-pressure. Adapted with permission from Deutsch *et al.*¹³⁶ Copyright 1981 WILEY-VCH Verlag GmbH & Co. KGaA, Weinheim.

1.2.3.1.1 Yasuda parameter

The Yasuda parameter, popularized by H. Yasuda in the late 1970s, represents the deposition rate of the plasma polymer film as a function of the apparent energy input, or density, per unit of monomer molecule.^{33,133} Fundamentally, the Yasuda parameter divides polymer deposition into three different regimes: the monomer deficient regime, the competition regime, and the energy deficient regime. This parameter is interesting since it has been shown that it

directly influences the properties, deposition rates, and application of the polymer films.^{32,133,137,138}

The Yasuda parameter is calculated as “ $Y=W/FM$ ”, where W is the discharge power, F is the monomer flow rate, and M is the molecular weight of the monomer. Figure 1.10 shows the influence of the Yasuda parameter on the deposition rate of the plasma polymer film, depicting the three different regimes. The energy deficient regime (also reported as monomer sufficient region) exhibits a direct increase in polymer deposition rate with increasing energy input per molecule (W/FM). Low W/FM values typically lead to the formation of plasma polymers with a more regular and well-defined structure, resembling conventional polymers.^{36,112,133} However, low power input per molecule often results in the incorporation of monomers and oligomers trapped within the polymeric chains of the deposited films.¹¹² As the energy input per molecule increases, thicker coatings are formed. The competition regime is encountered in a stable deposition rate (a plateau). The monomer deficient regime is characterized by higher energy/molecule input, where the deposition rate will gradually decrease. The fragmentation/recombination reactions in this regime are preponderant, associated with the loss of the monomer’s functional group.^{33,112,133}

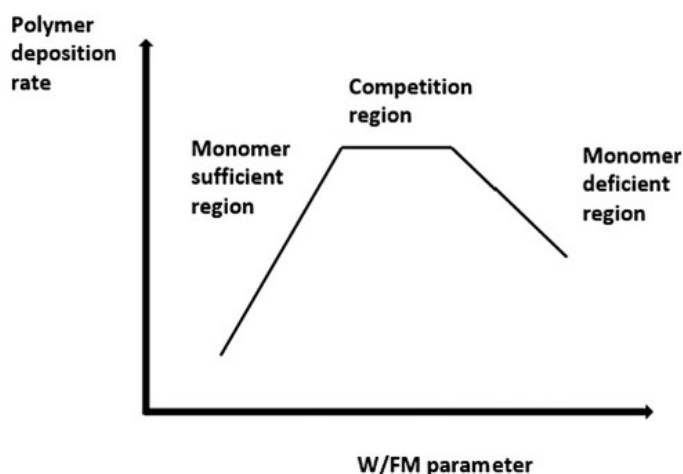


Figure 1.10: Schematic representation of the different regimes of plasma polymerization based as function of the Yasuda parameter. Reprinted with permission from Bitar *et al.*¹¹² Copyright 2018 Elsevier.

1.2.3.2 Plasma-induced free radical polymerization of vinyl monomers

As illustrated in the RSGP model in Figure 1.8, repeating the several reactions will enable the growth of the polymeric chain in plasma polymerization, and chain-growth is only one of these steps.

In this context, a promising approach in this field is plasma-induced or plasma-induced radical chain-growth polymerization (also referred to as plasma-induced free-radical polymerization). This approach aims to achieve a more regular and well-defined polymer structure with retained chemical functionalities from the initial monomer, resembling polymers obtained via conventional free-radical polymerization (FRP).³³⁻³⁵

The mechanisms governing plasma-induced FRP of monomers bearing vinyl groups resembles the initiation, propagation, termination, and chain-transfer reactions of FRP in conventional polymer chemistry.^{32,33} However, in plasma-induced FRP, the initiation is triggered by the free-radicals formed from the dissociation of monomers upon collision with the plasma reactive species (see Figure 1.11).¹²⁰ Where these plasma-formed radicals can react in several pathways through radical-radical and radical-molecule interactions.³² Hence, the plasma-state polymerization pathway occurs concurrently, leading to the formation of macromolecules through fragmentation and poly-recombination reactions.^{33,35,111}

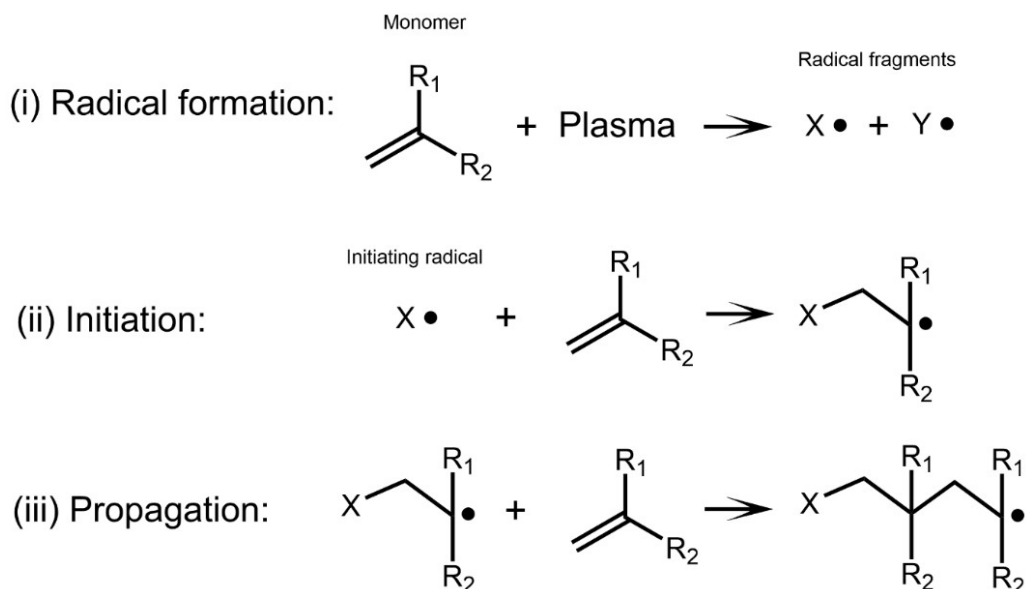


Figure 1.11: Schematic representation of radical formation, initiation, and propagation reactions of plasma-induced radical chain-growth polymerization.

Numerous studies have focused on minimizing these detrimental recombination/fragmentation reactions while promoting plasma-induced FRP to achieve greater control over the plasma polymer chemistry. Various approaches can be employed to reduce the detrimental aspect of the exposure of plasma, such as Yasuda parameter,¹³⁹ the reactor design,³⁹ the monomer chemistry,^{38,132,140} substrate temperature,¹⁴¹ post-discharge configuration,⁵⁰ and using pulsed plasma ignition.

1.2.3.2.1 Influence of plasma ignition in plasma-induced free-radical polymerization: Continuous wave versus pulsed plasma

Pulsed plasma represents a variation of the conventional continuous wave (CW) plasma ignition. Unlike CW plasma, which delivers a constant voltage, pulsed plasma interrupts the discharge ignition with periodic off-times (Figure 1.12).

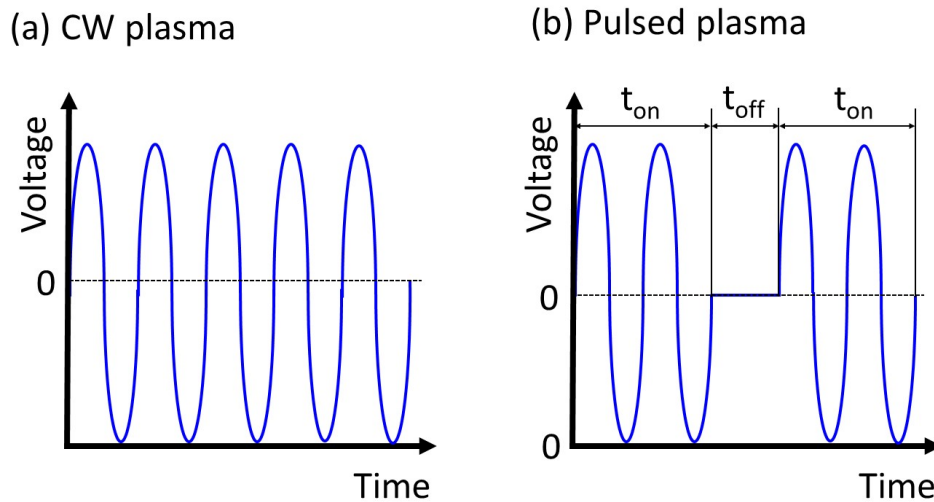


Figure 1.12: Schematic representation of the applied voltage in (a) continuous wave and (b) pulsed plasma.

The main parameters to characterize the pulsed plasma are plasma pulse frequency (the rate at which plasma ignition occurs over a time cycle), pulse period (the total time to complete a cycle), and the duty cycle (the percentage of time the plasma is "on" relative to the entire cycle).¹¹¹ These parameters are calculated as follows:

$$\text{Period} = t_{\text{on}} + t_{\text{off}} \quad (1.14)$$

$$\text{Plasma pulse frequency} = \frac{1}{t_{\text{on}} + t_{\text{off}}} \quad (1.15)$$

$$\text{Duty cycle (\%)} = \frac{t_{\text{on}}}{t_{\text{on}} + t_{\text{off}}} \quad (1.16)$$

Numerous studies have investigated to pulsed plasma to promote the plasma-induced FRP compared to the CW. The use of pulsed plasma aims to minimize the detrimental effect of plasma reactions and to form plasma polymers with retention of the monomer functionalities and chemical structures closer to conventional polymers prepared by wet chemistry methods.^{40,41,142–144} This approach aims to produce plasma polymers with greater control over chemistry through the temporal limitation of fragmentation/recombination reactions. During the "on" time (t_{ON}) of a pulse cycle, plasma exposure generates free radicals from fragmentation reactions, which can then initiate FRP. During the subsequent "off" time (t_{OFF}), the free radicals can recombine with other species or react with monomer molecules to initiate a FRP process. The deposition rate during t_{OFF} results mainly via chain-growth polymerization. By promoting this FRP pathway during the t_{OFF} , pulsed plasma can potentially lead to the formation of more chemically regular plasma polymers when compared to those obtained with CW discharges. Notably, Klages *et al.* demonstrated significant differences in the retention of epoxy groups in glycidyl methacrylate monomer between films obtained from pulsed and CW plasma ignitions.⁴⁰ This work showed up to 80% of epoxy groups were retained in pulsed plasma by varying t_{OFF} , compared to only around 15% in CW plasma. Furthermore, Tarducci *et al.* reported that plasma-polymerized HEMA obtained using pulsed plasma ($t_{\text{ON}} = 20 \mu\text{s}$, $t_{\text{OFF}} = 20 \text{ms}$) exhibited a structure more closely resembling the commercially acquired poly(HEMA) than the deposition obtained using CW plasma ignition.⁴¹

1.2.3.2.1.1 Nanosecond pulsed plasma

Reducing the plasma t_{on} and keeping the t_{off} in the range of milliseconds has been shown to reduce fragmentation/recombination reactions, while promoting self-sustained polymeric chain growth by FRP. Studies showed that varying the parameters of atmospheric-pressure nanosecond-pulsed plasma had a significant impact on the chemistry and polymeric growth of the films.^{42,43,145,146} Notably, Boscher *et al.* used the nanosecond pulsed plasma to polymerize the vapor-phase of glycidyl methacrylate monomer.⁴² This work demonstrated that employing

duty cycles as low as 0.01% showed high retention of the monomer structure and growth of high molecular weight plasma polymers. Boscher *et al.* attributed such results to favoring FRP pathway during long t_{OFF} while nanosecond t_{ON} limited the fragmentation/recombination reactions.⁴² Furthermore, Loyer *et al.* obtained an unprecedented weight-average molar mass of 94 000 $\text{g}\cdot\text{mol}^{-1}$ using nanosecond-pulsed plasma to polymerize the glycidyl methacrylate monomer.⁴³ This exceptional weight-average molar mass was never reported before in literature for atmospheric-pressure plasma-polymerization. In this context, there have been few studies on the plasma-induced FRP using atmospheric-pressure nanosecond-pulsed plasma to date, showcasing such an interesting approach to be further explored.

1.2.4 Atmospheric-pressure plasma polymerization from liquid phase monomers

Several studies have explored the use of pulsed plasma polymerization of monomer bearing polymerizable bonds at both low and atmospheric pressure.^{40,41,142–144} The ability to operate at atmospheric pressure, eliminating the need for vacuum equipment, presents a significant advantage for industrial upscaling. However, side reactions with the surrounding open atmosphere (air/moisture) cannot be ignored. Atmospheric-pressure pulsed plasma configurations have been successfully employed to obtain plasma polymers of monomers in vapor^{147–149} and liquid phase.^{46–48,150} The latter is very convenient for monomers with low vapor pressure, high molecular weight oligomers, and even solid phase molecules dissolved or dispersed in a liquid monomer.^{50–54}

The interactions between plasma and liquid have become of great interest and importance, not only for plasma polymerization but also for diverse applications in nanomaterial synthesis and plasma medicine. Since the knowledge gap in plasma polymerization of liquid layers still exists, a better comprehension was sought in other plasma-liquid systems. A great number of studies in plasma-liquid highlight different boundary regions characterized by differences in mass and energy transport. The interaction can be investigated under these regions: plasma gas phase, plasma-liquid interface, and bulk liquid (Figure 1.13).

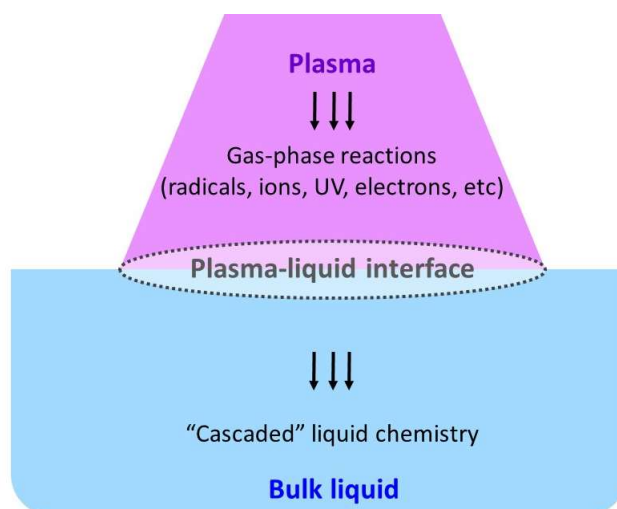


Figure 1.13: Schematic diagram of the different regions in the interaction in a plasma-liquid system. Adapted with permission from Mariotti *et al.*¹⁵¹ Copyright 2012 WILEY-VCH Verlag GmbH & Co. KGaA, Weinheim.

The plasma gas phase is the boundary region where plasma reactive species are present and is dominated by plasma gas phase chemistry.¹⁵² Furthermore, the plasma-liquid interface is the boundary region between the plasma and the liquid phase, where reactions will occur between plasma reactive species and the liquid.^{151,153} The reactions and products formed in the interface can lead to several cascading chemical reactions within the liquid phase.^{151,154} Moreover, the bulk liquid refers to the boundary region dominated by liquid-phase chemistry. The bulk liquid provides a medium for the propagation of chemical reactions initiated at the plasma-liquid interface.^{151,152}

1.3 Hydrogel synthesized by plasma polymerization

Plasma technology offers a unique and promising approach to hydrogel synthesis through the polymerization of vinyl-bearing monomers. In this sense, Table 1.4 summarizes several studies on the synthesis of hydrogels by plasma-induced FRP or plasma state polymerization. This later refers to the formation of the polymeric network structure mainly by fragmentation and polyrecombination reactions.

Table 1.4: Main plasma parameters and monomers used for the synthesis of hydrogels by plasma polymerization.

Plasma ignition	Reactor pressure	Monomer physical state	Monomer used*	Chemical cross-linker (concentration)*	Stated mechanism of polymerization	Target application	Reference
Pulsed	Low-pressure	Vapor	DMAEMA or HEMA	N.A.	FRP, plasma state polymerization	N.A.	155
			HEMA	N.A.	FRP	N.A.	41
	Atmospheric	Liquid	AAM and AAc	MBA (1 mol%)	FRP	N.A.	156
Continuous	Atmospheric	Liquid	NIPAAm	N.A.	FRP, plasma state polymerization	Stimuli-responsive	107
			NIPAAm	MBA (0.2-2 wt%)	FRP, plasma state polymerization	Stimuli-responsive	51
			HEMA and DEAEMA	N.A.	FRP	Functional and immobilization layers for biosensors	157
			HEMA and DEAEMA	N.A.	FRP	N.A.	108

			Chitosan and acrylic acid	N.A.	Plasma state polymerization for chitosan; FRP for acrylic acid	Biomedicine	158
			HEMA and DEAEMA	N.A.	FRP	Biosensors	159
			PVP	MBA (0.1-1.1 mol%)	FRP	Heavy-metal ions adsorption	109
Low-pressure	Vapor		NIPAAm	N.A.	Plasma state polymerization	N.A.	160
			NIPAAm	N.A.	Plasma state polymerization	N.A.	161

* DMAEMA: Dimethylaminoethyl methacrylate; HEMA: 2-hydroxymethyl methacrylate; AAm: acrylamide; AAc: acrylic acid; NIPAAm: N-isopropylacrylamide; DEAEMA: 2-(diethylamino)ethyl methacrylate; MBA: N,N'-Methylenebisacrylamide; PVP: Polyvinylpyrrolidone; N.A.: not applicable

As expected, the works in Table 1.4 did not rely on the use of a chemical initiator to trigger the growth of polymeric chains. Instead, the plasma-formed free radicals from water dissociation (such as OH• and H•) or monomer's bond cleavage were pointed out as species that initiate the FRP.^{51,109,156} Interestingly, Malik *et al.* compared in their work polymers formed by plasma and by conventional wet chemistry using the same apparatus (i.e., in the absence of plasma discharge).¹⁵⁶ The FTIR spectra in this work showed remarkable similarity between the samples, highlighting the potential to use plasma technology to induce free-radical polymerization.

Regarding the operational parameters, only a few studies have employed pulsed plasma ignition for hydrogel synthesis.^{41,155,156} Particularly, Veuilleit *et al.* explored the effect of variation in the duty cycle (from 2-100%) on the chemical and mechanical properties of dimethylaminoethyl methacrylate (DMAEMA) or HEMA films.¹⁵⁵ However, this study did not characterize the swelling ratio or swelling kinetics, which would have been valuable in confirming the formation of the desired polymeric network structure. Indeed, many studies did not measure hydrogel's swelling ratio or stability in liquid media. Instead, the focus is on the specific application, such as characterizing biosensing,¹⁵⁹ thermoresponsive properties,¹⁶⁰ or adsorption of heavy metal ions.¹⁰⁹ When swelling ratio measurements were conducted, the main two methods were quartz crystal microbalance^{41,161} and microbalance (gravimetric measurement).^{156,162}

In summary, while the plasma's complete mechanisms and effects on hydrogel formation remain under active investigation, numerous studies have demonstrated its effectiveness in generating initiating species or facilitating cross-linking (mainly through fragmentation/recombination reactions). Furthermore, detailed chemical and structural characterization of the polymeric network of hydrogels remains a significant challenge due to their intrinsic cross-linked nature. Consequently, studies inferring the number of cross-links and chemistry of the network structure of plasma-polymerized hydrogel films through in-depth chemical characterizations are scarce and remain relatively limited. Additionally, studies correlating the polymeric network structure with the properties of these plasma-formed hydrogels are scarce. Finally, most studies focus on biomedical applications, due to the well-established use of hydrogels in this field.

Chapter 2 : Deposition and characterization

2.1 AP-DBD set-up, electrodes and generator

All the deposition experiments described in this PhD thesis were performed in an atmospheric pressure dielectric barrier discharge (AP-DBD) setup (Figure 2.1). The AP-DBD system was purchased from Fraunhofer IST (Braunschweig, Germany). The AP-DBD setup was composed of two high-voltage electrodes (each 15 mm width and 300 mm length) covered with alumina dielectric and a stainless-steel moving table as a ground electrode. The moving table was set to move back and forth at a speed of $50 \text{ mm}\cdot\text{s}^{-1}$.

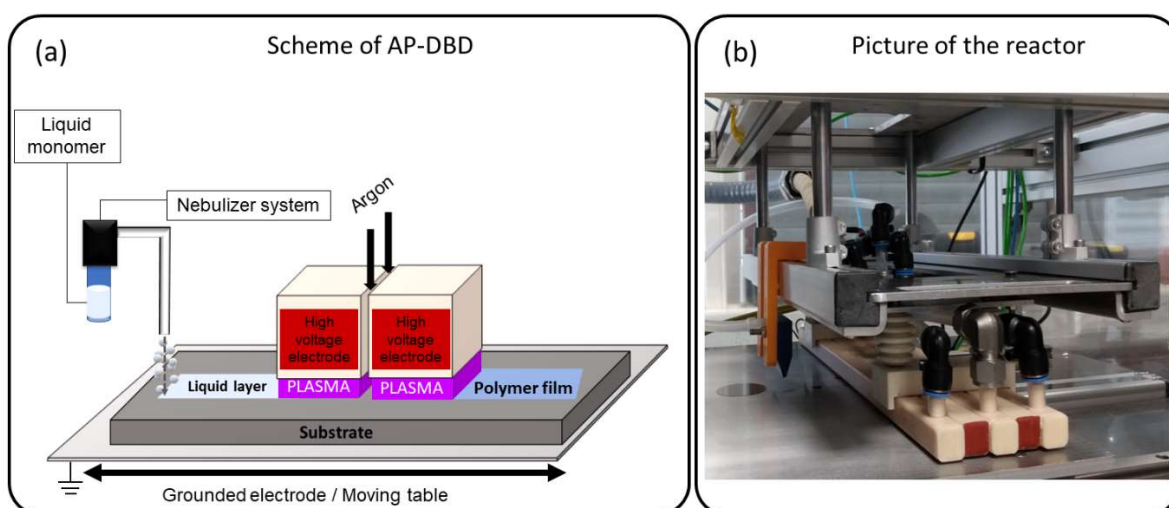


Figure 2.1: (a) Schematic representation and b) picture of the AP-DBD reactor used in this thesis.

2.2 Generator and nanopulsed-plasma electrical measurements

For every experiment, argon was used as the plasma gas at a flow of 20 slm, while maintaining a discharge gap of 1 mm. Two generators acquired from Effitech (Gif-sur-Yvette, France, www.effitech.fr), named AHTPB10F2 or AHTPB10Z were used for every experiment. Electrical measurements of the voltage pulse traces, and current discharges were investigated using a Teledyne Lecroy HDO4054A oscilloscope and a Teledyne Lecroy PPE 20 kV high-voltage probe. The plasma was ignited by $15 \mu\text{s}$ square pulses of 6.5 kV, generated by an

EFFITECH generator, resulting in the generation of two distinct discharges lasting several tens of nanoseconds ($t_{\text{on}} \approx 200$ ns), as shown in Figure 2.2a. Figure 2.2b illustrates the plasma pulse frequencies ranging from 30 Hz ($t_{\text{off}} \approx 33.33$ ms) up to 3000 Hz ($t_{\text{off}} \approx 0.33$ ms) used in the deposition of the polymeric films.

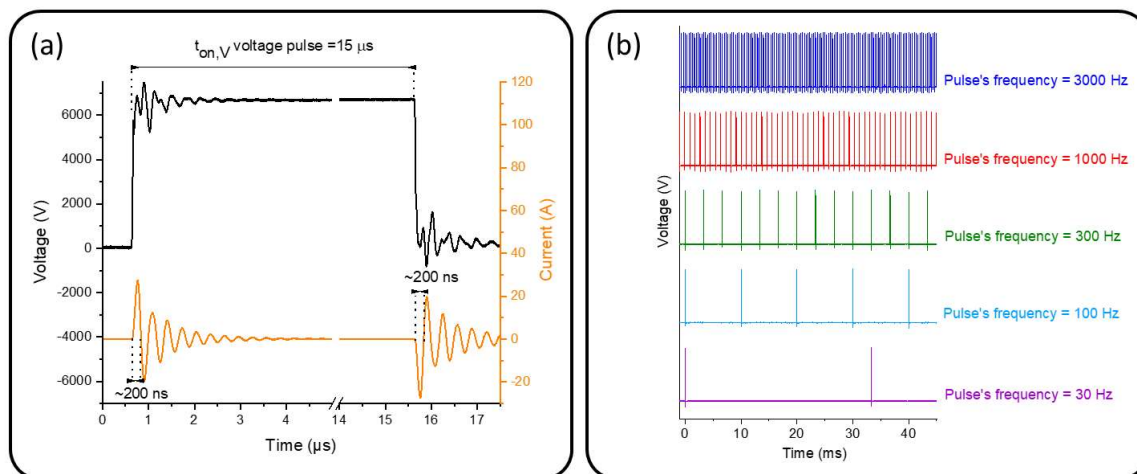
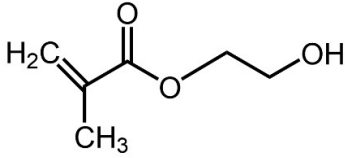
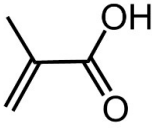
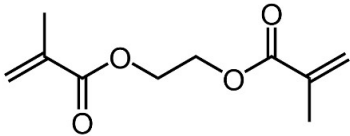
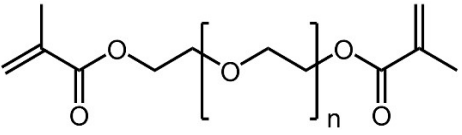


Figure 2.2: (a) Traces of voltage pulse and current discharges and (b) Voltage traces for the different plasma pulse frequencies ranging from 30-3000 Hz in this study.

2.3 Monomers

The monomers used in this thesis are summed in Table 2.1. The monomers were used as supplied for the plasma polymerization. 2-hydroxyethyl methacrylate (HEMA, 99%) was studied in Chapter 3, methacrylic acid (MAA, 99%) and ethylene glycol dimethacrylate (EGDMA, 98%) was studied in Chapter 4 and polyethylene glycol dimethacrylate (PEGDMA₄₀₀, $M_{w,PEG} = 400$ g/mol, 95-100%) was studied in Chapter 5. The conventionally polymerized reference for poly(2-hydroxyethyl methacrylate) (pHEMA) was bought from Sigma Aldrich, and poly(methacrylic acid) (pMAA) was purchased from Polysciences.

Table 2.1: Properties of the monomers used in this thesis, namely: MM is the molar weight, P_{sat} is the saturation vapor pressure, and ρ is the liquid density.

Abbreviation	Skeletal formula	MM (g.mol ⁻¹)	P _{sat} * (mmHg)	ρ* (g/mL)
HEMA		130.14	0.1	1.073
MAA		86.06	1	1.015
EGDMA		198.22	<0.1	1.051
PEGDMA ₄₀₀		554.06**	No data	1.117

* Values at room temperature. ** Molecular weight of PEG unit is approximately 400 (n≈9).

2.4 Liquid layer formation

The monomer was delivered to the surface of the substrate using a nozzle (3-D printed in our laboratory). The liquid was nebulized onto the substrate surface using a venturi-based nebulization system with Nitrogen (air liquid, 99.999%) as nebulization and carrier gas (Figure 2.3).

In the Venturi section, the gas that crosses the small orifice in the hole has a higher velocity associated to it than in the entrance (from A₁ to A₂). The resulting pressure drop draws out the liquid from the vessel through a small tube, and the interface liquid-gas in contact with the gas jet breaks the liquid into droplets. Larger droplets impact the nebulizer wall and return to the vessel. Droplets that are small enough will be carried away from the nebulizer by the gas flow and form the liquid layer. Subsequently, the entire substrate, coated with the liquid precursor layer, was introduced into the plasma discharge zone.

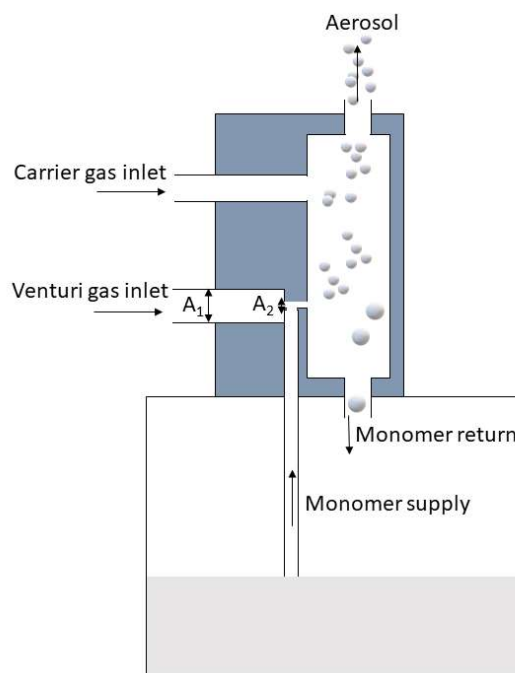


Figure 2.3: Scheme of the venturi-based atomizer used for the injection of liquid precursors.

2.5 Substrates

One-side polished doped silicon wafers (10-20 Ohm-cm, $\theta = 50.8 \pm 0.3$ mm from Siegert wafer) were used as substrates in Chapter 3, 4 and 5. In chapters 4 and 5, before each experiment, the substrates were cleaned and activated using an argon:oxygen (95%:5%) plasma (pulse frequency of 1000 Hz for 50 s).

For the study of swelling behavior and viscoelastic properties in chapters 4 and 5, the number of runs of the moving table were adjusted to ensure the deposition of a very thin film (from ~65-200), with the substrate being changed to sensors (QX-Q-sense). Before each deposition experiment, the sensors were cleaned and activated using an argon:oxygen (95%:5%) plasma (pulse frequency of 1000 Hz for 50 s).

In Chapter 5, a wide range of substrate was used to demonstrate the several field of application for the plasma polymerized hydrogel films. The chosen substrates were: polypropylene fabric (VWR®), gloves (VWR®), membrane Filter (Acrodisc®, PALL), kraft paper (260 g), polylactic acid (PLA) 3-D printed support, low density polyethylene (Goodfellow Cambridge), fabric (laboratory coat CAWE®).

2.6 Characterization

2.6.1 Profilometry

Growth rate and thickness increment per discharge were calculated by measuring the thickness of the as-deposited films using a KLA-Tencor P-17 Stylus profiler (Milpitas, CA). The growth rate in thickness was obtained from the measured thicknesses in profilometry and the time spent in the plasma zone. The growth rate was determined from the measured thicknesses of three independently grown films. The growth rate is the product of the high-voltage electrodes width (30 mm) and the number of passes of the moving table (100) and divided by the speed of the moving table ($50 \text{ mm}\cdot\text{s}^{-1}$). The thickness increment is a product of the growth rate per the period of each pulse.

2.6.2 Microbalance

The mass from three independently grown films were determined by weighing the substrate before and after exposure to plasma using a Sartorius ME36S scale (Goettingen, Germany). The mass growth rate is the product of the high-voltage electrodes width (30 mm) and the number of passes of the moving table (100) and divided by the speed of the moving table ($50 \text{ mm}\cdot\text{s}^{-1}$).

2.6.2.1 Mass stability (gravimetry)

In Chapter 4, stability in water of the films were indirectly measured by gravimetry. The detailed steps for this measurement can be seen in Figure 4.12. The mass from three independently films were determined the weights in each step.

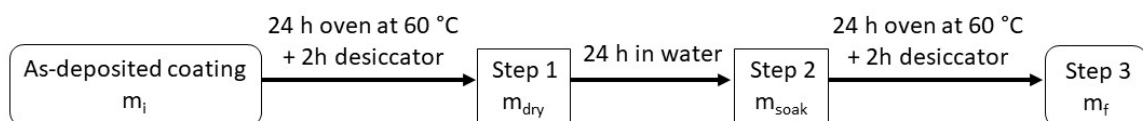


Figure 2.4: Scheme of the steps taken to measure the mass stability of the films in water.

“Step 1” is referred as a purification step implemented to minimize interference of unreacted monomers trapped within the films on the quantification of water stability results. In this step, the as-deposited films (m_i) were firstly placed in an oven at 60 °C for 24 hours and then cooled to room temperature for 2 hours inside a desiccator under vacuum (m_{dry}). The mass loss in Step 1 is determined by Equation 2.1.

$$\text{Mass loss step 1 (\%)} = \frac{m_i - m_{dry}}{m_i} \times 100 \quad (2.1)$$

After the purification step, the “Step 2” was the immersion of the films in water for 24 h (m_{soak}). “Step 3” referred to the subsequent drying of the films by placing them in an oven at 60 °C for 24 hours and then cooled to room temperature for 2 hours inside a desiccator under vacuum (m_f). The total loss of the mass from the as-deposited films (m_i) to the final mass (m_f) is given by Equation 2.2.

$$\text{Mass loss step 3 (\%)} = \frac{m_i - m_f}{m_i} \times 100 \quad (2.2)$$

The measured mass loss in water is given by Equation 2.3.

$$\text{Mass loss in water (Step 1 – Step3) (\%)} = \frac{m_{dry} - m_f}{m_{dry}} \times 100 \quad (2.3)$$

2.6.3 Fourier-transform infrared spectroscopy (FTIR)

Fourier transform infrared (FTIR) transmission measurements of the depositions on the silicon wafer were performed on a Bruker Vertex 70 spectrometer (Ettlingen, Germany). All film and layer depositions in this work were analyzed with a mercury cadmium telluride (MCT) detector. with an DTGS detector. FTIR data were all normalized according to the C=O stretching band. In chapter 3, the spectra were acquired between 4000-600 cm^{-1} with an accumulation of 256 scans and a resolution of 4 cm^{-1} . In chapter 4, the spectra were acquired between 4000-600 cm^{-1} with an accumulation of 128 scans and a resolution of 4 cm^{-1} . A 4 min nitrogen purge was performed for each measurement to diminish the contribution of carbon dioxide and moisture in the sample chamber.

Monomers and mixture of the monomers (all in liquid state) were analysed with the same FTIR spectrometer using an attenuated total reflectance (ATR) accessory with a diamond

crystal. The spectra were acquired between 4000-600 cm^{-1} with an accumulation of 50 scans and a resolution of 4 cm^{-1} .

FTIR analysis of the atmospheric-pressure plasma initiated chemical vapor deposition (AP-PiCVD) thin films, in Chapter 3, were performed in transmission mode on double polished silicon wafers. The spectra were obtained over a range of 4000-400 cm^{-1} with a resolution of 4 cm^{-1} . A 10 min nitrogen purge was performed for each measurement to diminish the contribution of carbon dioxide and moisture in the sample chamber.

In chapter 5, the spectra were acquired between 3500-600 cm^{-1} and a resolution of 4 cm^{-1} . A heated controlled stage (PMA ECO24) was used. The temperature at the surface of the stage was further calibrated using an IR thermometer (Fluke 62 Max). To do so, the coatings were prepared using 100 runs and were acquired using as a background the spectrum of the non-coated original substrate. Different mappings of up to 20 points were considered to ensure the homogeneity of the deposition.

Spectra acquisitions were processed using OPUS 7.5 software package (Bruker Corporation, Billerica, MA, USA).

2.6.4 X-ray photoelectron spectroscopy (XPS)

In chapter 3, XPS analyses (700 μm x 300 μm) were carried out with a Kratos Axis Ultra DLD with Al K_{α} source (1486.6 eV). Photoelectron emission was collected at 0° with respect to the normal surface with a survey scan pass energy of 160 eV and energy resolution of 1 eV. For the narrow scan pass energy was 20 eV and an energy resolution of 0.1 eV. In chapter 4, XPS analyses (800 μm x 400 μm) were carried out with a Thermofisher Nexsa G2 operating with Al K_{α} source (1486.6 eV). Photoelectron emission was collected at 0° with respect to the normal surface with a survey scan pass energy of 1.9 eV and energy resolution of 1 eV. For the narrow scan pass energy was 0.9 eV and an energy resolution of 0.1 eV. Both the survey spectra and high-resolution core-level spectra were recorded for carbon, nitrogen, and oxygen in three analysis points per sample. For peak analysis and bonds quantification, the Casa XPS software was used.

Chapter 4 showed a quantitative analysis of the copolymer films. To determine the MAA and EGDMA fractions in the copolymer, the C 1s core level spectra of the individual homopolymers (prepared at the same pulse frequency) were independently fitted. The resulting fitting parameters (full width at half maximum, peak position, and relative peak ratios) were

then fixed for the corresponding homopolymer in the copolymer spectra. The copolymer spectra were subsequently fitted, allowing only the C-CH peak area for each homopolymer to vary, thus quantifying its composition.

2.6.5 Gel permeation chromatography coupled with high-resolution mass spectrometry (GPC-MS)

Gel permeation chromatography coupled with high-resolution mass spectrometry (GPC-HRMS) analysis was performed using Thermo Scientific (Sunnyvale, CA, USA) Dionex UltiMate 3000 LC system coupled online to an LTQ/Orbitrap Elite mass spectrometer (Thermo Fisher Scientific, San Jose, CA, USA) with an Ion Max source, equipped with a heated electrospray probe (Thermo Scientific). The column (Mesopore and Oligopore column) had the exclusion limit of $25 \text{ kg}\cdot\text{mol}^{-1}$. Calibration curves were obtained with polystyrene narrow molecular weights standards. Analysis was held in the soluble part of the samples in THF and the elution time. Electro-Spray Ionization (ESI) is aided by post-column addition of cationization agents (Ammonium acetate).

2.6.6 Matrix-assisted laser desorption/ionization high-resolution mass spectrometry (MALDI-HRMS)

MALDI-HRMS measurements were performed on an AP MALDI PDF+ ion source from MassTech Inc. coupled to an LTQ/Orbitrap Elite from Thermo Scientific. Atmospheric Pressure Laser Desorption/Ionization is based on a Nd:YAG laser ($\lambda = 355\text{nm}$) operated at 5 kHz, Laser Attenuator setting = 2.0%. Orbitrap Exploris was tuned at 240k mass resolution at m/z 200 for positive ions, target HV was 3 kV, IT 350 ms. A matrix solution of DHB $10 \text{ mg}\cdot\text{mL}^{-1}$ in $\text{H}_2\text{O}/\text{ACN}$ was prepared. A $1 \mu\text{L}$ of this solution was spotted directly on the silicon wafer then irradiated. Mass assignments were carried out using PolyCalc web-based assignment tool.

2.6.7 Water contact angle (WCA)

WCA measurements were performed using a DSA100 Drop Shape Analyzer (Krüss, Hamburg, Germany). Each measurement is the average of five independent water droplets ($2 \mu\text{L}$) throughout the surface area of three different samples. The angle between the surface and

the droplet was quickly calculated just after droplet deposition based on the contour and baseline determined automatically by the software.

2.6.8 Coupled quartz crystal micro balance with dissipation (QCM-D) and spectroscopic ellipsometry (SE) measurements

Determination of the mass of the hydrogel ultra-thin films was determined comparing the frequencies of the naked and coated sensors (in the dry state) using the Sauerbrey as shown in Equation 2.4.

$$\Delta f = -\frac{2f_0^2}{A\sqrt{\rho_q\mu_q}}\Delta m = \delta\Delta m \quad (2.4)$$

where Δf is the normalized frequency (depending on the harmonic), Δm is the mass variation and δ is an experimental parameter obtained from the manufacturer specifications. A frequency-dependent Voigt model was assumed for the sample during wet and dynamic experiments. Thus, water viscosity and density were fixed at 10^{-3} Pa·s and $1 \text{ g}\cdot\text{cm}^{-3}$, respectively. The corresponding film thickness (d) and the shear modulus μ were directly obtained from the model used.

While conventional SE measurements were collected at three different angles (65° , 70° and 75°), the QCM-D/SE cell only allows measurements at 65° . Before collecting data, naked sensors were analyzed and fitted using the specifications provided by the manufacturer. The naked sensor consists in a three-layered system corresponding to: 1) Quartz Substrate, 2) Ti sublayer (KK B-Spline model) and 3) SiO_2 coating (Cauchy model). In order to achieve more accurate results, small range fittings of the thickness of each layer were initially considered. Moreover, analyses in the wet state were also tested for naked sensors to study the proper mathematical modeling (including water instead of air as the analysis media). Finally, the parameters of the 1st-3rd layers were fixed and the 4th layer was included in the mathematical fitting (Cauchy model), corresponding to the deposited ultra-thin film hydrogel.

Taking advantage of the data collected by both QCM-D and SE measurements, the swelling ratio was determined using the Equation 2.5.

$$S (\%) = \frac{w_{\text{wet}} - w_{\text{dry}}}{w_{\text{dry}}} \cdot 100 \quad 2.5$$

where w_{dry} and w_{wet} accounts for the weight of the hydrogels at the dry and wet states, correspondingly.

2.6.9 Confocal Microscopy

Images were carried by Confocal laser microscope (3D Laser Scanning Confocal Microscope Keyence VK-X Series). Each image was collected with a magnification of 50X that covered an area of $212.5 \times 283.427 \mu\text{m}$.

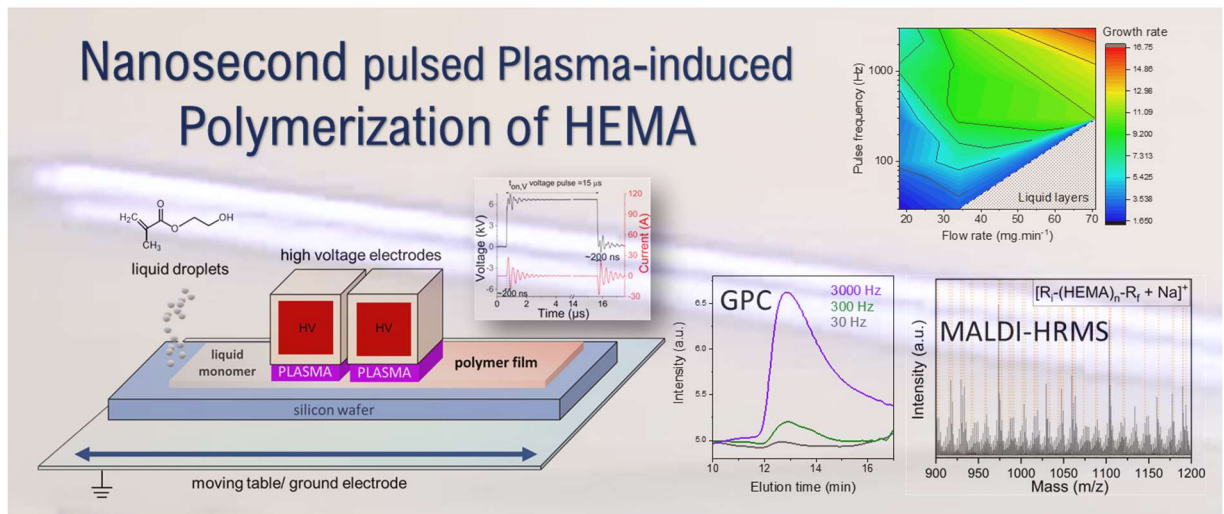
2.6.10 Atomic force microscopy (AFM)

Atomic Force Microscopy (AFM) was used to capture topography images in air using AC mode at 2 Hz scan rates and a resolution of 512×512 pixels². MFP3D INFINITY microscope (Oxford Instrument, UK) was the utilized equipment. The AFM tips employed were semi-contact silicon AC160TS from Olympus, Japan, with a cantilever spring constant of $26 \text{ N}\cdot\text{m}^{-1}$. The surface topography of the deposit was observed while maintaining a constant cantilever first resonance amplitude through the feedback loop of the AFM controlling the piezo Z direction. The root mean square roughness (Sq) was determined using the statistical application of the software provided by the manufacturer.

2.6.11 Nano-pulsed plasma characterization

Electrical measurements for the traces of the voltage pulse and current discharges from Effitech's generator were investigated using a Teledyne Lecroy HDO4054A oscilloscope, Teledyne Lecroy PPE 20 kV high voltage probe and Teledyne Lecroy CP030 current probe.

Chapter 3 : Free-radical polymerization of 2-(hydroxyethyl) methacrylate from liquid assisted thin film deposition using nanosecond pulsed atmospheric plasma



3.1 Introduction

Liquid-assisted plasma enhanced chemical vapor deposition (LA-PECVD),^{163–165} also called rapid spray plasma processing (RSPP),^{166–168} is a convenient method for the fast open-air deposition of functional thin films. LA-PECVD and RSPP have notably been applied for the preparation of photoactive metal halide perovskite thin films for solar cell applications^{166–168} and organosilicon-based coatings embedding molecules with sensing properties^{165,169,170} or fillers with optical^{171,172} or electrical properties.¹⁷³ In LA-PECVD and RSPP, a liquid layer is first deposited onto a substrate, mainly by spray deposition,^{166,169} followed by atmospheric plasma treatment that readily enable the conversion^{166–168,174,175} or polymerization^{163,173,176} of precursors without the need of additional annealing or curing processing. Both direct (e.g. dielectric barrier discharge)^{163,173,174,176} and remote (e.g. blown arc discharge)^{166–168,175} plasma configurations have been successfully used for the LA-PECVD or RSPP of functional thin films, making the approach suitable for up-scaling and in-line processing.¹⁷⁷

Taking advantage of the capability of atmospheric plasmas to cure or polymerize low-vapor pressure monomers, several works have also investigated the LA-PECVD approach for the polymerization of non-volatile vinylic compounds, i.e. allyl ether-substituted six-membered cyclic carbonate¹⁷⁸ and dopamine acrylamide^{163,176}. In this context, the quantity of liquid monomer deposited at the surface (in relation to the delivery rate) and the plasma exposure or curing time were highlighted as key parameters for the conversion of the liquid monomers into thin solid films.^{163,178} However, in contrast to the PECVD of monomers delivered from the vapor phase,^{33,36,139,179–181} only a scarce number of studies have focused on controlling the chemistry of organic thin films prepared from the plasma curing of liquid layers.^{182–184} In plasma polymerization from the vapor phase, the Yasuda parameter (W/FM), where W is the power of the discharge, and F and M are the flow rate and the molecular weight of the precursor, respectively, is often used to explain the properties of the resulting thin films and classify the process conditions into distinct deposition regimes, i.e. monomer-deficient, competition, and energy-deficient regimes.^{113,133,135} Yet, the applicability of such a classification to plasma-induced polymerization of liquid monomer layers requires further investigation.

LA-PECVD involves mechanisms occurring both in the gas phase, particularly for highly volatile precursors, at the liquid-plasma interface and in the bulk of the liquid layer.¹⁶³ In the polymerization of vinylic monomers, plasma-generated energetic species are the responsible of forming radical species at the liquid-plasma interface, mainly through monomer fragmentation

reactions.¹⁷⁸ These radicals diffuse into the liquid phase where they initiate the free-radical polymerization of the vinylic monomer. Therefore, to promote polymerization while preserving the chemical structure of most of the monomer units contained in the liquid layer, it is crucial to optimize the plasma energy inputs. A well-known and common strategy to initiate and sustain the free-radical polymerization reaction when operating from the vapor phase in PECVD is the use of pulsed plasmas. Several works have recently investigated the impact of pulse frequency on the free-radical polymerization of alkyl acrylates and the resulting chemical properties of the polymeric thin films.^{43,176,179,185} By precisely controlling the time between pulses (t_{off}), selected in accordance to the lifetime of free-radical propagation under these conditions (milliseconds) and employing extremely short pulse durations (t_{ON}) of 100 ns, high molecular weight polymers ($94,000 \text{ g}\cdot\text{mol}^{-1}$) were achieved.⁴³ The preservation of the monomer chemical properties is attributed to the ultrashort square pulse plasma, which allows to minimize plasma-state polymerization (involving fragmentation and recombination of monomer fragments) and promote a conventional free-radical polymerization pathway.

In this chapter, nanosecond plasma pulses in a dielectric barrier discharge (DBD) configuration are studied to ensure the plasma-induced polymerization of 2-hydroxyethyl methacrylate (HEMA), chosen as a model vinylic monomer. Different quantity of liquid HEMA monomer (controlled from the spray rates) and different nanosecond plasma pulses frequencies are investigated and their influence on deposition rates as well as on the chemical and polymeric structure (growth mechanisms, molecular weights) of the resulting thin films are elucidated using Fourier transform infrared spectroscopy, gel permeation chromatography and matrix-assisted laser desorption/ionization high resolution mass spectrometry. Comparative atmospheric-pressure plasma-enhanced chemical vapor deposition (AP-PECVD) experiments from the vapor phase emphasized the advantages of the plasma-induced polymerization of liquid monomer layers in terms of faster deposition rates and enhanced preservation of HEMA chemistry.

3.2 Results and discussion

3.2.1 Nanosecond pulsed plasma curing of liquid HEMA layers

As shown in Figure 2.1a, the atmospheric-pressure plasma-induced free-radical polymerization of 2-hydroxyethyl methacrylate (HEMA) was carried out by repeating several

times the steps of spraying the monomer over the silicon substrate surface followed by the exposition of the formed liquid layer to the nanosecond pulsed plasma discharge. Table 3.1 summarizes the 3 samples series studied in this chapter, characterized by the spray rate used: low (series A), medium (series B) or high (series C), and prepared with plasma pulses frequencies ranging from 30 to 3000 Hz. The different monomer spray rates were produced by varying the nebulizer inlet gas flow rate (see further details in the Annex A, Table A1). Increasing the spray rate led to both a thicker liquid layer and a larger sprayed surface (Figure A 1). Therefore, a proportional correlation between the spray rate and the thickness of the liquid layer formed over the substrate surface could not be accurately quantified. Otherwise, despite the moderate low vapor pressure of HEMA (0.08 mbar at 25 °C), the open configuration of the reactor will not prevent some monomer loss through evaporation during the deposition process. Upon exposure to the nanosecond pulsed plasma discharge, the liquid HEMA layers convert into solid thin films, except in two cases corresponding to the series C (high monomer spray rate). Within this series, the two lowest plasma pulses frequencies (30 to 100 Hz) yield liquid layers of viscous appearance. In comparison to these partially liquid samples, the formation of thin solid films could be attributed to a higher degree of polymerization of the monomer, and/or higher monomer conversion, and/or the occurrence of cross-link reactions (plasma-state polymerization) induced by the plasma exposure. All these factors will be further discussed on the following sections. The thin solid films exhibited a characteristic surface pattern ascribed to the droplets from the spray. As shown in Figure 3.1 the lobular shape of the pattern features, their sizes and surface clustering are affected both by the monomer spray rate and the plasma pulses frequency. No discontinuities or pinholes were observed on the thin films that cover the surface of the substrates.

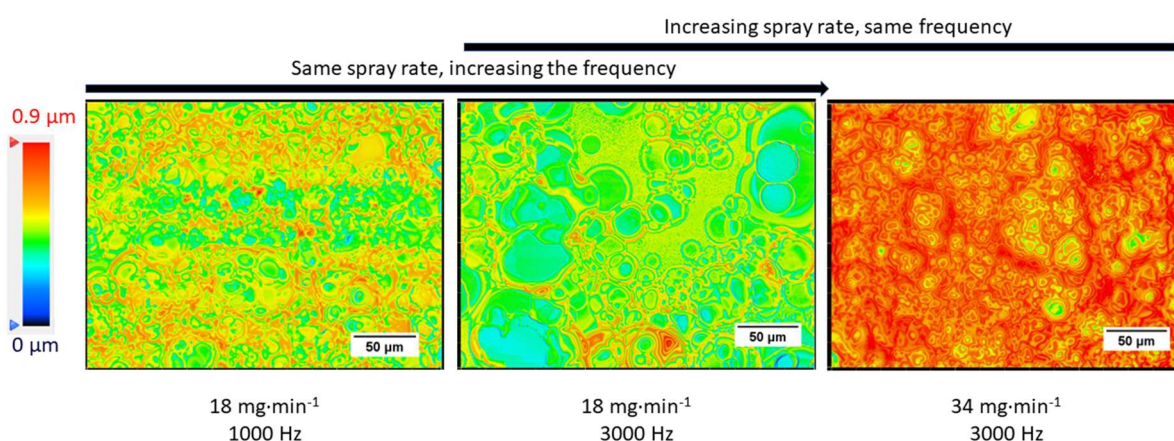


Figure 3.1: Confocal microscopy images of the thin films showing the effect on the surface topography of variations of spray rate and plasma pulses frequency.

Table 3.1: Summary table of the sample series deposited by LA-PECVD, their deposition conditions, thin film thickness, and polymer molecular weight.

Series	Flow rate ^b (mg·min ⁻¹)	Plasma pulses Frequency [t _{off}] ^a									
		30 Hz (33.3 ms)		100 Hz (10 ms)		300 Hz (3.3 ms)		1000 Hz (1 ms)		3000 Hz (0.3 ms)	
		Thickness ^c (nm)	Mp ^d (g/mol)	Thickness (nm)	Mp (g/mol)	Thickness (nm)	Mp (g/mol)	Thickness (nm)	Mp (g/mol)	Thickness (nm)	Mp (g/mol)
A	18	100 ± 27	7100	241 ± 85	6400	214 ± 45	5300	450 ± 148	4200	346 ± 52	3800
B	34	179 ± 51	6100	379 ± 102	4800	578 ± 131	6200	570 ± 46	5300	656 ± 146	4000
C	71	– ^e	NA	– ^e	6400	667 ± 131	5300	754 ± 76	5000	1003 ± 88	5500

^a Plasma pulses frequency and t_{off} between two current discharges of approx. 200 ns.

^b HEMA flow rare at nebulizer outlet.

^c Thin film thickness determined by profilometry.

^d Peak molecular weight determined from GPC curves using polystyrene as calibration standard.

^e Liquid layer.

Thin films with thicknesses ranging from approximately 100 to 1000 nm (Table 3.1) were deposited by varying spray rate and plasma pulses frequency, while maintaining a constant deposition time. The dependence of the thin film growth rate on the plasma pulses frequency is depicted in Figure 3.2a. For each spray rate, a logarithmic increase of the growth rate is observed with increasing plasma pulses frequency, indicating a self-limiting growth process.⁴⁷ Notably, increasing the plasma pulses frequency by two orders of magnitude (for the lowest spray rates) led to a ca. 3 to 4 increase of the thin film growth rate.

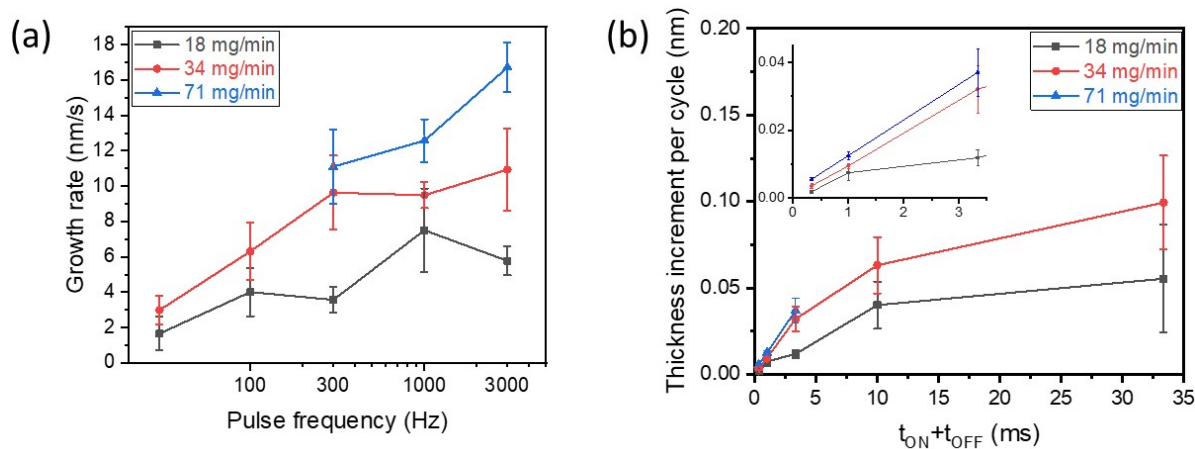


Figure 3.2: Thin film growth properties: (a) Growth rate vs. plasma pulses frequency, (b) thickness increment per cycle vs. cycle time ($t_{ON} + t_{OFF}$) for the different HEMA spray rates.

The correlation between increasing thin film growth rate and the number of plasma pulses suggests a faster polymerization rate upon increase of the plasma pulses frequency, which is consistent with the well-known effect of increasing initiator concentration in bulk free-radical polymerizations (FRP). In the studied system, the radical initiator species are generated by the nanosecond pulsed plasma discharges through fragmentation of the molecules of the reaction media (liquid layer). Figure 3.2b shows the apparent thickness increment per discharge cycle with the nanosecond pulse plasma frequency, expressed as cycle time ($t_{ON} + t_{OFF}$). As the duration of the discharge (t_{ON}) was kept constant, an increase on the pulse frequency reduces the t_{OFF} . For each spray rate, increasing the duration between two nanosecond pulsed plasma discharges (t_{OFF}) led to an increase on thickness increment per cycle. This indicates the occurrence of reactions contributing to the thin film growth during t_{OFF} . Yet, from a process point of view, it is interesting to note that while increasing t_{OFF} appears more efficient as more monomer is converted into thin film, increasing the plasma pulses frequency is more desirable

for thickness build up. Otherwise, while increasing spray rate led to higher thickness increment, the system reaches a limit where the formation of the solid film could not be obtained (series C).

3.2.2 Plasma-induced free-radical polymerization of liquid HEMA layers

FTIR analyses were carried out to assess the effect of plasma pulses frequency on the monomer structure. Figure 3.3a notably presents the FTIR spectra of samples prepared from the highest spray rate (series C), including spectra from samples from the conditions that failed to form thin solid films. In comparison with the HEMA monomer spectrum, it is possible to notice that the bands associated with the vinyl group (817 , 1324 , 1637 , and 3107 cm^{-1})¹⁸⁶ exhibited remarkably lower intensity as the plasma pulses frequency is increased. On the other hand, the FTIR spectra of the samples deposited at 30 and 100 Hz pulse frequencies have more prominent peaks at 1637 cm^{-1} indicating the presence of vinyl groups attributed to unreacted monomer. Such observation is consistent with viscous liquid appearance of these samples and confirms the incomplete conversion of HEMA monomer under these conditions. Additionally, the conversion of HEMA monomer into polymer can be assessed by the shift toward higher wavenumbers of the $\text{C}=\text{O}$ peak (from 1718 cm^{-1} to 1729 cm^{-1}). The shift can be associated to the loss of conjugation of the carbonyl group in the methacrylate group already observed for the plasma polymerization of HEMA.^{47,187–189} Moreover, it can be perceived a rise in the band related to $-\text{CH}_2-$ vibration at 1485 cm^{-1} becomes even more prominent at higher frequencies, coupled with a decrease of the CH_2 vibration band at 2931 cm^{-1} .^{43,186} Notably, these changes in the FTIR spectra are consistent with the free-radical polymerization of HEMA as supported by the strong resemblance to the spectrum acquired from a commercial poly(HEMA) produced by conventional wet chemistry (Sigma–Aldrich, M_v 20,000). This indicates a high degree of preservation of the characteristic HEMA functional groups, carbonyl and hydroxyl, in all the samples under the investigated conditions. This finding was supported by XPS analyses carried out on the thin film samples as well as on the commercial poly(HEMA). Both the atomic composition (Table A2) and the high-resolution $\text{C } 1s$ spectra (Figure A3) revealed no significant differences compared to the commercial product.

From the FTIR spectra, the effect of plasma pulses frequency on the apparent monomer conversion for each spray rate was determined as the peak intensity ratio of the vinyl (1637 cm^{-1}) band in the sample relative to the initial monomer, normalized to the carbonyl band. As

shown in Figure 3.3b, conversions over 90% were obtained for all the samples except for the two samples prepared from the highest spray rate and the lowest nanosecond pulsed plasma frequencies. In particular, the monomer conversion for the highest spray rate shows an evident logarithmic-like increase with increasing the plasma pulses frequency. On the other hand, a similar trend of the monomer conversion rate is observed for the samples prepared from the lowest spray rates, although the difference in conversion rate between plasma pulses frequencies is significantly smaller.

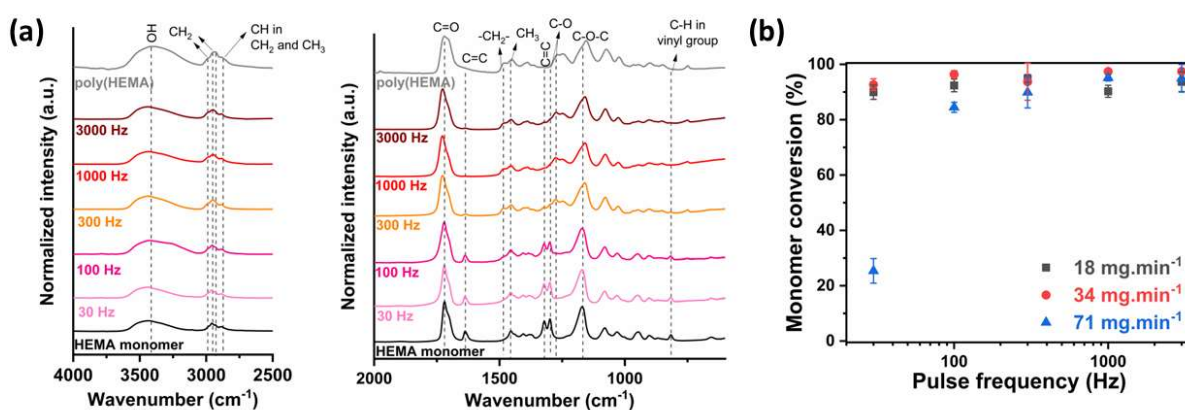


Figure 3.3: (a) FTIR spectra of the series C samples (highest spray rate) and a commercial poly(HEMA) produced by conventional wet chemistry and (b) apparent monomer conversion vs. plasma pulses frequency for all samples reported in this chapter (A, B, and C).

This behavior can be discussed based on the assumption that radical species formation due to plasma exposure occurs at the plasma-liquid interface and only extends up to a few nanometres of liquid phase.^{45,151,183,190} This implies for thicker liquid layers, a greater number of monomer molecules are not exposed to the plasma.^{182,183} From another perspective, the concentration of the formed initiator species decreases when the monomer spray rate increases. Hence, the presence of higher number of unreacted monomers in the samples prepared from the highest spray rate can be correlated with the conditions where the lowest initiator concentrations are expected from all the series, i.e., higher monomer flow rate and low pulse frequencies. These unfavourable conditions for converting monomer into polymer appear to be overcome by increasing the plasma pulses frequency at 1000 Hz (Figure 3.3b), obtaining apparent monomer conversions similar to the ones calculated in the two other series.

To correlate monomer conversion with polymer chain growth, GPC analyses were carried out for all the sample series (Figure 3.4). The presence of small insoluble fractions was observed in all thin films, which was attributed at the generation of cross-linked polymers. In Table 1.1 are summarized the peak molecular weight (M_p). The shape of the molecular weight distribution curves, asymmetrical with a large tail towards low molecular weights, is characteristic plasma-induced polymerized thin films,⁴³ indicating a large polydispersity. Therefore, M_p values are considered more appropriate for the discussion as they are independent of the molecular weight distribution.

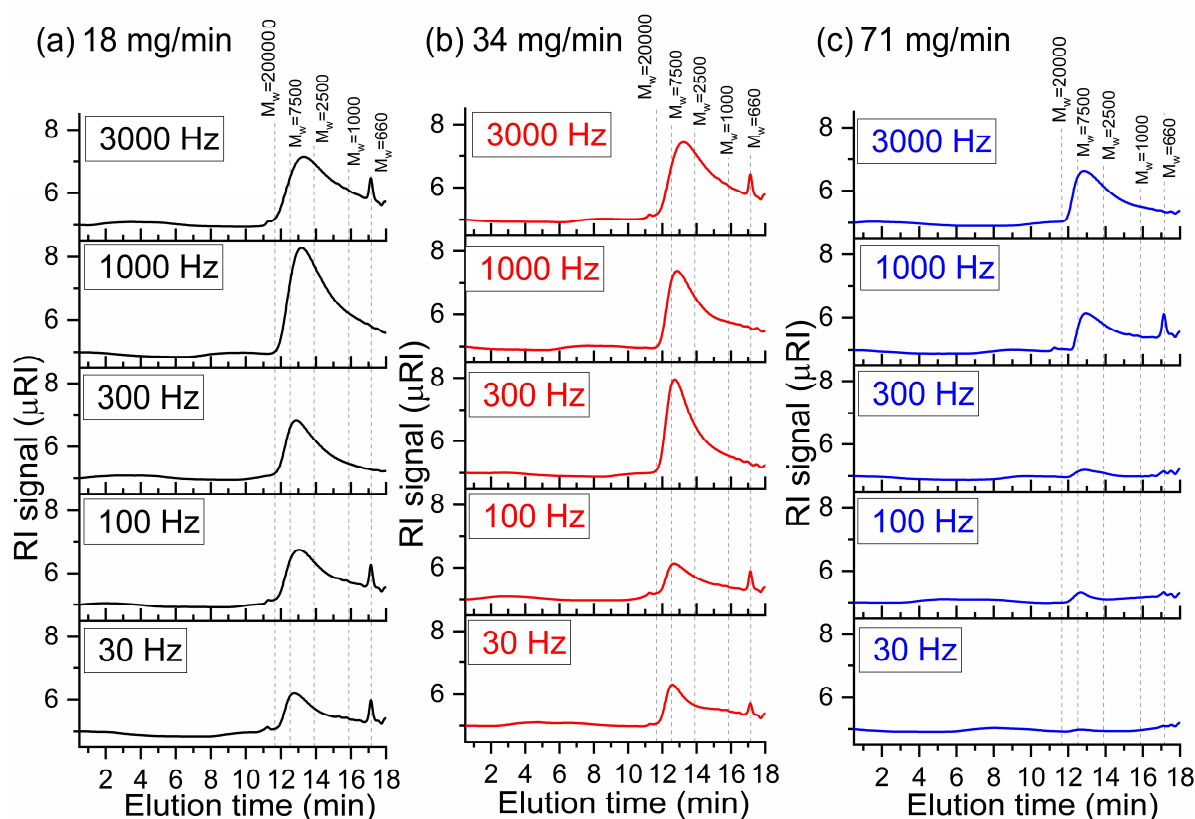


Figure 3.4: GPC chromatograms for the poly(HEMA) films at delivery rate of (a) 18 mg·min⁻¹, (b) 34 mg·min⁻¹ and (c) 71 mg·min⁻¹ for plasma pulses frequencies ranging from 30-3000 Hz.

For each series, the highest value was achieved for the lowest plasma pulses frequency (series B value was very close to the series maximum). Interestingly, the overall highest M_p (7100 g·mol⁻¹) was obtained using the lowest monomer spray rate combined to the lowest plasma pulses frequency. The effect of increasing the plasma pulses frequency on the molecular weight is different for each series. For the samples prepared from the lowest spray rate, the M_p shows a decreasing trend resulting in a molecular weight that was roughly halved. For the

samples prepared from the highest spray rates, while not clear trends are evident, the difference between the maximum and minimum M_p values is less significant with ratios of 1.6 and 1.3 for series B and C, respectively. Considering the chromatograms, the curves of series C clearly show an increase in the concentration of polymeric chains with increasing plasma pulses frequency, in accordance with the findings from the FTIR analysis. In each series is observed the presence of an additional peak at $M_w = 660$ (polystyrene standard), corresponding to oligomers up to 4 units.

From the results described above, it is still unclear if one should combine low spray rates with low pulse frequencies or high spray rates with high pulse frequencies to promote plasma-induced free-radical polymerization over plasma-state polymerization, responsible for the formation of highly branched and randomly terminated polymer chains with a high degree of cross-linking. Therefore, to gain further insight into the polymerization of liquid vinylic monomer layers using atmospheric plasma, matrix assisted laser desorption/ionization high resolution mass spectrometry (MALDI-HRMS) was performed directly on the as-deposited thin films (Figure 3.5). Indeed, GPC-MS, which was also carried out in this work (Figure A 4 and Figure A5), only provides information about the soluble part of the thin films. On the other hand, MALDI-HRMS uses a laser energy absorbing matrix (2,5-dihydroxybenzoic acid in the present work) to desorb and ionize large molecules with minimal fragmentation.¹⁹¹ Although the technique does not provide an exhaustive view into the mass distribution of polymers, it enables an accurate structural identification of the chain end-groups, providing essential information about the polymerization mechanism of polymers synthesised from conventional solution-based approaches¹⁹¹ and plasma-based processes.¹⁷⁹ Importantly, MALDI-HRMS can be used to elucidate the structure of non-soluble or partly soluble polymers.¹⁹²

The MALDI-HRMS spectra ($m/z = 300-2000$) of the solid thin films obtained from the highest spray rates (series B and C) are dominated by peaks related to sodium adducts of formula $[C_3H_5-(HEMA)_n-C_6H_9O_3 + Na]^+$ with n up to 13 (Figure 3.5). The proposed end groups (C_3H_5 and $C_6H_9O_3$) are both radicals that can originate from the plasma-induced breakdown of a single σ -bond in HEMA (Table A3). Irrespective of the selected spray rate and plasma pulses frequency, a non-negligible number of side-species is observed between two successive $[C_3H_5-(HEMA)_n-C_6H_9O_3 + Na]^+$ peaks (Figure 3.5b). Such mass distributions were previously shown not related to the polymer fragmentation during the ionization of the molecules under the laser radiation, but to the end-groups originating from the initiator.¹⁷⁹ Noteworthy, the peaks are arranged in 9 distinct sets of distributions from $[C_3H_5-(HEMA)_n-C_6H_9O_3 + Na]^+$ to their

successive $[\text{C}_3\text{H}_5(\text{HEMA})_{n+1}\text{-C}_6\text{H}_9\text{O}_3 + \text{Na}]^+$ oligomer units (Figure 3.5b). These different sets of distributions are shifted by roughly 14 m/z, which was previously ascribed to the single plasma-induced fragmentation of monomers composed of carbon and oxygen atoms, which possess close atomic masses (low atomic weight hydrogen atoms being excluded).¹⁷⁹ Particularly, the number of sets of distributions observed between two successive oligomer units was shown directly related to the summed number of carbon and oxygen atoms composing these monomers (7 for MMA ($\text{C}_5\text{H}_8\text{O}_2$) and 10 for GMA ($\text{C}_7\text{H}_{10}\text{O}_3$)).¹⁷⁹ Accordingly, in the case of HEMA ($\text{C}_6\text{H}_{10}\text{O}_3$), 9 sets of distributions are observed (Figure 3.5b).

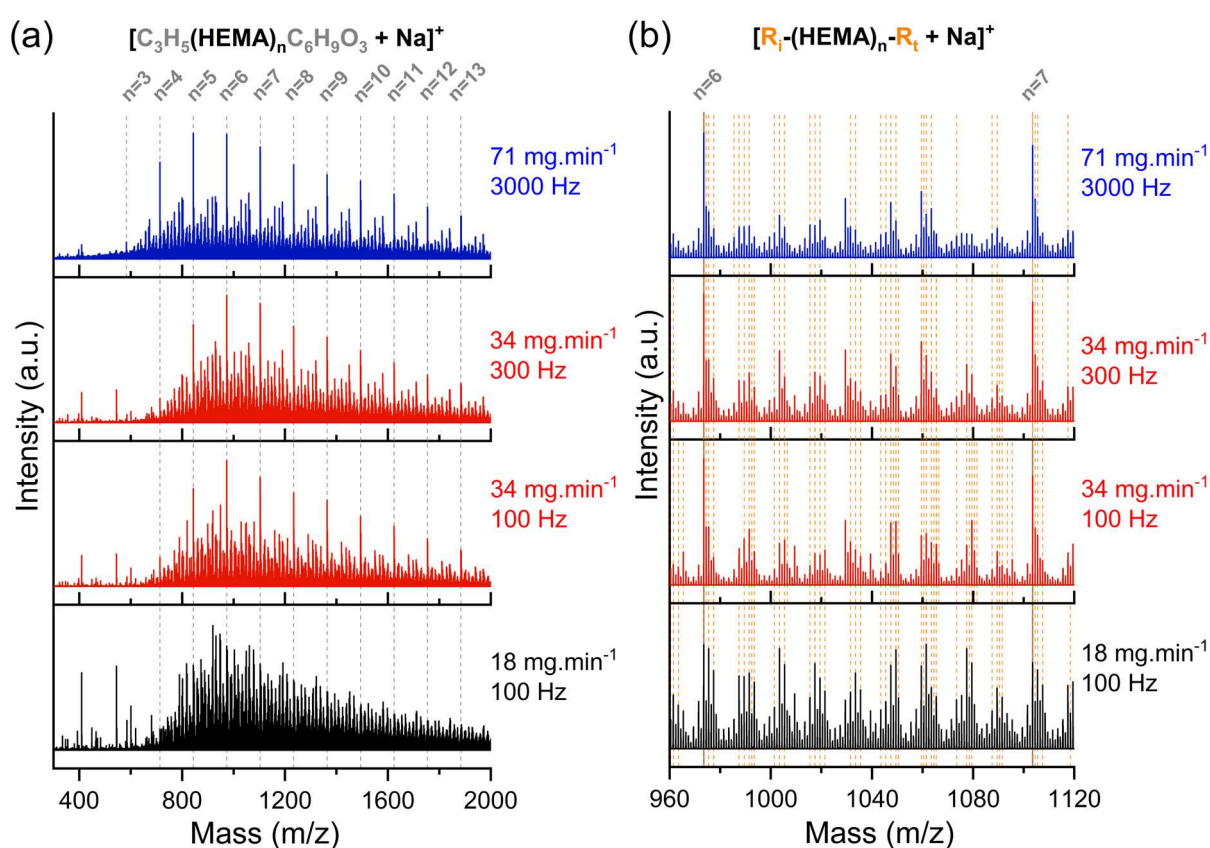


Figure 3.5: MALDI-HRMS spectra in the mass ranges (a) $m/z = 300\text{-}2000$ and (b) $m/z = 960\text{-}1120$ of the HEMA-based thin films prepared from various delivery rates and plasma pulses frequencies. The HRMS peaks related to ionized adducts of $[\text{C}_3\text{H}_5(\text{HEMA})_n\text{-C}_6\text{H}_9\text{O}_3 + \text{Na}]^+$ are indicated by grey dashed lines on (a). The HRMS peaks related to ionized adducts of $[\text{R}_i\text{-(HEMA)}_n\text{-R}_t + \text{Na}]^+$ are indicated by orange dashed lines on (b). The potential R_i and R_t end-groups are listed in Table A3 and the exact m/z values of the resulting of $[\text{R}_i\text{-(HEMA)}_n\text{-R}_t + \text{Na}]^+$ combinations are provided in Table A4.

Interestingly, for the thin film prepared from the highest spray rate (series C) and at 3000 Hz (Figure 3.5b), assigning as R_i and R_t end-groups the fragments originating from a single σ -

bond breakdown of the HEMA molecule (Table A3) allows to match all the main HRMS peaks with the formula $[R_i-(\text{HEMA})_n-R_t + \text{Na}]^+$. Under these conditions, exposure of the liquid HEMA layer to ultra-short plasma pulses produces a defined number of radical fragments, which play both the roles of polymerization initiation and termination groups. Therefore, plasma-induced free-radical polymerization is preponderant under these conditions and it can be assumed that the chemical structure of the poly(HEMA) thin film synthesized using the highest spray rate and at 3000 Hz mainly differ from its counterparts synthesized via conventional methods by the variety of its end-groups. The decrease of the spray rate (series B), coupled to a decrease of the plasma pulses frequency (100 Hz) is yielding a similar chemistry (Figure 3.5), although at a significantly lower growth rates, *i.e.* $6 \text{ nm}\cdot\text{s}^{-1}$ vs. $17 \text{ nm}\cdot\text{s}^{-1}$ for the highest spray rate and at 3000 Hz (Figure 3.2). Further decrease of the spray rate (series A) even coupled to plasma pulses frequencies as low as 100 Hz or 30 Hz, is responsible for a non-negligible range dissociation and recombination reactions that yield to additional peaks that cannot be addressed by the formula $[R_i-(\text{HEMA})_n-R_t + \text{Na}]^+$ using the fragments originating from a single σ -bond breakdown of the HEMA molecule as end-groups (Table A3). According to the thickness increment per discharge cycle curves (Figure 3.2), the growth of the thin films elaborated from the lowest spray rate is already significantly slowed down 1 ms after the ultrashort plasma pulse by comparison to the one of the thin films prepared from higher spray rates. Under these conditions (series A), the early termination of the free-radical polymerization is not related to a lack of initiation (change of thickness increment slope at 1000 Hz) but to termination reactions due to high concentration of growing radical species in comparison with unreacted monomer. As such, the monomer-deficient regime is observed for spray rates below $18 \text{ mg}\cdot\text{min}^{-1}$ where the high probability of interaction between the monomer and the reactive plasma species is responsible of a significant monomer dissociation that even a decrease of the plasma pulses frequency cannot attenuate.

Among the monomer alterations, the integration and some subtraction of oxygen, yielding structures with formula $[R_i-(\text{HEMA})_n-(\text{HEMA})_m^{\pm\text{O}\pm\text{CH}_4}-R_t + \text{Na}]^+$ evidenced by green dashed lines on Figure 3.6a, were detected by MALDI-HRMS. Integration and subtraction of oxygen was previously observed from the plasma-enhanced chemical vapor deposition of methacrylate monomers and ascribed to the oxygen radicals created from the ionization of the O_2 and H_2O from the surrounding atmosphere.¹⁷⁹ These radicals may react and integrate in the polymer chains, as well as terminate the free-radical polymerization reaction. Oxygen integration and subtraction are more prominent for the thin films synthesized from low spray rates and low

plasma pulses frequencies (e.g. series A, 100 Hz on Figure 3.6b) compared to the ones synthesised at high spray rates and high plasma pulse frequencies (e.g. series C, 3000 Hz on Figure 3.6b). Considering that the free-radical polymerization reaction is mainly initiated at the plasma-liquid interface, only monomer molecules in the vicinity of the surface of the liquid layer are exposed to the plasma reactive species and the monomer molecules located in the bulk of the liquid layer solely meet well defined radicals to undergo a conventional free-radical propagation reaction. Therefore, higher spray rates (series B and C) form thicker liquid layers that have a shielding effect on the monomer molecules located in the bulk of the liquid layer, even when using high pulse frequency (3000 Hz for series C).

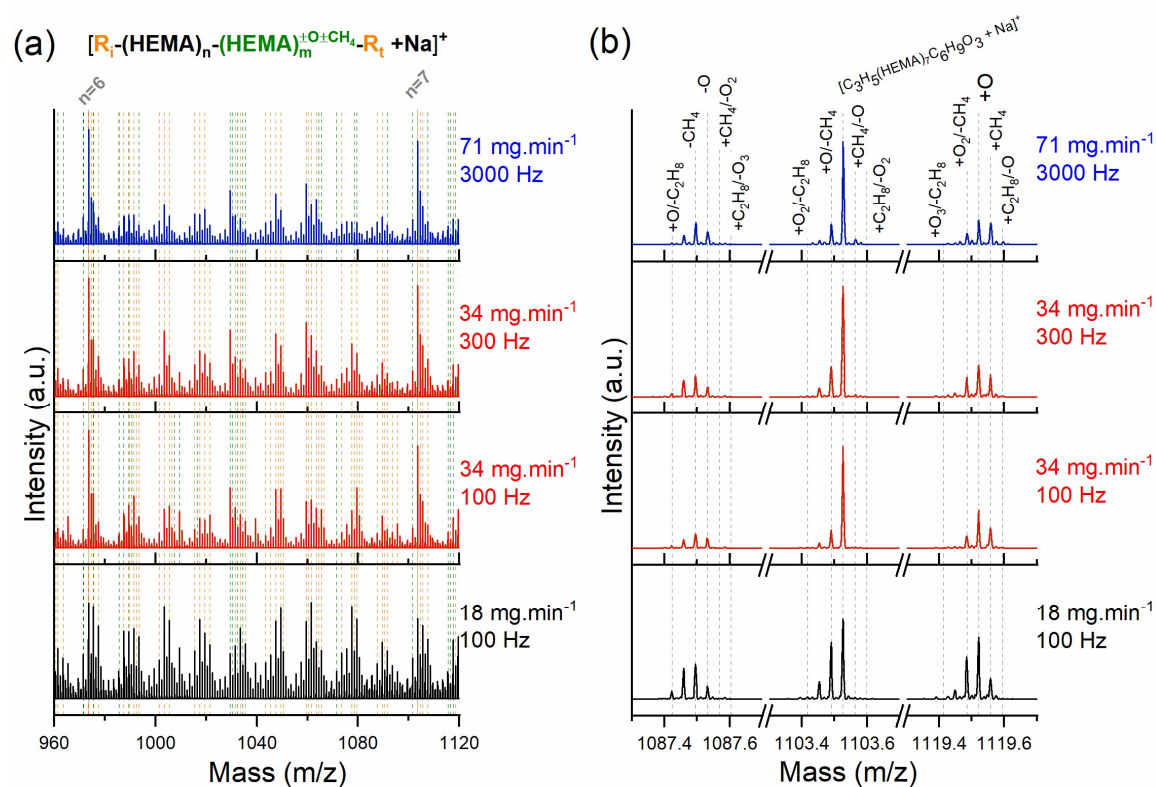


Figure 3.6: (a) MALDI-HRMS spectra in the mass ranges $m/z = 960-1120$ of the HEMA-based thin films prepared from various spray rates and plasma pulses frequencies. The HRMS peaks related to ionized adducts of $[R_i-(\text{HEMA})_n-R_t + \text{Na}]^+$ involving a single σ -bond plasma-induced fragmentation are indicated by orange dashed lines. The HRMS peaks related to ionized adducts of $[R_i-(\text{HEMA})_n-(\text{HEMA})_m^{\pm\text{O}\pm\text{CH}_4}-R_t + \text{Na}]^+$ involving a single σ -bond plasma-induced fragmentation and the integration or subtraction of oxygenated and/or alkyl groups are indicated by green dashed lines. (b) MALDI-HRMS spectra of HEMA-based thin films zoomed around the HEMA heptamer adduct with formula $[\text{C}_3\text{H}_5-(\text{HEMA})_7-\text{C}_6\text{H}_9\text{O}_3 + \text{Na}]^+$ ($m/z = 1103.526714$). The HRMS peaks related to HEMA heptamers adducts comprising the integration or subtraction of oxygenated and/or alkyl groups are indicated by grey dashed lines. The exact m/z values are listed in Table A4 and Table A5.

The combination of high spray rates and high plasma pulses frequencies enables the plasma-induced free-radical polymerization of liquid layers of vinylic compounds to form polymer-like thin films. Such an approach is particularly suitable for the plasma-induced free-radical polymerization of vinylic compounds possessing low saturation vapor pressure (P_{sat}). In the present case, HEMA possesses a P_{sat} (0.08 mbar at 25°C) that makes it also suitable for the plasma-enhanced chemical vapor deposition of HEMA-based thin films.¹⁹³ With the aim to evidence any differences between the thin films prepared from the liquid assisted approach described in this work and more traditional PECVD methods, we undertook the AP-PECVD of HEMA using the same atmospheric-pressure dielectric barrier discharge reactor and nanosecond plasma pulses generator (experimental conditions on Table A 6). In accordance with reports,^{43,185} the plasma pulses frequency was fixed to 100 Hz (*i.e.* $t_{\text{off}} = 10$ ms). A plasma off-time in the range of tens of millisecond, in accordance with the lifetime of the formed radical species, promotes plasma-induced polymerization over plasma-state polymerization in AP-PECVD.^{43,185} With the same objective, a high monomer saturation ratio ($P_{\text{M}}/P_{\text{sat}} = 80$ %, with P_{M} being the partial pressure of the monomer) was selected. In the case of HEMA, the use of lower $P_{\text{M}}/P_{\text{sat}}$ ratios engenders the system to operate in the monomer-deficient regime, yielding alteration of the monomer structure. A $P_{\text{M}}/P_{\text{sat}}$ ratio of 80 % also promote higher growth rate by comparison to the ones achieved for $P_{\text{M}}/P_{\text{sat}}$ ratio of 35% and 50% (Figure A6), confirming that the system operates in the monomer-deficient regime under low $P_{\text{M}}/P_{\text{sat}}$. Interestingly, one should point out that the growth rate achieved for a $P_{\text{M}}/P_{\text{sat}}$ of 80% in AP-PECVD, *i.e.* $1 \text{ nm} \cdot \text{s}^{-1}$, is more than one order of magnitude lower than the one achieved from the plasma-induced polymerization of HEMA liquid layers at high delivery rate (series C) and high frequency (3000 Hz), *i.e.* $17 \text{ nm} \cdot \text{s}^{-1}$. In contrast to what observed for the thin films prepared from the highest spray rate (series B and C), dominated by peaks related to sodium adducts of formula $[\text{C}_3\text{H}_5\text{-(HEMA)}_n\text{-C}_6\text{H}_9\text{O}_3 + \text{Na}]^+$ (Figure 3.5 and Figure 3.6), the MALDI-HRMS spectra of the AP-PECVD HEMA-based thin film is dominated by sodium adducts of formula $[\text{C}_2\text{H}_5\text{O}_2\text{-(HEMA)}_n\text{-C}_6\text{H}_9\text{O}_3 + \text{Na}]^+$ (Figure 3.7b). Both $\text{C}_2\text{H}_5\text{O}_2$ and $\text{C}_6\text{H}_9\text{O}_3$ end-groups can originate from the plasma-induced breakdown of a single σ -bond in HEMA (Table A3). Similarly to the thin films prepared from the liquid-assisted plasma-induced polymerization, a large number of peaks can be addressed by the formula $[\text{R}_i\text{-(HEMA)}_n\text{-R}_t + \text{Na}]^+$ using the fragments originating from a single σ -bond breakdown of the HEMA molecule as end-groups (Figure 3.7d). Besides, peaks related to HEMA oligomers involving the integration or subtraction of oxygenated and/or alkyl groups, structure $[\text{R}_i\text{-(HEMA)}_n\text{-(HEMA)}_m^{\pm\text{O}^{\pm}\text{CH}_4}\text{-R}_t + \text{Na}]^+$, are observed (Figure 3.7d).

Quite visually from the MALDI-HRMS spectra (Figure 3.7), the occurrence of the integration or subtraction of oxygenated and/or alkyl groups is more pronounced for the AP-PECVD thin film elaborated from the vapor phase at 100 Hz than for the plasma-induced polymerized thin film prepared from the highest spray rate in the liquid-assisted approach (series C) at 3000 Hz. The supply of the HEMA molecules from the vapor phase in AP-PECVD (virtually allowing interaction of all molecules with plasma reactive species)¹⁷⁹ is likely responsible for the greater alteration of the monomer structure compared to what observed when starting from liquid layers (granting a shielding effect).¹⁸³

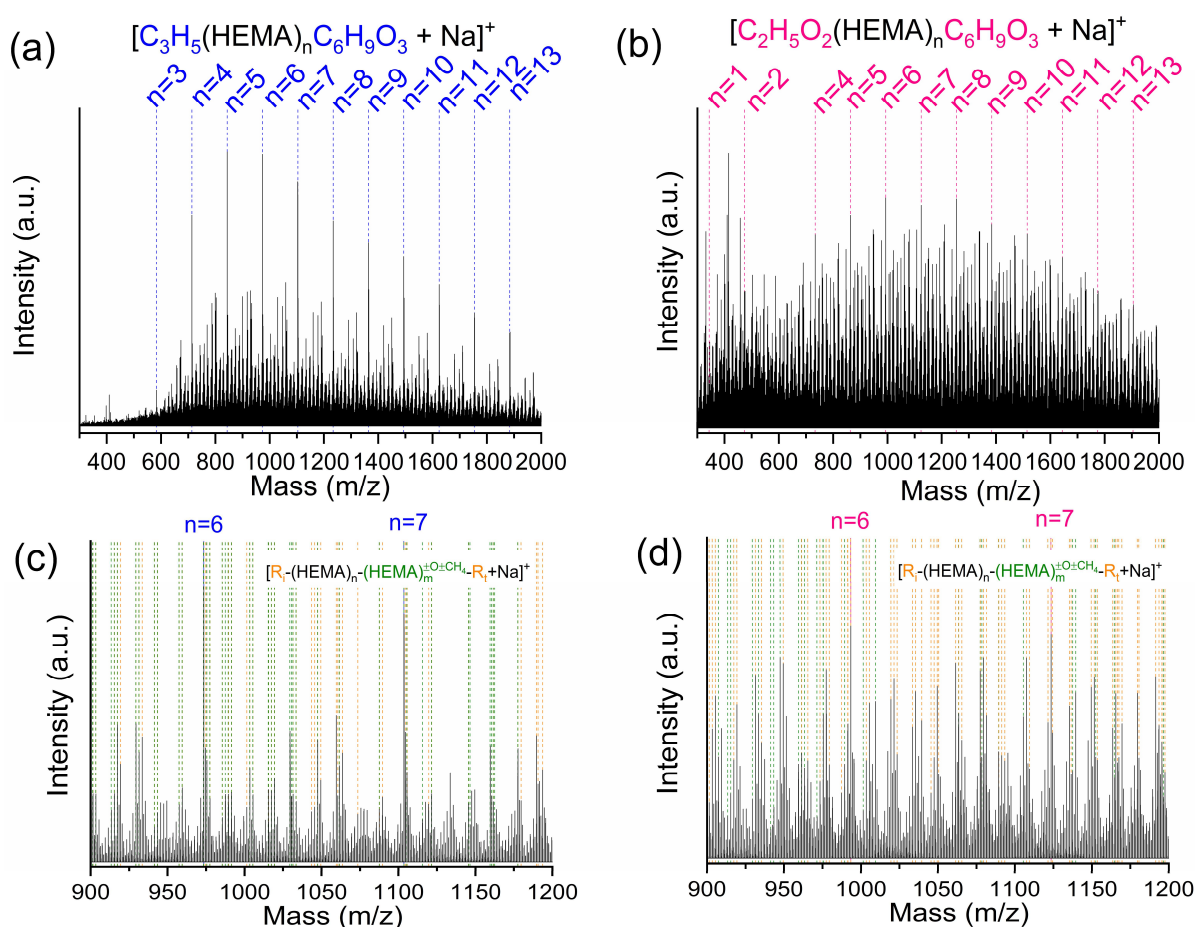


Figure 3.7: MALDI-HRMS spectra of the thin films prepared from (a & c) the plasma-induced polymerization of a liquid HEMA layer ($71 \text{ mg} \cdot \text{min}^{-1}$) at 3000 Hz and (b & d) the AP-PECVD of HEMA at 100 Hz. (a-b) mass range $m/z = 300\text{-}2000$ and (c-d) mass range $m/z = 900\text{-}1200$. The HRMS peaks assigned to ionized adducts of $[\text{C}_3\text{H}_5\text{-(HEMA)}_n\text{-C}_6\text{H}_9\text{O}_3 + \text{Na}]^+$ and $[\text{C}_2\text{H}_5\text{O}_2\text{-(HEMA)}_n\text{-C}_6\text{H}_9\text{O}_3 + \text{Na}]^+$ are identified by blue dashed lines and pink dashed lines on (a) and (b), respectively. The HRMS peaks related to ionized adducts of $[\text{R}_i\text{-(HEMA)}_n\text{-R}_t + \text{Na}]^+$ involving a single σ -bond plasma-induced fragmentation are indicated by orange dashed lines on (c & d). The HRMS peaks related to ionized adducts of $[\text{R}_i\text{-(HEMA)}_n\text{-(HEMA)}_m^{\pm\text{O}\pm\text{CH}_4}\text{-R}_t + \text{Na}]^+$ involving a single σ -bond plasma-induced fragmentation and the integration or subtraction

of oxygenated and/or alkyl groups are indicated by green dashed lines on (c & d). The exact m/z values are listed in Table A4, Table A5, Table A7 and Table A8.

3.2.3 Guidelines for thin film deposition by LA-PECVD

The most desirable conditions for the LA-PECVD of functional polymer thin films are those enabling the full conversion of the monomer liquid layer, translated in thickness built up, while preserving the chemical structure and functional groups of the monomer (reducing side-reactions occurrences). GPC and FTIR investigations highlighted that high delivery rates (series C) combined with too low plasma pulse frequencies (30 Hz and 100 Hz) do not allow the creation of a sufficient number of radical species (free-radical initiators) to ensure the full monomer conversion into a solid polymer thin film. Under these conditions, i.e. high monomer to initiator ratio, the system operates in the so-called energy-deficient regime. On the other hand, low spray rates (series A) and high pulse frequencies imply a high probability of interaction between the monomer and the plasma reactive species, which is responsible for a significant alteration of the monomer. Under these conditions, plasma-state polymerization appears predominant in comparison with the free-radical polymerization pathway, i.e. recombination vs. initiation, and the system operates in the so-called monomer-deficient regime. In accordance with previous AP-PECVD studies¹⁸¹, a rather large operating window (competition regime) for the plasma-induced free-radical polymerization of liquid HEMA layers into solid polymer-like thin films is identified. Particularly, the combination of intermediate spray rate (series B) with intermediate plasma pulses frequency (100 Hz), or high spray rate (series C) with high plasma pulse frequency (3000 Hz) enables the formation poly(HEMA) thin film with a low amount of side reactions. These poly(HEMA) thin films mainly differ from their counterparts synthesised by conventional solution-based approaches by their wider variety of end-groups that originate from the single σ -bond breakdown of some of HEMA molecules upon exposure to plasma (Figure A9). Gratifyingly, the thin film prepared from the highest plasma pulses frequency (3000 Hz) and highest spray rate studied is displaying both the highest growth rate and the most regular polymer structure among the thin films prepared from both the AP-PECVD at 100 Hz and the plasma-induced free-radical polymerization of liquid layers. Particularly, the growth rate achieved from 3000 Hz and at the highest spray rate ($17 \text{ nm}\cdot\text{s}^{-1}$) is more than one order of magnitude higher than the one achieved from the AP-PECVD of HEMA in the same AP-DBD reactor ($1 \text{ nm}\cdot\text{s}^{-1}$). Therefore, the plasma-induced free-radical polymerization of liquid layers provides an attractive strategy for the preparation of functional polymer thin films not only from low P_{sat} vinylic compounds, but also

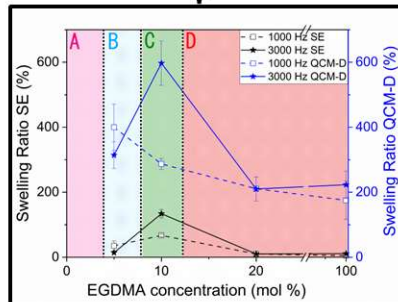
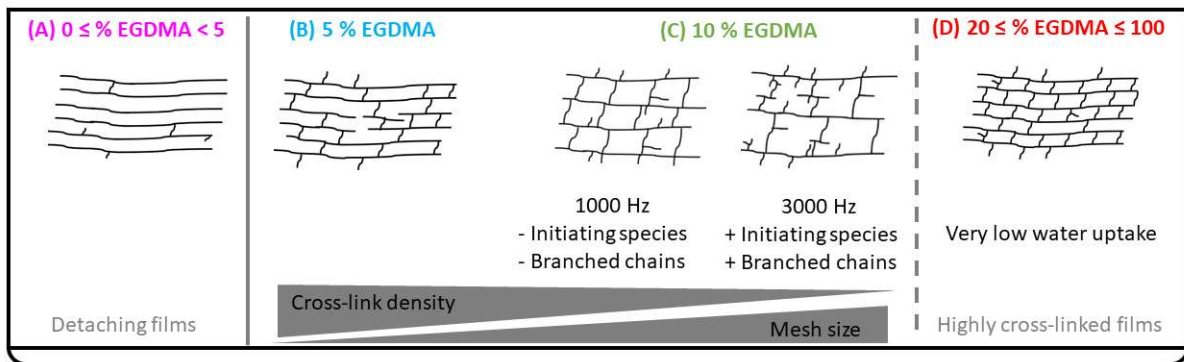
from vinylic compounds possessing intermediate P_{sat} and enabling the copolymerization of vinylic compounds with highly different P_{sat} to form stable hydrogel thin films.

3.3 Conclusion

While plasma deposition processes are often limited by the vapor pressure of the thin film precursors, this study demonstrates the potential of the LA-PECVD approach for the fast deposition of functional polymer thin films. The significance of the operating parameters, such as monomer spray rate and the plasma pulse frequency on the plasma-induced free-radical polymerization of HEMA are elucidated. Specifically, GPC analysis revealed M_w^* distribution up to ca. $8 \text{ kg}\cdot\text{mol}^{-1}$ for the thin film prepared from the lowest spray rate and lowest plasma pulses frequency. Yet, MALDI-HRMS and FTIR indicated a superior retention of the monomer structure and lower amount of side reactions by combining intermediate spray rate with intermediate plasma pulses frequency (300 Hz), or high spray rate with high plasma pulses frequency (3000 Hz). Particularly, the combination of the highest plasma pulses frequency (3000 Hz) and high spray rate resulted in the highest growth rate and the most regular polymer structure among the thin films prepared from LA-PECVD. Interestingly, alongside a superior retention of the monomer chemical structure, the LA-PECVD approach enable more than one order of magnitude higher growth rates compared to the traditional vapor phase AP-PECVD approach.

Plasma-induced free-radical polymerization of liquid layers provides an attractive method for preparing functional polymer thin films, not only from low P_{sat} vinylic compounds but also from vinylic compounds possessing intermediate P_{sat} , paving the way to the fast deposition of functional polymer thin solid films with a controlled degree of cross-linking.

Chapter 4 : Hydrogel synthesis via nanosecond pulsed plasma induced copolymerization of MAA and EGDMA from liquid layers



4.1 Introduction

In the previous chapter, it was demonstrated and characterized the plasma-induced free-radical polymerization (FRP) of a model functional monomer for the direct synthesis and deposition of a hydrophilic polymer thin films from liquid layers. Building on these findings, this chapter aims to investigate the plasma-induced FRP of liquid layers in the perspective to form hydrogel films.

Free-radical copolymerization of vinyl monomers in the presence of a cross-linking agent bearing two vinyl groups is a widely employed method for synthesizing hydrogels (Figure 4.1).^{27,28,100} In this approach both polymer chain growth and cross-linking occur simultaneously, leading to the formation of the desired network structure.^{27,28} Nonetheless, heterogeneity is expected in this approach due to the concurrent and random propagation and cross-linking reactions.²⁸ Furthermore, the termination mechanism, whether combination or disproportionation, can influence the network structure during the copolymerization. Both termination modes lead to different end-groups on the polymeric chains, which can subsequently affect cross-linking efficiency and network homogeneity.^{28,81} The final network structure often contains unreacted vinyl groups derived from the cross-linker and the presence of dangling chains (Figure 4.1).

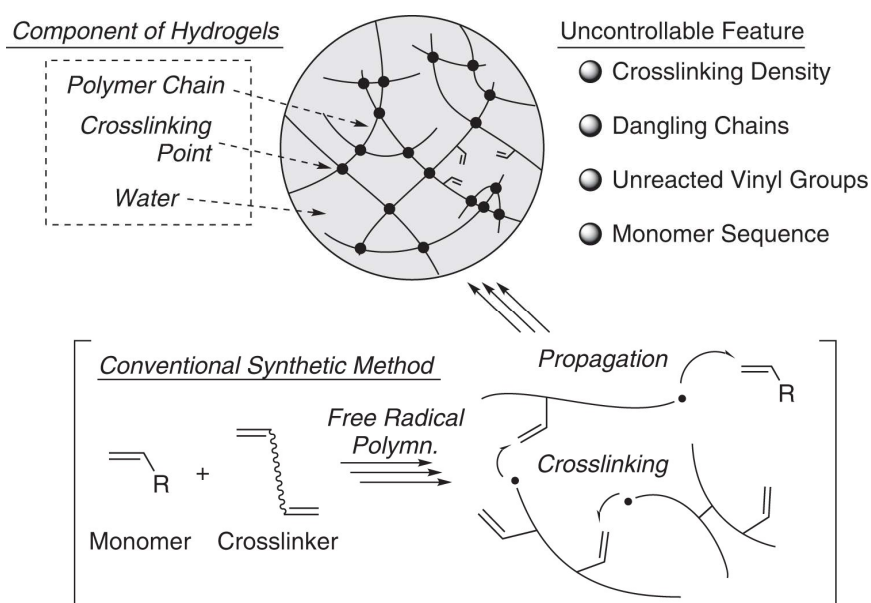


Figure 4.1: Structure and uncontrollable features in the copolymerization between a vinyl and divinyl hydrogel. Reprinted with permission from Ida.²⁸ Copyright 2019, The Society of Polymer Science, Japan.

On the other hand, few studies have investigated plasma polymerizations of a monomer and a cross-linker to form (bulk and thin film) hydrogels.^{45,51,109,156} Those studies usually synthesized them by exposing aqueous solutions of the monomers to the plasma reactive species. Such approach aims to create free radicals from water dissociation (such as, OH• and H•) to initiate FRP.^{51,109,156}

Malik *et al.* reported the synthesis of bulk hydrogels using atmospheric-pressure corona pulsed plasma with three monomers: acrylamide (AAm), acrylic acid (AAc) and N,N-methylene-bis-acrylamide (MBA).¹⁵⁶ The MBA was fixed at the concentration of 1 mol% of the monomers, as cross-linking agent, and AAc was varied between 0-50 mol%. Interestingly, the authors observed a swelling 14 times bigger for the sample produced without AAc compared to the samples with 50 mol% AAc in its composition (Figure 4.2a). Likewise, Lu *et al.* utilized glow discharge to synthesize hydrogel from AAc, polyvinylpyrrolidone (PVP), and MBA (cross-linker agent) in aqueous solutions.¹⁰⁹ Such synthesized hydrogels were investigated as absorbents for the removal of heavy-metal ions from wastewater. Lu *et al.* studied the variation of the cross-linker concentration (MBA) between 0.1 and 1.1 mol% in the properties of the plasma polymers. Although the swelling of the plasma polymerized was not determined for the hydrogel, the authors determined an optimum content of MBA as 0.7% for the studied adsorption of Pb (II) (Figure 4.2b). Knowing the influence of the cross-linker concentration, Molina *et al.* investigate the impact of chemical cross-linker concentration on physico-chemical properties of the poly(N-isopropylacrylamide-co-N,N-methylene-bis-acrylamide) (NIPAAm-co-MBA) bulk hydrogel (Figure 4.2 c and d).⁵¹ The authors observed that the swelling capacity of the p(NIPAAm-co-MBA) declines significantly when the MBA concentration increased (Figure 4.2c).

Due to the intrinsic cross-linked nature, the chemical and structural characterization of the plasma polymerized hydrogels in the studies were limited to the soluble fraction for some characterization techniques, such as nuclear magnetic resonance spectroscopy (NMR) and GPC. Consequently, these reports were mainly focused on the resulting hydrogel properties (such as swelling and mechanical properties) to infer the structure-property relationship. From the literature survey, it became evident that the chosen kind of monomers and their concentrations will play an important role in the properties of the plasma polymerized hydrogels, as have been largely reported on the wet chemistry synthesis of these materials.

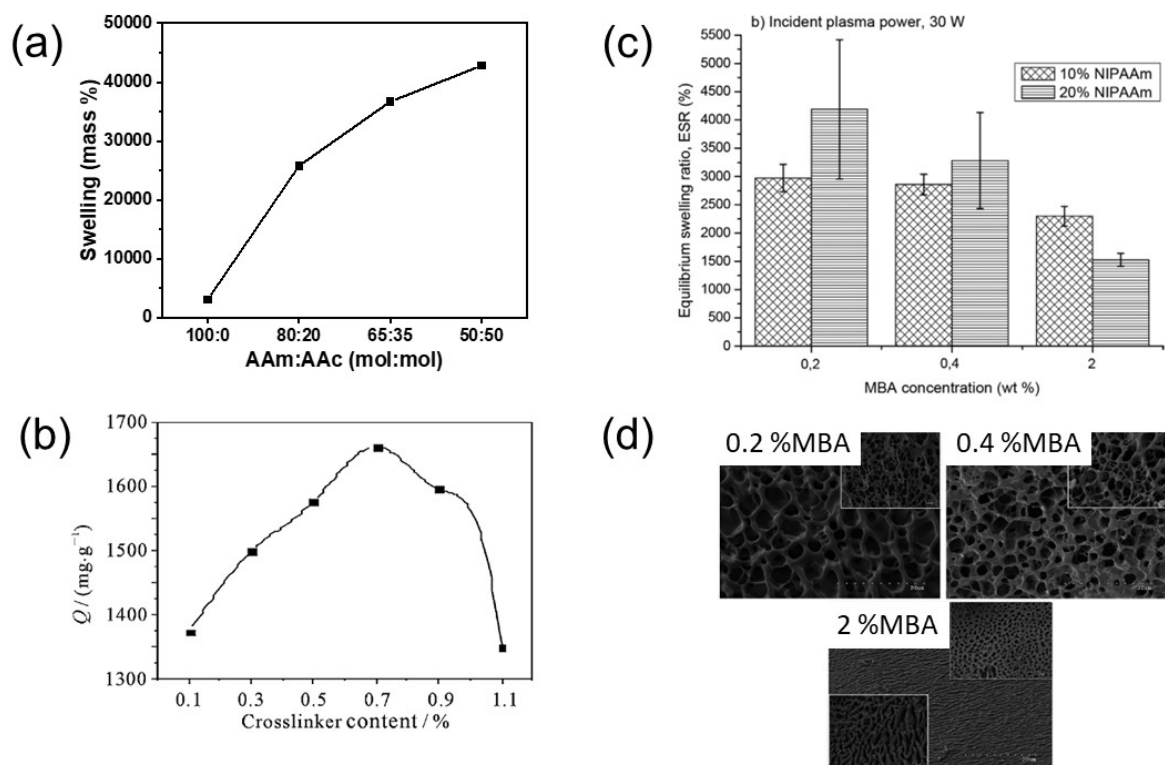


Figure 4.2: (a) Effect of AAc concentration in poly(AAm-co-AAc-co-MBA) in the swelling behavior of the plasma polymerized bulk hydrogels. MBA (cross-linker agent) was kept at 1 mol%. Adapted with permission from Malik *et al.*¹⁵⁶ Copyright 2003, Springer Nature, Plenum Publishing Corporation (b) Effect of MBA concentration on Pb(II) adsorption of plasma polymerized p(PVP-co-AAc-co-MBA) hydrogel. Reprinted with permission from Lu *et al.*¹⁰⁹ Copyright 2011 WILEY-VCH Verlag GmbH & Co. KGaA, Weinheim (c) Effect of MBA concentration on the (c) swelling ratio and (d) porous structure of the swollen hydrogels characterized by scanning electron microscopy of the plasma polymerized p(NIPAAm-co-MBA). Reprinted with permission from Jovančić *et al.*⁵¹ Copyright 2015 WILEY-VCH Verlag GmbH & Co. KGaA, Weinheim.

In this context, this chapter aims to study the deposition of hydrogel coatings from liquid mixtures of methacrylic acid (MAA) and ethylene glycol dimethacrylate (EGDMA). MAA has been extensively employed for hydrogel applications due to its high hydrophilicity and pH-responsiveness characteristics, thanks to the carboxyl group.^{194–196} While EGDMA was selected for its vast use as a cross-linker in FRP and as a chemical cross-linker in hydrogel applications.^{101,197} Figure 4.3 shows a representation of the chemical structure of EGDMA acting as a chemical cross-linking point and MAA as the polymeric backbone for the formation of a 3D network structure. From a process point of view, these selected methacrylates have low vapor pressure at room temperature (0.1 mmHg and 1 mmHg for EGDMA and MAA,

respectively), which will limit monomer losses by evaporation in the open configuration of the plasma reaction set-up.

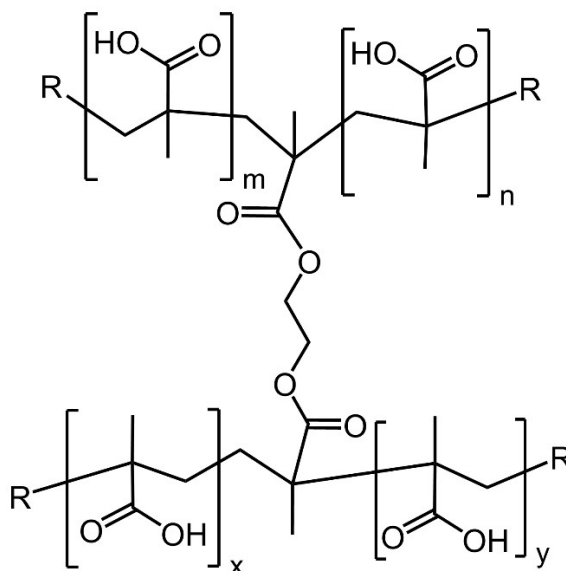


Figure 4.3: Representation of the expected chemical structure from the copolymerization between MAA and EGDMA.

The synthesis of p(MAA-co-EGDMA) hydrogel films via atmospheric-pressure (nanosecond) pulsed plasma polymerization of liquid layers has not yet been reported. Following the approach of the previous chapter, the first section of this chapter was focused on the plasma-induced FRP of MAA. Then, the copolymerization of MAA and EGDMA is studied by varying the plasma pulse frequency and the EGDMA concentration (chemical cross-linker) to analyze the impact on the properties of the network structure of the coatings. In particular, the chemical structure and hydrogel properties (swelling behavior and viscoelastic properties) of the coatings are characterized by spectroscopic methods and QCM-D measurements, respectively.

4.2 Results and discussion

4.2.1 Samples nomenclature

In Table 4.1 are summarized the seven series of samples studied in this chapter and its corresponding nomenclature. Each series was characterized by the EGDMA concentration used in the liquid mixture, spanning from 0 to 100 mol%, and within the series, three different f_{pe} were studied ca. 100, 1000 and 3000 Hz. Other deposition parameters such as spray rate (1.8 slm and 0.5 slm for nebulizer gas and carrier gas, respectively) and sample displacement speed through the plasma zone ($50 \text{ mm}\cdot\text{s}^{-1}$) were kept unchanged through the series. The number of deposition runs were 100, except for the samples dedicated for QCM-D studies.

A corresponding nomenclature for the samples is also provided. For ease of reference, these samples are hereafter referred to by the designations outlined. The specific parameters for each sample, including monomer composition in the liquid mixture and pulse frequency (f_{pe}), are outlined in Table 4.1.

Table 4.1: Nomenclature of the samples studied in this chapter.

EGDMA concentration in the liquid mixture (mol %)	Mass delivery rate ($\text{mg}\cdot\text{min}^{-1}$)	Plasma pulse frequency (Hz)		
		100	1000	3000
0	82 ± 6	ppMAA_100	ppMAA_1000	ppMAA_3000
1	83 ± 9	1EGDMA_100	1EGDMA_1000	1EGDMA_3000
2.5	87 ± 1	2.5EGDMA_100	2.5EGDMA_1000	2.5EGDMA_3000
5	79 ± 10	5EGDMA_100	5EGDMA_1000	5EGDMA_3000
10	86 ± 6	10EGDMA_100	10EGDMA_1000	10EGDMA_3000
20	52 ± 6	20EGDMA_100	20EGDMA_1000	20EGDMA_3000
100	51 ± 7	ppEGDMA_100	ppEGDMA_1000	ppEGDMA_3000

4.2.2 Deposition of water-soluble ppMAA films

Certainly, to develop a robust method to tune the polymeric network structure of hydrogels it would be extremely interesting to distinguish the effect of the cross-linker (*i.e.*, EGDMA concentration) from the effect of the f_{pe} in the growth of the polymeric network structure. Due to the foreseen highly cross-linked structure obtained at higher EGDMA

concentration in the films, chemical analysis techniques (such as mass spectrometry and GPC) are more complicated and perhaps not representative of the sample's chemistry. Therefore, this section aims at investigating the influence of the f_{pe} on the homopolymerization of the plasma polymerized MAA (ppMAA) films. As shown in the previous chapter on plasma-induced polymerization using nanosecond pulse discharge, the f_{pe} can influence the chemistry and molecular weight of the deposited thin films. For this purpose, f_{pe} ranging from 100 Hz to 3000 Hz was investigated for the growth of pp(MAA).

4.2.3.1 Study of the chemistry and polymeric growth of the films of the ppMAA

After deposition, naked eye observations readily revealed a change in physical state of the liquid MAA monomer into solid thin films for all studied f_{pe} , suggesting polymeric growth. To characterize the effects of plasma exposure on the monomer structure, FTIR analysis was performed (Figure 4.4). For the sake of comparison, a commercial poly(MAA) produced by conventional polymerization (pMAA_REF, Polysciences M_w 100 $\text{kg}\cdot\text{mol}^{-1}$) was also analyzed as a reference.

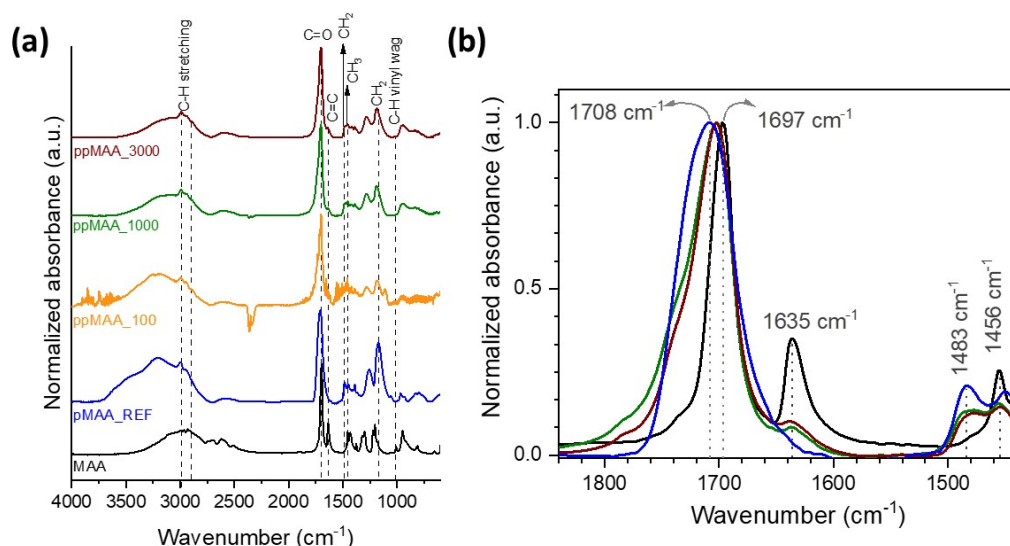


Figure 4.4: FTIR spectra of as-deposited ppMAA films obtained at different plasma pulse frequency (100-3000 Hz) (a) in the wavenumbers range of 4000-600 cm^{-1} and (b) overlay on the carbonyl and vinyl band region around 1700 and 1635 cm^{-1} , respectively. The monomer (MAA) and commercial poly(MAA) produced by conventional polymerization (pMAA_REF, Polysciences M_w 100 $\text{kg}\cdot\text{mol}^{-1}$) are shown as references.

FTIR spectra showed that the vinyl group bands at 1006 cm^{-1} and 1635 cm^{-1} exhibited significantly lower intensity in the plasma polymerized samples compared to the MAA monomer (Figure 4.4b).^{186,198–200} Additionally, a shift in the carbonyl group peak from 1697 cm^{-1} (MAA monomer) to 1700 cm^{-1} (ppMAA) and 1708 cm^{-1} (pMAA_REF) was observed. The disappearance of the C=C and the shift of the C=O indicated the growth of polymeric chains via a FRP pathway.^{199–201} A distinct difference between the monomer and polymerized samples (ppMAA and pMAA_REF) was observed in the hydroxyl group region ($3200 - 2900\text{ cm}^{-1}$). The broader OH band in the polymerized samples is attributed to intermolecular hydrogen bonding involving the carboxylic acid groups, which is consistent with previous studies on MAA polymerization in wet chemistry.^{186,201–203} Overall, FTIR analysis indicated structural similarities between pMAA and ppMAA, suggesting the preservation of functional groups on the plasma polymerized thin films. Likewise, XPS spectra of the thin films obtained at different f_{pe} showed no difference from the conventionally polymerized pMAA_REF sample. The XPS elemental analysis also showed similar values between the thin films, pMAA_REF and the theoretical values (Figure B2).

To gain insights into the polymeric chain growth, MALDI-HRMS analysis was performed for the ppMAA obtained at 100 and 3000 Hz (Figure 4.5). The MALDI-HRMS spectra ($m/z = 100-1000$) were dominated by ppMAA proton adduct of formula $[(\text{MAA})_n + \text{H}]^+$ with n up to 6 and 7 repetition units for ppMAA_100 and ppMAA_3000, respectively (Figure 4.5 a&b). Such oligomer was attributed to the formation of an unsaturation through hydrogen transfer as termination mechanism. The spectra was also dominated by peaks related to the proton adducts of formula $[\text{C}_3\text{H}_5 - (\text{MAA})_n - \text{C}_4\text{H}_5\text{O}_2 + \text{H}]^+$ up to $n = 7$ repetition units. These proposed end groups (C_3H_5 and $\text{C}_4\text{H}_5\text{O}_2$) are initiating/terminating groups originated from the plasma-induced breakdown of a single σ -bond in MAA (Figure B3). Additionally, irrespective of the f_{pe} , a non-negligible number of side-species is observed between the trimer and tetramer $[(\text{MAA})_n + \text{H}]^+$ peaks (Figure 4.5 b&d). In a similar manner as for the HEMA in the previous chapter, the sets of distribution were directly related to the summed number of C and O atoms composing the monomers (9 for HEMA ($\text{C}_6\text{H}_{10}\text{O}_3$) and 6 for MAA ($\text{C}_4\text{H}_6\text{O}_2$)). Likewise, some peaks could be addressed by the formula $[\text{R}_i - (\text{MAA})_n - \text{R}_t + \text{H}]^+$ using the fragments originating from a single σ -bond breakdown of the MAA molecule as end-groups (Figure 4.5 b&d, dashed orange lines), and the main modifications of the monomer structure could be assigned as integration or subtraction of O unit with a CH_4 unit. This side-mechanism and mass peaks that

could not be addressed (likely originate from fragmentation and polyrecombination reactions) likely from the plasma-state polymerization pathway.

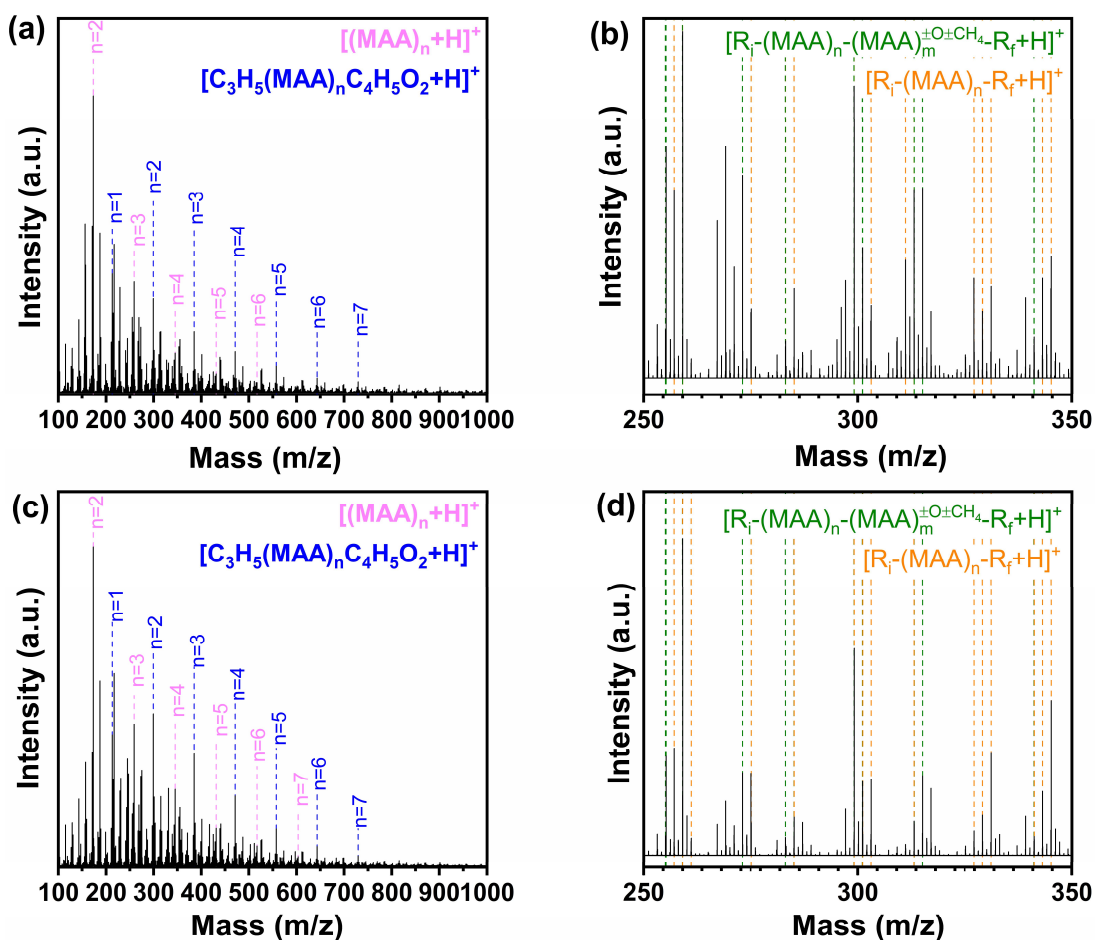


Figure 4.5: MALDI-HRMS spectra in the mass range $m/z = 100-1000$ of a thin film elaborated from MAA at (a) 100 Hz and (c) 3000 Hz. MALDI-HRMS spectra in the mass ranges $m/z = 250-350$ of ppMAA from MAA at (b) 100 Hz and (d) 3000 Hz. Peaks related to ionized adducts of oligomers $[R_f-(MAA)_n-R_f + H]^+$ indicated as dashed orange lines and oxygen side reactions are indicated as green lines.

To demonstrate the growth of the polymeric chains and gain insights of the molar mass distribution of the ppMAA, GPC analyses was performed for the soluble parts of these films (Figure B4). The molecular weight distribution and polydispersity index of the ppMAA films deposited at 1000 and 3000 Hz are shown in Table B 1. Both ppMAA_1000 and ppMAA_3000 exhibited an apparent weight average molar mass (M_w^*) around $2300 \text{ g}\cdot\text{mol}^{-1}$ with a relatively high polydispersity index around 1.7, indicating no significant influence of f_{pe} on the molar mass distribution within this range. Unfortunately, ppMAA_100 chromatogram exhibited

extremely low detectable peaks (sample to blank ratio), likely due to insufficient soluble polymer for analysis. Consequently, reliable molecular weight data could not be extracted for ppMAA_100.

4.2.3.2 Study of the solubility in water of the ppMAA

Poly(MAA) synthesized by conventional wet chemistry is readily soluble in water.^{204,205} To investigate whether the thin films deposited by plasma show this property, immersion tests in distilled water were conducted. Special attention was paid to the presence of any supernatant or insoluble material in the water where the samples were immersed. FTIR spectra of the samples after immersion in water showed only the OH vibration from moisture and Si-O vibration of the silicon substrate for all investigated f_{pe} (Figure 4.6a). Quantitatively, gravimetric analysis confirmed the dissolution of all ppMAA films, with mass losses ranging from 94% to 100% for ppMAA_100 and ppMAA_3000, respectively (Figure 4.6b).

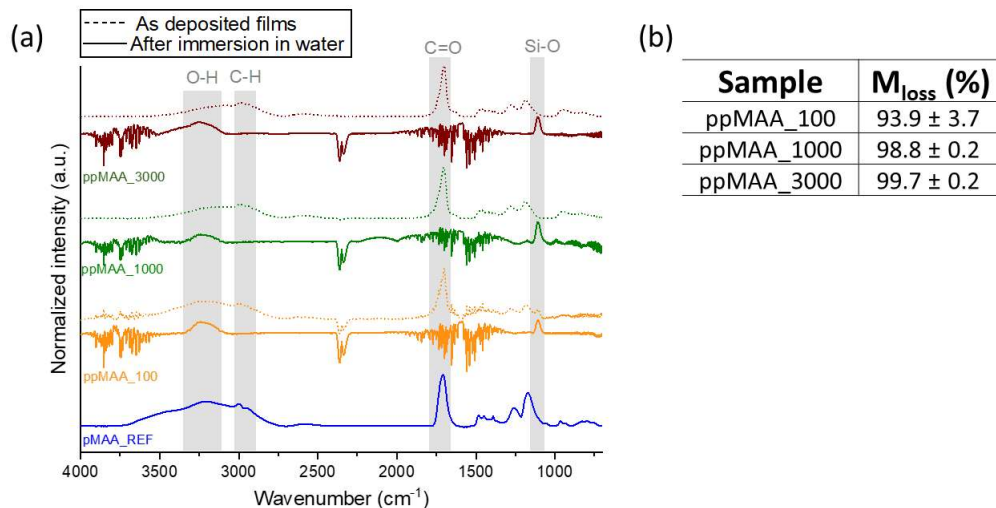


Figure 4.6: (a) FTIR spectra of ppMAA film at different pulse frequencies measured after immersion in water (continuous line). The as-deposited films grown at the same pulse frequencies (dashed lines) and commercial conventionally polymerized (pMAA_REF) are shown as references. For the plasma polymerized films after immersion in water (green continuous lines), the spectra were normalized from 0 - 1 to be able to adjust the values to a common scale. (b) Mass losses of thin film (M_{loss}) were calculated after 24 h immersion in water and subsequent drying in an oven at 60 °C.

The absence of bands associated with polymeric chains in the FTIR spectra, along with the mass loss, indicates near-complete dissolution of the ppMAA. The complete dissolution indicates the absence of sufficient cross-linking within the plasma polymerized films. Indeed, several studies have showed that fragmentation and polyrecombination reactions during plasma-based processes can form highly cross-linked and insoluble networks.^{206–208} The solubility in water and analyzed chemical structure suggests a predominantly linear polymer chain structure for the ppMAA films, formed primarily through plasma-initiated FRP. Interestingly, these results indicate that the f_{pe} used in the deposition does not seem to have any significant effect on the solubility of the ppMAA thin film. This is of significance for studying the copolymerization of MAA with EGDMA as the role of EGDMA as cross-linking agent would not be significantly influenced by plasma-induced cross-linking reactions.

4.2.3 Nanosecond-pulsed plasma copolymerization of MAA and EGDMA

4.2.3.1 Effect on the chemistry

After deposition, naked-eye observation readily enables evidence of physical state differences for some samples. In particular, liquid thin layers were obtained when combining the highest EGDMA concentration (≥ 5 mol%) to the lowest plasma pulse frequencies (100 Hz). Decrease of EGDMA concentration or use of higher pulse frequencies (1000 or 3000 Hz) yield the formation of solid thin films. The difference in the physical state of the samples, appearing as a liquid thin layer, suggests the presence of non-polymerized monomers or short oligomers, as concluded in the previous chapter.

Hence, FTIR analysis was performed to investigate the chemistry of the films and liquid layers (Figure 4.7 and Figure B5). As expected, compared to the liquid mixture, a decrease in the band associated with the vinyl group (1637 cm^{-1}) is noticeable for all the samples. Additionally, the thin liquid layers, obtained when combining higher EGDMA concentration with the lower f_{pe} , exhibited a higher intensity of the C=C, corroborating the assumption of a higher concentration of unreacted monomers. These findings align with the reported results in the literature for the free-radical copolymerization of similar methacrylate (i.e., methyl methacrylate, MMA) and EGDMA in wet chemistry.^{81,209,210} For instance, Carswell *et al.* reported the monomer conversion close to 40% and 85% for homopolymerization of EGDMA

and MMA, respectively.²⁰⁹ Furthermore, they also showed that for comonomer mixtures containing up to 6 mol% of EGDMA, the conversion was close to 80% and decreased at higher EGDMA concentrations. Similarly, Czuba *et al.* work on atmospheric-pressure plasma polymerization of methyl methacrylate and EGDMA mixtures demonstrated comparable behavior.²¹¹ Czuba *et al.* showed that higher EGDMA concentrations (2 mol%) exhibited thinner films, when compared to lower concentration of the cross-linker (0.05 - 0.4 mol%). Such behavior was attributed to the evaporation of the unreacted volatile MMA monomer and, consequently, originating thinner thickness of the films. In both studies, the lower monomer conversion at the higher cross-linker content was attributed to the Trommsdorff–Norrish effect, also called gel effect.^{210,212} Furthermore, our results showed that combining of high EGDMA concentration (≥ 5 mol%) and higher pulse frequency (1000 - 3000 Hz) formed solid films. Although an explanation for the observed trend cannot be proposed, such differences already highlight an effect between the EGDMA fraction in liquid mixture and the pulse frequency used in the deposition.

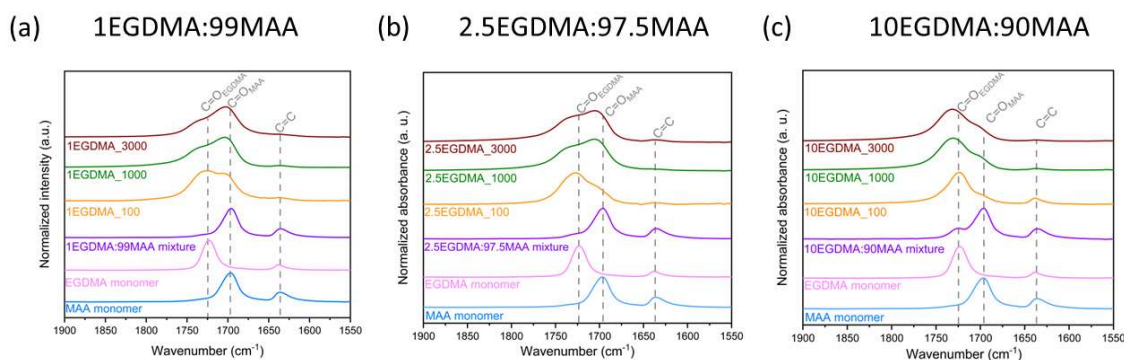


Figure 4.7: FTIR spectra of the 1900-1550 cm^{-1} region, corresponding to the carbonyl stretching of EGDMA and MAA monomer and the pp(EGDMA:MAA) copolymer films for different EGDMA:MAA molar ratios grown from 100 to 3000 Hz. MAA and EGDMA monomers, and the liquid mixture solution prepared with its corresponding concentration of each monomer are shown as references.

Regarding the effect of the EGDMA concentration in the liquid mixture on composition of the films, the spectra of pp(EGDMA:MAA) copolymer films show the distinctive vibrations at 1697 and 1725 cm^{-1} attributed to the ester moiety (C=O stretching) contained in the MAA and EGDMA monomers, respectively.¹⁸⁶ As expected, by comparing the same f_{pe} , the intensity of the peak at 1752 cm^{-1} become more pronounced with increasing the EGDMA content in the

liquid mixture. In addition to the noticeable decrease of the OH stretching vibrations at the 3600-3100 cm^{-1} attributed to the COOH group of MAA, for higher EGDMA contents in the copolymers (Figure B5).

Furthermore, the effect of f_{pe} on the resulting structure of the copolymers is evident in all the spectra of the samples across the studied range of cross-linker concentrations (1 - 20 mol%). Where the C=O band observed on the samples obtained with lower f_{pe} (100 Hz) has shifted towards the characteristic absorbance peak of the carboxylic groups of EGDMA rather than MAA. While at very low concentration of EGDMA in the liquid mixture (1 - 2.5 mol%) the carbonyl peaks from EGDMA located at 1752 cm^{-1} are barely noticeable, while it is more pronounced in the copolymer film's spectra.

To further analyze the bond arrangements, XPS studies of pp(EGDMA:MAA) films were carried out (Figure 4.8 and Table B 2). The C1s high resolution core level spectra from the films exhibited four distinct peaks, corresponding to C*-(C,H) (B.E.= 285.0 eV), C*-COO (B.E.= 285.8 eV), C-O (B.E.= 286.7 eV), and O=C*-O (B.E.=289.33 eV).²¹³ The presence of EGDMA in the copolymers was clearly indicated by an increase in the C–O peak associated with the EGDMA backbone (Figure 4.8b). Notably, the C-O components were more pronounced in copolymer films synthesized at 100 Hz (Figure 4.8a), suggesting a higher concentration of EGDMA in the polymeric backbone at low f_{pe} . Similar behavior was observed in FTIR, where 1EGDMA_100 and 2.5EGDMA_100 exhibited more pronounced peaks in the C=O related to the ester of EGDMA compared to their counterparts obtained at higher pulse frequencies (1000 and 3000 Hz).

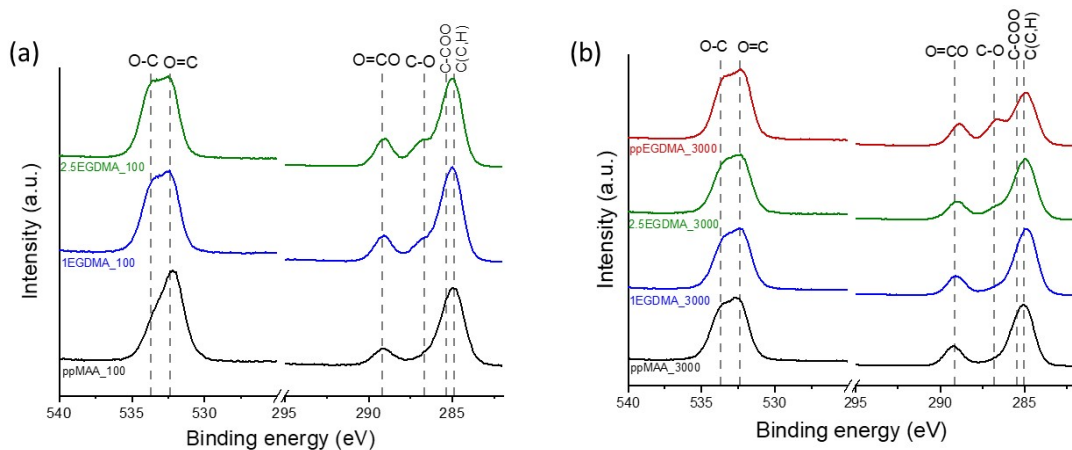


Figure 4.8: XPS spectra of the O 1s and C 1s core levels of as-deposited pp(EGDMA:MAA) copolymer layers grown for different EGDMA concentration at (a) 100 Hz and (b) 3000 Hz.

4.2.3.2 Insights into molecular composition of pp(MAA-co-EGDMA)

Figure 4.9 shows the high-resolution XPS C 1s spectra used to attempt the quantification of the MAA molar fraction in the thin films. A comparison between the MAA molar fraction in the liquid monomer mixture used in the deposition and the fraction determined by XPS in the thin film is plotted in Figure 4.9b & c. While higher molar fractions of MAA (in the range of 95 - 100%) in the monomer mixture led to values similar to those obtained in the copolymer films, a significant deviation was observed upon increasing EGDMA fraction in the liquid mixture.

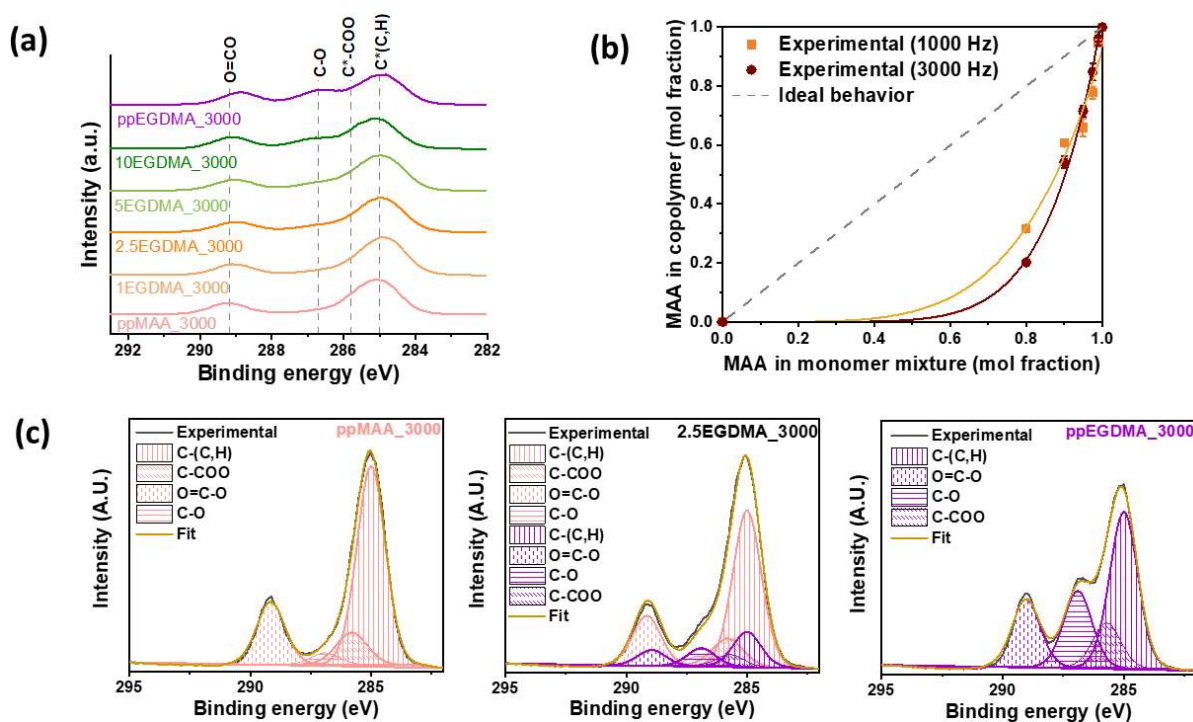


Figure 4.9: (a) XPS spectrum of the C 1s core levels of the pp(EGDMA:MAA) copolymer films for different EGDMA:MAA molar ratios grown at 3000 Hz. (b) A plot of the MAA molar fraction in the copolymer film (obtained by XPS) versus MAA molar fraction in the liquid mixture before exposure to plasma zone. Error bars: means \pm SD ($n=3$). The dotted grey line indicates the ideal case where molar fraction in the feed is fully conserved within the thin film.

The deconvolution of the XPS spectra might be affected by the new groups originating from the plasma-induced fragmentation and recombination reactions, affecting the estimation of EGDMA concentration in the copolymer. Nevertheless, the clear trend observed in Figure 4.9c is likely related to the reactivity ratio between this comonomer pair. For comparison,

reactivity ratio values reported in the literature between methacrylate monomer pairs with similar chemistry from this work were shown in Table B3. The trend thus suggests a higher tendency of EGDMA to self-polymerize than to add MAA units. Indeed, this nonlinear behaviour between the monomer fraction obtained in the copolymers compared to the initial monomer mixture has been reported previously between a (meth)acrylate and divinyl monomers, bearing similar moieties.^{90,214} Under these circumstances, the formation of a polymer network rich in poly(EGDMA) could be expected, increasing the possibility of unreacted MAA monomer loss through evaporation. This is accentuated by the higher vapor pressure of MAA (1 mmHg) compared to EGDMA (0.1 mmHg) at room temperature.

While XPS results provided useful information of the monomer fractions in the film, the results do not provide information to reveal the mechanism responsible for the growth of polymeric chains, whether by separate homopolymerization of MAA or EGDMA, copolymerization, oxygen side-reactions, etc. In this context, chemical structural analysis were carried out by MALDI-HRMS. In Figure 4.10 and Figure B6 (in black lines) are shown the MALDI-HRMS spectra of a representative sample (10EGDMA_3000). This sample was chosen for illustrative purposes as it corresponds to the midpoint of the EGDMA fractions in the copolymer film, as determined by XPS. Also, these figures also show the filtered peaks (colored spectra) from the full spectra that could be assigned to different mechanisms of polymeric growth. One should note that MALDI-HRMS is not the ideal characterization for oligomers with high cross-linker concentration such as expected for ppEGDMA, implying the results might not fully describe the film's chemistry. For the filtering of the peaks, the investigated mechanisms were the homopolymerization (orange and green lines), copolymerization (blue lines) and the structure of oligomers with modified repeat units (pink lines, corresponding to the integration or subtraction of an oxygen unit with an alkyl unit). Polymeric's distributions considering either proton, hydroxyl, C₄H₅O₂ and C₄H₅O as end groups were investigated. In addition, the formation of an unsaturation through hydrogen transfer or disproportionation was also considered as a terminating process, yielding the oligomer form [(MAA)_n + H]⁺, [(EGDMA)_n + H]⁺, [(MAA)_n-(EGDMA)_m + H]⁺ or [(MAA)_n-(MAA)^{±O±CH₄}_m + H]⁺. As evidenced by the higher number of filtered peaks in Figure 4.10 and Figure B6, the matching peaks were more pronounced for the structure [R_i-(MAA)_n(EGDMA)_m-R_f + H]⁺. The predominance of matches for the copolymer-related peaks (blue lines) suggests that copolymerization is the primary growth mechanism rather than homopolymerization of ppMAA or ppEGDMA. This indicates that despite the higher

concentration of EGDMA in the films, as concluded from the XPS analysis, the copolymerization is still the primary growth mechanism.

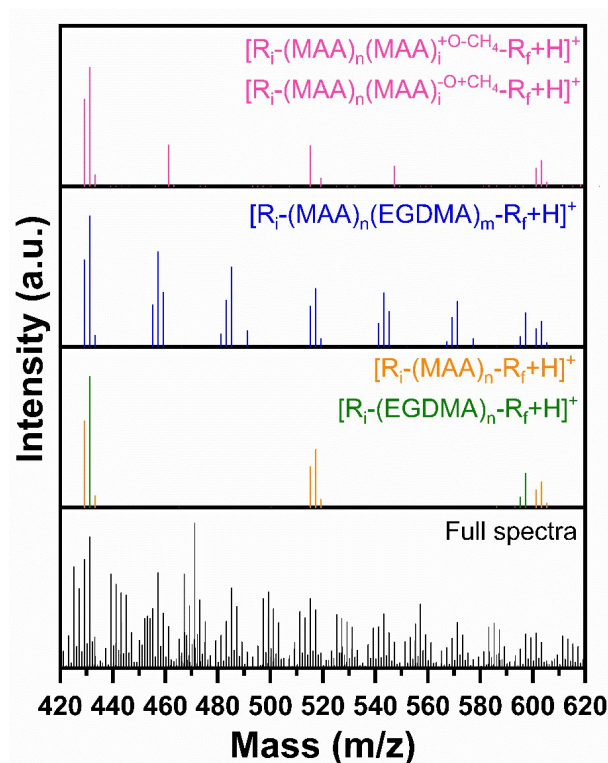


Figure 4.10: MALDI-HRMS spectra of the pp(10EGDMA:90MAA) copolymer films grown at a discharge frequency of 3000 Hz in the mass range $m/z = 420 - 620$. The full spectra of the sample are indicated in black line. Filtration of the full spectra from the sample to the matching mass are indicated in coloured lines.

4.2.3.3 Effect on the hydrophilicity of the surface of the films

Water contact angle (WCA) measurements were used to characterize the hydrophilicity of the surface of pp(EGDMA:MAA) films (Figure 4.11). For the following analysis, only the as-deposited solid films are considered, therefore excluding samples with 5 - 100 mol% EGDMA at 100 Hz. As expected, ppEGDMA exhibited higher WCA values than ppMAA films for all the f_{pe} . The WCA values for the homopolymers of ppMAA and ppEGDMA were approximately 15° and 70° , respectively, which align well with values reported in the literature for these homopolymers in conventional free-radical polymerization. The suggested influence of f_{pe} on the network structure of pp(EGDMA:MAA) likely accounts for the observed differences in WCA between the copolymers. The most notable difference was observed

between 100 Hz and 3000 Hz, with the WCA being approximately three times higher for 1 mol% EGDMA and twice as high for 2.5 mol% EGDMA.

Given our assumption that polymerizing films at 100 Hz resulted in a higher concentration of EGDMA in the polymer backbone, the observed increase in WCA values is consistent. To properly evaluate this assumption, it is expected that a higher concentration of EGDMA in these copolymers would lead to a greater degree of cross-linking within the polymeric network. This increased cross-linking would enhance the water stability of the thin film and demonstrate the formation of hydrogel materials. Consequently, the next section will focus on the differences in water stability among these films.

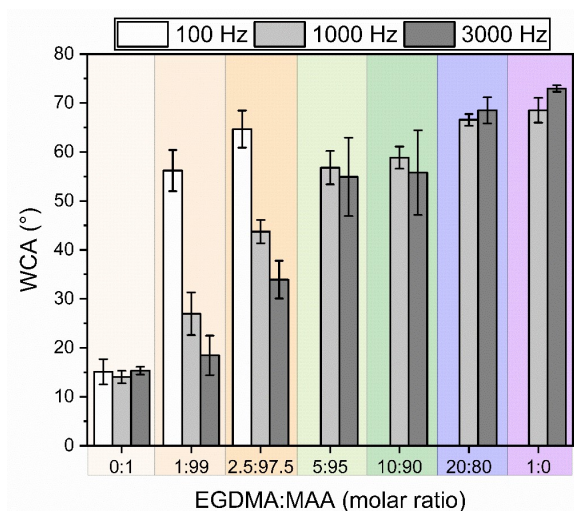


Figure 4.11: Water contact angle measurements of copolymer pp(EGDMA:MAA) films polymerized with different EGDMA:MAA molar ratios and pulse frequencies (100 - 3000 Hz). Error bars: means \pm SD (n=3).

4.2.3.4 Effect on the stability in water

In order to have a better understanding of any influence of f_{pe} and the ratio between comonomers in the liquid mixture on the stability in water of the plasma-polymerized films, the stability study was conducted in multiple steps. The detailed quantification of mass loss and the steps performed are described in Chapter 2. Hence, the mass loss in Step 1 is expected to be correlated with unreacted monomers trapped within the films and the mass loss in Step 3 is expected to be from the ppMAA homopolymers and oligomers (Figure 4.12). As previously

mentioned, the hydrophilic nature of ppMAA (across all f_{pe}) led to significant mass loss upon immersion in water, indicating a predominantly linear polymer structure with limited cross-linking. Conversely, ppEGDMA exhibited exceptional water stability, with negligible mass loss, suggesting the formation of a highly cross-linked network. The addition of EGDMA to the comonomer mixture resulted in a proportional decrease in mass loss, with the values in between the ones obtained for ppMAA and ppEGDMA. The effect of f_{pe} on water stability was pronounced at lower EGDMA concentrations (1 and 2.5 mol%). Notably, the addition of 1 mol% EGDMA resulted in a dramatic difference in mass loss, from 9.7% to 91.1% when obtained at 100 Hz and 3000 Hz, respectively. This low solubility in water can be attributed to a higher content of EGDMA in the polymeric network, as suggested by the previous results. Furthermore, from 5 mol% EGDMA, no significant differences in the mass loss were detected when varying the f_{pe} from 1000 to 3000 Hz.

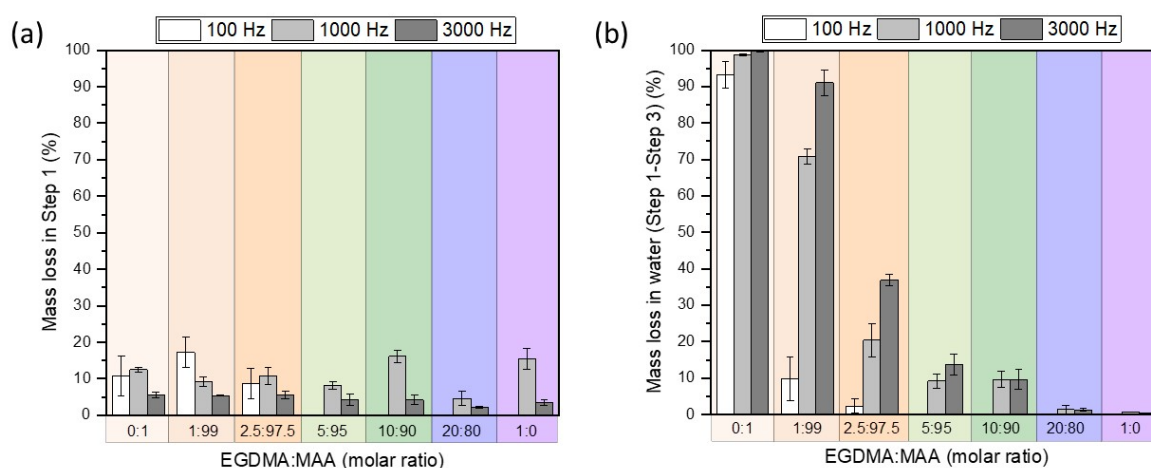


Figure 4.12: (a) Mass loss after step 1 and (b) mass loss between step 2 and step 3 of the pp(EGDMA:MAA) copolymer films for different EGDMA:MAA molar ratios grown from 100-3000 Hz. In “Step 1”, the as-deposited films were firstly placed in an oven at 60 °C for 24 hours and then cooled to room temperature for 2 hours inside a vacuum desiccator. After the purification process, the considered “Mass loss in water (Step 1-Step3)” was obtained. The mass loss in water is considered as the dried films (dried 24 h at 60 °C in drying oven and cooled at room temperature for 2 h in vacuum desiccator) of the films previously immersed in water for 24h. Error bars: means ± SD (n=3).

Overall, the plasma-polymerized films at 1000-3000 Hz led to the formation of solid films, apparent lower cross-linking of the polymeric networks and higher thickness and mass

growth rate (Figure B1) when compared to 100 Hz. Hence, further investigation for the samples prepared at 1000 and 3000 Hz with varying EGDMA concentrations (1-100%) were conducted.

4.2.3.5 Hydrogel films: swelling and viscoelastic properties

Certainly, to determine whether the poly(MAA-co-EGDMA) thin films produced in this chapter form hydrogel network structures, they should absorb and retain water while maintaining their structural integrity.^{1,2} Hence, the following section presents an analysis of the film's behavior in aqueous medium, focusing on determining swelling ratio and viscoelastic modulus.

4.2.3.5.1 QCM-D coupled with SE

A common method for determining hydrogel swelling ratio involves measuring the mass difference between the dry and swollen states. However, applying this approach to thin films deposited on a substrate can introduce significant inaccuracies due to the negligible mass of the thin film compared to the supporting substrate. Otherwise, the determination of the mechanical properties is typically assessed through surface analysis techniques such as AFM or nanoindentation since thin films are often not self-standing. Nevertheless, reporting data acquisition from such techniques is challenging due to the soft nature of hydrogels and the presence of water, making these time-consuming measurements and complex, especially when quantitative precision is required.^{215,216}

In this context, QCM-D coupled with SE offers a promising approach for characterizing the mechanical properties and swelling behavior of plasma-polymerized hydrogel films from dry to swollen states. For QCM-D measurements of hydrogels, it is often recommended to work with layers that have a thickness below 500 nm in their swollen state.^{217,218} To this end, the deposition process to coat QCM-D sensors was carried out using a reduced number of deposition passes. All plasma-polymerized films in their dry state were prepared with thickness ranging from ~ 65 to 145 nm (Table B4). Importantly, these films were designed not to follow a trend based on thickness for either the f_{pe} or EGDMA concentration. This ensures that the discussion of results focuses on effect of the variable parameters in the hydrogel properties (swelling and mechanical properties), rather than variations in these properties due to thickness.

Figure 4.13 presents QCM-D data, the vibrational dissipation (Figure 4.13) and resonant frequencies (Figure 4.13b) were recorded for approximately 60 minutes under wet dynamical measurements. The pp(EGDMA-co-MAA) copolymer films samples were produced at f_{pe} 3000 Hz from EGDMA:MAA mixtures with different molar ratios. Since QCM-D measures frequency changes of a quartz crystal caused by mass changes on its surface, the data can show qualitative information associated with mass uptake or loss in the medium.^{217–220} The slight drifting of the frequency signal towards higher values (inset in Figure 4.13b) observed on 1EGDMA_3000 and 2.5EGDMA_3000 likely suggests mass loss from the films in water. This mass loss could be attributed to unreacted monomers or water-soluble linear polymer chains. Figure 4.13b also indicates that 1EGDMA_3000 and 2.5EGDMA_3000 did not show a stable baseline within the measurement timeframe. In contrast, the 5EGDMA_3000 exhibited a potential initial mass loss followed by a stable baseline after a few minutes of water exposure.

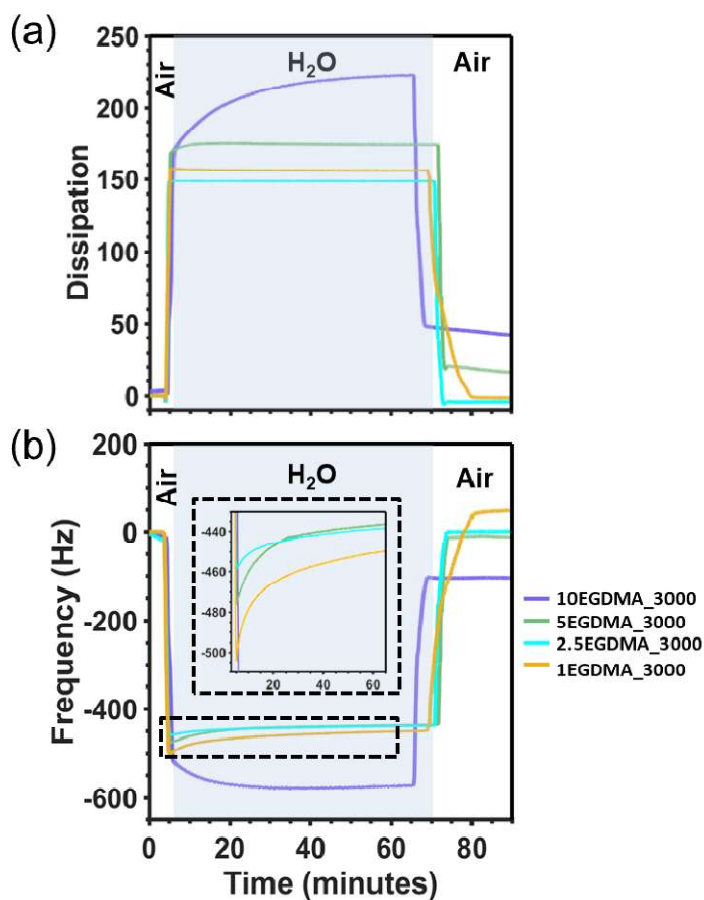


Figure 4.13: Representative QCM-D data obtained for the pp(EGDMA-co-MAA) copolymer films deposited at 3000 Hz from EGDMA:MAA mixtures with different molar ratios. Measured (a) vibrational dissipation (related to the viscoelastic behaviour) and (b) resonant frequencies (related with difference in mass) according to time passed during experiment.

Qualitative information can also be obtained by analyzing the behavior of the thin film when the water flow is stopped, the water is pump out from the chamber and replaced by air (time higher than 75 min in Figure 4.13). The difference between the thin film response under wet and air environments is evident and interesting. The 10EGDMA_3000 series demonstrates characteristic hydrogel film properties, as it absorbed water and exhibits a viscoelastic response with values different from the initial values (0 for $t = 0$ min) for resonant frequencies and vibrational dissipation, respectively.

Ultimately, a stable baseline signal is crucial for applying mathematical models to calculate swelling and viscoelastic modulus using QCM-D data. Therefore, further evaluation and discussion of these properties will focus on samples prepared with EGDMA concentrations ranging from 5 to 100 mol% and deposited at plasma frequencies of 1000 Hz and 3000 Hz, as these samples exhibited stable baselines during the measurement time.

4.2.3.5.2 Swelling ratio and viscoelastic properties

Figure 4.14 presents the swelling ratios obtained for the pp(EGDMA-co-MAA) hydrogels using both QCM-D and SE techniques. A clear difference is observed between the values obtained between the two methods. The consistently higher swelling ratios obtained by QCM-D (Figure 4.14a) measurements compared to SE (Figure 4.14b) likely originate from inherent differences in their sensitivities. SE relies on the change of the polarization state of the light as it is reflected from the film, providing information on the thickness and optical properties of the hydrogel film.^{221,222} On the other hand, QCM-D is sensible not only to the film mass itself but also to the mass of the water that is hydrodynamically bounded to the hydrogel surface.^{85,223–225} This explains the higher swelling ratios observed using QCM-D compared to SE, which aligns with previous findings for hydrogel films in aqueous environments.⁸⁵

To confirm that the significant difference in swelling ratios obtained by QCM-D and SE is attributed to the presence of a hydrated layer, further studies on these samples were conducted using a 3-step protocol. This protocol involved measurements in both heavy water (deuterium oxide, D₂O) and deionized water. While the experimental synthesis was performed by the author, the analysis and discussion of the results were carried out collaboratively by other researchers from the laboratory and published elsewhere.²²⁶ These findings are presented in

Annex C. In summary, the results corroborated with the presence of a hydrated layer at the hydrogel surface. Furthermore, the data suggested the possibility of a less-bounded water layer superstructure with a specific order that also vibrates with the sensor in response to the QCM-D measurement.

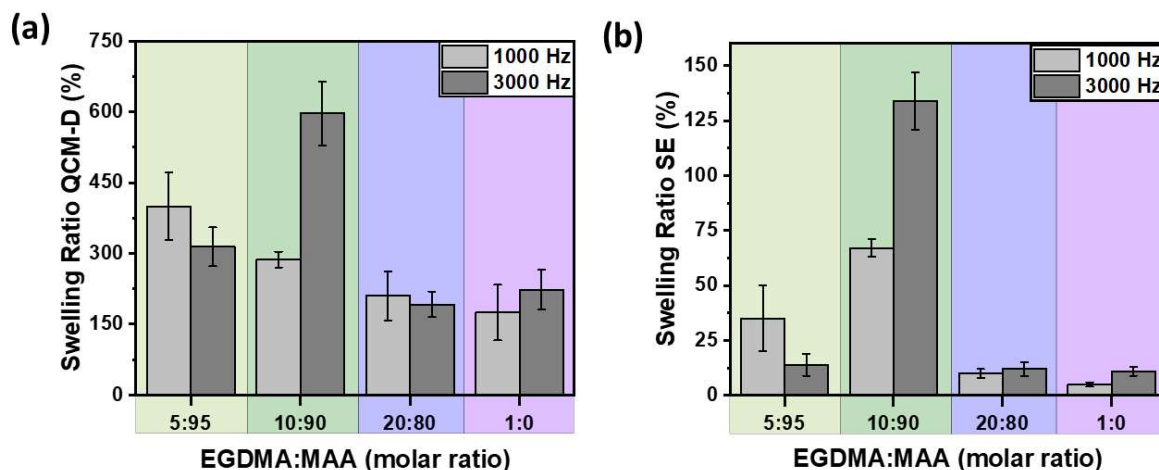


Figure 4.14: Swelling ratio in distilled water medium determined by (a) QCM-D and (b) SE of the pp(EGDMA-co-MAA) copolymer films grown at 1000 and 3000 Hz for different EGDMA:MAA molar ratios. Error bars: means \pm SD (n=2).

As expected, higher EGDMA concentrations in the liquid monomer mixture (i.e., 20 and 100 mol%) resulted in lower swelling ratios for both studied f_{pe} . The 20 mol% EGDMA concentration was chosen to induce a cross-linked network structure similar to ppEGDMA. The idea relied on increasing the probability for 1 mol of EGDMA to react 4 molecules of MAA and produce a structure such as shown in Figure 4.3. However, XPS analysis (Figure 4.9) indicated higher EGDMA reactivity. This resulted in an unforeseen cross-linker concentration reaching values of 68% and 80% for 1000 Hz and 3000 Hz, respectively, suggesting that a polymeric network structure would be closer to the ones formed in ppEGDMA. Notably, water stability measurements (Figure 4.12b) anticipated a highly cross-linked structure for these two concentrations, exhibiting neglectable mass loss, and the independence of the f_{pe} . Similarly, the swelling behavior of these samples also exhibited similar values and independence from f_{pe} . The very low swelling behavior observed for high chemical cross-linker concentrations during polymerization aligns with reports in the literature for hydrogel films, not only for plasma-

polymerized films.^{51,59,70,105} Higher chemical cross-linker concentration during polymerization decreases the swelling most likely by yielding smaller mesh size.^{69,227,228}

While it remains inconclusive if increasing the cross-linker concentration from 5 to 10% for the films grown at 1000 Hz will lead to higher swelling ratios, a clear trend is observed for films grown at 3000 Hz. For these films, increasing the concentration from 5 to 10% EGDMA leads to an increase in swelling ratios, while a further increase in EGDMA in the mixture leads to a decrease in the values measured by both techniques.

The most common tendency reported in the hydrogel literature is that increasing the cross-linking agent concentration decreases hydrogel swelling ratios.^{59,69,228} However, the influence of f_{pe} in this work cannot be disregarded. An increase in the plasma pulse frequency is expected to increase the fragmentation of molecules in the medium, consequently, increasing the plasma-formed free radicals.^{43,135,229} The free radicals can increase the termination by reaction with a growing chain, with mid-chain radicals or pendant vinyl groups of EGDMA already incorporated into a polymer backbone.^{81,230,231} The combined effects of f_{pe} and the presence of EGDMA molecules in all possible scenarios become evident. Ultimately, the formation of dangling chains (unattached polymer chains within the hydrogel network that are not fully cross-linked to the rest of the structure) can affect the properties of the formed structure. The result can be a network structure with increased branching and higher average molecular weight of the polymer chains between cross-links. Such network structure could explain the unexpectedly high swelling ratio measured.

Interestingly, Lee *et al.* also reported an unusual behavior in the swelling ratio of the hydrogel synthesized with a methacrylate and a cross-linking agent bearing vinyl groups using UV-initiated FRP.²³² In their study, increasing the concentration of chemical initiator or UV intensity also led to an increase in swelling ratios. A parallelism can be made to this work in the sense that increasing f_{pe} can indirectly lead to an increase in the concentration of initiating species by fragmentation. Furthermore, Lee *et al.* also considered chain scissions and an increase in dangling chains occurring at higher UV intensity, similar to the potential effects of increasing f_{pe} in this study.

In addition to the swelling ratio, the viscoelastic modulus of the swollen hydrogel films was also determined by QCM-D (Table 4.2). As expected from the swelling results, the 10EGDMA_3000 series exhibited the lowest viscoelastic modulus among the samples series

analyzed. Since the higher swelling ratios indicate a higher presence of absorbed water, a lower viscoelastic modulus of the entire system (film and water mass) is expected.

Table 4.2: Viscoelastic modulus determined in distilled water medium of the pp(EGDMA-co-MAA) copolymer films deposited at 1000 and 3000 Hz for EGDMA:MAA mixture of different molar ratios. Error bars: means \pm SD (n=2).

Pulse frequency (Hz)	EGDMA:MAA (mol:mol)	Viscoelastic Modulus (MPa)
1000	5:95	6.25 \pm 0.25
	10:90	0.11 \pm 0.02
	20:80	5.1 \pm 3.0
3000	5:95	3.2 \pm 0.6
	10:90	0.02 \pm 0.001
	20:80	11.5 \pm 0.7

4.2.3.5.3 Thickness and topography of the thin films

Motivated by the ability to control swelling ratio and viscoelastic modulus for the 10EGDMA:90MAA copolymer with varying f_{pe} of the nanosecond-pulsed plasma frequency, further characterizations were performed in these experimental conditions. Therefore, the following discussion will explore the effects of f_{pe} (1000 Hz and 3000 Hz) on the films with 10 mol% EGDMA.

The ability to tune film thickness from a few nanometers to micrometers by adjusting the number of runs of deposition runs can be interesting for the application of hydrogel (thin) films.^{85,233,234} For this reason, the film thickness evolution curves based on the f_{pe} and number of runs of the moving table are shown in Figure 4.15. Step-height procedure (scratching the coating with a sharp needle tip) by AFM and SE were used to determine the thickness of the studied hydrogel films.

Interestingly, for a low number of runs (up to 15), f_{pe} does not considerably affect the thickness of the hydrogel films (Figure 4.15b). Furthermore, the thickness seems to exhibit a linear relationship ($R^2=0.9$) with the number of runs in this range. In contrast, a higher number of runs (55 - 100) leads to a divergence in thickness between the two f_{pe} values. It is worth remarking that from profilometry measurements (Figure B1), 10EGDMA:90MAA copolymer thin films did not reveal a discrepancy between the thickness obtained at 1000 and 3000 Hz.

This apparent difference in trend likely arises from the resolution between these surface contact instruments. AFM measurements were the average of $20 \times 20 \mu\text{m}^2$ different regions, while profilometry relied on the measurement of approximately $300 \mu\text{m}$ profiles.

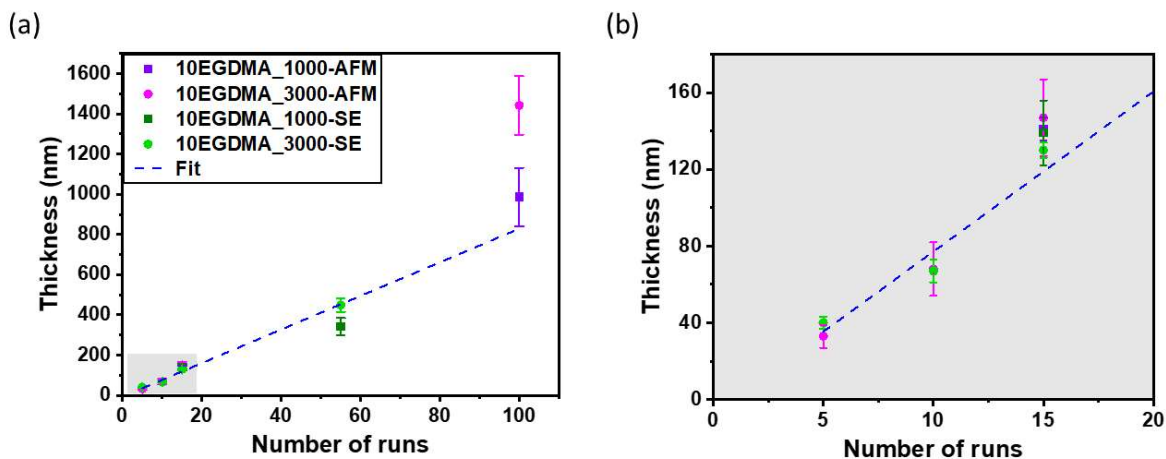


Figure 4.15: (a) Thickness values for different number of runs (0 - 100 runs) and f_{pe} determined by AFM and SE techniques. (b) Thickness values for different number of runs (0 - 15 runs) and f_{pe} determined by means of AFM and SE techniques.

Agreement between film thickness obtained by AFM and SE is noteworthy, particularly for samples with thicknesses ranging from 40 - 160 nm (used for dry hydrogel films in QCM-D/SE measurements). This consistency supports the proper fitting of the Cauchy layer considered within the physical model for thickness determination using SE data. Ultimately, thickness obtained by SE was not only used for swelling ratio calculations but also to determine the density for hydrogels in dry state in QCM-D measurements. Consequently, influencing the swelling ratios obtained by QCM-D.

Regarding topography of the plasma-polymerized hydrogels, AFM topography pictures are shown in Figure 4.16 and Figure B7, and roughness parameters summarized in Table B5. AFM analysis reveals apparently smooth surfaces at the nanoscale ($S_q = 0.8 \pm 0.4 \text{ nm}$, in average) regardless of f_{pe} or the number of runs of the moving table. The most interesting result comes from the phase images depicted in Figure 4.16c. A closer examination of these images reveals a consistent, small phase shift between samples obtained at 1000 Hz and 3000 Hz. This finding aligned with the mechanical differences observed in the viscoelastic modulus (Table

4.2).^{216,235} Samples showed in Figure B7 also showed the same trend. Furthermore, the phase images show homogenous cross-link distributions across the analyzed areas (evident from the well-defined Gaussian distributions), regardless of f_{pe} or the number of runs of the moving table.

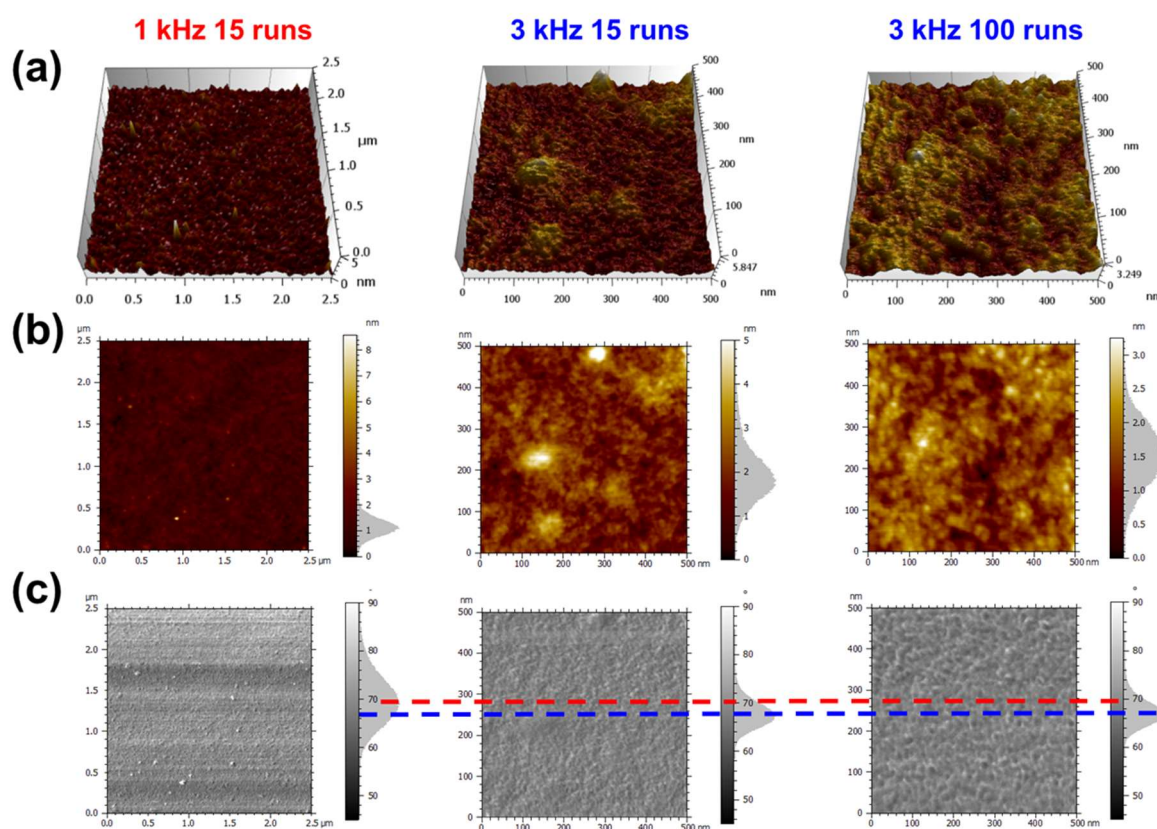


Figure 4.16: AFM pictures of the pp(10EGDMA:90MAA) films obtained at 1000 and 3000 Hz with the number of runs of the moving table of 15 and 100. (a) 3D height topographic images, (b) 2D height image; and (c) Phase images.

4.3 Conclusion

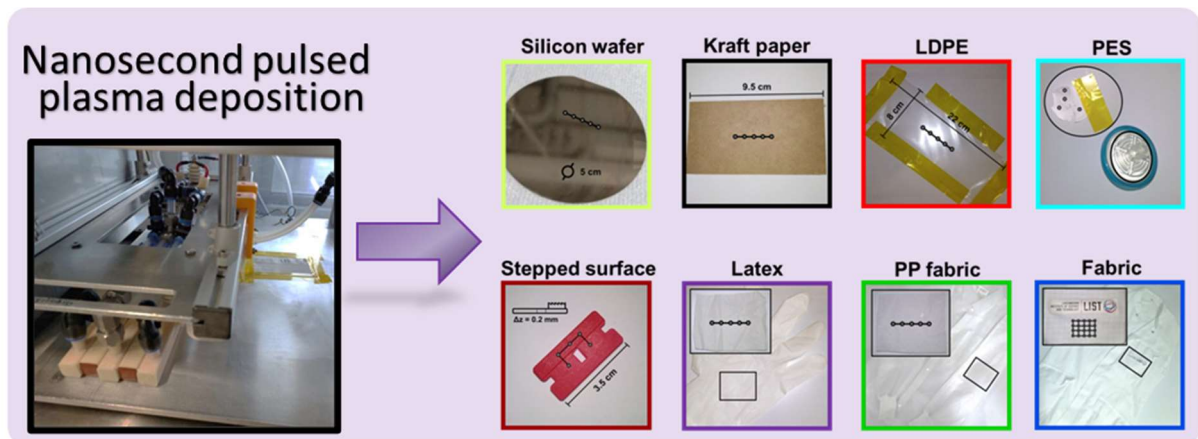
This chapter investigated the influence of pulse frequency and EGDMA as cross-linker agent in the synthesis of hydrogel films via nanosecond pulsed plasma polymerization of methacrylate monomers from liquid layers. Water-soluble ppMAA films were obtained for the investigated range of plasma pulse frequency. A comprehensive analysis of the film's chemistry, supported by FTIR, XPS, and MALDI-HRMS, revealed that growth of the

polymeric chains was most likely promoted by a FRP pathway. Furthermore, XPS and FTIR present functional group retention by comparing to the spectra of the commercially acquired pMAA.

Conversely, water-stable pp(MAA-co-EGDMA) copolymer films were successfully achieved by controlling pulse frequency and EGDMA concentrations. An important finding was that the fraction of EGDMA in the polymeric film was higher compared to its fraction in the liquid mixture, suggesting differing comonomer reactivity ratios. MALDI-HRMS complemented the results obtained by XPS, suggesting that the copolymerization is the primary growth mechanism rather than homopolymerization of ppMAA or ppEGDMA. Notably, hydrogels prepared at 3000 Hz with 10 mol% EGDMA exhibited significantly higher swelling ratios compared to those prepared at other combinations of pulse frequency and EGDMA concentration. Hence, this thesis reported for the first time the synthesis of MAA:EGDMA hydrogels with different swelling ratios and viscoelastic modulus by tuning the plasma pulse frequency.

These findings underscore the potential of nanosecond-pulsed plasma polymerization from methacrylate in liquid layers as a versatile technique for producing hydrogel films. Further exploration for the application of such engineered soft materials can be accessed in future works, focusing on the potential to be used as pH-responsive thanks to the retention of the carboxylic acid group in MAA.

Chapter 5 : Synthesis of thermoresponsive pp(PEGDMA₄₀₀) hydrogel films via liquid-assisted plasma-induced free-radical polymerization from liquid layers



5.1 Introduction

The previous chapter demonstrated the formation of hydrogels through the copolymerization of mono and bifunctional monomers to create a cross-linked network structure. An alternative strategy to synthesize hydrogel films is using a hydrophilic, bifunctional oligomer to induce chemical cross-linking via plasma-induced free-radical polymerization (FRP). In this approach, films containing polyethylene glycol (PEG) in their backbone are particularly attractive due to their well-established hydrophilicity, biocompatibility, and anti-biofouling properties.^{236–238}

The use of PEG in various biomedical and industrial applications is supported by extensive research.^{239–241} PEG-based polymers can be obtained by grafting PEG into polymer brushes (demonstrating superior antifouling characteristics)²⁴² or incorporating it into different systems, such as interpenetrating networks (leading to selective membranes with improved mechanical properties)^{243,244} or hydrogels (resulting in multi-platform systems with enhanced biocompatibility).^{245–247} In this sense, the development of PEG-based film hydrogels has generated lots of interest.^{248,249} However, the synthesis of controlled responsive PEG-hydrogels often involves complex and multi-step processes.³ The use of poly(ethylene glycol) dimethacrylate (PEGDMA) has been widely investigated due to the presence of the carboxylic groups and polymerizable bonds to grow polymeric chains.^{250,251} Hydrogels from PEGDMA can be easily initiated by introducing redox initiators like ammonium persulfate mixed with tetramethylethylenediamine, among others.^{252,253} Nonetheless, the incorporation of chemical cross-linkers and other additives might be detrimental for desired properties, such as biocompatibility and anti-biofouling.^{254,255}

In this chapter, the atmospheric-pressure nanosecond pulsed plasma polymerization from liquid layer of poly(ethylene glycol) dimethacrylate (PEGDMA₄₀₀, $M_{w,PEG} = 400$ g/mol) was demonstrated without the presence of chemical initiator and solvent. The chemistry and swelling of this one-step obtained hydrogel films were investigated. This chapter highlighted the potential for scalability and applicability to various substrates, including those with complex surface geometries and textiles. Furthermore, recent studies have demonstrated that textiles coated with plasma polymers exhibit tailored surface modifications without compromising the bulk properties and flexibility of the fabric.^{256–260} Motivated by this potential application,

hydrophilic properties before and after laundering test (washing machine) of the plasma polymerized PEGDMA₄₀₀ were also analyzed in this chapter.

5.2 Results and discussion

5.2.1 Coating deposition of PEGDMA₄₀₀ hydrogel films onto different substrates

Plasma polymerization is a well-established technique for depositing thin films on various material substrates, including ceramics and metals.^{31,32} To demonstrate the versatility of the approach used in this thesis for synthesizing hydrogels in a diverse range of interesting substrates (Table 5.1), plasma-polymerized PEGDMA₄₀₀ films were obtained at 3000 Hz. These substrates were selected to represent not only a wide spectrum of materials with different chemical nature, but also for their relevance to the clothing, food packaging and biomedical industries. It is important to note that while this approach offers versatility in substrate selection, one limitation exists. The discharge gap between the high-voltage electrodes and the bottom electrode (where the substrates are placed) was 1 mm for the DBD reactor used in this study. Larger gap distances are detrimental to achieve a stable laminar discharge in the plasma zone.^{261–263}

Table 5.1: List of the substrates investigated.

#	Substrate	Extracted from	Potential application
1	Polypropylene (PP) fabric	Laboratory coat (VWR [®])	Sportswear, food packaging, ropes, tapes, tote bags
2	Latex	Gloves (VWR [®])	Medical supplies, tire industry, clothing
3	Polyethersulfone (PES)	Membrane Filter (Acrodisc [®] , PALL)	Filtration system, respirator nebulizers, electrical insulator
4	Kraft paper	Paper foil (260 gr)	Food packaging

5	Stepped surface	Poly(lactic acid) (PLA) 3D printed support	Deposition on 3D materials with complex surface geometries. The support has a gap of 0.2 mm.
6	Low density polyethylene (LDPE)	Roll (Goodfellow Cambridge)	Enable to show scalability by applying to larger surface (22 cm x 8 cm)
7	Fabric	Laboratory coat (CAWE [®])	Clothing, shoes, bags, homewares

Compared to conventional methods to synthesize hydrogel films like combining UV curing with spin coating, this approach can offer some advantages. First, it enables scalable deposition on non-rigid and non-symmetrical materials (such as fabrics, paper and latex in Table 5.1), which can be challenging for spin coating technique. Second, it eliminates the need for solvents used in conventional methods, avoiding the additional steps of solvent dissolution and removal. Finally, plasma polymerization provides more homogeneous coatings on rough surfaces and those with complex geometries (such as 3D printed support in Table 5.1).

Naked-eye observations readily showed that the liquid and viscous monomer was converted into solid thin films after the plasma deposition process. This observation, consistent with findings from previous chapters, strongly suggest occurrence of a polymerization process. The films exhibited a change in physical state (indicative of polymer chain growth) and strong adhesion of the films to all the studied substrates as evidenced by finger-rubbing tests. The presence of the PEGDMA₄₀₀ films onto the substrates was further confirmed by FTIR analysis (Figure 5.1). To ensure coating homogeneity, several mappings were performed on the samples (circular marks in Figure 5.1).

Due to the inherent challenges in carrying out FTIR measurements on ultra-thin films (less than 200 nm) deposited on substrates of different nature, films prepared with a higher number of runs i.e. 100 were analyzed to improve the detection of the hydrogel coating. To identify the presence of PEGDMA₄₀₀ thin film hydrogels, uncoated substrates were measured beforehand and used as background references. Therefore, negative vibration bands, such as the characteristic vibrations appearing at 1350 – 1500 cm⁻¹ for latex substrate (indicated as purple line in Figure 5.1) attributed to the CH₃ asymmetric deformation of the polyisoprene compound,²⁶⁴ are expected.

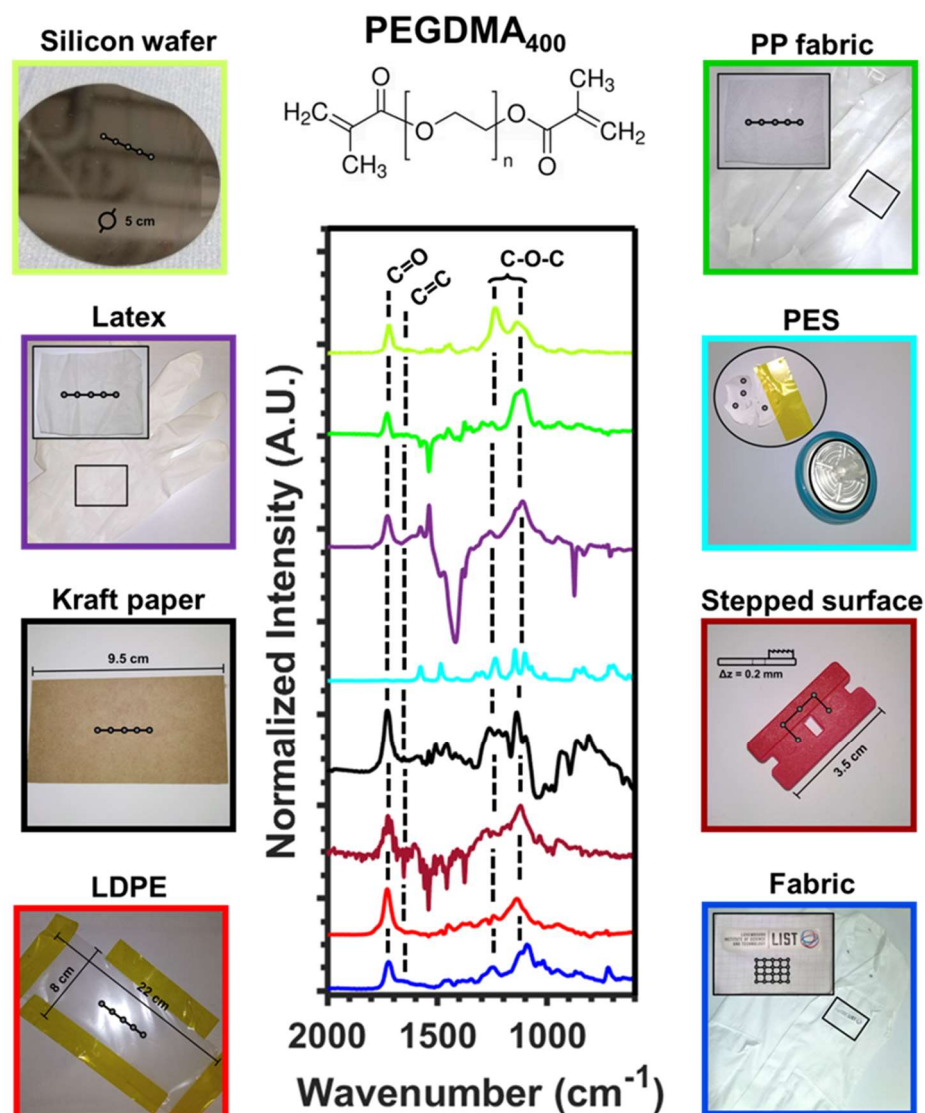


Figure 5.1: FTIR spectra of the films grown from PEGDMA₄₀₀ obtained at 3000 Hz coatings different substrates from manufactured materials. Above is shown the monomer PEGDMA₄₀₀ chemical structure. Circular marks inside the pictures indicate the positions of the measurements performed in each sample.

Figure 5.1 evidenced the deposition of PEGDMA₄₀₀ onto different substrates based on the characteristic vibrations bands observed at 1050 – 1300 and 1722 cm⁻¹ attributed to the C–O–C and C=O, respectively.¹⁸⁶ Interestingly, the sample deposited in PES substrate is the only one that does not show the distinctive C=O vibration. However, the presence of other identifiable band vibrations in this sample suggested a potential reaction between PEGDMA₄₀₀ and PES through C=O activation. Additionally, a comparison between the PEGDMA₄₀₀ monomer and the plasma polymer film deposited on a silicon wafer (Figure D1 in Annex D)

showed a great reduction of the bands at 1652 and 655 cm^{-1} , attributed to the vinyl groups, and shift of the C=O group to higher wavenumbers. These observations suggest the plasma-induced FRP polymerization of PEGDMA₄₀₀, triggering the cleavage of the C=C bond for the growth of the polymeric chains. The deposition on various substrates using nanosecond pulsed plasma polymerization, granting the deposition on delicate substrates (kraft paper or fabrics), large surfaces (LDPE) and stepped and rough surfaces.

5.2.2 Stability of the PEGDMA₄₀₀ hydrogel films deposited on textile substrate

Due to the high relevance of fabrics, further wettability studies on the PEGDMA₄₀₀ thin film hydrogels were performed by WCA measurements (Figure 5.2). As it is seen in Figure 5.2a, the laboratory fabric coat (without coating) shows a clear and stable hydrophobic behavior (WCA = 124.8°). On the contrary, the hydrophilic nature of the thin films appears for the coated fabric in Figure 2b, where the water droplets are clearly absorbed in < 60 s demonstrating the effect of the deposited PEGDMA₄₀₀.

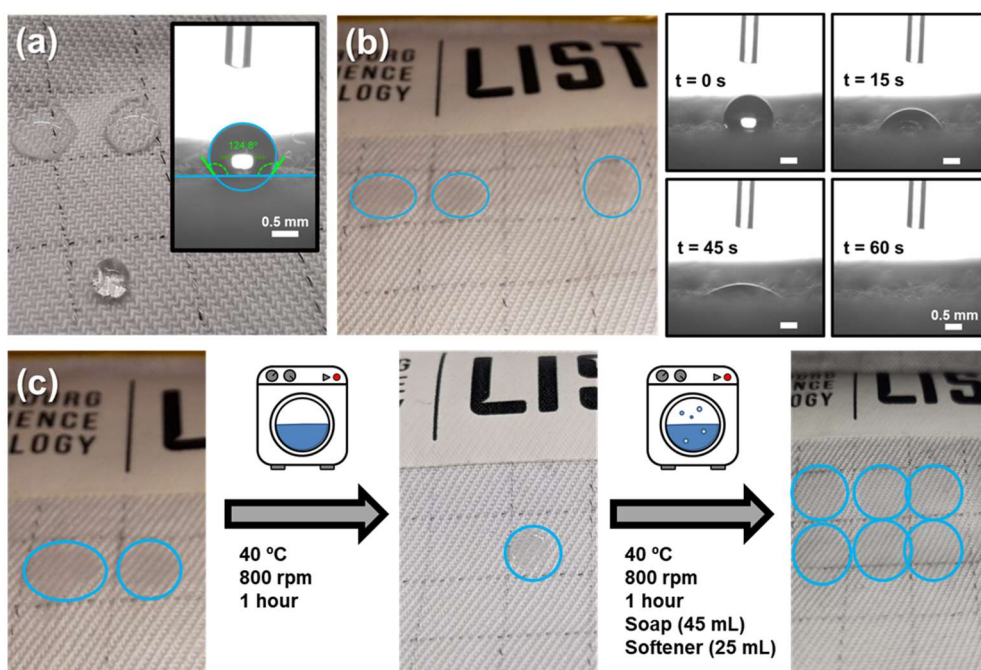


Figure 5.2: Wettability tests by means of WCA measurements conducted on (a) non coated laboratory coat fabric and (b) fabric coated with PEGDMA₄₀₀ thin film hydrogel. (c) Stability tests carried out on commercial laundry machines. Blue circles highlight the absorption of the water droplets.

Additionally, stability tests were carried out by washing the coated fabric in a commercial laundry machine considering two independent washing cycles (40 °C, 800 rpm and 1 hour) separated by 7 days. Gratifyingly, the wettability tests conducted after drying the samples at room temperature for 24 h confirmed the presence of the PEGDMA₄₀₀ hydrogel coatings even after using commercial soap and detergent (Figure 5.2c). Besides, WCA measurements were also performed to a non-coated laboratory fabric coat (Figure D2) after the washing tests to discard any effects arising from residual softener and/or soap on the fabric's wettability. Thus, the excellent stability and adhesion of the film was demonstrated by WCA and supported by FTIR analyses (Figure D3).

5.2.3 Swelling ratio and topology of the PEGDMA₄₀₀ hydrogel films

In order to study the swelling ratio and stability of the films under *in operando* conditions, samples were prepared with 5 runs and analyzed by QCM-D/SE technique. Results presented in Figure 5.3 show the mass change of hydrogel directly attributed to water absorption (increase and decrease of Δf and ΔD , respectively). Additionally, when the samples were exposed to air again (indicated as “wet” in Figure 5.3a) the hydrogels kept retaining some swollen water as indicated by $\Delta f < 0$. For all the conditions, the samples reached a plateau, confirming the stability of the coatings and allowing the quantification of the thickness of the swollen hydrogels, and thus, swelling ratio and extended viscoelastic model.^{217–220} Similar to the last chapter, the as-deposited thickness (dry film) showed similar values when analyzed by SE and by AFM (scratched film for step-height measurement in Figure 5.3b). Therefore, the swelling ratio could be obtained for the swollen samples in aqueous and air media in Figure 5.3b. Furthermore, from fitting the experimental data to the extended viscoelastic model of the immersed films, the viscoelastic modulus of the coatings of 4.97 kPa were obtained.

However, swelling ratios from the immersed samples showed higher values for QCM-D when compared to SE. Similar behavior for the values between techniques was observed in Chapter 4 for pp(MAA-co-EGDMA) films. Accordingly, the expected contribution of the mass of the hydrated layer can contribute to such divergence in values. Interestingly, similar values obtained by QCM-D and SE from the wet samples (swollen samples exposed to air) were measured. In air medium, the water trapped in the interface, and vibrating together with the sample during immersed condition, may be removed. Such behavior further corroborated with

the assumption that the hydrated layer and branched structure formed by plasma polymerized hydrogels can lead to these higher values measured by QCM-D technique, mentioned in the previous chapter. Finally, the topological characterization by AFM revealed smooth surfaces ($S_q = 3$ nm, Figure 5.3c) and homogenous coatings as indicated by the small variations observed in the AFM phase image (Figure 5.3d).

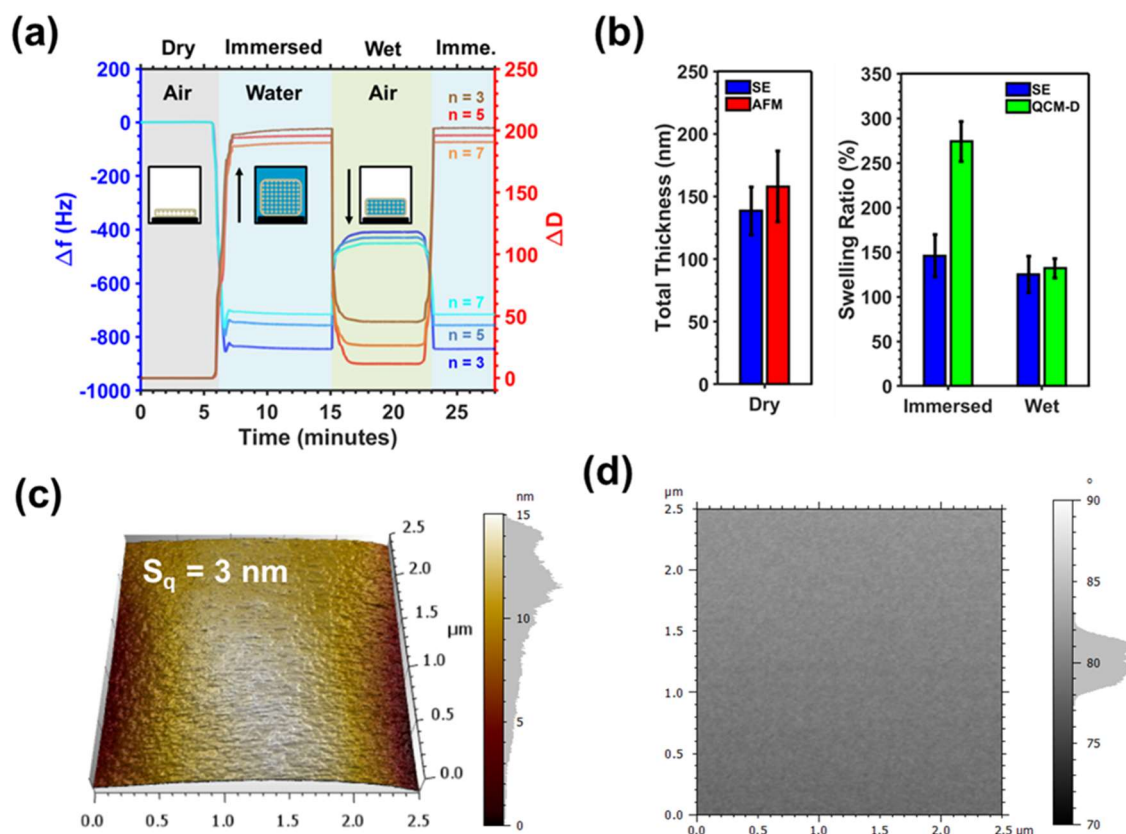


Figure 5.3: (a) QCM-D data obtained for PEGDMA₄₀₀. (b) Total thickness of the as-deposited films obtained by AFM and SE (left graph). Swelling ratio obtained from QCM-D and SE (right graph). (c) 3D height topographic images and (d) phase maps obtained by AFM analysis.

5.2.4 Thermoresponsive properties of the PEGDMA₄₀₀ hydrogel films

The thermoresponsive properties of the plasma polymerized PEDMA₄₀₀ were assessed from the QCM-D measurement carried out from room temperature to 44 °C in de-ionized water (Figure 5.4). Interestingly, a linear relationship between swelling ratio and temperature was observed (Figure 5.4b). Continuous changes in the swelling ratio with temperature might be related to hydrogen bonding exerting a force that constrains the polymer network. To confirm

this hypothesis, the same experiments were performed using D₂O, as it results in stronger hydrogen bonding.²⁶⁵ Accordingly, a higher decrease in the swelling ratio was observed for this condition (3.38 %·°C⁻¹) as compared to H₂O (1.43 %·°C⁻¹). The observed temperature responsiveness demonstrates potential for further studies for its application as stimulus responsive hydrogels.^{26,51,93}

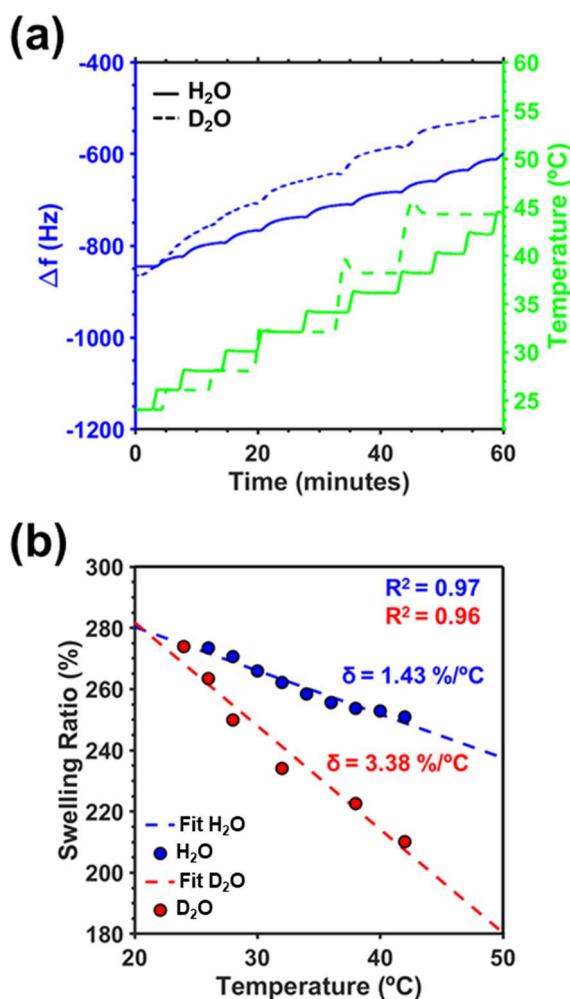


Figure 5.4: QCM-D measurements at different temperatures obtained for both de-ionized water (H₂O) and deuterium oxide (D₂O) media. (a) Raw data obtained and (b) dependence between swelling ratio and temperature.

5.3 Conclusion

This chapter demonstrated the use of nanosecond pulsed plasma for the polymerization and deposition of a PEG oligomer bearing dimethacrylate as polymerizable bond

(PEGDMA₄₀₀). The synthesis of the hydrogel films onto various substrates, such as paper, plastic, and textile, was confirmed by FTIR analysis. Further investigation into the application of this coating on textile substrates revealed a significant change in WCA, from 124.4° to a superhydrophilic character (less than 10° in a rapid water droplet spreading under a minute), observed before and after deposition, respectively. The coating even showed stability after the laundering test (two independent cycles in a washing machine), demonstrated by FTIR and WCA. Additionally, the swelling ratio of the films, analyzed by QCM-D in two different media (deionized water and D₂O), showed a linear relationship between the temperature and the swelling ratio, hinting at a potential thermo-responsive property.

This approach overcomes the limitations associated with conventional hydrogel thin film fabrication methods based only on high vapor pressure monomers, offering a scalable and environmentally friendly process. Furthermore, the deposited PEGDMA₄₀₀ hydrogels exhibited exceptional stability by laundering tests in fabrics, in water and thermoresponsive behavior. The swelling ratio obtained by *in operando* conditions through QCM-D coupled SE showed the retention of the swollen water in air media. Such properties highlight the potential biomedical application and further research of the plasma polymerized films as sensors or even as smart drug delivery hydrogels.

Chapter 6 : Conclusion and outlooks

This PhD dissertation provides an in-depth investigation of hydrogel films synthesized through plasma-induced free-radical polymerization (FRP). The deposition was carried out using nanosecond pulsed plasma discharges to induce the polymerization of hydrophilic methacrylate monomers as liquid layers. While previous studies have explored hydrogel synthesis via plasma polymerization, the correlation between the polymeric network structure and the properties of plasma-formed hydrogel films is still limited. Furthermore, this thesis aimed to gain further insight into the polymerization mechanism of liquid vinylic monomer layers using atmospheric-pressure plasma. Hence, this research aimed to bridge that gap by examining how various synthesis parameters in both the plasma and liquid phases influence the properties of the resulting films.

Firstly, the experimental work focused on studying the plasma-induced FRP of a model functional monomer for the deposition of hydrophilic polymer thin film (Chapter three). By varying important operational parameters, monomer spray rate and plasma pulse frequency were found to affect the resulting film characteristics of plasma-polymerized 2-hydroxyethyl methacrylate (HEMA).

Monomer conversion increased when combining high spray rates with frequencies above 100 Hz. Indeed, conversions over 90% were achieved under these conditions, and a logarithmic trend in monomer conversion from 30 to 3000 Hz was observed. Decreasing the spray rate enabled the achievement of a higher degree of conversion for all other conditions. It is worth noting that the lower monomer conversion was corroborated by GPC studies, which confirmed the formation of lower molecular weight oligomers compared to other conditions. These results were attributed to the concentration of free radicals in the liquid phase due to the fragmentation occurring during on-times of the plasma discharges. Particularly, the plasma-formed radicals can affect the molecular weight of the oligomers by affecting initiation and termination reactions in the FRP pathway.

Interestingly, MALDI-HRMS analysis provided essential information about the polymerization mechanism. HRMS enabled the identification of the end groups of the polymers grown in the FRP pathway as originating from the plasma-induced breakdown of a single σ -

bond in the monomer. Finally, in order to optimize the FRP pathway and minimize fragmentation and recombination reactions, guidelines were established based on the properties of the films. In particular, the combination of the highest plasma pulse frequency and high spray rate yielded the highest growth rate and the most regular polymer structure among the films studied.

The fourth chapter employed the same apparatus to synthesize hydrogel films via the copolymerization of methacrylic acid (MAA) and ethylene glycol dimethacrylate (EGDMA) used as the cross-linking agent. The deposition of water-soluble ppMAA homopolymers and pp(MAA-co-EGDMA) copolymers was obtained by varying the plasma pulse frequency and EGDMA concentration in the liquid mixture.

While the plasma pulse frequency had a negligible effect on the chemistry and water solubility of ppMAA homopolymer films, its influence on the chemistry and hydrogel properties was noticeable for pp(MAA-co-EGDMA) copolymer films. An important finding was that the fraction of EGDMA in the polymeric film was higher than in the liquid mixture, suggesting differing comonomer reactivity ratios. Additionally, samples with higher EGDMA fractions in the feed liquid mixture resulted in highly cross-linked structure, characterized by water stability and low water uptake, as evidenced by gravimetric measurements and QCM-D coupled SE, respectively. Notably, this study also revealed distinctive swelling ratios and viscoelastic properties by tuning the plasma pulse frequency (from 1000 to 3000 Hz). Finally, QCM-D and SE were shown to be powerful tools for characterizing hydrogel properties such as swelling ratios and viscoelastic modulus in ultrathin films synthesized by plasma, with film thicknesses on the order of 100 nm.

To further demonstrate the versatility of nanosecond-pulsed plasma in synthesizing hydrogels, plasma-induced FRP of polyethylene glycol dimethacrylate (PEGDMA₄₀₀, $M_{w,PEG} = 400 \text{ g}\cdot\text{mol}^{-1}$), a high molecular weight oligomer, was conducted in the fifth chapter. The plasma technology utilized in this thesis enabled the application of such films onto various substrates, including paper, plastic, and textiles. Additionally, the water-stable hydrogels exhibited thermo-responsive behaviour, as evidenced by QCM-D coupled SE. The QCM-D coupled SE technique proved to be a crucial tool for characterizing PEGDMA₄₀₀ and (MAA-co-EGDMA) hydrogels, providing insights into the hydrated layer, swelling ratio, and viscoelastic modulus.

Overall, this research provides a comprehensive understanding of the chemical structure and properties of hydrogels synthesized using atmospheric pressure nanosecond pulsed plasma from liquid layers. The findings lay the groundwork for future studies focused on understanding the influence of plasma pulse frequency and liquid parameters on hydrogel film network structures and properties.

Further studies on plasma-liquid interactions would significantly enhance the approach of forming hydrogels through plasma-induced FRP from liquid layers. In particular, investigating the penetration of the plasma species into the liquid phase by combining experimental data and simulations would offer valuable insights. Determining the kinetic parameters of polymerization would also be a notable advancement in the field of plasma-liquid interactions and plasma polymerization. Additionally, in situ chemical characterizations, such as FTIR, could provide valuable data to infer the lifetime and concentration of plasma-formed free radicals in the liquid phase.

Regarding the copolymerization to form hydrogels, future works could investigate other comonomer pairs with differing reactivity ratio and similar vapor pressures to enable a more comprehensive understanding of the copolymerization process. Also studying monomers with different functionalities (such as amines and methacrylates) would facilitate better quantification of the monomers in chemical analysis due to the presence of heteroatoms in one of them.

By combining experimental studies with simulations, future research could explore further the underlying polymerization mechanism and hydrogel formation. This would enable a macromolecular level of understanding of the polymer topology (such as long or short branches) and molecular arrangement in the copolymer (i.e., random or blocky). Additionally, applicative studies of these materials in various fields, such as biomedical devices, drug delivery, and tissue engineering, as well as their potential smart/stimuli responsiveness properties represent promising fields for further investigation.

Lastly, understanding other polymerization mechanisms, such as ring-opening polymerization induced by plasma, and combining this knowledge with plasma-induced FRP could represent a potential pathway to form interpenetrated polymer networks hydrogels solely through plasma technology.

PUBLICATION LIST

1. List of conferences

- Poster presentation at MRT/DPhyMS PhD day and DPPM General Assembly 2022
- Oral presentation at the international conference Plasma tech 2023
- Poster presentation at international conference PLATHINIUM 2023

2. List of publications

- Azevedo Gonçalves, I.; Abessolo Ondo, D.; Boscher, N. D.; Quintana, R. Free-Radical Polymerization of Liquid Hydroxyethyl Methacrylate Layers Using Nanosecond Plasma Pulses. <https://doi.org/10.1002/ppap.202400224>
- Sans, J., Azevedo Gonçalves, I., Quintana, R. Ultrathin Film Hydrogels with Controlled Swelling and Viscoelastic Properties Deposited by Nanosecond Pulsed Plasma Induced-Polymerization. *Adv. Mater. Interfaces* **2024**, *11* (2), 2300644. <https://doi.org/10.1002/admi.202300644>.
- Sans, J.; Azevedo Gonçalves, I.; Quintana, R. Establishing Quartz Crystal Microbalance with Dissipation (QCM-D) Coupled with Spectroscopic Ellipsometry (SE) as an Advantageous Technique for the Characterization of Ultra-Thin Film Hydrogels. *Small* **2024**, *20* (30), 2312041. <https://doi.org/10.1002/sml.202312041>.
- J. Sans, I. Azevedo Gonçalves, D. Cardenas-Morcoso, R. Quintana, Synthesis of Ultrathin Film PEGDMA Hydrogels Coated onto Different Surfaces by Atmospheric Pressure Plasma: Characterization and Potential Features for the Biomedical Field. *Macromol. Mater. Eng.* **2024**, 2400230. <https://doi.org/10.1002/mame.202400230>

REFERENCES

- (1) Richbourg, N. R.; Peppas, N. A. The Swollen Polymer Network Hypothesis: Quantitative Models of Hydrogel Swelling, Stiffness, and Solute Transport. *Prog. Polym. Sci.* **2020**, *105*, 101243. <https://doi.org/10.1016/j.progpolymsci.2020.101243>.
- (2) Peppas, N. A.; Huang, Y.; Torres-Lugo, M.; Ward, J. H.; Zhang, J. Physicochemical Foundations and Structural Design of Hydrogels in Medicine and Biology. *Annu. Rev. Biomed. Eng.* **2000**, *2*, 9–29. <https://doi.org/10.1146/annurev.bioeng.2.1.9>.
- (3) Sikdar, P.; Uddin, M. M.; Dip, T. M.; Islam, S.; Hoque, M. S.; Dhar, A. K.; Wu, S. Recent Advances in the Synthesis of Smart Hydrogels. *Mater. Adv.* **2021**, *2* (14), 4532–4573. <https://doi.org/10.1039/D1MA00193K>.
- (4) Sandolo, C.; Coviello, T.; Matricardi, P.; Alhaique, F. Characterization of Polysaccharide Hydrogels for Modified Drug Delivery. *European Biophysics Journal.* 2007. <https://doi.org/10.1007/s00249-007-0158-y>.
- (5) Singhal, R.; Gupta, K. A Review: Tailor-Made Hydrogel Structures (Classifications and Synthesis Parameters). *Polym. Plast. Technol. Eng.* **2016**, *55* (1), 54–70. <https://doi.org/10.1080/03602559.2015.1050520>.
- (6) Tang, G.; Zhou, B.; Li, F.; Wang, W.; Liu, Y.; Wang, X.; Liu, C.; Ye, X. Advances of Naturally Derived and Synthetic Hydrogels for Intervertebral Disk Regeneration. *Front. Bioeng. Biotechnol.* **2020**, *8*.
- (7) Gyles, D. A.; Castro, L. D.; Silva, J. O. C.; Ribeiro-Costa, R. M. A Review of the Designs and Prominent Biomedical Advances of Natural and Synthetic Hydrogel Formulations. *Eur. Polym. J.* **2017**, *88*, 373–392. <https://doi.org/https://doi.org/10.1016/j.eurpolymj.2017.01.027>.
- (8) Hameed, H.; Faheem, S.; Paiva-Santos, A. C.; Sarwar, H. S.; Jamshaid, M. A Comprehensive Review of Hydrogel-Based Drug Delivery Systems: Classification, Properties, Recent Trends, and Applications. *AAPS PharmSciTech* **2024**, *25* (4), 64. <https://doi.org/10.1208/s12249-024-02786-x>.
- (9) Aswathy, S. H.; Narendrakumar, U.; Manjubala, I. Commercial Hydrogels for

- Biomedical Applications. *Heliyon* **2020**, *6* (4), e03719. <https://doi.org/https://doi.org/10.1016/j.heliyon.2020.e03719>.
- (10) Steele, A. N.; Stapleton, L. M.; Farry, J. M.; Lucian, H. J.; Paulsen, M. J.; Eskandari, A.; Hironaka, C. E.; Thakore, A. D.; Wang, H.; Yu, A. C.; Chan, D.; Appel, E. A.; Woo, Y. J. A Biocompatible Therapeutic Catheter-Deliverable Hydrogel for in Situ Tissue Engineering. *Advanced Healthcare Materials*. 2019. <https://doi.org/10.1002/adhm.201801147>.
- (11) Tovar-Carrillo, K. L.; Saucedo-Acuña, R. A.; Ríos-Arana, J. V; Tamayo, G.; Guzmán-Gastellum, D. A.; Díaz-Torres, B. A.; Nava-Martínez, S. D.; Espinosa-Cristóbal, L. F.; Cuevas-González, J. C. Synthesis, Characterization, and *In Vitro* and *In Vivo* Evaluations of Cellulose Hydrogels Enriched With *Larrea Tridentata* for Regenerative Applications. *Biomed Res. Int.* **2020**, 1–11. <https://doi.org/10.1155/2020/1425402>.
- (12) Hu, S.; Pei, X.; Duan, L.; Zhu, Z.; Liu, Y.; Chen, J.; Chen, T.; Ji, P.; Wan, Q.; Wang, J. A Mussel-Inspired Film for Adhesion to Wet Buccal Tissue and Efficient Buccal Drug Delivery. *Nat. Commun.* **2021**, *12* (1), 1689. <https://doi.org/10.1038/s41467-021-21989-5>.
- (13) Tian, Y.; Wang, Z.; Cao, S.; Liu, D.; Zhang, Y.; Chen, C.; Jiang, Z.; Ma, J.; Wang, Y. Connective Tissue Inspired Elastomer-Based Hydrogel for Artificial Skin via Radiation-Induced Penetrating Polymerization. *Nat. Commun.* **2024**, *15* (1), 636. <https://doi.org/10.1038/s41467-024-44949-1>.
- (14) El-Husseiny, H. M.; Mady, E. A.; Hamabe, L.; Abugomaa, A.; Shimada, K.; Yoshida, T.; Tanaka, T.; Yokoi, A.; Elbadawy, M.; Tanaka, R. Smart/Stimuli-Responsive Hydrogels: Cutting-Edge Platforms for Tissue Engineering and Other Biomedical Applications. *Mater. Today Bio* **2022**, *13*, 100186. <https://doi.org/https://doi.org/10.1016/j.mtbio.2021.100186>.
- (15) Tran, C. M.; Kim, J.; Yoon, J. Oxygen-Tolerant Fabrication of Large-Area Hydrogel Films via Photoinduced Electron/Energy Transfer-Reversible Addition–Fragmentation Chain Transfer Polymerization. *ACS Appl. Polym. Mater.* **2024**, *6* (6), 3326–3334. <https://doi.org/10.1021/acsapm.3c03146>.
- (16) Liu, Y.; Yang, T.; Zhang, Y.; Qu, G.; Wei, S.; Liu, Z.; Kong, T. Ultrastretchable and

- Wireless Bioelectronics Based on All-Hydrogel Microfluidics. *Adv. Mater.* **2019**, *31* (39). <https://doi.org/10.1002/adma.201902783>.
- (17) Ohm, Y.; Pan, C.; Ford, M. J.; Huang, X.; Liao, J.; Majidi, C. An Electrically Conductive Silver–Polyacrylamide–Alginate Hydrogel Composite for Soft Electronics. *Nat. Electron.* **2021**, *4* (3), 185–192. <https://doi.org/10.1038/s41928-021-00545-5>.
- (18) Zhang, X.; Guan, Y.; Zhang, Y. Ultrathin Hydrogel Films for Rapid Optical Biosensing. *Biomacromolecules* **2012**, *13* (1), 92–97. <https://doi.org/10.1021/bm2012696>.
- (19) Liu, Z.; Wang, Y.; Ren, Y.; Jin, G.; Zhang, C.; Chen, W.; Yan, F. Poly(Ionic Liquid) Hydrogel-Based Anti-Freezing Ionic Skin for a Soft Robotic Gripper. *Mater. Horizons* **2020**, *7* (3), 919–927. <https://doi.org/10.1039/C9MH01688K>.
- (20) Zhang, Y.; Wang, Y.; Wang, H.; Yu, Y.; Zhong, Q.; Zhao, Y. Super-Elastic Magnetic Structural Color Hydrogels. *Small* **2019**, *15* (35). <https://doi.org/10.1002/smll.201902198>.
- (21) Kang, Y.; Walish, J. J.; Gorishnyy, T.; Thomas, E. L. Broad-Wavelength-Range Chemically Tunable Block-Copolymer Photonic Gels. *Nat. Mater.* **2007**, *6* (12), 957–960. <https://doi.org/10.1038/nmat2032>.
- (22) Dong, M.; Jiao, D.; Zheng, Q.; Wu, Z. L. Recent Progress in Fabrications and Applications of Functional Hydrogel Films. *J. Polym. Sci.* **2023**, *61* (11), 1026–1039. <https://doi.org/10.1002/pol.20220451>.
- (23) Liu, J.; Qu, S.; Suo, Z.; Yang, W. Functional Hydrogel Coatings. *Natl. Sci. Rev.* **2021**, *8* (2). <https://doi.org/10.1093/nsr/nwaa254>.
- (24) Correa, S.; Grosskopf, A. K.; Lopez Hernandez, H.; Chan, D.; Yu, A. C.; Stapleton, L. M.; Appel, E. A. Translational Applications of Hydrogels. *Chem. Rev.* **2021**, *121* (18), 11385–11457. <https://doi.org/10.1021/acs.chemrev.0c01177>.
- (25) Lee, S. C.; Kwon, I. K.; Park, K. Hydrogels for Delivery of Bioactive Agents: A Historical Perspective. *Adv. Drug Deliv. Rev.* **2013**, *65* (1), 17–20. <https://doi.org/https://doi.org/10.1016/j.addr.2012.07.015>.
- (26) White, E. M.; Yatvin, J.; Grubbs, J. B.; Bilbrey, J. A.; Locklin, J. Advances in Smart Materials: Stimuli-Responsive Hydrogel Thin Films. *J. Polym. Sci. Part B Polym. Phys.*

- 2013**, *51* (14), 1084–1099. <https://doi.org/10.1002/polb.23312>.
- (27) Di Lorenzo, F.; Seiffert, S. Nanostructural Heterogeneity in Polymer Networks and Gels. *Polym. Chem.* **2015**, *6* (31), 5515–5528. <https://doi.org/10.1039/C4PY01677G>.
- (28) Ida, S. Structural Design of Vinyl Polymer Hydrogels Utilizing Precision Radical Polymerization. *Polym. J.* **2019**, *51* (9), 803–812. <https://doi.org/10.1038/s41428-019-0204-5>.
- (29) Bauer, M.; Duerkop, A.; Baeumner, A. J. Critical Review of Polymer and Hydrogel Deposition Methods for Optical and Electrochemical Bioanalytical Sensors Correlated to the Sensor's Applicability in Real Samples. *Anal. Bioanal. Chem.* **2023**, *415* (1), 83–95. <https://doi.org/10.1007/s00216-022-04363-2>.
- (30) Guimarães, C. F.; Ahmed, R.; Marques, A. P.; Reis, R. L.; Demirci, U. Engineering Hydrogel-Based Biomedical Photonics: Design, Fabrication, and Applications. *Adv. Mater.* **2021**, *33* (23). <https://doi.org/10.1002/adma.202006582>.
- (31) Jarvis, K. L.; Majewski, P. Optimization of Plasma Polymerized Ethylenediamine Film Chemistry on Quartz Particles. *Plasma Process. Polym.* **2013**, *10* (7), 619–626. <https://doi.org/https://doi.org/10.1002/ppap.201200143>.
- (32) Khelifa, F.; Ershov, S.; Habibi, Y.; Snyders, R.; Dubois, P. Free-Radical-Induced Grafting from Plasma Polymer Surfaces. *Chem. Rev.* **2016**, *116* (6), 3975–4005. <https://doi.org/10.1021/acs.chemrev.5b00634>.
- (33) Friedrich, J. Mechanisms of Plasma Polymerization – Reviewed from a Chemical Point of View. *Plasma Process. Polym.* **2011**, *8* (9), 783–802. <https://doi.org/https://doi.org/10.1002/ppap.201100038>.
- (34) Thiry, D.; Reniers, F.; Snyders, R. A Joint Mechanistic Description of Plasma Polymers Synthesized at Low and Atmospheric Pressure; Pinson, J., Thiry, D., Eds.; 2019; pp 67–106. <https://doi.org/10.1002/9783527819249.ch3>.
- (35) Fridman, A. Organic and Polymer Plasma Chemistry. In *Plasma Chemistry*; Fridman, A., Ed.; Cambridge University Press: Cambridge, 2008; pp 589–675. <https://doi.org/DOI: 10.1017/CBO9780511546075.011>.
- (36) Hegemann, D.; Körner, E.; Guimond, S. Plasma Polymerization of Acrylic Acid

- Revisited. *Plasma Process. Polym.* **2009**, *6* (4), 246–254.
<https://doi.org/10.1002/ppap.200800089>.
- (37) Mertens, J.; Baneton, J.; Ozkan, A.; Pospisilova, E.; Nysten, B.; Delcorte, A.; Reniers, F. Atmospheric Pressure Plasma Polymerization of Organics: Effect of the Presence and Position of Double Bonds on Polymerization Mechanisms, Plasma Stability and Coating Chemistry. *Thin Solid Films* **2019**, *671*, 64–76.
<https://doi.org/https://doi.org/10.1016/j.tsf.2018.12.036>.
- (38) Michelmore, A.; Gross-Kosche, P.; Al-Bataineh, S. A.; Whittle, J. D.; Short, R. D. On the Effect of Monomer Chemistry on Growth Mechanisms of Nonfouling PEG-like Plasma Polymers. *Langmuir* **2013**, *29* (8), 2595–2601.
<https://doi.org/10.1021/la304713b>.
- (39) Hegemann, D.; Michlíček, M.; Blanchard, N. E.; Schütz, U.; Lohmann, D.; Vandenbossche, M.; Zajíčková, L.; Drábik, M. Deposition of Functional Plasma Polymers Influenced by Reactor Geometry in Capacitively Coupled Discharges. *Plasma Process. Polym.* **2016**, *13* (2), 279–286.
<https://doi.org/https://doi.org/10.1002/ppap.201500078>.
- (40) Klages, C.-P.; Höpfner, K.; Kläke, N.; Thyen, R. Surface Functionalization at Atmospheric Pressure by DBD-Based Pulsed Plasma Polymerization. *Plasmas Polym.* **2000**, *5* (2), 79–89. <https://doi.org/10.1023/A:1009583815474>.
- (41) Tarducci, C.; Schofield, W. C. E.; Badyal, J. P. S.; Brewer, S. A.; Willis, C. Monomolecular Functionalization of Pulsed Plasma Deposited Poly(2-Hydroxyethyl Methacrylate) Surfaces. *Chem. Mater.* **2002**, *14* (6), 2541–2545.
<https://doi.org/10.1021/cm010939z>.
- (42) Boscher, N. D.; Hilt, F.; Duday, D.; Frache, G.; Fouquet, T.; Choquet, P. Atmospheric Pressure Plasma Initiated Chemical Vapor Deposition Using Ultra-Short Square Pulse Dielectric Barrier Discharge. *Plasma Process. Polym.* **2015**, *12* (1), 66–74.
<https://doi.org/https://doi.org/10.1002/ppap.201400094>.
- (43) Loyer, F.; Frache, G.; Choquet, P.; Boscher, N. D. Atmospheric Pressure Plasma-Initiated Chemical Vapor Deposition (AP-PiCVD) of Poly(Alkyl Acrylates): An Experimental Study. *Macromolecules* **2017**, *50* (11), 4351–4362.

<https://doi.org/10.1021/acs.macromol.7b00461>.

- (44) Abessolo Ondo, D.; Loyer, F.; Boscher, N. D. Influence of Double Bonds and Cyclic Structure on the AP-PECVD of Low-k Organosilicon Insulating Layers. *Plasma Process. Polym.* **2021**. <https://doi.org/10.1002/ppap.202000222>.
- (45) Hegemann, D.; Gaiser, S. Plasma Surface Engineering for Manmade Soft Materials: A Review. *J. Phys. D. Appl. Phys.* **2022**, *55* (17), 173002. <https://doi.org/10.1088/1361-6463/ac4539>.
- (46) Hieda, J.; Nakashima, H.; Hirano, M. Synthesis of Poly(N-Isopropylacrylamide) by Plasma-in-Liquid Process. *Jpn. J. Appl. Phys.* **2021**, *60* (4), 046004. <https://doi.org/10.35848/1347-4065/abec9b>.
- (47) Jalaber, V.; Del Frari, D.; De Winter, J.; Mehennaoui, K.; Planchon, S.; Choquet, P.; Detrembleur, C.; Moreno-Couranjou, M. Atmospheric Aerosol Assisted Pulsed Plasma Polymerization: An Environmentally Friendly Technique for Tunable Catechol-Bearing Thin Films. *Front. Chem.* **2019**, *7* (APR), 1–12. <https://doi.org/10.3389/fchem.2019.00183>.
- (48) Carton, O.; Salem, D. Ben; Pulpytel, J.; Arefi-Khonsari, F. Improvement of the Water Stability of Plasma Polymerized Acrylic Acid/MBA Coatings Deposited by Atmospheric Pressure Air Plasma Jet. *Plasma Chem. Plasma Process.* **2015**, *35* (5), 819–829. <https://doi.org/10.1007/s11090-015-9634-9>.
- (49) Jang, H. J.; Jung, E. Y.; Parsons, T.; Tae, H. S.; Park, C. S. A Review of Plasma Synthesis Methods for Polymer Films and Nanoparticles under Atmospheric Pressure Conditions. *Polymers (Basel)*. **2021**, *13* (14). <https://doi.org/10.3390/polym13142267>.
- (50) Carton, O.; Ben Salem, D.; Bhatt, S.; Pulpytel, J.; Arefi-Khonsari, F. Plasma Polymerization of Acrylic Acid by Atmospheric Pressure Nitrogen Plasma Jet for Biomedical Applications. *Plasma Process. Polym.* **2012**, *9* (10), 984–993. <https://doi.org/10.1002/ppap.201200044>.
- (51) Jovančić, P.; Vílchez, A.; Molina, R. Synthesis of Thermo-Sensitive Hydrogels from Free Radical Copolymerization of NIPAAm with MBA Initiated by Atmospheric Plasma Treatment. *Plasma Process. Polym.* **2016**, *13* (7), 752–760.

<https://doi.org/10.1002/ppap.201500194>.

- (52) Czuba, U.; Quintana, R.; De Pauw-Gillet, M. C.; Bourguignon, M.; Moreno-Couranjou, M.; Alexandre, M.; Detrembleur, C.; Choquet, P. Atmospheric Plasma Deposition of Methacrylate Layers Containing Catechol/Quinone Groups: An Alternative to Polydopamine Bioconjugation for Biomedical Applications. *Adv. Healthc. Mater.* **2018**, *7* (11), 1–11. <https://doi.org/10.1002/adhm.201701059>.
- (53) Makhneva, E.; Barillas, L.; Farka, Z.; Pastucha, M.; Skládal, P.; Weltmann, K. D.; Fricke, K. Functional Plasma Polymerized Surfaces for Biosensing. *ACS Appl. Mater. Interfaces* **2020**, *12* (14), 17100–17112. <https://doi.org/10.1021/acsami.0c01443>.
- (54) Molina, R.; Maria Teixido, J.; Kan, C.-W.; Jovancic, P. Hydrophobic Coatings on Cotton Obtained by in Situ Plasma Polymerization of a Fluorinated Monomer in Ethanol Solutions. *ACS Appl. Mater. Interfaces* **2017**, *9* (6), 5513–5521. <https://doi.org/10.1021/acsami.6b15812>.
- (55) Klinger, D.; Landfester, K. Stimuli-Responsive Microgels for the Loading and Release of Functional Compounds: Fundamental Concepts and Applications. *Polymer (Guildf)*. **2012**, *53* (23), 5209–5231. <https://doi.org/10.1016/j.polymer.2012.08.053>.
- (56) Khurana, B.; Gierlich, P.; Meindl, A.; Gomes-da-Silva, L. C.; Senge, M. O. Hydrogels: Soft Matters in Photomedicine. *Photochem. Photobiol. Sci.* **2019**, *18* (11), 2613–2656. <https://doi.org/10.1039/c9pp00221a>.
- (57) Patel, A.; Mequanint, K. Hydrogel Biomaterials. In *Biomedical Engineering*; Fazel-Rezai, R., Ed.; IntechOpen: Rijeka, 2011. <https://doi.org/10.5772/24856>.
- (58) Gu, S.; Cheng, G.; Yang, T.; Ren, X.; Gao, G. Mechanical and Rheological Behavior of Hybrid Cross-Linked Polyacrylamide/Cationic Micelle Hydrogels. *Macromolecular Materials and Engineering*. 2017. <https://doi.org/10.1002/mame.201700402>.
- (59) Lin, C.-C.; Anseth, K. S. PEG Hydrogels for the Controlled Release of Biomolecules in Regenerative Medicine. *Pharm. Res.* **2009**, *26* (3), 631–643. <https://doi.org/10.1007/s11095-008-9801-2>.
- (60) Norioka, C.; Inamoto, Y.; Hajime, C.; Kawamura, A.; Miyata, T. A Universal Method

- to Easily Design Tough and Stretchable Hydrogels. *NPG Asia Mater.* **2021**, *13* (1), 34. <https://doi.org/10.1038/s41427-021-00302-2>.
- (61) Wang, L.; Zhang, X.; Yang, K.; Fu, Y. V.; Xu, T.; Li, S.; Zhang, D.; Wang, L.-N.; Lee, C.-S. A Novel Double-Crosslinking-Double-Network Design for Injectable Hydrogels with Enhanced Tissue Adhesion and Antibacterial Capability for Wound Treatment. *Adv. Funct. Mater.* **2020**, *30* (1), 1904156. <https://doi.org/https://doi.org/10.1002/adfm.201904156>.
- (62) Xu, C.; Hung, C.; Cao, Y.; Liu, H. H. Tunable Crosslinking, Reversible Phase Transition, and 3D Printing of Hyaluronic Acid Hydrogels via Dynamic Coordination of Innate Carboxyl Groups and Metallic Ions. *ACS Appl. Bio Mater.* **2021**, *4* (3), 2408–2428. <https://doi.org/10.1021/acsabm.0c01300>.
- (63) Wang, B.; Xu, W.; Yang, Z.; Wu, Y.; Pi, F. An Overview on Recent Progress of the Hydrogels: From Material Resources, Properties, to Functional Applications. *Macromolecular Rapid Communications.* **2022**. <https://doi.org/10.1002/marc.202100785>.
- (64) Hu, W.; Wang, Z.; Xiao, Y.; Zhang, S.; Wang, J. Advances in Crosslinking Strategies of Biomedical Hydrogels. *Biomater. Sci.* **2019**, *7* (3), 843–855. <https://doi.org/10.1039/C8BM01246F>.
- (65) Paiva, M. T. P.; Kishima, J. O. F.; Silva, J. B. M. D.; Mantovan, J.; Colodi, F. G.; Mali, S. Crosslinking Methods in Polysaccharide-Based Hydrogels for Drug Delivery Systems. *Biomed. Mater. Devices* **2024**, *2* (1), 288–306. <https://doi.org/10.1007/s44174-023-00118-4>.
- (66) Taaca, K. L. M.; Prieto, E. I.; Vasquez, M. R. Current Trends in Biomedical Hydrogels: From Traditional Crosslinking to Plasma-Assisted Synthesis. *Polymers (Basel)*. **2022**, *14* (13). <https://doi.org/10.3390/polym14132560>.
- (67) Song, F.; Hu, W.; Xiao, L.; Cao, Z.; Li, X.; Zhang, C.; Liao, L.; Liu, L. Enzymatically Cross-Linked Hyaluronic Acid/Graphene Oxide Nanocomposite Hydrogel with pH-Responsive Release. *J. Biomater. Sci. Polym. Ed.* **2015**, *26* (6), 339–352. <https://doi.org/10.1080/09205063.2015.1007413>.

- (68) Ye, D.; Cheng, Q.; Zhang, Q.; Wang, Y.; Chang, C.; Li, L.; Peng, H.; Zhang, L. Deformation Drives Alignment of Nanofibers in Framework for Inducing Anisotropic Cellulose Hydrogels with High Toughness. *ACS Appl. Mater. & Interfaces* **2017**, *9* (49), 43154–43162. <https://doi.org/10.1021/acsami.7b14900>.
- (69) Shi, K.; Liu, Z.; Wei, Y.-Y.; Wang, W.; Ju, X.-J.; Xie, R.; Chu, L.-Y. Near-Infrared Light-Responsive Poly(N-Isopropylacrylamide)/Graphene Oxide Nanocomposite Hydrogels with Ultrahigh Tensibility. *ACS Appl. Mater. Interfaces* **2015**, *7* (49), 27289–27298. <https://doi.org/10.1021/acsami.5b08609>.
- (70) Unger, K.; Resel, R.; Coclite, A. M. Dynamic Studies on the Response to Humidity of Poly (2-Hydroxyethyl Methacrylate) Hydrogels Produced by Initiated Chemical Vapor Deposition. *Macromolecular Chemistry and Physics*. **2016**. <https://doi.org/10.1002/macp.201600271>.
- (71) Ullah, F.; Othman, M. B. H.; Javed, F.; Ahmad, Z.; Akil, H. M. Classification, Processing and Application of Hydrogels: A Review. *Mater. Sci. Eng. C* **2015**, *57*, 414–433. <https://doi.org/https://doi.org/10.1016/j.msec.2015.07.053>.
- (72) Li, X.; Sun, Q.; Li, Q.; Kawazoe, N.; Chen, G. Functional Hydrogels With Tunable Structures and Properties for Tissue Engineering Applications. *Frontiers in Chemistry*. **2018**. <https://www.frontiersin.org/articles/10.3389/fchem.2018.00499>.
- (73) Babić, M. M.; Vukomanović, M.; Štefanič, M.; Nikodinović-Runić, J.; Tomić, S. L. Controlled Curcumin Release From Hydrogel Scaffold Platform Based on 2-Hydroxyethyl Methacrylate/Gelatin/Alginate/Iron(III) Oxide. *Macromolecular Chemistry and Physics*. **2020**. <https://doi.org/10.1002/macp.202000186>.
- (74) Harrison, I. P.; Spada, F. Hydrogels for Atopic Dermatitis and Wound Management: A Superior Drug Delivery Vehicle. *Pharmaceutics*. **2018**. <https://doi.org/10.3390/pharmaceutics10020071>.
- (75) Li, S.; Yan, S.; Yu, J. Removal of Cationic Dyes from Aqueous Solution by Hydrophobically Modified Poly(Acrylic Acid) Hydrogels. *Polym. Plast. Technol. Eng.* **2011**, *50* (8), 783–790. <https://doi.org/10.1080/03602559.2010.551444>.
- (76) Su, G.; Zhou, T.; Zhang, Y.; Liu, X.; Zhang, A. Microdynamics Mechanism of D₂O

- Absorption of the Poly(2-Hydroxyethyl Methacrylate)-Based Contact Lens Hydrogel Studied by Two-Dimensional Correlation ATR-FTIR Spectroscopy. *Soft Matter* **2016**, *12* (4), 1145–1157. <https://doi.org/10.1039/C5SM02542G>.
- (77) Stile, R. A.; Burghardt, W. R.; Healy, K. E. Synthesis and Characterization of Injectable Poly(N-Isopropylacrylamide)-Based Hydrogels That Support Tissue Formation in Vitro. *Macromolecules* **1999**, *32* (22), 7370–7379. <https://doi.org/10.1021/ma990130w>.
- (78) Gong, C.; Shi, S.; Dong, P.; Kan, B.; Gou, M.; Wang, X.; Li, X.; Luo, F.; Zhao, X.; Wei, Y.; Qian, Z. Synthesis and Characterization of PEG-PCL-PEG Thermosensitive Hydrogel. *Int. J. Pharm.* **2009**, *365* (1), 89–99. <https://doi.org/https://doi.org/10.1016/j.ijpharm.2008.08.027>.
- (79) Odian, G. *Principles of Polymerization*; John Wiley & Sons, 2004.
- (80) Matiyashevskiy, K.; Thomas, P. D. *Handbook of Radical Polymerization*, ; *Matyjaszewski, K., Davis, TP, Eds*; John Wiley & Sons: Hoboken, NJ, USA, 2002.
- (81) Tripathi, A. K.; Neenan, M. L.; Sundberg, D. C.; Tsavalas, J. G. Influence of N-Alkyl Ester Groups on Efficiency of Crosslinking for Methacrylate Monomers Copolymerized with EGDMA: Experiments and Monte Carlo Simulations of Reaction Kinetics and Sol–Gel Structure. *Polymer (Guildf)*. **2016**, *96*, 130–145. <https://doi.org/https://doi.org/10.1016/j.polymer.2016.04.017>.
- (82) Murray, D. L.; Piirma, I. Mechanism of the Emulsion-Precipitation Polymerization of Chlorotrifluoroethylene. 1. Kinetics of the Polymerization. *Macromolecules* **1993**, *26* (21), 5577–5586. <https://doi.org/10.1021/ma00073a008>.
- (83) Anene, A.; Kalfat, R.; Chevalier, Y.; Hbaieb, S. Design of Molecularly Imprinted Polymeric Materials: The Crucial Choice of Functional Monomers. *Chem. Africa* **2020**, *3* (3), 769–781. <https://doi.org/10.1007/s42250-020-00180-1>.
- (84) Chen, L.; Guo, M. Highly Transparent, Stretchable, and Conductive Supramolecular Ionogels Integrated with Three-Dimensional Printable, Adhesive, Healable, and Recyclable Character. *ACS Appl. Mater. Interfaces* **2021**. <https://doi.org/10.1021/acsami.1c04255>.
- (85) Wiener, C. G.; Weiss, R. A.; Vogt, B. D. Overcoming Confinement Limited Swelling in

- Hydrogel Thin Films Using Supramolecular Interactions. *Soft Matter* **2014**, *10* (35), 6705–6712. <https://doi.org/10.1039/C4SM00815D>.
- (86) Cao, Z.; Du, B.; Chen, T.; Li, H.; Xu, J.; Fan, Z. Fabrication and Properties of Thermosensitive Organic/Inorganic Hybrid Hydrogel Thin Films. *Langmuir* **2008**, *24* (10), 5543–5551. <https://doi.org/10.1021/la8000653>.
- (87) Schmaljohann, D.; Nitschke, M.; Schulze, R.; Eing, A.; Werner, C.; Eichhorn, K.-J. In Situ Study of the Thermo-responsive Behavior of Micropatterned Hydrogel Films by Imaging Ellipsometry. *Langmuir* **2005**, *21* (6), 2317–2322. <https://doi.org/10.1021/la0476128>.
- (88) Khan, B. A.; Ullah, S.; Khan, M. K.; Uzair, B.; Mena, F.; Braga, V. A. Fabrication, Physical Characterizations, and In Vitro, In Vivo Evaluation of Ginger Extract-Loaded Gelatin/Poly(Vinyl Alcohol) Hydrogel Films Against Burn Wound Healing in Animal Model. *AAPS PharmSciTech* **2020**, *21* (8), 323. <https://doi.org/10.1208/s12249-020-01866-y>.
- (89) Nguyen, H. K.; Fujinami, S.; Nakajima, K. Elastic Modulus of Ultrathin Polymer Films Characterized by Atomic Force Microscopy: The Role of Probe Radius. *Polymer (Guildf)*. **2016**, *87*, 114–122. <https://doi.org/10.1016/j.polymer.2016.01.080>.
- (90) Arunbabu, D.; Shahsavan, H.; Zhang, W.; Zhao, B. Poly(AAc-Co-MBA) Hydrogel Films: Adhesive and Mechanical Properties in Aqueous Medium. *J. Phys. Chem. B* **2013**, *117* (1), 441–449. <https://doi.org/10.1021/jp3101688>.
- (91) Künniger, T.; Grüneberger, F.; Fischer, B.; Walder, C. Nanofibrillated Cellulose in Wood Coatings: Viscoelastic Properties of Free Composite Films. *J. Mater. Sci.* **2017**, *52* (17), 10237–10249. <https://doi.org/10.1007/s10853-017-1193-4>.
- (92) Correa-Baena, J.-P.; Artyushkova, K.; Santoro, C.; Atanassov, P.; Agrios, A. G. Morphological Characterization of ALD and Doping Effects on Mesoporous SnO₂ Aerogels by XPS and Quantitative SEM Image Analysis. *ACS Appl. Mater. Interfaces* **2016**, *8* (15), 9849–9854. <https://doi.org/10.1021/acsami.6b00019>.
- (93) Zhang, N.; Knoll, W. Thermally Responsive Hydrogel Films Studied by Surface

- Plasmon Diffraction. *Anal. Chem.* **2009**, *81* (7), 2611–2617. <https://doi.org/10.1021/ac802527j>.
- (94) Ma, L.; Cheng, C.; He, C.; Nie, C.; Deng, J.; Sun, S.; Zhao, C. Substrate-Independent Robust and Heparin-Mimetic Hydrogel Thin Film Coating via Combined LbL Self-Assembly and Mussel-Inspired Post-Cross-Linking. *ACS Appl. Mater. Interfaces* **2015**, *7* (47), 26050–26062. <https://doi.org/10.1021/acsami.5b09634>.
- (95) Tang, Z.; Wang, Y.; Podsiadlo, P.; Kotov, N. A. Biomedical Applications of Layer-by-Layer Assembly: From Biomimetics to Tissue Engineering. *Adv. Mater.* **2006**, *18* (24), 3203–3224. <https://doi.org/10.1002/adma.200600113>.
- (96) Lazar, S.; Garcia-Valdez, O.; Kennedy, E.; Champagne, P.; Cunningham, M. F.; Grunlan, J. C. Crosslinkable-Chitosan-Enabled Moisture-Resistant Multilayer Gas Barrier Thin Film. *Macromol. Rapid Commun.* **2019**, *40* (6). <https://doi.org/10.1002/marc.201800853>.
- (97) Nash, M. E.; Carroll, W. M.; Foley, P. J.; Maguire, G.; Connell, C. O.; Gorelov, A. V.; Beloshapkin, S.; Rochev, Y. A. Ultra-Thin Spin Coated Crosslinkable Hydrogels for Use in Cell Sheet Recovery—Synthesis, Characterisation to Application. *Soft Matter* **2012**, *8* (14), 3889–3899. <https://doi.org/10.1039/C2SM06466A>.
- (98) Biring, S.; Sadhu, A. S.; Deb, M. An Effective Optical Dual Gas Sensor for Simultaneous Detection of Oxygen and Ammonia. *Sensors*. **2019**. <https://doi.org/10.3390/s19235124>.
- (99) Kenney, R. M.; Boyce, M. W.; Whitman, N. A.; Kromhout, B. P.; Lockett, M. R. A PH-Sensing Optode for Mapping Spatiotemporal Gradients in 3D Paper-Based Cell Cultures. *Anal. Chem.* **2018**, *90* (3), 2376–2383. <https://doi.org/10.1021/acs.analchem.7b05015>.
- (100) Madduma-Bandarage, U. S. K.; Madihally, S. V. Synthetic Hydrogels: Synthesis, Novel Trends, and Applications. *J. Appl. Polym. Sci.* **2020**, *138* (19). <https://doi.org/10.1002/app.50376>.
- (101) Li, Z.; Cheng, H.; Ke, L.; Liu, M.; Wang, C.-G.; Jun Loh, X.; Li, Z.; Wu, Y.-L. Recent Advances in New Copolymer Hydrogel-Formed Contact Lenses for Ophthalmic Drug Delivery. *ChemNanoMat* **2021**, *7* (6), 564–579. <https://doi.org/https://doi.org/10.1002/cnma.202100008>.

- (102) Dong, M.; Jiao, D.; Zheng, Q.; Wu, Z. L. Recent Progress in Fabrications and Applications of Functional Hydrogel Films. *J. Polym. Sci.* **2022**, *61* (11), 1026–1039. <https://doi.org/10.1002/pol.20220451>.
- (103) Gleason, K. K. Nanoscale Control by Chemically Vapour-Deposited Polymers. *Nat. Rev. Phys.* **2020**, *2* (7), 347–364. <https://doi.org/10.1038/s42254-020-0192-6>.
- (104) Martin, T. P.; Chan, K.; Gleason, K. K. Combinatorial Initiated Chemical Vapor Deposition (ICVD) for Polymer Thin Film Discovery. *Thin Solid Films* **2008**, *516* (5), 681–683. <https://doi.org/https://doi.org/10.1016/j.tsf.2007.06.113>.
- (105) Christian, P.; Tumphart, S.; Ehmann, H. M. A.; Riegler, H.; Coclite, A. M.; Werzer, O. Controlling Indomethacin Release through Vapor-Phase Deposited Hydrogel Films by Adjusting the Cross-Linker Density. *Sci. Rep.* **2018**, *8* (1), 7134. <https://doi.org/10.1038/s41598-018-24238-w>.
- (106) Sun, L.; Yuan, G.; Gao, L.; Yang, J.; Chhowalla, M.; Gharahcheshmeh, M. H.; Gleason, K. K.; Choi, Y. S.; Hong, B. H.; Liu, Z. Chemical Vapour Deposition. *Nat. Rev. Methods Prim.* **2021**, *1* (1), 5. <https://doi.org/10.1038/s43586-020-00005-y>.
- (107) Molina, R.; Ligeró, C.; Jovančić, P.; Bertran, E. In Situ Polymerization of Aqueous Solutions of NIPAAm Initiated by Atmospheric Plasma Treatment. *Plasma Process. Polym.* **2013**, *10* (6), 506–516. <https://doi.org/10.1002/ppap.201200121>.
- (108) Levien, M.; Fricke, K. Fabrication of Hydrogel Coatings by Atmospheric-Pressure Plasma Polymerization: Function by Structure and Chemistry. *Mater. Today* **2020**, *41* (December), 316–317. <https://doi.org/10.1016/j.mattod.2020.10.020>.
- (109) Lu, Q.; Yu, J.; Gao, J.; Yang, W.; Li, Y. Glow-Discharge Electrolysis Plasma Induced Synthesis of Polyvinylpyrrolidone/Acrylic Acid Hydrogel and Its Adsorption Properties for Heavy-Metal Ions. *Plasma Process. Polym.* **2011**, *8* (9), 803–814. <https://doi.org/https://doi.org/10.1002/ppap.201000144>.
- (110) Fridman, A. Introduction to Theoretical and Applied Plasma Chemistry. In *Plasma Chemistry*; Cambridge University Press: Cambridge, 2008; pp 1–11. <https://doi.org/DOI: 10.1017/CBO9780511546075.003>.
- (111) Denes, F. S.; Manolache, S. Macromolecular Plasma-Chemistry: An Emerging Field of

- Polymer Science. *Prog. Polym. Sci.* **2004**, *29* (8), 815–885. <https://doi.org/https://doi.org/10.1016/j.progpolymsci.2004.05.001>.
- (112) Bitar, R.; Cools, P.; De Geyter, N.; Morent, R. Acrylic Acid Plasma Polymerization for Biomedical Use. *Appl. Surf. Sci.* **2018**, *448*, 168–185. <https://doi.org/https://doi.org/10.1016/j.apsusc.2018.04.129>.
- (113) Bitar, R.; Cools, P.; De Geyter, N.; Morent, R. Acrylic Acid Plasma Polymerization for Biomedical Use. *Appl. Surf. Sci.* **2018**, *448*, 168–185. <https://doi.org/10.1016/j.apsusc.2018.04.129>.
- (114) Tendero, C.; Tixier, C.; Tristant, P.; Desmaison, J.; Leprince, P. Atmospheric Pressure Plasmas: A Review. *Spectrochim. Acta Part B At. Spectrosc.* **2006**, *61* (1), 2–30. <https://doi.org/https://doi.org/10.1016/j.sab.2005.10.003>.
- (115) Boulos, M. I. Thermal Plasma Processing. *IEEE Trans. Plasma Sci.* **1991**, *19* (6), 1078–1089. <https://doi.org/10.1109/27.125032>.
- (116) Morent, R.; Geyter, N. De; Desmet, T.; Dubruel, P.; Leys, C. Plasma Surface Modification of Biodegradable Polymers: A Review. *Plasma Process. Polym.* **2011**, *8* (3), 171–190. <https://doi.org/10.1002/ppap.201000153>.
- (117) Bertin, M.; Leitao, E. M.; Bickerton, S.; Verbeek, C. J. R. A Review of Polymer Surface Modification by Cold Plasmas Toward Bulk Functionalization. *Plasma Process. Polym.* **2024**, *21* (5). <https://doi.org/10.1002/ppap.202300208>.
- (118) Heyse, P.; Dams, R.; Paulussen, S.; Houthoofd, K.; Janssen, K.; Jacobs, P. A.; Sels, B. F. Dielectric Barrier Discharge at Atmospheric Pressure as a Tool to Deposit Versatile Organic Coatings at Moderate Power Input. *Plasma Process. Polym.* **2007**, *4* (2), 145–157. <https://doi.org/https://doi.org/10.1002/ppap.200600087>.
- (119) Islam, R.; Xie, S.; Englund, K. R.; Pedrow, P. D. Plasma Polymerized Acetylene Deposition Using a Return Corona Enhanced Plasma Reactor. *Plasma Sci. Technol.* **2017**, *19* (8), 85501. <https://doi.org/10.1088/2058-6272/aa6bef>.
- (120) Li, P. H.; Chu, P. K. Thin Film Deposition Technologies and Processing of Biomaterials; In *Thin film coatings for biomaterials and biomedical applications*, Ed.; Woodhead Publishing, **2016**; pp 3–28. <https://doi.org/https://doi.org/10.1016/B978-1-78242-453->

6.00001-8.

- (121) Chu, P. K. Recent Developments and Applications of Plasma Immersion Ion Implantation. *J. Vac. Sci. Technol. B Microelectron. Nanom. Struct. Process. Meas. Phenom.* **2004**, *22* (1), 289–296. <https://doi.org/10.1116/1.1632920>.
- (122) Arolkar, G. A.; Jacob, S. M.; Pandiyaraj, K. N.; Kelkar-Mane, V. R.; Deshmukh, R. R. Effect of TEOS Plasma Polymerization on Corn Starch/Poly(ϵ -Caprolactone) Film: Characterization, Properties and Biodegradation. *RSC Adv.* **2016**, *6* (20), 16779–16789. <https://doi.org/10.1039/C5RA23414J>.
- (123) Schneider, J.; Baumgärtner, K. M.; Feichtinger, J.; Krüger, J.; Muranyi, P.; Schulz, A.; Walker, M.; Wunderlich, J.; Schumacher, U. Investigation of the Practicability of Low-Pressure Microwave Plasmas in the Sterilisation of Food Packaging Materials at Industrial Level. *Surf. Coatings Technol.* **2005**, *200* (1), 962–966. <https://doi.org/10.1016/j.surfcoat.2005.01.114>.
- (124) Ejenstam, L.; Tuominen, M.; Haapanen, J.; Mäkelä, J. M.; Pan, J.; Swerin, A.; Claesson, P. M. Long-Term Corrosion Protection by a Thin Nano-Composite Coating. *Appl. Surf. Sci.* **2015**, *357*, 2333–2342. <https://doi.org/10.1016/j.apsusc.2015.09.238>.
- (125) Ershov, S.; Khelifa, F.; Druart, M.-E.; Habibi, Y.; Olivier, M.-G.; Snyders, R.; Dubois, P. Free Radical-Induced Grafting from Plasma Polymers for the Synthesis of Thin Barrier Coatings. *RSC Adv.* **2015**, *5* (19), 14256–14265. <https://doi.org/10.1039/C4RA16424E>.
- (126) Khelifa, F.; Ershov, S.; Druart, M.-E.; Habibi, Y.; Chicot, D.; Olivier, M.-G.; Snyders, R.; Dubois, P. A Multilayer Coating with Optimized Properties for Corrosion Protection of Al. *J. Mater. Chem. A* **2015**, *3* (31), 15977–15985. <https://doi.org/10.1039/C5TA01920F>.
- (127) Vasilev, K.; Poulter, N.; Martinek, P.; Griesser, H. J. Controlled Release of Levofloxacin Sandwiched between Two Plasma Polymerized Layers on a Solid Carrier. *ACS Appl. Mater. Interfaces* **2011**, *3* (12), 4831–4836. <https://doi.org/10.1021/am201320a>.
- (128) Michl, T. D.; Coad, B. R.; Doran, M.; Osiecki, M.; Kafshgari, M. H.; Voelcker, N. H.; Hüsler, A.; Vasilev, K.; Griesser, H. J. Nitric Oxide Releasing Plasma Polymer Coating

- with Bacteriostatic Properties and No Cytotoxic Side Effects. *Chem. Commun.* **2015**, *51* (32), 7058–7060. <https://doi.org/10.1039/C5CC01722J>.
- (129) Bouaidat, S.; Berendsen, C.; Thomsen, P.; Petersen, S. G.; Wolff, A.; Jonsmann, J. Micro Patterning of Cell and Protein Non-Adhesive Plasma Polymerized Coatings for Biochip Applications. *Lab Chip* **2004**, *4* (6), 632–637. <https://doi.org/10.1039/B406285J>.
- (130) Hegemann, D.; Hossain, M. M.; Körner, E.; Balazs, D. J. Macroscopic Description of Plasma Polymerization. *Plasma Process. Polym.* **2007**, *4* (3), 229–238. <https://doi.org/10.1002/ppap.200600169>.
- (131) Hegemann, D. Macroscopic Control of Plasma Polymerization Processes. *Pure Appl. Chem.* **2008**, *80* (9), 1893–1900. <https://doi.org/10.1351/pac200880091893>.
- (132) Mertens, J.; Baneton, J.; Ozkan, A.; Pospisilova, E.; Nysten, B.; Delcorte, A.; Reniers, F. Atmospheric Pressure Plasma Polymerization of Organics: Effect of the Presence and Position of Double Bonds on Polymerization Mechanisms, Plasma Stability and Coating Chemistry. *Thin Solid Films* **2019**, *671* (December 2018), 64–76. <https://doi.org/10.1016/j.tsf.2018.12.036>.
- (133) Yasuda, H.; Wang, C. R. Plasma Polymerization Investigated by the Substrate Temperature Dependence. *J. Polym. Sci. Polym. Chem. Ed.* **1985**, *23* (1), 87–106. <https://doi.org/https://doi.org/10.1002/pol.1985.170230110>.
- (134) Yasuda, H. New Insights into Aging Phenomena from Plasma Chemistry. *Nucl. Instruments Methods Phys. Res. Sect. A Accel. Spectrometers, Detect. Assoc. Equip.* **2003**, *515* (1), 15–30. <https://doi.org/https://doi.org/10.1016/j.nima.2003.08.125>.
- (135) Yasuda, H. K. Some Important Aspects of Plasma Polymerization. *Plasma Process. Polym.* **2005**, *2* (4), 293–304. <https://doi.org/https://doi.org/10.1002/ppap.200400071>.
- (136) Deutsch, H.; Schmidt, M. On the Quantitative Treatment of the Growth Rate of Thin Polymer Films Produced in Glow Discharges. *Beiträge aus der Plasmaphys.* **1981**, *21* (4), 279–292. <https://doi.org/https://doi.org/10.1002/ctpp.19810210405>.
- (137) Nisol, B.; Watson, S.; Lerouge, S.; Wertheimer, M. R. Energetics of Reactions in a Dielectric Barrier Discharge with Argon Carrier Gas: III Esters. *Plasma Process. Polym.* **2016**, *13* (9), 900–907. <https://doi.org/10.1002/ppap.201600003>.

- (138) Nisol, B.; Watson, S.; Lerouge, S.; Wertheimer, M. R. Energetics of Reactions in a Dielectric Barrier Discharge with Argon Carrier Gas: V Hydrocarbons. *Plasma Process. Polym.* **2017**, *14* (8), 1600191. <https://doi.org/https://doi.org/10.1002/ppap.201600191>.
- (139) Kakaroglou, A.; Nisol, B.; Baert, K.; De Graeve, I.; Reniers, F.; Van Assche, G.; Terryn, H. Evaluation of the Yasuda Parameter for the Atmospheric Plasma Deposition of Allyl Methacrylate. *RSC Adv.* **2015**, *5* (35), 27449–27457. <https://doi.org/10.1039/C5RA02684A>.
- (140) Michelmore, A.; Steele, D. A.; Robinson, D. E.; Whittle, J. D.; Short, R. D. The Link between Mechanisms of Deposition and the Physico-Chemical Properties of Plasma Polymer Films. *Soft Matter* **2013**, *9* (26), 6167–6175. <https://doi.org/10.1039/C3SM51039E>.
- (141) G. Lopez, B. D. R. Cryogenic Control of Chemistry in Plasma-Deposited Organic Films. *ACS Polym. Mater. Sci. Eng.* **1990**, *62*, 14.
- (142) Manakhov, A.; Moreno-Couranjou, M.; Boscher, N. D.; Rogé, V.; Choquet, P.; Pireaux, J.-J. Atmospheric Pressure Pulsed Plasma Copolymerisation of Maleic Anhydride and Vinyltrimethoxysilane: Influence of Electrical Parameters on Chemistry, Morphology and Deposition Rate of the Coatings. *Plasma Process. Polym.* **2012**, *9* (4), 435–445. <https://doi.org/https://doi.org/10.1002/ppap.201100184>.
- (143) Coulson, S. R.; Woodward, I. S.; Badyal, J. P. S.; Brewer, S. A.; Willis, C. Ultralow Surface Energy Plasma Polymer Films. *Chem. Mater.* **2000**, *12* (7), 2031–2038. <https://doi.org/10.1021/cm000193p>.
- (144) Detomaso, L.; Gristina, R.; Senesi, G. S.; d’Agostino, R.; Favia, P. Stable Plasma-Deposited Acrylic Acid Surfaces for Cell Culture Applications. *Biomaterials* **2005**, *26* (18), 3831–3841. <https://doi.org/https://doi.org/10.1016/j.biomaterials.2004.10.011>.
- (145) Liguori, A.; Pollicino, A.; Stancampiano, A.; Tarterini, F.; Focarete, M. L.; Colombo, V.; Gherardi, M. Deposition of Plasma-Polymerized Polyacrylic Acid Coatings by a Non-Equilibrium Atmospheric Pressure Nanopulsed Plasma Jet. *Plasma Process. Polym.* **2016**, *13* (3), 375–386. <https://doi.org/10.1002/ppap.201500080>.
- (146) Loyer, F.; Combrisson, A.; Omer, K.; Moreno-Couranjou, M.; Choquet, P.; Boscher, N.

- D. Thermoresponsive Water-Soluble Polymer Layers and Water-Stable Copolymer Layers Synthesized by Atmospheric Plasma Initiated Chemical Vapor Deposition. *ACS Appl. Mater. Interfaces* **2019**, *11* (1), 1335–1343. <https://doi.org/10.1021/acsami.8b14806>.
- (147) Topala, I.; Dumitrascu, N.; Popa, G. Properties of the Acrylic Acid Polymers Obtained by Atmospheric Pressure Plasma Polymerization. *Nucl. Instruments Methods Phys. Res. Sect. B Beam Interact. with Mater. Atoms* **2009**, *267* (2), 442–445. <https://doi.org/10.1016/j.nimb.2008.10.029>.
- (148) Herbert, P. A. F.; O’Neill, L.; Jaroszynska-Wolinska, J.; Stallard, C. P.; Ramamoorthy, A.; Dowling, D. P. A Comparison between Gas and Atomized Liquid Precursor States in the Deposition of Functional Coatings by Pin Corona Plasma. *PLASMA Process. Polym.* **2011**, *8* (3), 230–238. <https://doi.org/10.1002/ppap.201000119>.
- (149) Morent, R.; De Geyter, N.; Van Vlierberghe, S.; Dubruel, P.; Leys, C.; Schacht, E. Organic-Inorganic Behaviour of HMDSO Films Plasma-Polymerized at Atmospheric Pressure. *Surf. Coatings Technol.* **2009**, *203* (10–11), 1366–1372. <https://doi.org/10.1016/j.surfcoat.2008.11.008>.
- (150) Donegan, M.; Dowling, D. P. Protein Adhesion on Water Stable Atmospheric Plasma Deposited Acrylic Acid Coatings. *Surf. Coatings Technol.* **2013**, *234*, 53–59. <https://doi.org/10.1016/j.surfcoat.2013.03.002>.
- (151) Mariotti, D.; Patel, J.; Švrček, V.; Maguire, P. Plasma-Liquid Interactions at Atmospheric Pressure for Nanomaterials Synthesis and Surface Engineering. *Plasma Process. Polym.* **2012**, *9* (11–12), 1074–1085. <https://doi.org/10.1002/ppap.201200007>.
- (152) Vanraes, P.; Bogaerts, A. The Essential Role of the Plasma Sheath in Plasma–Liquid Interaction and Its Applications—A Perspective. *J. Appl. Phys.* **2021**, *129* (22), 220901. <https://doi.org/10.1063/5.0044905>.
- (153) Baba, K.; Okada, T.; Kaneko, T.; Hatakeyama, R. Atmospheric Pressure Glow-Discharge Plasmas with Gas–Liquid Interface. *Jpn. J. Appl. Phys.* **2006**, *45* (10S), 8286. <https://doi.org/10.1143/JJAP.45.8286>.
- (154) Tachibana, K.; Yasuoka, K. Understanding of Chemical Reactions Induced by Argon

- Plasma in Contact with Sodium Halide Solutions: Importance of Surface Properties for Plasma–Liquid Interactions. *J. Phys. D. Appl. Phys.* **2020**, *53* (12), 125203. <https://doi.org/10.1088/1361-6463/ab5ebe>.
- (155) Veuillet, M.; Ploux, L.; Airoudj, A.; Gourbeyre, Y.; Gaudichet-Maurin, E.; Roucoules, V. Macroscopic Control of DMAHEMA and HEMA Plasma Polymerization to Tune the Surface Mechanical Properties of Hydrogel-like Coatings. *Plasma Process. Polym.* **2017**, *14* (10), 1600215. <https://doi.org/https://doi.org/10.1002/ppap.201600215>.
- (156) Malik, M. A.; Ahmed, M.; Ejaz-ur-Rehman; Naheed, R.; Ghaffar, A. Synthesis of Superabsorbent Copolymers by Pulsed Corona Discharges in Water. *Plasmas Polym.* **2003**, *8* (4), 271–279. <https://doi.org/10.1023/A:1026385110522>.
- (157) Levien, M.; Nasri, Z.; Weltmann, K.-D.; Fricke, K. Study on the Interaction of Plasma-Polymerized Hydrogel Coatings with Aqueous Solutions of Different pH. *Gels*. **2023**. <https://doi.org/10.3390/gels9030237>.
- (158) Taaca, K. L. M.; De Leon, M. J. D.; Thumanu, K.; Nakajima, H.; Chanlek, N.; Prieto, E. I.; Vasquez, M. R. Probing the Structural Features of a Plasma-Treated Chitosan-Acrylic Acid Hydrogel. *Colloids Surfaces A Physicochem. Eng. Asp.* **2022**, *637*, 128233. <https://doi.org/https://doi.org/10.1016/j.colsurfa.2021.128233>.
- (159) Levien, M.; Farka, Z.; Pastucha, M.; Skládal, P.; Nasri, Z.; Weltmann, K.-D.; Fricke, K. Functional Plasma-Polymerized Hydrogel Coatings for Electrochemical Biosensing. *Appl. Surf. Sci.* **2022**, *584*, 152511. <https://doi.org/10.1016/j.apsusc.2022.152511>.
- (160) Tamirisa, P. A.; Koskinen, J.; Hess, D. W. Plasma Polymerized Hydrogel Thin Films. *Thin Solid Films* **2006**, *515* (4), 2618–2624. <https://doi.org/https://doi.org/10.1016/j.tsf.2006.03.021>.
- (161) Tamirisa, P. A.; Hess, D. W. Water and Moisture Uptake by Plasma Polymerized Thermoresponsive Hydrogel Films. *Macromolecules* **2006**, *39* (20), 7092–7097. <https://doi.org/10.1021/ma060944u>.
- (162) Jovancic, P.; Vilchez, A.; Molina, R. Synthesis of Thermo-Sensitive Hydrogels from Free Radical Copolymerization of NIPAAm with MBA Initiated by Atmospheric Plasma Treatment. *PLASMA Process. Polym.* **2016**, *13* (7), 752–760.

<https://doi.org/10.1002/ppap.201500194>.

- (163) Mauchauffé, R.; Moreno-Couranjou, M.; Boscher, N. D.; Duwez, A.-S.; Choquet, P. Liquid-Assisted Plasma-Enhanced Chemical Vapor Deposition of Catechol and Quinone-Functionalized Coatings: Insights into the Surface Chemistry and Morphology. *Plasma Process. Polym.* **2016**, *13* (8), 843–856. <https://doi.org/10.1002/ppap.201600002>.
- (164) Schäfer, J.; Fricke, K.; Mika, F.; Pokorná, Z.; Zajíčková, L.; Foest, R. Liquid Assisted Plasma Enhanced Chemical Vapour Deposition with a Non-Thermal Plasma Jet at Atmospheric Pressure. *Thin Solid Films* **2017**, *630*, 71–78. <https://doi.org/10.1016/j.tsf.2016.09.022>.
- (165) Boscher, N. D.; Obaton, A.-F.; Choquet, P.; Duday, D. Liquid- Assisted Plasma-Enhanced Chemical Vapor Deposition of α -Cyclodextrin/PDMS Composite Thin Film for the Preparation of Interferometric Sensors- Application to the Detection of Benzene in Water. *J. Nanosci. Nanotechnol.* **2016**, *16* (9). <https://doi.org/10.1166/jnn.2016.12846>.
- (166) Hilt, F.; Hovish, M. Q.; Rolston, N.; Brüning, K.; Tassone, C. J.; Dauskardt, R. H. Rapid Route to Efficient, Scalable, and Robust Perovskite Photovoltaics in Air. *Energy Environ. Sci.* **2018**, *11* (8), 2102–2113. <https://doi.org/10.1039/C8EE01065J>.
- (167) Hovish, M. Q.; Rolston, N.; Brüning, K.; Hilt, F.; Tassone, C.; Dauskardt, R. H. Crystallization Kinetics of Rapid Spray Plasma Processed Multiple Cation Perovskites in Open Air. *J. Mater. Chem. A* **2020**, *8* (1), 169–176. <https://doi.org/10.1039/C9TA07980G>.
- (168) Rolston, N.; Scheideler, W. J.; Flick, A. C.; Chen, J. P.; Elmaraghi, H.; Sleugh, A.; Zhao, O.; Woodhouse, M.; Dauskardt, R. H. Rapid Open-Air Fabrication of Perovskite Solar Modules. *Joule* **2020**, *4* (12), 2675–2692. <https://doi.org/https://doi.org/10.1016/j.joule.2020.11.001>.
- (169) Boscher, N. D.; Duday, D.; Heier, P.; Heinze, K.; Hilt, F.; Choquet, P. Plasma Polymer Membranes for Immobilising Metalloporphyrins. *Plasma Process. Polym.* **2013**, *10* (4). <https://doi.org/10.1002/ppap.201200132>.
- (170) Boscher, N. D.; Bohn, T.; Heier, P.; Moisy, F.; Untereiner, B.; Heinze, K.; Choquet, P.

- Optical Sensing Responses of Cr^{III}Cl(TPP)(H₂O)-Based Coatings Obtained by an Atmospheric Pressure Plasma Method - Application to the Detection of Volatile Amines. *Sensors Actuators, B Chem.* **2014**, *191*, 553–560. <https://doi.org/10.1016/j.snb.2013.10.044>.
- (171) Boscher, N. D.; Choquet, P.; Duday, D.; Kerbellec, N.; Lambrechts, J.-C.; Maurau, R. Luminescent Lanthanide-Based Hybrid Coatings Deposited by Atmospheric Pressure Plasma Assisted Chemical Vapour Deposition. *J. Mater. Chem.* **2011**, *21* (47). <https://doi.org/10.1039/c1jm14659a>.
- (172) Ding, Y.; Dong, S.; Hilt, F.; Dauskardt, R. H. Open-Air Spray Plasma Deposited UV-Absorbing Nanocomposite Coatings. *Nanoscale* **2018**, *10* (30), 14525–14533. <https://doi.org/10.1039/C8NR04095H>.
- (173) Boscher, N.; Chemin, J.-B. Method for Forming an Electrically Conductive Multilayer Coating with Anti-Corrosion Properties onto a Metallic Substrate. United States patent application US 17/048,822. **2021**.
- (174) Knapp, C. E.; Chemin, J.-B.; Douglas, S. P.; Ondo, D. A.; Guillot, J.; Choquet, P.; Boscher, N. D. Room-Temperature Plasma-Assisted Inkjet Printing of Highly Conductive Silver on Paper. *Adv. Mater. Technol.* **2018**, *3* (3). <https://doi.org/10.1002/admt.201700326>.
- (175) Knapp, C. E.; Metcalf, E. A.; Mrig, S.; Sanchez-Perez, C.; Douglas, S. P.; Choquet, P.; Boscher, N. D. Precursors for Atmospheric Plasma-Enhanced Sintering: Low-Temperature Inkjet Printing of Conductive Copper. *ChemistryOpen* **2018**, *7* (11). <https://doi.org/10.1002/open.201800131>.
- (176) Mauchauffé, R.; Bonot, S.; Moreno-Couranjou, M.; Detrembleur, C.; Boscher, N. D.; Van De Weerd, C.; Duwez, A.-S.; Choquet, P. Fast Atmospheric Plasma Deposition of Bio-Inspired Catechol/Quinone-Rich Nanolayers to Immobilize NDM-1 Enzymes for Water Treatment. *Adv. Mater. Interfaces* **2016**, *3* (8). <https://doi.org/10.1002/admi.201500520>.
- (177) Rolston, N.; Sleugh, A.; Chen, J. P.; Zhao, O.; Colburn, T. W.; Flick, A. C.; Dauskardt, R. H. Perspectives of Open-Air Processing to Enable Perovskite Solar Cell Manufacturing. *Front. Energy Res.* **2021**, *9*. <https://doi.org/10.3389/fenrg.2021.684082>.

- (178) Niemczyk, E. M.; Gomez-Lopez, A.; Haler, J. R. N.; Frache, G.; Sardon, H.; Quintana, R. Insights on the Atmospheric-Pressure Plasma-Induced Free-Radical Polymerization of Allyl Ether Cyclic Carbonate Liquid Layers. *Polymers (Basel)*. **2021**, *13* (17). <https://doi.org/10.3390/polym13172856>.
- (179) Loyer, F.; Bengasi, G.; Frache, G.; Choquet, P.; Boscher, N. D. Insights in the Initiation and Termination of Poly(Alkyl Acrylates) Synthesized by Atmospheric Pressure Plasma-Initiated Chemical Vapor Deposition (AP-PiCVD). *Plasma Process. Polym.* **2018**, *15* (5), 1800027. <https://doi.org/10.1002/ppap.201800027>.
- (180) Loyer, F.; Bulou, S.; Choquet, P.; Boscher, N. D. Pulsed Plasma Initiated Chemical Vapor Deposition (PiCVD) of Polymer Layers – A Kinetic Model for the Description of Gas Phase to Surface Interactions in Pulsed Plasma Discharges. *Plasma Process. Polym.* **2018**, *15* (12). <https://doi.org/10.1002/ppap.201800121>.
- (181) Abessolo Ondo, D.; Leturcq, R.; Boscher, N. D. Plasma-Initiated Chemical Vapour Deposition of Organosiloxane Thin Films: From the Growth Mechanisms to Ultrathin Low-k Polymer Insulating Layers. *Plasma Process. Polym.* **2020**, *17* (7). <https://doi.org/10.1002/ppap.202000032>.
- (182) Gaiser, S.; Schütz, U.; Rupper, P.; Hegemann, D. Plasma Processing of Low Vapor Pressure Liquids to Generate Functional Surfaces. *Molecules* **2020**, *25* (24), 15–19. <https://doi.org/10.3390/molecules25246024>.
- (183) Gaiser, S.; Schütz, U.; Hegemann, D. Top-down Approach to Attach Liquid Polyethylene Glycol to Solid Surfaces by Plasma Interaction. *Plasma Process. Polym.* **2020**, *17* (2), 1900211. <https://doi.org/https://doi.org/10.1002/ppap.201900211>.
- (184) Barillas, L.; Makhneva, E.; An, S.; Fricke, K. Functional Thin Films Synthesized from Liquid Precursors by Combining Mist Chambers and Atmospheric-Pressure Plasma Polymerization. *Coatings* **2021**, *11* (11). <https://doi.org/10.3390/coatings11111336>.
- (185) Boscher, N. D.; Hilt, F.; Duday, D.; Frache, G.; Fouquet, T.; Choquet, P. Atmospheric Pressure Plasma Initiated Chemical Vapor Deposition Using Ultra-Short Square Pulse Dielectric Barrier Discharge. *Plasma Process. Polym.* **2015**, *12* (1), 66–74. <https://doi.org/10.1002/ppap.201400094>.

- (186) Socrates, G. *Infrared and Raman Characteristic Group Frequencies: Tables and Charts*, 3rd ed.; John Wiley & Sons, 2001.
- (187) Bodas, D. S.; Desai, S. M.; Gangal, S. A. Deposition of Plasma-Polymerized Hydroxyethyl Methacrylate (HEMA) on Silicon in Presence of Argon Plasma. *Appl. Surf. Sci.* **2005**, *245* (1), 186–190. <https://doi.org/https://doi.org/10.1016/j.apsusc.2004.10.010>.
- (188) Lao, H.-K.; Renard, E.; Langlois, V.; Vallée-Rehel, K.; Linossier, I. Surface Functionalization of PHBV by HEMA Grafting via UV Treatment: Comparison with Thermal Free Radical Polymerization. *J. Appl. Polym. Sci.* **2010**, *116* (1), 288–297. <https://doi.org/https://doi.org/10.1002/app.31507>.
- (189) Huang, C.-W.; Sun, Y.-M.; Huang, W.-F. Curing Kinetics of the Synthesis of Poly(2-Hydroxyethyl Methacrylate) (PHEMA) with Ethylene Glycol Dimethacrylate (EGDMA) as a Crosslinking Agent. *J. Polym. Sci. Part A Polym. Chem.* **1997**, *35* (10), 1873–1889. [https://doi.org/https://doi.org/10.1002/\(SICI\)1099-0518\(19970730\)35:10<1873::AID-POLA2>3.0.CO;2-P](https://doi.org/https://doi.org/10.1002/(SICI)1099-0518(19970730)35:10<1873::AID-POLA2>3.0.CO;2-P).
- (190) Vanraes, P.; Bogaerts, A. The Essential Role of the Plasma Sheath in Plasma-Liquid Interaction and Its Applications—A Perspective. *J. Appl. Phys.* **2021**, *129* (22). <https://doi.org/10.1063/5.0044905>.
- (191) Ladavière, C.; Lacroix-Desmazes, P.; Delolme, F. First Systematic MALDI/ESI Mass Spectrometry Comparison to Characterize Polystyrene Synthesized by Different Controlled Radical Polymerizations. *Macromolecules* **2009**, *42* (1), 70–84. <https://doi.org/10.1021/ma8013788>.
- (192) Baba, K.; Bengasi, G.; El Assad, D.; Grysan, P.; Lentzen, E.; Heinze, K.; Frache, G.; Boscher, N. D. Conductive Directly Fused Poly(Porphyrin) Coatings by Oxidative Chemical Vapour Deposition – From Single- to Triple-Fused. *European J. Org. Chem.* **2019**, *2019* (13), 2368–2375. <https://doi.org/10.1002/ejoc.201900045>.
- (193) Fei, X. M.; Kondo, Y.; Qian, X. Y.; Kuroda, S.; Mori, T.; Hosoi, K. Functional-Group-Retaining Polymerization of Hydroxyethyl Methacrylate by Atmospheric Pressure Non-Equilibrium Plasma. *Key Eng. Mater.* **2014**, *596*, 65–69. <https://doi.org/10.4028/www.scientific.net/KEM.596.65>.

- (194) Safarzadeh, H.; Peighambaroust, S. J.; Mousavi, S. H.; Foroutan, R.; Mohammadi, R.; Peighambaroust, S. H. Adsorption Ability Evaluation of the Poly(Methacrylic Acid-Co-Acrylamide)/Cloisite 30B Nanocomposite Hydrogel as a New Adsorbent for Cationic Dye Removal. *Environ. Res.* **2022**, *212*, 113349. <https://doi.org/https://doi.org/10.1016/j.envres.2022.113349>.
- (195) Nasser, R.; Bouzari, N.; Huang, J.; Golzar, H.; Jankhani, S.; Tang, X. (Shirley); Mekonnen, T. H.; Aghakhani, A.; Shahsavan, H. Programmable Nanocomposites of Cellulose Nanocrystals and Zwitterionic Hydrogels for Soft Robotics. *Nat. Commun.* **2023**, *14* (1), 6108. <https://doi.org/10.1038/s41467-023-41874-7>.
- (196) Ali, A.; Haseeb, M. T.; Hussain, M. A.; Tulain, U. R.; Muhammad, G.; Azhar, I.; Hussain, S. Z.; Hussain, I.; Ahmad, N. A pH Responsive and Superporous Biocomposite Hydrogel of Salvia Spinosa Polysaccharide-Co-Methacrylic Acid for Intelligent Drug Delivery. *RSC Adv.* **2023**, *13* (8), 4932–4948. <https://doi.org/10.1039/D2RA05240G>.
- (197) Ismail, O.; Kipcak, A. S.; Piskin, S. Modeling of Absorption Kinetics of Poly(Acrylamide) Hydrogels Crosslinked by EGDMA and PEGDMAs. *Res. Chem. Intermed.* **2013**, *39* (3), 907–919. <https://doi.org/10.1007/s11164-012-0604-z>.
- (198) Orgill, M.; Baker, B. L.; Owen, N. L. FTIR Studies of Conformational Isomerism in Acrylates and Acrylic Acids. *Spectrochim. Acta - Part A Mol. Biomol. Spectrosc.* **1999**, *55* (5), 1021–1024. [https://doi.org/10.1016/S1386-1425\(98\)00242-X](https://doi.org/10.1016/S1386-1425(98)00242-X).
- (199) Soppera, O.; Croutxé-Barghorn, C. Real-Time Fourier Transform Infrared Study of Free-Radical UV-Induced Polymerization of Hybrid Sol–Gel. I. Effect of Silicate Backbone on Photopolymerization Kinetics. *J. Polym. Sci. Part A Polym. Chem.* **2003**, *41* (5), 716–724. <https://doi.org/https://doi.org/10.1002/pola.10622>.
- (200) Arya, A.; Pathak, D. P.; Majumdar, D. K.; Manchanda, S. Methacrylic Acid-Co-Butylmethacrylate Copolymers: Design, Characterization and Evaluation as Encapsulating Material for Colon Targeted Formulations. *Des. Monomers Polym.* **2016**, *19* (1), 34–46. <https://doi.org/10.1080/15685551.2015.1092011>.
- (201) García, D. M.; Escobar, J. L.; Bada, N.; Casquero, J.; Hernández, E.; Katime, I. Synthesis and Characterization of Poly(Methacrylic Acid) Hydrogels for Metoclopramide Delivery. *Eur. Polym. J.* **2004**, *40* (8), 1637–1643.

<https://doi.org/https://doi.org/10.1016/j.eurpolymj.2004.03.011>.

- (202) Lee, T. Y.; Roper, T. M.; Jönsson, E. S.; Guymon, C. A.; Hoyle, C. E. Influence of Hydrogen Bonding on Photopolymerization Rate of Hydroxyalkyl Acrylates. *Macromolecules* **2004**, *37* (10), 3659–3665. <https://doi.org/10.1021/ma0305277>.
- (203) Beuermann, S.; Paquet, D. A.; McMinn, J. H.; Hutchinson, R. A. Propagation Kinetics of Methacrylic Acid Studied by Pulsed-Laser Polymerization. *Macromolecules* **1997**, *30* (2), 194–197. <https://doi.org/10.1021/ma9611073>.
- (204) Leclercq, L.; Pollet, A.; Morcellet, M.; Martel, B. Conformation of Water Soluble Copolymers of Methacrylic Acid and Benzyl Methacrylate. *Eur. Polym. J.* **1999**, *35* (2), 185–193. [https://doi.org/https://doi.org/10.1016/S0014-3057\(98\)00124-4](https://doi.org/https://doi.org/10.1016/S0014-3057(98)00124-4).
- (205) Chu, D. Y.; Thomas, J. K. Photophysical Studies of a Water-Soluble Copolymer of Methacrylic Acid and 1-Pyreneacrylic Acid. *Macromolecules* **1984**, *17* (10), 2142–2147. <https://doi.org/10.1021/ma00140a047>.
- (206) Fang, Q.; Meier, M.; Yu, J. J.; Wang, Z. M.; Zhang, J.-Y.; Wu, J. X.; Kenyon, A.; Hoffmann, P.; Boyd, I. W. FTIR and XPS Investigation of Er-Doped SiO₂–TiO₂ Films. *Mater. Sci. Eng. B* **2003**, *105* (1), 209–213. <https://doi.org/https://doi.org/10.1016/j.mseb.2003.08.047>.
- (207) Primeau, N.; Vautey, C.; Langlet, M. The Effect of Thermal Annealing on Aerosol-Gel Deposited SiO₂ Films: A FTIR Deconvolution Study. *Thin Solid Films* **1997**, *310* (1), 47–56. [https://doi.org/https://doi.org/10.1016/S0040-6090\(97\)00340-4](https://doi.org/https://doi.org/10.1016/S0040-6090(97)00340-4).
- (208) Osswald, J.; Fehr, K. T. FTIR Spectroscopic Study on Liquid Silica Solutions and Nanoscale Particle Size Determination. *J. Mater. Sci.* **2006**, *41* (5), 1335–1339. <https://doi.org/10.1007/s10853-006-7327-8>.
- (209) Carswell, T. G.; Hill, D. J. T.; Kellman, R.; Londero, D. I.; O'Donnell, J. H.; Pomery, P. J.; Winzor, C. L. Mechanisms of Polymerization of Methacrylate Copolymers of Biological Interest. *Makromol. Chemie. Macromol. Symp.* **1991**, *51* (1), 183–191. <https://doi.org/https://doi.org/10.1002/masy.19910510116>.
- (210) Zhu, S.; Hamielec, A. Kinetics of Polymeric Network Synthesis via Free-Radical Mechanisms - Polymerization and Polymer Modification. *Makromol. Chemie.*

- Macromol. Symp.* **1992**, *63* (1), 135–182.
<https://doi.org/https://doi.org/10.1002/masy.19920630112>.
- (211) Czuba, U.; Quintana, R.; Lassaux, P.; Bombera, R.; Ceccone, G.; Bañuls-Ciscar, J.; Moreno-Couranjou, M.; Detrembleur, C.; Choquet, P. Anti-Biofouling Activity of Ranaspumin-2 Bio-Surfactant Immobilized on Catechol-Functional PMMA Thin Layers Prepared by Atmospheric Plasma Deposition. *Colloids Surfaces B Biointerfaces* **2019**, *178*, 120–128. <https://doi.org/https://doi.org/10.1016/j.colsurfb.2019.02.049>.
- (212) Scranton, A. B.; Peppas, N. A. A Statistical Model of Free-Radical Copolymerization/Crosslinking Reactions. *J. Polym. Sci. Part A Polym. Chem.* **1990**, *28* (1), 39–57. <https://doi.org/https://doi.org/10.1002/pola.1990.080280103>.
- (213) Beamson, G. High Resolution XPS of Organic Polymer. *Anal. Chim. Acta* **1993**, *276*, 469–470.
- (214) Corfield, G. C.; Monks, H. H.; Ellinger, L. P. Copolymerization Behaviour of N,N' — Divinylureas. *Polymer (Guildf)*. **1975**, *16* (11), 770–772. [https://doi.org/https://doi.org/10.1016/0032-3861\(75\)90103-2](https://doi.org/https://doi.org/10.1016/0032-3861(75)90103-2).
- (215) Bruggeman, P. J.; Frontiera, R. R.; Kortshagen, U. R.; Kushner, M. J.; Linic, S.; Schatz, G. C.; Andaraarachchi, H.; Exarhos, S.; Jones, L. O.; Mueller, C. M.; Rich, C. C.; Xu, C.; Yue, Y.; Zhang, Y. Plasma-Driven Solution Electrolysis. *J. Appl. Phys.* **2021**, *129* (20). <https://doi.org/10.1063/5.0044261>.
- (216) Cosas Fernandes, J. P.; Federico, C. E.; Basterra-Beroiz, B.; Weydert, M.; Quintana, R. Revealing Phase-Specific Properties of Elastomeric Blends and Their Molecular Structure at the Nanoscale by AFM. *Polymer (Guildf)*. **2022**, *257*, 125229. <https://doi.org/https://doi.org/10.1016/j.polymer.2022.125229>.
- (217) Reviakine, I.; Johannsmann, D.; Richter, R. P. Hearing What You Cannot See and Visualizing What You Hear: Interpreting Quartz Crystal Microbalance Data from Solvated Interfaces. *Anal. Chem.* **2011**, *83* (23), 8838–8848. <https://doi.org/10.1021/ac201778h>.
- (218) M V Voinova; M Rodahl; M Jonson; B Kasemo. Viscoelastic Acoustic Response of Layered Polymer Films at Fluid-Solid Interfaces: Continuum Mechanics Approach.

- Phys. Scr.* **1999**, *59* (5), 391. <https://doi.org/10.1238/Physica.Regular.059a00391>.
- (219) Easley, A. D.; Ma, T.; Eneh, C. I.; Yun, J.; Thakur, R. M.; Lutkenhaus, J. L. A Practical Guide to Quartz Crystal Microbalance with Dissipation Monitoring of Thin Polymer Films. *J. Polym. Sci.* **2022**, *60* (7), 1090–1107. <https://doi.org/https://doi.org/10.1002/pol.20210324>.
- (220) Chen, Q.; Xu, S.; Liu, Q.; Masliyah, J.; Xu, Z. QCM-D Study of Nanoparticle Interactions. *Adv. Colloid Interface Sci.* **2016**, *233*, 94–114. <https://doi.org/10.1016/j.cis.2015.10.004>.
- (221) Minamikawa, T.; Hsieh, Y.-D.; Shibuya, K.; Hase, E.; Kaneoka, Y.; Okubo, S.; Inaba, H.; Mizutani, Y.; Yamamoto, H.; Iwata, T.; Yasui, T. Dual-Comb Spectroscopic Ellipsometry. *Nat. Commun.* **2017**, *8* (1), 610. <https://doi.org/10.1038/s41467-017-00709-y>.
- (222) Bertin, F.; Baron, T.; Mariolle, D.; Martin, F.; Chabli, A.; Dupuy, M. Characterization of Deposited Nanocrystalline Silicon by Spectroscopic Ellipsometry. *Phys. status solidi* **1999**, *175* (1), 405–412. [https://doi.org/https://doi.org/10.1002/\(SICI\)1521-396X\(199909\)175:1<405::AID-PSSA405>3.0.CO;2-U](https://doi.org/https://doi.org/10.1002/(SICI)1521-396X(199909)175:1<405::AID-PSSA405>3.0.CO;2-U).
- (223) Guzmán, E.; Chuliá-Jordán, R.; Ortega, F.; Rubio, R. G. Influence of the Percentage of Acetylation on the Assembly of LbL Multilayers of Poly(Acrylic Acid) and Chitosan. *Phys. Chem. Chem. Phys.* **2011**, *13* (40), 18200–18207. <https://doi.org/10.1039/C1CP21609K>.
- (224) Guzmán, E.; Cavallo, J. A.; Chuliá-Jordán, R.; Gómez, C.; Strumia, M. C.; Ortega, F.; Rubio, R. G. PH-Induced Changes in the Fabrication of Multilayers of Poly(Acrylic Acid) and Chitosan: Fabrication, Properties, and Tests as a Drug Storage and Delivery System. *Langmuir* **2011**, *27* (11), 6836–6845. <https://doi.org/10.1021/la200522r>.
- (225) Osypova, A.; Thakar, D.; Dejeu, J.; Bonnet, H.; Van der Heyden, A.; Dubacheva, G. V.; Richter, R. P.; Defrancq, E.; Spinelli, N.; Coche-Guérente, L.; Labbé, P. Sensor Based on Aptamer Folding to Detect Low-Molecular Weight Analytes. *Anal. Chem.* **2015**, *87* (15), 7566–7574. <https://doi.org/10.1021/acs.analchem.5b01736>.
- (226) Sans, J.; Azevedo Gonçalves, I.; Quintana, R. Ultrathin Film Hydrogels with Controlled

- Swelling and Viscoelastic Properties Deposited by Nanosecond Pulsed Plasma Induced-Polymerization. *Adv. Mater. Interfaces* **2024**, *11* (2), 2300644. <https://doi.org/https://doi.org/10.1002/admi.202300644>.
- (227) Liang, K.; Grebowicz, J.; Valles, E.; Karasz, F. E.; MacKnight, W. J. Thermal and Rheological Properties of Miscible Polyethersulfone/Polyimide Blends. *J. Polym. Sci. Part B Polym. Phys.* **1992**, *30* (5), 465–476. <https://doi.org/https://doi.org/10.1002/polb.1992.090300506>.
- (228) Mao, Y. Copolymerization and Crosslinking. In *CVD Polymers*; 2015; pp 45–63. <https://doi.org/https://doi.org/10.1002/9783527690275.ch3>.
- (229) Chauvin, J.; Judée, F.; Yousfi, M.; Vicendo, P.; Merbahi, N. Analysis of Reactive Oxygen and Nitrogen Species Generated in Three Liquid Media by Low Temperature Helium Plasma Jet. *Sci. Rep.* **2017**, *7* (1), 4562. <https://doi.org/10.1038/s41598-017-04650-4>.
- (230) Tobita, H.; Hamielec, A. E. Control of Network Structure in Free-Radical Crosslinking Copolymerization. *Polymer (Guildf)*. **1992**, *33* (17), 3647–3657. [https://doi.org/https://doi.org/10.1016/0032-3861\(92\)90651-C](https://doi.org/https://doi.org/10.1016/0032-3861(92)90651-C).
- (231) Landin, D. T.; Macosko, C. W. Cyclization and Reduced Reactivity of Pendant Vinyls during the Copolymerization of Methyl Methacrylate and Ethylene Glycol Dimethacrylate. *Macromolecules* **1988**, *21* (3), 846–851. <https://doi.org/10.1021/ma00181a048>.
- (232) Lee, J. H.; Bucknall, D. G. Swelling Behavior and Network Structure of Hydrogels Synthesized Using Controlled UV-Initiated Free Radical Polymerization. *J. Polym. Sci. Part B Polym. Phys.* **2008**, *46* (14), 1450–1462. <https://doi.org/https://doi.org/10.1002/polb.21481>.
- (233) Wang, C.; Chen, X.; Wang, L.; Makihata, M.; Liu, H.-C.; Zhou, T.; Zhao, X. Bioadhesive Ultrasound for Long-Term Continuous Imaging of Diverse Organs. *Science (80-.)*. **2022**, *377* (6605), 517–523. <https://doi.org/10.1126/science.abo2542>.
- (234) Wu, Z.; Ding, H.; Tao, K.; Wei, Y.; Gui, X.; Shi, W.; Xie, X.; Wu, J. Ultrasensitive, Stretchable, and Fast-Response Temperature Sensors Based on Hydrogel Films for

- Wearable Applications. *ACS Appl. Mater. Interfaces* **2021**, *13* (18), 21854–21864. <https://doi.org/10.1021/acsami.1c05291>.
- (235) Cosas Fernandes, J. P.; Federico, C. E.; Lentzen, E.; Valle, N.; Basterra-Beroiz, B.; Weydert, M.; Quintana, R. AFM-NanoSIMS Correlative Microscopy on Multiphase Elastomeric Systems: Nanomechanical Properties and Elemental Distribution at the Nanoscale. *Polym. Test.* **2023**, *121*, 107996. <https://doi.org/https://doi.org/10.1016/j.polymertesting.2023.107996>.
- (236) Hoffman, A. S. Non-Fouling Surface Technologies. *J. Biomater. Sci. Polym. Ed.* **1999**, *10* (10), 1011–1014. <https://doi.org/10.1163/156856299X00658>.
- (237) Wyman, P. 1 - Hydrophilic Coatings for Biomedical Applications in and Ex Vivo. In *Woodhead Publishing Series in Biomaterials*; Driver, M. B. T.-C. for B. A., Ed.; Woodhead Publishing, 2012; pp 3–42. <https://doi.org/https://doi.org/10.1533/9780857093677.1.3>.
- (238) Lee, J. H.; Lee, H. B.; Andrade, J. D. Blood Compatibility of Polyethylene Oxide Surfaces. *Prog. Polym. Sci.* **1995**, *20* (6), 1043–1079. [https://doi.org/https://doi.org/10.1016/0079-6700\(95\)00011-4](https://doi.org/https://doi.org/10.1016/0079-6700(95)00011-4).
- (239) Nam, E.; Wong, E. H. H.; Tan, S.; Fu, Q.; Blencowe, A.; Qiao, G. G. Antifogging Surface Facilitated by Nanoscale Coatings with Controllable Hydrophobicity and Cross-Linking Density. *Macromol. Mater. Eng.* **2017**, *302* (1), 1600199. <https://doi.org/https://doi.org/10.1002/mame.201600199>.
- (240) Li, X.; Liu, K. L.; Li, J.; Tan, E. P. S.; Chan, L. M.; Lim, C. T.; Goh, S. H. Synthesis, Characterization, and Morphology Studies of Biodegradable Amphiphilic Poly[(R)-3-Hydroxybutyrate]-Alt-Poly(Ethylene Glycol) Multiblock Copolymers. *Biomacromolecules* **2006**, *7* (11), 3112–3119. <https://doi.org/10.1021/bm060675f>.
- (241) Choi, C.; Hwang, I.; Cho, Y.-L.; Han, S. Y.; Jo, D. H.; Jung, D.; Moon, D. W.; Kim, E. J.; Jeon, C. S.; Kim, J. H.; Chung, T. D.; Lee, T. G. Fabrication and Characterization of Plasma-Polymerized Poly(Ethylene Glycol) Film with Superior Biocompatibility. *ACS Appl. Mater. Interfaces* **2013**, *5* (3), 697–702. <https://doi.org/10.1021/am302208f>.
- (242) Dehghani, E. S.; Spencer, N. D.; Ramakrishna, S. N.; Benetti, E. M. Crosslinking

- Polymer Brushes with Ethylene Glycol-Containing Segments: Influence on Physicochemical and Antifouling Properties. *Langmuir* **2016**, *32* (40), 10317–10327. <https://doi.org/10.1021/acs.langmuir.6b02958>.
- (243) Zhang, J.; Wang, J.; Zhang, H.; Lin, J.; Ge, Z.; Zou, X. Macroporous Interpenetrating Network of Polyethylene Glycol (PEG) and Gelatin for Cartilage Regeneration. *Biomed. Mater.* **2016**, *11* (3), 35014. <https://doi.org/10.1088/1748-6041/11/3/035014>.
- (244) Deng, J.; Yu, J.; Dai, Z.; Deng, L. Cross-Linked PEG Membranes of Interpenetrating Networks with Ionic Liquids as Additives for Enhanced CO₂ Separation. *Ind. Eng. Chem. Res.* **2019**, *58* (13), 5261–5268. <https://doi.org/10.1021/acs.iecr.9b00241>.
- (245) Lv, T.-R.; Zhang, W.-H.; Yang, Y.-Q.; Zhang, J.-C.; Yin, M.-J.; Yin, Z.; Yong, K.-T.; An, Q.-F. Micro/Nano-Fabrication of Flexible Poly(3,4-Ethylenedioxythiophene)-Based Conductive Films for High-Performance Microdevices. *Small* **2023**, *19* (30), 2301071. <https://doi.org/https://doi.org/10.1002/sml.202301071>.
- (246) Liang, Y.; Li, M.; Yang, Y.; Qiao, L.; Xu, H.; Guo, B. PH/Glucose Dual Responsive Metformin Release Hydrogel Dressings with Adhesion and Self-Healing via Dual-Dynamic Bonding for Athletic Diabetic Foot Wound Healing. *ACS Nano* **2022**, *16* (2), 3194–3207. <https://doi.org/10.1021/acsnano.1c11040>.
- (247) Yu, Y.; Cheng, Y.; Tong, J.; Zhang, L.; Wei, Y.; Tian, M. Recent Advances in Thermo-Sensitive Hydrogels for Drug Delivery. *J. Mater. Chem. B* **2021**, *9* (13), 2979–2992. <https://doi.org/10.1039/D0TB02877K>.
- (248) Zhao, Z.; Das, S.; Zharnikov, M. Tuning the Properties of Poly(Ethylene Glycol) Films and Membranes by the Molecular Weight of the Precursors. *ACS Appl. Polym. Mater.* **2022**, *4* (1), 645–653. <https://doi.org/10.1021/acsapm.1c01569>.
- (249) Martwong, E.; Tran, Y. Lower Critical Solution Temperature Phase Transition of Poly(PEGMA) Hydrogel Thin Films. *Langmuir* **2021**, *37* (28), 8585–8593. <https://doi.org/10.1021/acs.langmuir.1c01165>.
- (250) Killion, J. A.; Geever, L. M.; Devine, D. M.; Kennedy, J. E.; Higginbotham, C. L. Mechanical Properties and Thermal Behaviour of PEGDMA Hydrogels for Potential Bone Regeneration Application. *J. Mech. Behav. Biomed. Mater.* **2011**, *4* (7), 1219–

1227. <https://doi.org/10.1016/j.jmbbm.2011.04.004>.
- (251) Karakurt, I.; Aydoğdu, A.; Çıkrıkçı, S.; Orozco, J.; Lin, L. Stereolithography (SLA) 3D Printing of Ascorbic Acid Loaded Hydrogels: A Controlled Release Study. *Int. J. Pharm.* **2020**, *584*, 119428. <https://doi.org/10.1016/j.ijpharm.2020.119428>.
- (252) Patel, N. R.; Whitehead, A. K.; Newman, J. J.; Caldorera-Moore, M. E. Poly(Ethylene Glycol) Hydrogels with Tailorable Surface and Mechanical Properties for Tissue Engineering Applications. *ACS Biomater. Sci. Eng.* **2017**, *3* (8), 1494–1498. <https://doi.org/10.1021/acsbiomaterials.6b00233>.
- (253) Johannsmeier, S.; Nguyen, M. T. T.; Hohndorf, R.; Dräger, G.; Heinemann, D.; Ripken, T.; Heisterkamp, A. PEGDMA Hydrogels for Cell Adhesion and Optical Waveguiding. *ACS Appl. Bio Mater.* **2020**, *3* (10), 7011–7020. <https://doi.org/10.1021/acsabm.0c00885>.
- (254) Yang, J.; Liang, G.; Xiang, T.; Situ, W. Effect of Crosslinking Processing on the Chemical Structure and Biocompatibility of a Chitosan-Based Hydrogel. *Food Chem.* **2021**, *354*, 129476. <https://doi.org/10.1016/j.foodchem.2021.129476>.
- (255) Yang, G.; Xiao, Z.; Long, H.; Ma, K.; Zhang, J.; Ren, X.; Zhang, J. Assessment of the Characteristics and Biocompatibility of Gelatin Sponge Scaffolds Prepared by Various Crosslinking Methods. *Sci. Rep.* **2018**, *8* (1), 1616. <https://doi.org/10.1038/s41598-018-20006-y>.
- (256) Hegemann, D.; Hossain, M. M.; Balazs, D. J. Nanostructured Plasma Coatings to Obtain Multifunctional Textile Surfaces. *Prog. Org. Coatings* **2007**, *58* (2), 237–240. <https://doi.org/10.1016/j.porgcoat.2006.08.027>.
- (257) Rehman, A.; Houshyar, S.; Reineck, P.; Padhye, R.; Wang, X. Multifunctional Smart Fabrics through Nanodiamond-Polyaniline Nanocomposites. *ACS Appl. Polym. Mater.* **2020**, *2* (11), 4848–4855. <https://doi.org/10.1021/acsapm.0c00789>.
- (258) Singh, M.; Vajpayee, M.; Ledwani, L. Eco-Friendly Surface Modification and Nanofinishing of Textile Polymers to Enhance Functionalisation BT - Nanotechnology for Energy and Environmental Engineering; Ledwani, L., Sangwai, J. S., Eds.; Springer International Publishing: Cham, 2020; pp 529–559. <https://doi.org/10.1007/978-3-030->

33774-2_23.

- (259) Prado, M.; Marski, S. R. D. S.; Pacheco, L. P.; Barros, A. W. da C.; Gerardo, C. F.; Carvalho Prado, M.; Marques, F. D.; Lunz, J. do N.; de Carvalho Silva, G. C.; Archanjo, B. S.; Lione, V. de O. F.; Achete, C. A.; Simão, R. A. Hexamethyldisiloxane Coating by Plasma to Create a Superhydrophobic Surface for Fabric Masks. *J. Mater. Res. Technol.* **2022**, *17*, 913–924. <https://doi.org/https://doi.org/10.1016/j.jmrt.2022.01.003>.
- (260) Carneiro de Oliveira, J.; de Meireles Brioude, M.; Airoudj, A.; Bally-Le Gall, F.; Roucoules, V. Plasma Polymerization in the Design of New Materials: Looking through the Lens of Maleic Anhydride Plasma Polymers. *Mater. Today Chem.* **2022**, *23*, 100646. <https://doi.org/10.1016/j.mtchem.2021.100646>.
- (261) Yuan, C.; Zhou, C.; Demidov, M. V.; Gyergyek, T.; Kovačič, J.; Koepke, M. E.; Kurlyandskaya, I. P.; Demidov, V. I.; Costea, S.; Zhou, Z. Correlation Between Fluctuating Electron Temperature and Fluctuating Space-Potential Challenges the Probe Determination of Turbulent Electric Field Spectrum. *IEEE Trans. Plasma Sci.* **2024**, *52* (4), 1162–1167. <https://doi.org/10.1109/TPS.2023.3337008>.
- (262) Archambault-Caron, M.; Gagnon, H.; Nisol, B.; Piyakis, K.; Wertheimer, M. R. Precise Energy and Temperature Measurements in Dielectric Barrier Discharges at Atmospheric Pressure. *Plasma Sources Sci. Technol.* **2015**, *24* (4), 45004. <https://doi.org/10.1088/0963-0252/24/4/045004>.
- (263) Brandenburg, R. Dielectric Barrier Discharges: Progress on Plasma Sources and on the Understanding of Regimes and Single Filaments. *Plasma Sources Sci. Technol.* **2017**, *26* (5), 53001. <https://doi.org/10.1088/1361-6595/aa6426>.
- (264) Arjunan, V.; Subramanian, S.; Mohan, S. Fourier Transform Infrared and Raman Spectral Analysis of Trans-1,4-Polyisoprene. *Spectrochim. Acta Part A Mol. Biomol. Spectrosc.* **2001**, *57* (13), 2547–2554. [https://doi.org/https://doi.org/10.1016/S1386-1425\(01\)00426-7](https://doi.org/https://doi.org/10.1016/S1386-1425(01)00426-7).
- (265) Paesani, F. Hydrogen Bond Dynamics in Heavy Water Studied with Quantum Dynamical Simulations. *Phys. Chem. Chem. Phys.* **2011**, *13* (44), 19865–19875. <https://doi.org/10.1039/C1CP21863H>.

ANNEX A

Table A1: Nebulizer parameters to obtain the mass delivery rates applied in the study. The delivery rates were obtained based on the gravimetric measurements of three independent measurements.

Low delivery rate	
Nebulizing gas inlet	$1.2 \text{ L}\cdot\text{min}^{-1}$
Carrier gas inlet for the nebulizer	$0.5 \text{ L}\cdot\text{min}^{-1}$
Pressure drop	1 bar
Mass delivery rate	$18.5 \pm 7.6 \text{ mg}\cdot\text{min}^{-1}$
Medium delivery rate	
Nebulizing gas inlet	$1.8 \text{ L}\cdot\text{min}^{-1}$
Carrier gas inlet for the nebulizer	$0.5 \text{ L}\cdot\text{min}^{-1}$
Pressure drop	1.9 bar
Mass delivery rate	$33.8 \pm 1.1 \text{ mg}\cdot\text{min}^{-1}$
High delivery rate	
Nebulizing gas inlet	$4 \text{ L}\cdot\text{min}^{-1}$
Carrier gas inlet for the nebulizer	$0.5 \text{ L}\cdot\text{min}^{-1}$
Pressure drop	5 bar
Mass delivery rate	$71.3 \pm 5.0 \text{ mg}\cdot\text{min}^{-1}$

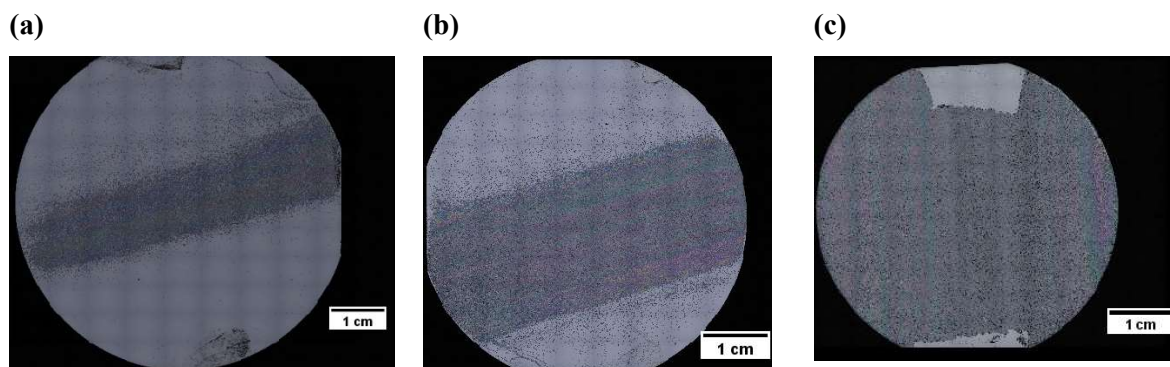


Figure A1: Picture of the coatings obtained at (a) $18 \text{ mg}\cdot\text{min}^{-1}$ and 3000 Hz, (b) $34 \text{ mg}\cdot\text{min}^{-1}$ and 3000 Hz and (c) $71 \text{ mg}\cdot\text{min}^{-1}$ and 3000 Hz.

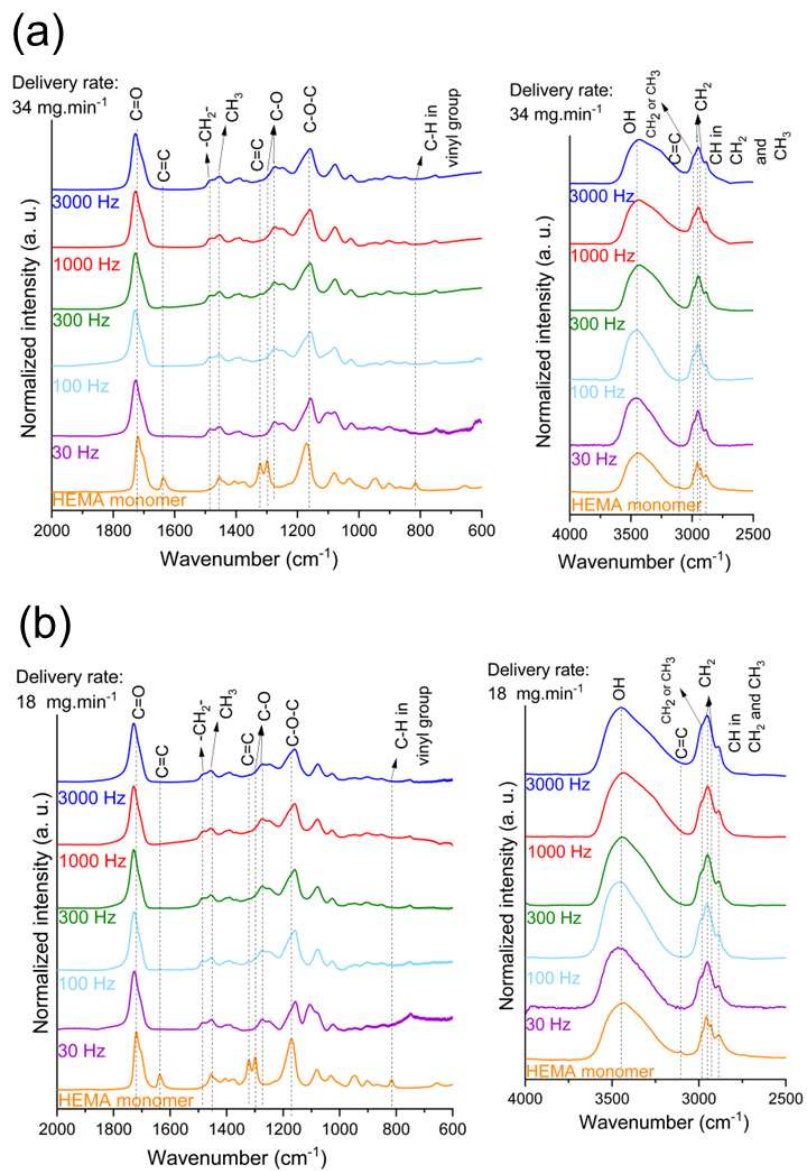


Figure A2: FT-IR spectra of coatings obtained at different frequencies and spray rates of (a) 34 mg·min⁻¹ and (b) 18 mg·min⁻¹.

Table A2: Atomic ratios and functional group distribution determined from XPS high-resolution C 1s spectra of the obtained plasma polymerized thin films and commercial poly(HEMA) (pHEMA_REF) prepared by wet chemistry.

		Atomic ratios		Binding in C 1s (%)			
		C (%)	O (%)	C*-(C,H)	C*-O	C*-COO	O-C*=O
pHEMA_REF		65.0	35.0	43.9 ± 1.2	30.0 ± 1.6	14.6 ± 0.2	14.6 ± 0.2
Series A	30 Hz	67.0	33.0	40.6 ± 0.5	28.2 ± 0.1	15.6 ± 0.2	15.6 ± 0.2
	100 Hz	67.5	32.5	39.8 ± 0.1	27.0 ± 0.3	16.6 ± 0.2	16.7 ± 0.2
	300 Hz	69.9	30.1	33.7 ± 0.6	32.0 ± 0.3	17.1 ± 0.1	17.2 ± 0.1
	1000 Hz	71.7	28.3	38.7 ± 0.6	28.3 ± 0.5	16.5 ± 0.1	16.5 ± 0.1
	3000 Hz	72.1	27.9	40.7 ± 0.4	25.3 ± 0.2	17.0 ± 0.1	17.0 ± 0.1
Series B	30 Hz	67.4	32.6	38.0 ± 0.3	30.0 ± 0.2	16.0 ± 0.1	16.0 ± 0.1
	100 Hz	66.2	33.8	41.8 ± 0.9	27.1 ± 0.5	15.5 ± 0.3	15.6 ± 0.2
	300 Hz	70.2	29.8	34.6 ± 1.3	31.1 ± 0.8	17.1 ± 0.2	17.2 ± 0.2
	1000 Hz	70.4	29.6	34.6 ± 0.3	31.4 ± 0.3	17.0 ± 0.0	17.0 ± 0.0
	3000 Hz	71.6	28.4	39.0 ± 0.3	27.3 ± 0.5	16.8 ± 0.1	16.8 ± 0.1
Series C	300 Hz	70.4	29.6	34.6 ± 0.1	30.3 ± 0.2	17.5 ± 0.1	17.5 ± 0.1
	1000 Hz	70.2	29.8	34.9 ± 0.4	29.6 ± 0.6	17.7 ± 0.1	17.8 ± 0.1
	3000 Hz	70.7	29.3	35.4 ± 0.8	29.8 ± 0.3	17.4 ± 0.2	17.4 ± 0.2

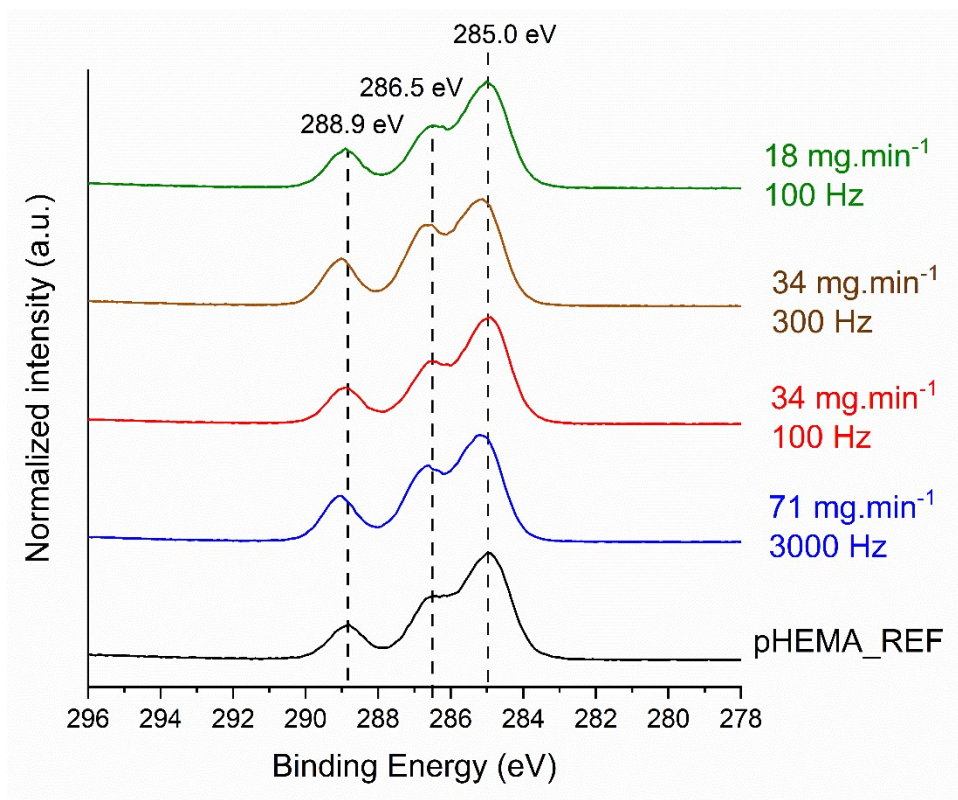


Figure A3: XPS spectrum of the and C 1s core levels for obtained plasma polymerized thin films. C 1s core level of the conventionally polymerized poly(HEMA) (pHEMA_REF) powder is shown as reference.

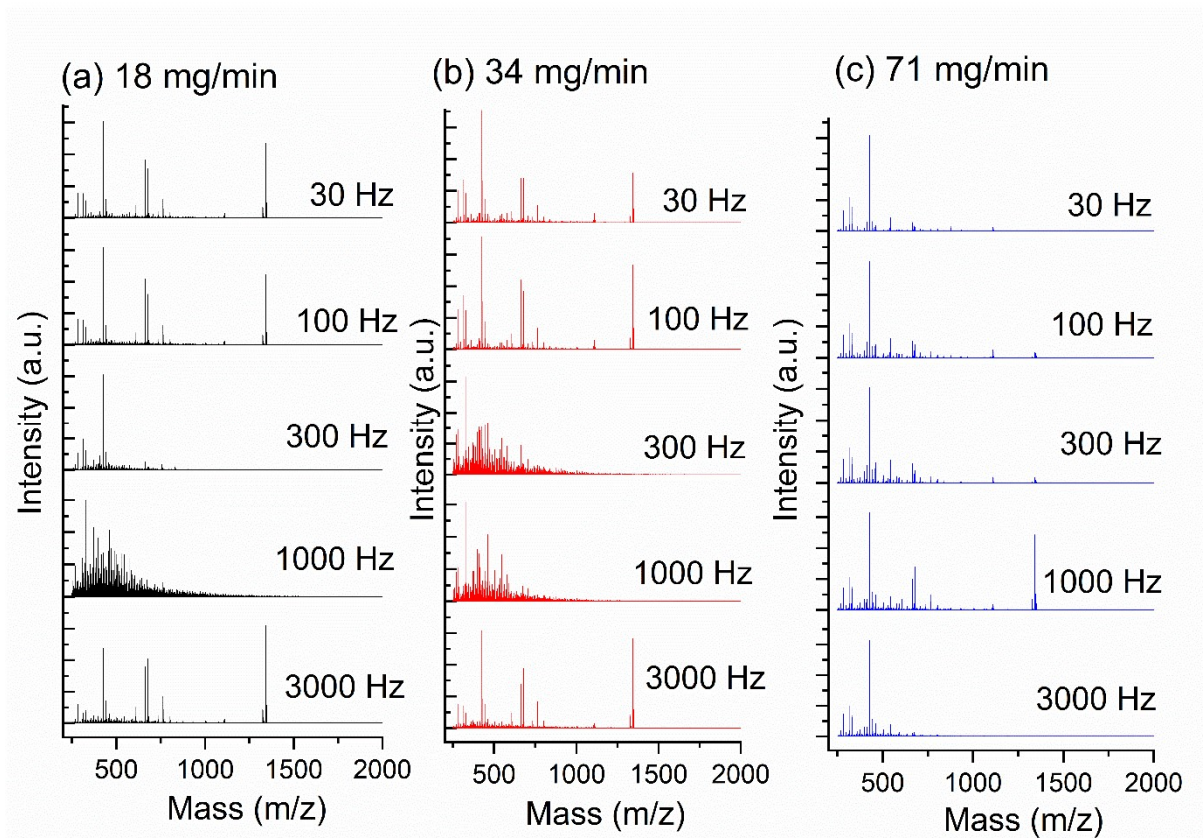


Figure A 4: GPC-MS spectra in the mass range $m/z= 200 - 2000$ of (a) $18 \text{ mg} \cdot \text{min}^{-1}$, (b) $34 \text{ mg} \cdot \text{min}^{-1}$ and (c) $71 \text{ mg} \cdot \text{min}^{-1}$. The data plotted are the average spectra for the elution time between 11.5 and 17.7 min.

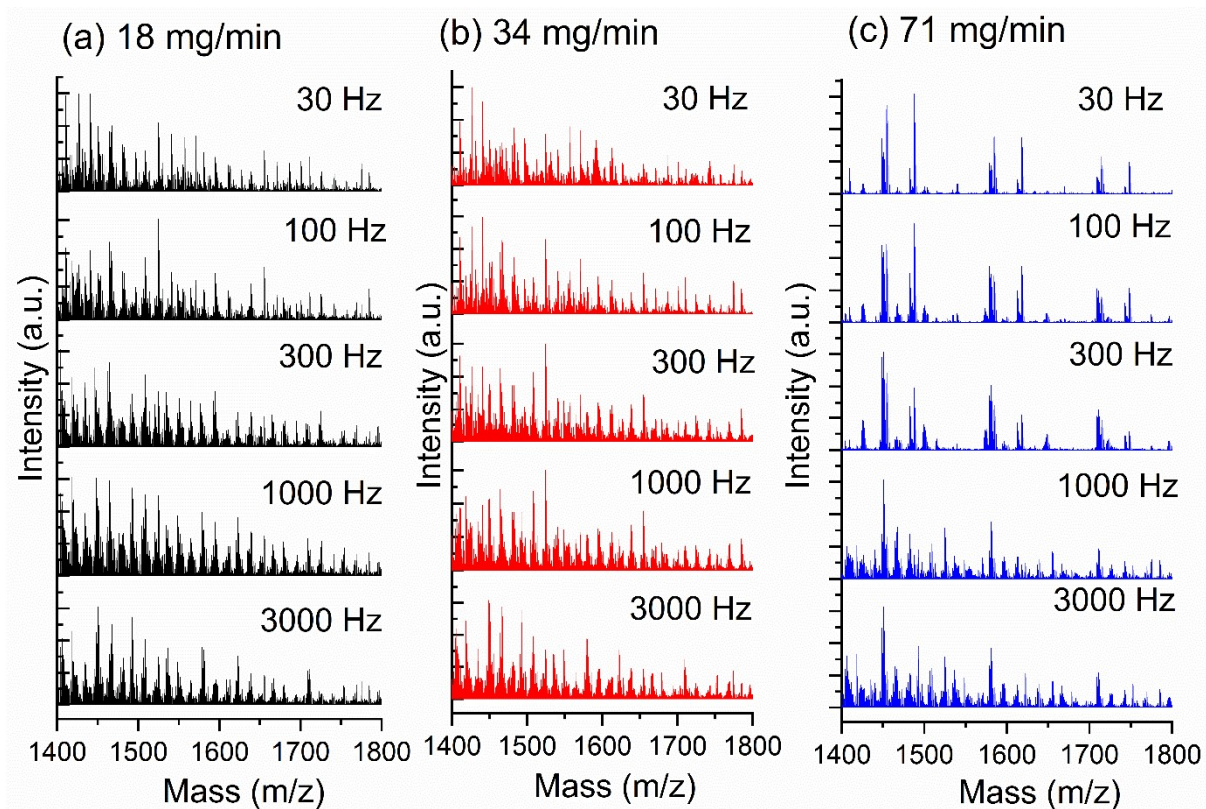


Figure A5: GPC-MS spectra in the mass range $m/z = 1400-1800$ of (a) $18 \text{ mg}\cdot\text{min}^{-1}$, (b) $34 \text{ mg}\cdot\text{min}^{-1}$ and (c) $71 \text{ mg}\cdot\text{min}^{-1}$. The data plotted are the average spectra for the elution time between 11.5 and 17.7 min.

Table A3: Proposed list of radical fragments originating from a single σ -bond breakdown of the HEMA molecule.

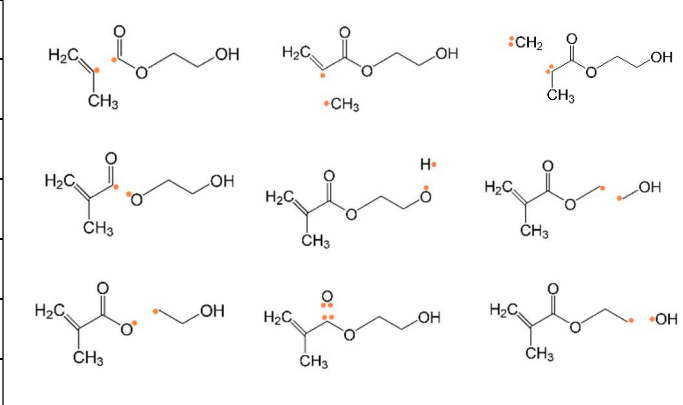
C ₆ H ₁₀ O ₃ (HEMA)		
CH ₃ •	C ₅ H ₇ O ₃ •	
CH ₂ •	C ₅ H ₈ O ₃ •	
O•	C ₆ H ₁₀ O ₂ •	
C ₃ H ₅ •	C ₄ H ₅ O ₃ •	
C ₄ H ₅ O•	C ₂ H ₅ O ₂ •	
C ₄ H ₅ O ₂ •	C ₂ H ₅ O•	
C ₅ H ₇ O ₂ •	CH ₃ O•	
C ₆ H ₉ O ₂ •	OH•	
C ₆ H ₉ O ₃ •	H•	

Table A4: List of relevant species monitored by MALDI-HRMS in LA-PECVD (Na⁺ as reagent ions) with their corresponding m/z values. Only the HRMS peaks related to ionized adducts of [R_i-(HEMA)_n-R_f + Na]⁺ are indicated. Mass assignments were carried out using PolyCalc web-based assignment tool (error mass tolerance below 3 ppm and height threshold of 5%).

m/z = 300-2000			
Sample: 71 mg·min ⁻¹ , 3000 Hz		Sample: 34 mg·min ⁻¹ , 300 Hz	
Assignment	(m/z) _{exp}	Assignment	(m/z) _{exp}
C ₃ H ₅ -(HEMA) ₃ -C ₆ H ₉ O ₃	583.27294	C ₃ H ₅ -(HEMA) ₄ -C ₆ H ₉ O ₃	713.33649
C ₃ H ₅ -(HEMA) ₄ -C ₆ H ₉ O ₃	713.33709	C ₃ H ₅ -(HEMA) ₅ -C ₆ H ₉ O ₃	843.39989
C ₃ H ₅ -(HEMA) ₅ -C ₆ H ₉ O ₃	843.40061	C ₃ H ₅ -(HEMA) ₆ -C ₆ H ₉ O ₃	973.46305
C ₃ H ₅ -(HEMA) ₆ -C ₆ H ₉ O ₃	973.46374	C ₃ H ₅ -(HEMA) ₇ -C ₆ H ₉ O ₃	1103.52603
C ₃ H ₅ -(HEMA) ₇ -C ₆ H ₉ O ₃	1103.52671	C ₃ H ₅ -(HEMA) ₈ -C ₆ H ₉ O ₃	1233.58923
C ₃ H ₅ -(HEMA) ₈ -C ₆ H ₉ O ₃	1233.58993	C ₃ H ₅ -(HEMA) ₉ -C ₆ H ₉ O ₃	1363.65253
C ₃ H ₅ -(HEMA) ₉ -C ₆ H ₉ O ₃	1363.65341	C ₃ H ₅ -(HEMA) ₁₀ -C ₆ H ₉ O ₃	1493.71561
C ₃ H ₅ -(HEMA) ₁₀ -C ₆ H ₉ O ₃	1493.71641	C ₃ H ₅ -(HEMA) ₁₁ -C ₆ H ₉ O ₃	1623.77901
C ₃ H ₅ -(HEMA) ₁₁ -C ₆ H ₉ O ₃	1623.77979	C ₃ H ₅ -(HEMA) ₁₂ -C ₆ H ₉ O ₃	1753.84182
C ₃ H ₅ -(HEMA) ₁₂ -C ₆ H ₉ O ₃	1753.84269	C ₃ H ₅ -(HEMA) ₁₃ -C ₆ H ₉ O ₃	1883.90486
C ₃ H ₅ -(HEMA) ₁₃ -C ₆ H ₉ O ₃	1883.90577		

Sample: 34 mg·min ⁻¹ , 100 Hz		Sample: 18 mg·min ⁻¹ , 100 Hz	
Assignment	(m/z) _{exp}	Assignment	(m/z) _{exp}
C ₃ H ₅ -(HEMA) ₄ -C ₆ H ₉ O ₃	713.33634	C ₃ H ₅ -(HEMA) ₄ -C ₆ H ₉ O ₃	713.33634
C ₃ H ₅ -(HEMA) ₅ -C ₆ H ₉ O ₃	843.39989	C ₃ H ₅ -(HEMA) ₅ -C ₆ H ₉ O ₃	843.39987
C ₃ H ₅ -(HEMA) ₆ -C ₆ H ₉ O ₃	973.46306	C ₃ H ₅ -(HEMA) ₆ -C ₆ H ₉ O ₃	973.46297
C ₃ H ₅ -(HEMA) ₇ -C ₆ H ₉ O ₃	1103.52601	C ₃ H ₅ -(HEMA) ₇ -C ₆ H ₉ O ₃	1103.52585
C ₃ H ₅ -(HEMA) ₈ -C ₆ H ₉ O ₃	1233.58927	C ₃ H ₅ -(HEMA) ₈ -C ₆ H ₉ O ₃	1233.58936
C ₃ H ₅ -(HEMA) ₉ -C ₆ H ₉ O ₃	1363.65258	C ₃ H ₅ -(HEMA) ₉ -C ₆ H ₉ O ₃	1363.65279
C ₃ H ₅ -(HEMA) ₁₀ -C ₆ H ₉ O ₃	1493.71568	C ₃ H ₅ -(HEMA) ₁₀ -C ₆ H ₉ O ₃	1493.71605
C ₃ H ₅ -(HEMA) ₁₁ -C ₆ H ₉ O ₃	1623.77882	C ₃ H ₅ -(HEMA) ₁₁ -C ₆ H ₉ O ₃	1623.77946
C ₃ H ₅ -(HEMA) ₁₂ -C ₆ H ₉ O ₃	1753.84167	C ₃ H ₅ -(HEMA) ₁₂ -C ₆ H ₉ O ₃	1753.84222
C ₃ H ₅ -(HEMA) ₁₃ -C ₆ H ₉ O ₃	1883.90486	C ₃ H ₅ -(HEMA) ₁₃ -C ₆ H ₉ O ₃	1883.90471

m/z = 960-1120			
Sample: 71 mg·min ⁻¹ , 3000 Hz		Sample: 34 mg·min ⁻¹ , 300 Hz	
Assignment	(m/z) _{exp}	Assignment	(m/z) _{exp}
C ₂ H ₅ O(HEMA) ₆ C ₆ H ₉ O ₃	977.45912	C ₅ H ₈ O ₃ (HEMA) ₆ C ₃ H ₅	960.45101
C ₄ H ₅ O(HEMA) ₆ C ₆ H ₉ O ₂	985.46426	C ₃ H ₅ O ₃ (HEMA) ₆ C ₄ H ₅ O	961.42682
C ₄ H ₅ O ₂ (HEMA) ₆ C ₅ H ₇ O ₂	987.44307	C ₃ H ₅ (HEMA) ₆ C ₆ H ₉ O ₃	973.46305
CH ₃ (HEMA) ₇ C ₃ H ₅	989.49529	C ₆ H ₁₀ O ₃ (HEMA) ₆ C ₃ H ₅	974.46641
OH(HEMA) ₇ C ₃ H ₅	991.47443	H(HEMA) ₇ C ₃ H ₅	975.47932
C ₄ H ₅ O(HEMA) ₆ C ₆ H ₉ O ₃	1001.45893	C ₃ H ₅ O ₃ (HEMA) ₆ C ₄ H ₅ O ₂	977.42158
C ₅ H ₇ O ₃ (HEMA) ₆ C ₄ H ₅ O ₂	1003.43799	C ₂ H ₅ O(HEMA) ₆ C ₆ H ₉ O ₃	977.45835
H(HEMA) ₇ C ₄ H ₅ O	1003.47488	C ₄ H ₅ O ₂ (HEMA) ₆ C ₅ H ₇ O ₂	987.44245
C ₃ H ₅ O ₃ (HEMA) ₆ C ₆ H ₉ O ₂	1005.45367	CH ₃ (HEMA) ₇ C ₃ H ₅	989.49451
C ₅ H ₇ O ₂ (HEMA) ₆ C ₆ H ₉ O ₂	1015.47438	C ₃ H ₅ O ₃ (HEMA) ₆ C ₅ H ₇ O ₂	991.43721
C ₃ H ₅ (HEMA) ₇ C ₃ H ₅	1015.51131	OH(HEMA) ₇ C ₃ H ₅	991.47363
CH ₃ (HEMA) ₇ C ₄ H ₅ O	1017.49045	CH ₂ (HEMA) ₇ C ₂ H ₅ O	992.47708
H(HEMA) ₇ C ₄ H ₅ O ₂	1019.46925	C ₂ H ₅ O ₂ (HEMA) ₆ C ₆ H ₉ O ₃	993.45299
C ₆ H ₁₀ O ₂ (HEMA) ₆ C ₆ H ₁₀ O ₂	1031.50559	C ₄ H ₅ O(HEMA) ₆ C ₆ H ₉ O ₃	1001.45816
C ₄ H ₅ O(HEMA) ₇ CH ₃ O	1033.48492	C ₅ H ₇ O ₃ (HEMA) ₆ C ₄ H ₅ O ₂	1003.43722
C ₃ H ₅ (HEMA) ₇ C ₄ H ₅ O	1043.5061	H(HEMA) ₇ C ₄ H ₅ O	1003.47396
C ₆ H ₉ O ₂ (HEMA) ₆ C ₆ H ₉ O ₃	1045.48508	C ₃ H ₅ O ₃ (HEMA) ₆ C ₆ H ₉ O ₂	1005.45293

C ₅ H ₇ O ₃ (HEMA) ₆ C ₆ H ₉ O ₃	1047.46407	C ₅ H ₇ O ₂ (HEMA) ₆ C ₆ H ₉ O ₂	1015.47366
H(HEMA) ₇ C ₆ H ₉ O ₂	1047.50093	C ₃ H ₅ (HEMA) ₇ C ₃ H ₅	1015.51021
C ₄ H ₅ O ₂ (HEMA) ₇ CH ₃ O	1049.47993	C ₄ H ₅ O ₂ (HEMA) ₆ C ₆ H ₉ O ₃	1017.45287
C ₃ H ₅ (HEMA) ₇ C ₄ H ₅ O ₂	1059.50033	CH ₃ (HEMA) ₇ C ₄ H ₅ O	1017.48982
CH ₂ (HEMA) ₇ C ₆ H ₉ O ₂	1060.50385	H(HEMA) ₇ C ₄ H ₅ O ₂	1019.46852
CH ₃ (HEMA) ₇ C ₆ H ₉ O ₂	1061.51661	C ₃ H ₅ O ₃ (HEMA) ₆ C ₆ H ₉ O ₃	1021.44777
H(HEMA) ₇ C ₆ H ₉ O ₃	1063.49542	C ₆ H ₁₀ O ₂ (HEMA) ₆ C ₆ H ₁₀ O ₂	1031.50485
C ₃ H ₅ (HEMA) ₇ C ₅ H ₇ O ₂	1073.5164	C ₄ H ₅ O(HEMA) ₇ CH ₃ O	1033.48416
C ₃ H ₅ (HEMA) ₇ C ₆ H ₉ O ₂	1087.53233	OH(HEMA) ₇ C ₄ H ₅ O ₂	1035.46347
C ₅ H ₇ O ₃ (HEMA) ₇ C ₃ H ₅	1089.51125	C ₃ H ₅ (HEMA) ₇ C ₄ H ₅ O	1043.50511
C ₃ H ₅ (HEMA) ₇ C ₆ H ₉ O ₃	1103.52671	C ₆ H ₉ O ₂ (HEMA) ₆ C ₆ H ₉ O ₃	1045.48422
HEMA(HEMA) ₇ C ₃ H ₅	1104.53008	C ₅ H ₇ O ₃ (HEMA) ₆ C ₆ H ₉ O ₃	1047.4633
H(HEMA) ₈ C ₃ H ₅	1105.54292	H(HEMA) ₇ C ₆ H ₉ O ₂	1047.4999
C ₄ H ₅ O ₂ (HEMA) ₇ C ₅ H ₇ O ₂	1117.50613	C ₄ H ₅ O ₂ (HEMA) ₇ CH ₃ O	1049.479
		H(HEMA) ₇ C ₅ H ₈ O ₃	1050.48249
		C ₃ H ₅ (HEMA) ₇ C ₄ H ₅ O ₂	1059.49967
		CH ₂ (HEMA) ₇ C ₆ H ₉ O ₂	1060.50304
		C ₆ H ₉ O ₃ (HEMA) ₆ C ₆ H ₉ O ₃	1061.47896
		CH ₃ (HEMA) ₇ C ₆ H ₉ O ₂	1061.51604
		H(HEMA) ₇ C ₆ H ₉ O ₃	1063.49476
		C ₅ H ₈ O ₃ (HEMA) ₇ O	1065.47382
		H(HEMA) ₈ H	1065.51088
		C ₃ H ₅ (HEMA) ₇ C ₅ H ₇ O ₂	1073.51554
		CH ₃ (HEMA) ₇ C ₆ H ₉ O ₃	1077.51053
		OH(HEMA) ₇ C ₆ H ₉ O ₃	1079.48969
		C ₃ H ₅ (HEMA) ₇ C ₆ H ₉ O ₂	1087.53179
		C ₅ H ₇ O ₃ (HEMA) ₇ C ₃ H ₅	1089.51062
		C ₅ H ₈ O ₃ (HEMA) ₇ C ₃ H ₅	1090.51401
		C ₃ H ₅ O ₃ (HEMA) ₇ C ₄ H ₅ O	1091.48983
		C ₃ H ₅ (HEMA) ₇ C ₆ H ₉ O ₃	1103.52603
		C ₆ H ₁₀ O ₃ (HEMA) ₇ C ₃ H ₅	1104.52947
		H(HEMA) ₈ C ₃ H ₅	1105.54223
		C ₂ H ₅ O(HEMA) ₇ C ₆ H ₉ O ₃	1107.52143
		C ₄ H ₅ O ₂ (HEMA) ₇ C ₅ H ₇ O ₂	1117.50541

Sample: 34 mg·min ⁻¹ , 100 Hz		Sample: 18 mg·min ⁻¹ , 100 Hz	
Assignment	(m/z) _{exp}	Assignment	(m/z) _{exp}
C ₅ H ₈ O ₃ (HEMA) ₆ C ₃ H ₅	960.45078	C ₅ H ₈ O ₃ (HEMA) ₆ C ₃ H ₅	960.45085
C ₃ H ₅ O ₃ (HEMA) ₆ C ₄ H ₅ O	961.42673	C ₃ H ₅ O ₃ (HEMA) ₆ C ₄ H ₅ O	961.42657
CH ₃ O(HEMA) ₆ C ₆ H ₉ O ₃	963.44256	CH ₃ O(HEMA) ₆ C ₆ H ₉ O ₃	963.44287
O(HEMA) ₇ O	965.42156	C ₄ H ₅ O ₂ (HEMA) ₆ C ₄ H ₅ O ₂	973.42663
C ₃ H ₅ (HEMA) ₆ C ₆ H ₉ O ₃	973.46306	C ₃ H ₅ (HEMA) ₆ C ₆ H ₉ O ₃	973.46297
HEMA(HEMA) ₆ C ₃ H ₅	974.46644	H(HEMA) ₇ C ₃ H ₅	975.47922
H(HEMA) ₇ C ₃ H ₅	975.47903	C ₃ H ₅ O ₃ (HEMA) ₆ C ₄ H ₅ O ₂	977.42146
C ₃ H ₅ O ₃ (HEMA) ₆ C ₄ H ₅ O ₂	977.42162	C ₂ H ₅ O(HEMA) ₆ C ₆ H ₉ O ₃	977.45838
C ₂ H ₅ O(HEMA) ₆ C ₆ H ₉ O ₃	977.45832	C ₄ H ₅ O ₂ (HEMA) ₆ C ₅ H ₇ O ₂	987.44221
CH ₃ (HEMA) ₇ C ₃ H ₅	989.49429	CH ₃ (HEMA) ₇ C ₃ H ₅	989.49443
OH(HEMA) ₇ C ₃ H ₅	991.47352	C ₃ H ₅ O ₃ (HEMA) ₆ C ₅ H ₇ O ₂	991.43718
CH ₂ (HEMA) ₇ C ₂ H ₅ O	992.47695	OH(HEMA) ₇ C ₃ H ₅	991.4735
C ₂ H ₅ O ₂ (HEMA) ₆ C ₆ H ₉ O ₃	993.45287	CH ₂ (HEMA) ₇ C ₂ H ₅ O	992.47695
C ₄ H ₅ O(HEMA) ₆ C ₆ H ₉ O ₃	1001.45815	C ₂ H ₅ O ₂ (HEMA) ₆ C ₆ H ₉ O ₃	993.45278
H(HEMA) ₇ C ₄ H ₅ O	1003.47367	C ₄ H ₅ O(HEMA) ₆ C ₆ H ₉ O ₃	1001.45794
C ₃ H ₅ O ₃ (HEMA) ₆ C ₆ H ₉ O ₂	1005.45274	C ₅ H ₇ O ₃ (HEMA) ₆ C ₄ H ₅ O ₂	1003.43711
C ₃ H ₅ (HEMA) ₇ CH ₃ O	1005.48988	H(HEMA) ₇ C ₄ H ₅ O	1003.4738

C ₆ H ₁₀ O ₂ (HEMA) ₆ C ₃ H ₅ O ₃	1006.45621	C ₃ H ₅ O ₃ (HEMA) ₆ C ₆ H ₉ O ₂	1005.45276
C ₅ H ₇ O ₂ (HEMA) ₆ C ₆ H ₉ O ₂	1015.47356	C ₅ H ₇ O ₂ (HEMA) ₆ C ₆ H ₉ O ₂	1015.47357
C ₃ H ₅ (HEMA) ₇ C ₃ H ₅	1015.51013	C ₄ H ₅ O ₂ (HEMA) ₆ C ₆ H ₉ O ₃	1017.45268
C ₄ H ₅ O ₂ (HEMA) ₆ C ₆ H ₉ O ₃	1017.45282	CH ₃ (HEMA) ₇ C ₄ H ₅ O	1017.48967
CH ₃ (HEMA) ₇ C ₄ H ₅ O	1017.48966	H(HEMA) ₇ C ₄ H ₅ O ₂	1019.46832
H(HEMA) ₇ C ₄ H ₅ O ₂	1019.46853	C ₃ H ₅ O ₃ (HEMA) ₆ C ₆ H ₉ O ₃	1021.44752
C ₃ H ₅ O ₃ (HEMA) ₆ C ₆ H ₉ O ₃	1021.44775	C ₆ H ₁₀ O ₂ (HEMA) ₆ C ₆ H ₁₀ O ₂	1031.50468
C ₆ H ₁₀ O ₂ (HEMA) ₆ C ₆ H ₁₀ O ₂	1031.50482	C ₄ H ₅ O(HEMA) ₇ CH ₃ O	1033.48395
C ₄ H ₅ O(HEMA) ₇ CH ₃ O	1033.48407	OH(HEMA) ₇ C ₄ H ₅ O ₂	1035.46327
OH(HEMA) ₇ C ₄ H ₅ O ₂	1035.46345	C ₃ H ₅ (HEMA) ₇ C ₄ H ₅ O	1043.50499
C ₃ H ₅ (HEMA) ₇ C ₄ H ₅ O	1043.50496	C ₆ H ₉ O ₂ (HEMA) ₆ C ₆ H ₉ O ₃	1045.48419
C ₆ H ₉ O ₂ (HEMA) ₆ C ₆ H ₉ O ₃	1045.48412	H(HEMA) ₇ C ₆ H ₉ O ₂	1047.49987
H(HEMA) ₇ C ₆ H ₉ O ₂	1047.49974	C ₄ H ₅ O ₂ (HEMA) ₇ CH ₃ O	1049.47883
H(HEMA) ₇ C ₆ H ₁₀ O ₂	1048.50326	H(HEMA) ₇ C ₅ H ₈ O ₃	1050.48225
C ₄ H ₅ O ₂ (HEMA) ₇ CH ₃ O	1049.47895	C ₃ H ₅ (HEMA) ₇ C ₄ H ₅ O ₂	1059.49946
H(HEMA) ₇ C ₅ H ₈ O ₃	1050.48239	CH ₂ (HEMA) ₇ C ₆ H ₉ O ₂	1060.50298
C ₃ H ₅ (HEMA) ₇ C ₄ H ₅ O ₂	1059.49964	C ₆ H ₉ O ₃ (HEMA) ₆ C ₆ H ₉ O ₃	1061.47889
CH ₂ (HEMA) ₇ C ₆ H ₉ O ₂	1060.50298	CH ₃ (HEMA) ₇ C ₆ H ₉ O ₂	1061.51602
CH ₃ (HEMA) ₇ C ₆ H ₉ O ₂	1061.51585	H(HEMA) ₇ C ₆ H ₉ O ₃	1063.49472
H(HEMA) ₇ C ₆ H ₉ O ₃	1063.49457	OH(HEMA) ₇ C ₆ H ₁₀ O ₂	1064.49799
OH(HEMA) ₇ C ₆ H ₁₀ O ₂	1064.49797	C ₃ H ₈ O ₃ (HEMA) ₇ O	1065.47383
C ₃ H ₈ O ₃ (HEMA) ₇ O	1065.47385	C ₃ H ₅ (HEMA) ₇ C ₅ H ₇ O ₂	1073.51537
H(HEMA) ₈ H	1065.51069	CH ₃ (HEMA) ₇ C ₆ H ₉ O ₃	1077.51044
OH(HEMA) ₇ C ₅ H ₈ O ₃	1066.47739	C ₆ H ₁₀ O ₂ (HEMA) ₇ CH ₃ O	1078.51391
C ₃ H ₅ (HEMA) ₇ C ₅ H ₇ O ₂	1073.51557	OH(HEMA) ₇ C ₆ H ₉ O ₃	1079.48958
CH ₃ (HEMA) ₇ C ₆ H ₉ O ₃	1077.51038	C ₃ H ₅ (HEMA) ₇ C ₆ H ₉ O ₂	1087.53155
C ₆ H ₁₀ O ₂ (HEMA) ₇ CH ₃ O	1078.5139	C ₅ H ₇ O ₃ (HEMA) ₇ C ₃ H ₅	1089.51033
OH(HEMA) ₇ C ₆ H ₉ O ₃	1079.48968	C ₅ H ₈ O ₃ (HEMA) ₇ C ₃ H ₅	1090.51377
C ₅ H ₈ O ₃ (HEMA) ₇ CH ₃ O	1080.49305	C ₃ H ₅ O ₃ (HEMA) ₇ C ₄ H ₅ O	1091.48973
H(HEMA) ₈ OH	1081.50563	C ₃ H ₅ (HEMA) ₇ C ₆ H ₉ O ₃	1103.52585
C ₃ H ₅ (HEMA) ₇ C ₆ H ₉ O ₂	1087.53122	C ₆ H ₁₀ O ₃ (HEMA) ₇ C ₃ H ₅	1104.52926
C ₅ H ₇ O ₃ (HEMA) ₇ C ₃ H ₅	1089.51038	H(HEMA) ₈ C ₃ H ₅	1105.54245
C ₅ H ₈ O ₃ (HEMA) ₇ C ₃ H ₅	1090.51383	C ₃ H ₅ O ₃ (HEMA) ₇ C ₄ H ₅ O ₂	1107.48446
C ₃ H ₅ O ₃ (HEMA) ₇ C ₄ H ₅ O	1091.48976	C ₂ H ₅ O(HEMA) ₇ C ₆ H ₉ O ₃	1107.52134
CH ₃ O(HEMA) ₇ C ₆ H ₉ O ₃	1093.50561	CH ₂ (HEMA) ₈ C ₃ H ₅	1118.54515
O(HEMA) ₈ O	1095.48447		
C ₃ H ₅ (HEMA) ₇ C ₆ H ₉ O ₃	1103.52601		
HEMA(HEMA) ₇ C ₃ H ₅	1104.52938		
H(HEMA) ₈ C ₃ H ₅	1105.54206		
C ₂ H ₅ O(HEMA) ₇ C ₆ H ₉ O ₃	1107.52137		

m/z = 900-1200

Sample: 71 mg·min⁻¹, 3000 Hz

Assignment	(m/z) _{exp}
C ₅ H ₇ O ₂ (HEMA) ₅ C ₆ H ₉ O ₃	901.40631
C ₆ H ₁₀ O ₂ (HEMA) ₅ C ₆ H ₁₀ O ₂	901.4425
C ₄ H ₅ O(HEMA) ₆ CH ₃ O	903.42196
C ₆ H ₉ O ₂ (HEMA) ₅ C ₆ H ₉ O ₃	915.42186
C ₅ H ₇ O ₃ (HEMA) ₅ C ₆ H ₉ O ₃	917.40107
C ₄ H ₅ O ₂ (HEMA) ₆ CH ₃ O	919.41673
C ₃ H ₅ (HEMA) ₆ C ₄ H ₅ O ₂	929.43747
C ₆ H ₉ O ₃ (HEMA) ₅ C ₆ H ₉ O ₃	931.41669
H(HEMA) ₆ C ₆ H ₉ O ₃	933.43236

$C_4H_5O(HEMA)_6C_4H_5O$	941.43795
$C_3H_5(HEMA)_6C_5H_7O_2$	943.45339
$C_4H_5O(HEMA)_6C_4H_5O_2$	957.43264
$C_5H_7O_3(HEMA)_6C_3H_5$	959.44834
$C_4H_5O_2(HEMA)_6C_4H_5O_2$	973.42764
$C_3H_5(HEMA)_6C_6H_9O_3$	973.46374
$HEMA(HEMA)_6C_3H_5$	974.46719
$H(HEMA)_7C_3H_5$	975.47998
$C_2H_5O(HEMA)_6C_6H_9O_3$	977.45912
$C_4H_5O(HEMA)_6C_6H_9O_2$	985.46426
$C_4H_5O_2(HEMA)_6C_5H_7O_2$	987.44307
$CH_3(HEMA)_7C_3H_5$	989.49529
$OH(HEMA)_7C_3H_5$	991.47443
$C_4H_5O(HEMA)_6C_6H_9O_3$	1001.45893
$C_5H_7O_3(HEMA)_6C_4H_5O_2$	1003.43799
$H(HEMA)_7C_4H_5O$	1003.47488
$C_3H_5O_3(HEMA)_6C_6H_9O_2$	1005.45367
$C_5H_7O_2(HEMA)_6C_6H_9O_2$	1015.47438
$C_3H_5(HEMA)_7C_3H_5$	1015.51131
$CH_3(HEMA)_7C_4H_5O$	1017.49045
$H(HEMA)_7C_4H_5O_2$	1019.46925
$C_6H_{10}O_2(HEMA)_6C_6H_{10}O_2$	1031.50559
$C_4H_5O(HEMA)_7CH_3O$	1033.48492
$C_3H_5(HEMA)_7C_4H_5O$	1043.5061
$C_6H_9O_2(HEMA)_6C_6H_9O_3$	1045.48508
$C_5H_7O_3(HEMA)_6C_6H_9O_3$	1047.46407
$H(HEMA)_7C_6H_9O_2$	1047.50093
$C_4H_5O_2(HEMA)_7CH_3O$	1049.47993
$C_3H_5(HEMA)_7C_4H_5O_2$	1059.50033
$CH_2(HEMA)_7C_6H_9O_2$	1060.50385
$CH_3(HEMA)_7C_6H_9O_2$	1061.51661
$H(HEMA)_7C_6H_9O_3$	1063.49542
$C_3H_5(HEMA)_7C_5H_7O_2$	1073.5164
$C_3H_5(HEMA)_7C_6H_9O_2$	1087.53233
$C_5H_7O_3(HEMA)_7C_3H_5$	1089.51125
$C_3H_5(HEMA)_7C_6H_9O_3$	1103.52671
$C_6H_{10}O_3(HEMA)_7C_3H_5$	1104.53008
$H(HEMA)_8C_3H_5$	1105.54292
$CH_3(HEMA)_8C_3H_5$	1119.55833
$OH(HEMA)_8C_3H_5$	1121.53734
$C_3H_5(HEMA)_8C_3H_5$	1145.57397
$C_6H_{10}O_2(HEMA)_7C_6H_{10}O_2$	1161.56869
$C_5H_7O_3(HEMA)_7C_6H_9O_3$	1177.52694
$C_4H_5O_2(HEMA)_8CH_3O$	1179.54292
$C_3H_5(HEMA)_8C_4H_5O_2$	1189.56339
$CH_2(HEMA)_8C_6H_9O_2$	1190.5667
$H(HEMA)_8C_6H_9O_3$	1193.5584

Table A5: List of relevant species monitored by MALDI-HRMS in LA-PECVD (Na^+ as reagent ions) with their corresponding m/z values. Only the HRMS peaks related to ionized adducts of $[\text{R}_i\text{-(HEMA)}_n\text{-(HEMA)}^{\pm\text{O}=\text{CH}}_4\text{-R}_t + \text{Na}]^+$ are indicated. Mass assignments were carried out using PolyCalc web-based assignment tool (error mass tolerance below 3 ppm and height threshold of 5%).

$m/z = 960\text{-}1120$			
Sample: 71 $\text{mg}\cdot\text{min}^{-1}$, 3000 Hz		Sample: 34 $\text{mg}\cdot\text{min}^{-1}$, 300 Hz	
Assignment	$(m/z)_{\text{exp}}$	Assignment	$(m/z)_{\text{exp}}$
$\text{C}_2\text{H}_5\text{O(HEMA)}_5(\text{C}_5\text{H}_6\text{O}_4)\text{C}_6\text{H}_9\text{O}_2$	961.42657	$\text{C}_2\text{H}_5\text{O(HEMA)}_5(\text{C}_5\text{H}_6\text{O}_4)\text{C}_6\text{H}_9\text{O}_2$	961.42682
$\text{CH}_3(\text{HEMA)}_6(\text{C}_5\text{H}_6\text{O}_4)\text{CH}_3$	963.44287	$\text{C}_4\text{H}_5\text{O(HEMA)}_5(\text{C}_5\text{H}_6\text{O}_4)\text{C}_5\text{H}_7\text{O}_2$	971.41116
$\text{C}_4\text{H}_5\text{O(HEMA)}_5(\text{C}_5\text{H}_6\text{O}_4)\text{C}_5\text{H}_7\text{O}_2$	971.41101	$\text{C}_4\text{H}_5\text{O}_2(\text{HEMA)}_5(\text{C}_7\text{H}_{14}\text{O}_2)\text{C}_4\text{H}_5\text{O}_2$	973.46305
$\text{C}_4\text{H}_5\text{O(HEMA)}_5(\text{C}_7\text{H}_{14}\text{O}_2)\text{C}_5\text{H}_7\text{O}_2$	971.48462	$\text{H(HEMA)}_6(\text{C}_5\text{H}_6\text{O}_4)\text{C}_3\text{H}_5$	975.44235
$\text{C}_3\text{H}_5(\text{HEMA)}_5(\text{C}_5\text{H}_6\text{O}_4)\text{C}_6\text{H}_9\text{O}_3$	973.42663	$\text{C}_2\text{H}_5\text{O(HEMA)}_5(\text{C}_5\text{H}_6\text{O}_4)\text{C}_6\text{H}_9\text{O}_3$	977.42158
$\text{C}_4\text{H}_5\text{O}_2(\text{HEMA)}_5(\text{C}_7\text{H}_{14}\text{O}_2)\text{C}_4\text{H}_5\text{O}_2$	973.46297	$\text{C}_3\text{H}_5\text{O}_3(\text{HEMA)}_5(\text{C}_7\text{H}_{14}\text{O}_2)\text{C}_4\text{H}_5\text{O}_2$	977.45835
$\text{H(HEMA)}_6(\text{C}_5\text{H}_6\text{O}_4)\text{C}_3\text{H}_5$	975.44222	$\text{C}_4\text{H}_5\text{O(HEMA)}_5(\text{C}_7\text{H}_{14}\text{O}_2)\text{C}_6\text{H}_9\text{O}_2$	985.49941
$\text{C}_2\text{H}_5\text{O(HEMA)}_5(\text{C}_5\text{H}_6\text{O}_4)\text{C}_6\text{H}_9\text{O}_3$	977.42146	$\text{C}_4\text{H}_5\text{O}_2(\text{HEMA)}_5(\text{C}_7\text{H}_{14}\text{O}_2)\text{C}_5\text{H}_7\text{O}_2$	987.47868
$\text{C}_3\text{H}_5\text{O}_3(\text{HEMA)}_5(\text{C}_7\text{H}_{14}\text{O}_2)\text{C}_4\text{H}_5\text{O}_2$	977.45838	$\text{CH}_3(\text{HEMA)}_6(\text{C}_5\text{H}_6\text{O}_4)\text{C}_3\text{H}_5$	989.45806
$\text{C}_4\text{H}_5\text{O(HEMA)}_5(\text{C}_7\text{H}_{14}\text{O}_2)\text{C}_6\text{H}_9\text{O}_2$	985.49949	$\text{OH(HEMA)}_6(\text{C}_5\text{H}_6\text{O}_4)\text{C}_3\text{H}_5$	991.43721
$\text{C}_4\text{H}_5\text{O}_2(\text{HEMA)}_5(\text{C}_7\text{H}_{14}\text{O}_2)\text{C}_5\text{H}_7\text{O}_2$	987.47867	$\text{C}_3\text{H}_5\text{O}_3(\text{HEMA)}_5(\text{C}_7\text{H}_{14}\text{O}_2)\text{C}_5\text{H}_7\text{O}_2$	991.47363
$\text{CH}_3(\text{HEMA)}_6(\text{C}_5\text{H}_6\text{O}_4)\text{C}_3\text{H}_5$	989.45784	$\text{CH}_3(\text{HEMA)}_6(\text{C}_5\text{H}_6\text{O}_4)\text{C}_2\text{H}_5\text{O}$	993.45299
$\text{OH(HEMA)}_6(\text{C}_5\text{H}_6\text{O}_4)\text{C}_3\text{H}_5$	991.43718	$\text{H(HEMA)}_6(\text{C}_5\text{H}_6\text{O}_4)\text{C}_4\text{H}_5\text{O}$	1003.43722
$\text{C}_3\text{H}_5\text{O}_3(\text{HEMA)}_5(\text{C}_7\text{H}_{14}\text{O}_2)\text{C}_5\text{H}_7\text{O}_2$	991.4735	$\text{C}_5\text{H}_7\text{O}_3(\text{HEMA)}_5(\text{C}_7\text{H}_{14}\text{O}_2)\text{C}_4\text{H}_5\text{O}_2$	1003.47396
$\text{CH}_3(\text{HEMA)}_6(\text{C}_5\text{H}_6\text{O}_4)\text{C}_2\text{H}_5\text{O}$	993.45278	$\text{C}_3\text{H}_5(\text{HEMA)}_6(\text{C}_5\text{H}_6\text{O}_4)\text{CH}_3\text{O}$	1005.45293
$\text{H(HEMA)}_6(\text{C}_5\text{H}_6\text{O}_4)\text{C}_4\text{H}_5\text{O}$	1003.43711	$\text{C}_3\text{H}_5(\text{HEMA)}_6(\text{C}_5\text{H}_6\text{O}_4)\text{C}_3\text{H}_5$	1015.47366
$\text{C}_5\text{H}_7\text{O}_3(\text{HEMA)}_5(\text{C}_7\text{H}_{14}\text{O}_2)\text{C}_4\text{H}_5\text{O}_2$	1003.4738	$\text{C}_5\text{H}_7\text{O}_2(\text{HEMA)}_5(\text{C}_7\text{H}_{14}\text{O}_2)\text{C}_6\text{H}_9\text{O}_2$	1015.51021
$\text{C}_3\text{H}_5(\text{HEMA)}_6(\text{C}_5\text{H}_6\text{O}_4)\text{CH}_3\text{O}$	1005.45276	$\text{CH}_3(\text{HEMA)}_6(\text{C}_5\text{H}_6\text{O}_4)\text{C}_4\text{H}_5\text{O}$	1017.45287
$\text{C}_3\text{H}_5(\text{HEMA)}_6(\text{C}_5\text{H}_6\text{O}_4)\text{C}_3\text{H}_5$	1015.47357	$\text{C}_4\text{H}_5\text{O}_2(\text{HEMA)}_5(\text{C}_7\text{H}_{14}\text{O}_2)\text{C}_6\text{H}_9\text{O}_3$	1017.48982
$\text{CH}_3(\text{HEMA)}_6(\text{C}_5\text{H}_6\text{O}_4)\text{C}_4\text{H}_5\text{O}$	1017.45268	$\text{C}_3\text{H}_5(\text{HEMA)}_6(\text{C}_5\text{H}_6\text{O}_4)\text{C}_2\text{H}_5\text{O}$	1019.46852
$\text{C}_4\text{H}_5\text{O}_2(\text{HEMA)}_5(\text{C}_7\text{H}_{14}\text{O}_2)\text{C}_6\text{H}_9\text{O}_3$	1017.48967	$\text{C}_3\text{H}_5\text{O}_3(\text{HEMA)}_5(\text{C}_7\text{H}_{14}\text{O}_2)\text{C}_6\text{H}_9\text{O}_3$	1021.48513
$\text{C}_3\text{H}_5(\text{HEMA)}_6(\text{C}_5\text{H}_6\text{O}_4)\text{C}_2\text{H}_5\text{O}$	1019.46832	$\text{C}_6\text{H}_9\text{O}_2(\text{HEMA)}_5(\text{C}_7\text{H}_{14}\text{O}_2)\text{C}_6\text{H}_9\text{O}_2$	1029.52553
$\text{C}_6\text{H}_9\text{O}_2(\text{HEMA)}_5(\text{C}_7\text{H}_{14}\text{O}_2)\text{C}_6\text{H}_9\text{O}_2$	1029.5254	$\text{C}_5\text{H}_7\text{O}_2(\text{HEMA)}_5(\text{C}_7\text{H}_{14}\text{O}_2)\text{C}_6\text{H}_9\text{O}_3$	1031.50485
$\text{C}_6\text{H}_{10}\text{O}_2(\text{HEMA)}_5(\text{C}_7\text{H}_{14}\text{O}_2)\text{C}_6\text{H}_9\text{O}_2$	1030.52895	$\text{C}_5\text{H}_8\text{O}_3(\text{HEMA)}_5(\text{C}_7\text{H}_{14}\text{O}_2)\text{C}_6\text{H}_9\text{O}_2$	1032.50818
$\text{C}_5\text{H}_7\text{O}_2(\text{HEMA)}_5(\text{C}_7\text{H}_{14}\text{O}_2)\text{C}_6\text{H}_9\text{O}_3$	1031.50468	$\text{C}_5\text{H}_7\text{O}_3(\text{HEMA)}_5(\text{C}_7\text{H}_{14}\text{O}_2)\text{C}_5\text{H}_7\text{O}_3$	1033.48416
$\text{C}_5\text{H}_8\text{O}_3(\text{HEMA)}_5(\text{C}_7\text{H}_{14}\text{O}_2)\text{C}_6\text{H}_9\text{O}_2$	1032.50825	$\text{O(HEMA)}_6(\text{C}_7\text{H}_{14}\text{O}_2)\text{C}_4\text{H}_5\text{O}_2$	1034.48755
$\text{C}_5\text{H}_7\text{O}_3(\text{HEMA)}_5(\text{C}_7\text{H}_{14}\text{O}_2)\text{C}_5\text{H}_7\text{O}_3$	1033.48395	$\text{C}_3\text{H}_5(\text{HEMA)}_6(\text{C}_5\text{H}_6\text{O}_4)\text{C}_2\text{H}_5\text{O}_2$	1035.46347
$\text{O(HEMA)}_6(\text{C}_7\text{H}_{14}\text{O}_2)\text{C}_4\text{H}_5\text{O}_2$	1034.48749	$\text{C}_3\text{H}_5(\text{HEMA)}_6(\text{C}_5\text{H}_6\text{O}_4)\text{C}_4\text{H}_5\text{O}$	1043.46853
$\text{C}_3\text{H}_5(\text{HEMA)}_6(\text{C}_5\text{H}_6\text{O}_4)\text{C}_2\text{H}_5\text{O}_2$	1035.46327	$\text{H(HEMA)}_6(\text{C}_5\text{H}_6\text{O}_4)\text{C}_6\text{H}_9\text{O}_2$	1047.4633
$\text{C}_5\text{H}_7\text{O}_3(\text{HEMA)}_5(\text{C}_7\text{H}_{14}\text{O}_2)\text{C}_6\text{H}_9\text{O}_3$	1047.49987	$\text{C}_5\text{H}_7\text{O}_3(\text{HEMA)}_5(\text{C}_7\text{H}_{14}\text{O}_2)\text{C}_6\text{H}_9\text{O}_3$	1047.4999
$\text{CH}_3(\text{HEMA)}_6(\text{C}_5\text{H}_6\text{O}_4)\text{C}_6\text{H}_9\text{O}_2$	1061.47889	$\text{CH}_3(\text{HEMA)}_6(\text{C}_5\text{H}_6\text{O}_4)\text{C}_6\text{H}_9\text{O}_2$	1061.47896
$\text{C}_6\text{H}_9\text{O}_3(\text{HEMA)}_5(\text{C}_7\text{H}_{14}\text{O}_2)\text{C}_6\text{H}_9\text{O}_3$	1061.51602	$\text{C}_6\text{H}_9\text{O}_3(\text{HEMA)}_5(\text{C}_7\text{H}_{14}\text{O}_2)\text{C}_6\text{H}_9\text{O}_3$	1061.51604
$\text{C}_5\text{H}_7\text{O}_3(\text{HEMA)}_6(\text{C}_7\text{H}_{14}\text{O}_2)\text{O}$	1064.49799	$\text{H(HEMA)}_7(\text{C}_5\text{H}_6\text{O}_4)\text{H}$	1065.47382
$\text{H(HEMA)}_7(\text{C}_5\text{H}_6\text{O}_4)\text{H}$	1065.47383	$\text{C}_5\text{H}_8\text{O}_3(\text{HEMA)}_6(\text{C}_7\text{H}_{14}\text{O}_2)\text{O}$	1065.51088
$\text{C}_4\text{H}_5\text{O(HEMA)}_6(\text{C}_7\text{H}_{14}\text{O}_2)\text{C}_4\text{H}_5\text{O}$	1071.53642	$\text{CH}_3(\text{HEMA)}_6(\text{C}_5\text{H}_6\text{O}_4)\text{C}_6\text{H}_9\text{O}_3$	1077.47404
$\text{O(HEMA)}_6(\text{C}_7\text{H}_{14}\text{O}_2)\text{C}_6\text{H}_9\text{O}_3$	1078.51391	$\text{H(HEMA)}_7(\text{C}_5\text{H}_6\text{O}_4)\text{CH}_3$	1079.48969
$\text{H(HEMA)}_7(\text{C}_5\text{H}_6\text{O}_4)\text{CH}_3$	1079.48958	$\text{C}_4\text{H}_5\text{O(HEMA)}_6(\text{C}_7\text{H}_{14}\text{O}_2)\text{C}_4\text{H}_5\text{O}_2$	1087.53179
$\text{C}_4\text{H}_5\text{O(HEMA)}_6(\text{C}_7\text{H}_{14}\text{O}_2)\text{C}_4\text{H}_5\text{O}_2$	1087.53155	$\text{C}_2\text{H}_5\text{O(HEMA)}_6(\text{C}_5\text{H}_6\text{O}_4)\text{C}_6\text{H}_9\text{O}_2$	1091.48983
$\text{C}_5\text{H}_7\text{O}_3(\text{HEMA)}_6(\text{C}_5\text{H}_6\text{O}_4)\text{C}_3\text{H}_5$	1089.47388	$\text{C}_4\text{H}_5\text{O(HEMA)}_6(\text{C}_7\text{H}_{14}\text{O}_2)\text{C}_5\text{H}_7\text{O}_2$	1101.54758
$\text{C}_2\text{H}_5\text{O(HEMA)}_6(\text{C}_5\text{H}_6\text{O}_4)\text{C}_6\text{H}_9\text{O}_2$	1091.48973	$\text{C}_4\text{H}_5\text{O}_2(\text{HEMA)}_6(\text{C}_7\text{H}_{14}\text{O}_2)\text{C}_4\text{H}_5\text{O}_2$	1103.52603
$\text{C}_4\text{H}_5\text{O(HEMA)}_6(\text{C}_7\text{H}_{14}\text{O}_2)\text{C}_5\text{H}_7\text{O}_2$	1101.54754	$\text{H(HEMA)}_7(\text{C}_5\text{H}_6\text{O}_4)\text{C}_3\text{H}_5$	1105.50531
$\text{C}_4\text{H}_5\text{O}_2(\text{HEMA)}_6(\text{C}_7\text{H}_{14}\text{O}_2)\text{C}_4\text{H}_5\text{O}_2$	1103.52585	$\text{C}_3\text{H}_5\text{O}_3(\text{HEMA)}_6(\text{C}_7\text{H}_{14}\text{O}_2)\text{C}_4\text{H}_5\text{O}_2$	1107.52143
$\text{H(HEMA)}_7(\text{C}_5\text{H}_6\text{O}_4)\text{C}_3\text{H}_5$	1105.50521	$\text{C}_4\text{H}_5\text{O(HEMA)}_6(\text{C}_7\text{H}_{14}\text{O}_2)\text{C}_6\text{H}_9\text{O}_2$	1115.56239
$\text{C}_2\text{H}_5\text{O(HEMA)}_6(\text{C}_5\text{H}_6\text{O}_4)\text{C}_6\text{H}_9\text{O}_3$	1107.48446	$\text{C}_6\text{H}_{10}\text{O}_2(\text{HEMA)}_6(\text{C}_7\text{H}_{14}\text{O}_2)\text{C}_4\text{H}_5\text{O}$	1116.56607
$\text{C}_3\text{H}_5\text{O}_3(\text{HEMA)}_6(\text{C}_7\text{H}_{14}\text{O}_2)\text{C}_4\text{H}_5\text{O}_2$	1107.52134	$\text{C}_4\text{H}_5\text{O}_2(\text{HEMA)}_6(\text{C}_7\text{H}_{14}\text{O}_2)\text{C}_5\text{H}_7\text{O}_2$	1117.5415
$\text{C}_4\text{H}_5\text{O(HEMA)}_6(\text{C}_7\text{H}_{14}\text{O}_2)\text{C}_6\text{H}_9\text{O}_2$	1115.56237		
$\text{C}_6\text{H}_{10}\text{O}_2(\text{HEMA)}_6(\text{C}_7\text{H}_{14}\text{O}_2)\text{C}_4\text{H}_5\text{O}$	1116.566		
$\text{C}_4\text{H}_5\text{O}_2(\text{HEMA)}_6(\text{C}_7\text{H}_{14}\text{O}_2)\text{C}_5\text{H}_7\text{O}_2$	1117.5416		
$\text{C}_5\text{H}_8\text{O}_3(\text{HEMA)}_6(\text{C}_7\text{H}_{14}\text{O}_2)\text{C}_4\text{H}_5\text{O}$	1118.54515		

Sample: 34 mg·min ⁻¹ , 100 Hz		Sample: 18 mg·min ⁻¹ , 100 Hz	
Assignment	(m/z) _{exp}	Assignment	(m/z) _{exp}
C ₄ H ₅ O(HEMA) ₅ (C ₇ H ₁₄ O ₂)C ₆ H ₉ O ₂	961.42673	C ₂ H ₅ O(HEMA) ₅ (C ₅ H ₆ O ₄)C ₆ H ₉ O ₂	961.42657
C ₄ H ₅ O ₂ (HEMA) ₅ (C ₇ H ₁₄ O ₂)C ₅ H ₇ O ₂	963.44256	CH ₃ (HEMA) ₆ (C ₅ H ₆ O ₄)CH ₃	963.44287
CH ₃ (HEMA) ₆ (C ₅ H ₆ O ₄)C ₃ H ₅	965.42156	C ₄ H ₅ O(HEMA) ₅ (C ₅ H ₆ O ₄)C ₅ H ₇ O ₂	971.41101
O(HEMA) ₆ (C ₇ H ₁₄ O ₂)C ₃ H ₅	971.4845	C ₄ H ₅ O(HEMA) ₅ (C ₇ H ₁₄ O ₂)C ₅ H ₇ O ₂	971.48462
C ₃ H ₅ O ₃ (HEMA) ₅ (C ₇ H ₁₄ O ₂)C ₅ H ₇ O ₂	973.46306	C ₃ H ₅ (HEMA) ₅ (C ₅ H ₆ O ₄)C ₆ H ₉ O ₃	973.42663
CH ₃ (HEMA) ₆ (C ₅ H ₆ O ₄)C ₂ H ₅ O	975.44234	C ₄ H ₅ O ₂ (HEMA) ₅ (C ₇ H ₁₄ O ₂)C ₄ H ₅ O ₂	973.46297
C ₅ H ₇ O ₃ (HEMA) ₅ (C ₇ H ₁₄ O ₂)C ₄ H ₅ O ₂	977.42162	H(HEMA) ₆ (C ₅ H ₆ O ₄)C ₃ H ₅	975.44222
C ₃ H ₅ (HEMA) ₆ (C ₅ H ₆ O ₄)CH ₃ O	977.45832	C ₂ H ₅ O(HEMA) ₅ (C ₅ H ₆ O ₄)C ₆ H ₉ O ₃	977.42146
C ₃ H ₅ O ₃ (HEMA) ₅ (C ₇ H ₁₄ O ₂)C ₆ H ₉ O ₂	985.49936	C ₃ H ₅ O ₃ (HEMA) ₅ (C ₇ H ₁₄ O ₂)C ₄ H ₅ O ₂	977.45838
C ₅ H ₇ O ₃ (HEMA) ₅ (C ₇ H ₁₄ O ₂)C ₃ H ₅ O ₃	987.4787	C ₄ H ₅ O(HEMA) ₅ (C ₇ H ₁₄ O ₂)C ₆ H ₉ O ₂	985.49949
C ₂ H ₅ O(HEMA) ₆ (C ₅ H ₆ O ₄)CH ₃ O	989.45799	C ₄ H ₅ O ₂ (HEMA) ₅ (C ₇ H ₁₄ O ₂)C ₃ H ₇ O ₂	987.47867
C ₃ H ₅ (HEMA) ₆ (C ₅ H ₆ O ₄)C ₃ H ₅	990.49774	CH ₃ (HEMA) ₆ (C ₅ H ₆ O ₄)C ₃ H ₅	989.45784
C ₅ H ₇ O ₂ (HEMA) ₅ (C ₇ H ₁₄ O ₂)C ₆ H ₉ O ₂	991.47352	OH(HEMA) ₆ (C ₅ H ₆ O ₄)C ₃ H ₅	991.43718
C ₆ H ₁₀ O ₂ (HEMA) ₅ (C ₇ H ₁₄ O ₂)C ₅ H ₇ O ₂	993.45287	C ₃ H ₅ O ₃ (HEMA) ₅ (C ₇ H ₁₄ O ₂)C ₅ H ₇ O ₂	991.4735
CH ₃ (HEMA) ₆ (C ₅ H ₆ O ₄)C ₄ H ₅ O	1003.47367	CH ₃ (HEMA) ₆ (C ₅ H ₆ O ₄)C ₂ H ₅ O	993.45278
C ₄ H ₅ O ₂ (HEMA) ₅ (C ₇ H ₁₄ O ₂)C ₆ H ₉ O ₃	1005.45274	H(HEMA) ₆ (C ₅ H ₆ O ₄)C ₄ H ₅ O	1003.43711
C ₃ H ₅ (HEMA) ₆ (C ₅ H ₆ O ₄)C ₂ H ₅ O	1005.48988	C ₅ H ₇ O ₃ (HEMA) ₅ (C ₇ H ₁₄ O ₂)C ₄ H ₅ O ₂	1003.4738
C ₃ H ₅ O ₃ (HEMA) ₅ (C ₇ H ₁₄ O ₂)C ₆ H ₉ O ₃	1007.46884	C ₃ H ₅ (HEMA) ₆ (C ₅ H ₆ O ₄)CH ₃ O	1005.45276
C ₆ H ₉ O ₂ (HEMA) ₅ (C ₇ H ₁₄ O ₂)C ₆ H ₉ O ₂	1009.44776	C ₃ H ₅ (HEMA) ₆ (C ₅ H ₆ O ₄)C ₃ H ₅	1015.47357
C ₆ H ₁₀ O ₂ (HEMA) ₅ (C ₇ H ₁₄ O ₂)C ₆ H ₉ O ₂	1015.47356	CH ₃ (HEMA) ₆ (C ₅ H ₆ O ₄)C ₄ H ₅ O	1017.45268
C ₅ H ₇ O ₂ (HEMA) ₅ (C ₇ H ₁₄ O ₂)C ₆ H ₉ O ₃	1015.51013	C ₄ H ₅ O ₂ (HEMA) ₅ (C ₇ H ₁₄ O ₂)C ₆ H ₉ O ₃	1017.48967
C ₅ H ₈ O ₃ (HEMA) ₅ (C ₇ H ₁₄ O ₂)C ₆ H ₉ O ₂	1016.51339	C ₃ H ₅ (HEMA) ₆ (C ₅ H ₆ O ₄)C ₂ H ₅ O	1019.46832
C ₅ H ₇ O ₃ (HEMA) ₅ (C ₇ H ₁₄ O ₂)C ₅ H ₇ O ₃	1017.45282	C ₆ H ₉ O ₂ (HEMA) ₅ (C ₇ H ₁₄ O ₂)C ₆ H ₉ O ₂	1029.5254
O(HEMA) ₆ (C ₇ H ₁₄ O ₂)C ₄ H ₅ O ₂	1017.48966	C ₆ H ₁₀ O ₂ (HEMA) ₅ (C ₇ H ₁₄ O ₂)C ₆ H ₉ O ₂	1030.52895
C ₃ H ₅ (HEMA) ₆ (C ₅ H ₆ O ₄)C ₂ H ₅ O ₂	1019.46853	C ₅ H ₇ O ₂ (HEMA) ₅ (C ₇ H ₁₄ O ₂)C ₆ H ₉ O ₃	1031.50468
C ₅ H ₇ O ₃ (HEMA) ₅ (C ₇ H ₁₄ O ₂)C ₆ H ₉ O ₃	1021.48489	C ₅ H ₈ O ₃ (HEMA) ₅ (C ₇ H ₁₄ O ₂)C ₆ H ₉ O ₂	1032.50825
C ₅ H ₈ O ₃ (HEMA) ₅ (C ₇ H ₁₄ O ₂)C ₆ H ₉ O ₃	1029.52553	C ₅ H ₇ O ₃ (HEMA) ₅ (C ₇ H ₁₄ O ₂)C ₃ H ₇ O ₃	1033.48395
C ₆ H ₉ O ₃ (HEMA) ₅ (C ₇ H ₁₄ O ₂)C ₆ H ₉ O ₃	1030.52883	O(HEMA) ₆ (C ₇ H ₁₄ O ₂)C ₄ H ₅ O ₂	1034.4875
C ₅ H ₇ O ₃ (HEMA) ₆ (C ₇ H ₁₄ O ₂)O	1031.50482	C ₃ H ₅ (HEMA) ₆ (C ₅ H ₆ O ₄)C ₂ H ₅ O ₂	1035.46327
H(HEMA) ₇ (C ₅ H ₆ O ₄)H	1032.50818	C ₅ H ₇ O ₃ (HEMA) ₅ (C ₇ H ₁₄ O ₂)C ₆ H ₉ O ₃	1047.49987
C ₅ H ₈ O ₃ (HEMA) ₆ (C ₇ H ₁₄ O ₂)O	1033.48407	CH ₃ (HEMA) ₆ (C ₅ H ₆ O ₄)C ₆ H ₉ O ₂	1061.47889
C ₄ H ₅ O(HEMA) ₆ (C ₇ H ₁₄ O ₂)C ₄ H ₅ O	1034.48754	C ₆ H ₉ O ₃ (HEMA) ₅ (C ₇ H ₁₄ O ₂)C ₆ H ₉ O ₃	1061.51602
O(HEMA) ₆ (C ₇ H ₁₄ O ₂)C ₆ H ₉ O ₃	1035.46345	C ₅ H ₇ O ₃ (HEMA) ₆ (C ₇ H ₁₄ O ₂)O	1064.49799
H(HEMA) ₇ (C ₅ H ₆ O ₄)CH ₃	1047.49974	H(HEMA) ₇ (C ₅ H ₆ O ₄)H	1065.47383
C ₄ H ₅ O(HEMA) ₆ (C ₇ H ₁₄ O ₂)C ₄ H ₅ O ₂	1048.50326	C ₄ H ₅ O(HEMA) ₆ (C ₇ H ₁₄ O ₂)C ₄ H ₅ O	1071.53642
C ₂ H ₅ O(HEMA) ₆ (C ₅ H ₆ O ₄)C ₆ H ₉ O ₂	1061.51585	O(HEMA) ₆ (C ₇ H ₁₄ O ₂)C ₆ H ₉ O ₃	1078.51391
CH ₃ (HEMA) ₇ (C ₅ H ₆ O ₄)CH ₃	1064.49797	H(HEMA) ₇ (C ₅ H ₆ O ₄)CH ₃	1079.48958
H(HEMA) ₇ (C ₅ H ₆ O ₄)CH ₃ O	1065.47385	C ₄ H ₅ O(HEMA) ₆ (C ₇ H ₁₄ O ₂)C ₄ H ₅ O ₂	1087.53155
C ₄ H ₅ O(HEMA) ₆ (C ₇ H ₁₄ O ₂)C ₅ H ₇ O ₂	1065.51069	C ₅ H ₇ O ₃ (HEMA) ₆ (C ₅ H ₆ O ₄)C ₃ H ₅	1089.47388
C ₄ H ₅ O ₂ (HEMA) ₆ (C ₇ H ₁₄ O ₂)C ₄ H ₅ O ₂	1071.53654	C ₂ H ₅ O(HEMA) ₆ (C ₅ H ₆ O ₄)C ₆ H ₉ O ₂	1091.48973
H(HEMA) ₇ (C ₅ H ₆ O ₄)C ₃ H ₅	1078.5139	C ₄ H ₅ O(HEMA) ₆ (C ₇ H ₁₄ O ₂)C ₅ H ₇ O ₂	1101.54754
C ₃ H ₅ O ₃ (HEMA) ₆ (C ₇ H ₁₄ O ₂)C ₄ H ₅ O ₂	1079.48968	C ₄ H ₅ O ₂ (HEMA) ₆ (C ₇ H ₁₄ O ₂)C ₄ H ₅ O ₂	1103.52585
C ₄ H ₅ O(HEMA) ₆ (C ₇ H ₁₄ O ₂)C ₆ H ₉ O ₂	1087.53122	H(HEMA) ₇ (C ₅ H ₆ O ₄)C ₃ H ₅	1105.50521
C ₆ H ₁₀ O ₂ (HEMA) ₆ (C ₇ H ₁₄ O ₂)C ₄ H ₅ O	1091.48976	C ₂ H ₅ O(HEMA) ₆ (C ₅ H ₆ O ₄)C ₆ H ₉ O ₃	1107.48446
C ₄ H ₅ O ₂ (HEMA) ₆ (C ₇ H ₁₄ O ₂)C ₅ H ₇ O ₂	1093.50561	C ₃ H ₅ O ₃ (HEMA) ₆ (C ₇ H ₁₄ O ₂)C ₄ H ₅ O ₂	1107.52134
C ₄ H ₅ O(HEMA) ₅ (C ₇ H ₁₄ O ₂)C ₆ H ₉ O ₂	1095.48447	C ₄ H ₅ O(HEMA) ₆ (C ₇ H ₁₄ O ₂)C ₆ H ₉ O ₂	1115.56237
C ₄ H ₅ O ₂ (HEMA) ₅ (C ₇ H ₁₄ O ₂)C ₅ H ₇ O ₂	1101.54714	C ₆ H ₁₀ O ₂ (HEMA) ₆ (C ₇ H ₁₄ O ₂)C ₄ H ₅ O	1116.566
CH ₃ (HEMA) ₆ (C ₅ H ₆ O ₄)C ₃ H ₅	1103.52601	C ₄ H ₅ O ₂ (HEMA) ₆ (C ₇ H ₁₄ O ₂)C ₅ H ₇ O ₂	1117.5416
O(HEMA) ₆ (C ₇ H ₁₄ O ₂)C ₃ H ₅	1105.50534	C ₅ H ₈ O ₃ (HEMA) ₆ (C ₇ H ₁₄ O ₂)C ₄ H ₅ O	1118.54515
C ₃ H ₅ O ₃ (HEMA) ₅ (C ₇ H ₁₄ O ₂)C ₅ H ₇ O ₂	1107.52137		
CH ₃ (HEMA) ₆ (C ₅ H ₆ O ₄)C ₂ H ₅ O	1115.56228		
C ₅ H ₇ O ₃ (HEMA) ₅ (C ₇ H ₁₄ O ₂)C ₄ H ₅ O ₂	1116.56564		
C ₃ H ₅ (HEMA) ₆ (C ₅ H ₆ O ₄)CH ₃ O	1117.54152		

m/z = 900-1200	
Sample: 71 mg·min ⁻¹ , 3000 Hz	
Assignment	(m/z) _{exp}
C ₆ H ₁₀ O ₂ (HEMA) ₄ (C ₅ H ₆ O ₄)C ₆ H ₁₀ O ₂	901.40631
C ₅ H ₇ O ₂ (HEMA) ₄ (C ₇ H ₁₄ O ₂)C ₆ H ₉ O ₃	901.4425
C ₅ H ₇ O ₃ (HEMA) ₄ (C ₇ H ₁₄ O ₂)C ₅ H ₇ O ₃	903.42196
C ₃ H ₅ (HEMA) ₄ (C ₅ H ₆ O ₄) ₂ C ₄ H ₅ O	913.36974
C ₃ H ₅ (HEMA) ₅ (C ₅ H ₆ O ₄)C ₄ H ₅ O	913.4063
C ₆ H ₉ O ₂ (HEMA) ₄ (C ₅ H ₆ O ₄)C ₆ H ₉ O ₃	915.38542
H(HEMA) ₅ (C ₅ H ₆ O ₄)C ₆ H ₉ O ₂	917.40107
C ₃ H ₅ (HEMA) ₅ (C ₅ H ₆ O ₄)C ₄ H ₅ O ₂	929.40108
CH ₃ (HEMA) ₅ (C ₅ H ₆ O ₄)C ₆ H ₉ O ₂	931.41669
C ₄ H ₅ O(HEMA) ₅ (C ₅ H ₆ O ₄)C ₄ H ₅ O	941.40134
C ₃ H ₅ (HEMA) ₅ (C ₅ H ₆ O ₄)C ₅ H ₇ O ₂	943.417
C ₃ H ₅ (HEMA) ₅ (C ₅ H ₆ O ₄)C ₆ H ₉ O ₂	957.43264
C ₅ H ₇ O ₃ (HEMA) ₅ (C ₅ H ₆ O ₄)C ₃ H ₅	959.41183
C ₃ H ₅ (HEMA) ₅ (C ₅ H ₆ O ₄)C ₆ H ₉ O ₃	973.42764
C ₄ H ₅ O ₂ (HEMA) ₅ (C ₇ H ₁₄ O ₂)C ₄ H ₅ O ₂	973.46374
H(HEMA) ₆ (C ₅ H ₆ O ₄)C ₃ H ₅	975.44306
C ₃ H ₅ O ₃ (HEMA) ₅ (C ₇ H ₁₄ O ₂)C ₄ H ₅ O ₂	977.45912
C ₄ H ₅ O(HEMA) ₅ (C ₇ H ₁₄ O ₂)C ₆ H ₉ O ₂	985.50022
C ₄ H ₅ O ₂ (HEMA) ₅ (C ₇ H ₁₄ O ₂)C ₅ H ₇ O ₂	987.47946
CH ₃ (HEMA) ₆ (C ₅ H ₆ O ₄)C ₃ H ₅	989.45875
C ₃ H ₅ O ₃ (HEMA) ₅ (C ₇ H ₁₄ O ₂)C ₅ H ₇ O ₂	991.47443
H(HEMA) ₆ (C ₅ H ₆ O ₄)C ₄ H ₅ O	1003.43799
C ₅ H ₇ O ₃ (HEMA) ₅ (C ₇ H ₁₄ O ₂)C ₄ H ₅ O ₂	1003.47488
C ₃ H ₅ (HEMA) ₆ (C ₅ H ₆ O ₄)CH ₃ O	1005.45367
C ₃ H ₅ (HEMA) ₆ (C ₅ H ₆ O ₄)C ₃ H ₅	1015.47438
C ₅ H ₇ O ₂ (HEMA) ₅ (C ₇ H ₁₄ O ₂)C ₆ H ₉ O ₂	1015.51131
C ₄ H ₅ O ₂ (HEMA) ₅ (C ₇ H ₁₄ O ₂)C ₆ H ₉ O ₃	1017.49045
C ₃ H ₅ (HEMA) ₆ (C ₅ H ₆ O ₄)C ₂ H ₅ O	1019.46925
C ₆ H ₉ O ₂ (HEMA) ₅ (C ₇ H ₁₄ O ₂)C ₆ H ₉ O ₂	1029.52619
C ₆ H ₁₀ O ₂ (HEMA) ₅ (C ₇ H ₁₄ O ₂)C ₆ H ₉ O ₂	1030.52976
C ₅ H ₇ O ₂ (HEMA) ₅ (C ₇ H ₁₄ O ₂)C ₆ H ₉ O ₃	1031.50559
C ₅ H ₇ O ₃ (HEMA) ₅ (C ₇ H ₁₄ O ₂)C ₅ H ₇ O ₃	1033.48492
H(HEMA) ₆ (C ₅ H ₆ O ₄)C ₆ H ₉ O ₂	1047.46407
C ₅ H ₇ O ₃ (HEMA) ₅ (C ₇ H ₁₄ O ₂)C ₆ H ₉ O ₃	1047.50093
C ₆ H ₉ O ₃ (HEMA) ₅ (C ₇ H ₁₄ O ₂)C ₆ H ₉ O ₃	1061.51661
C ₄ H ₅ O(HEMA) ₆ (C ₇ H ₁₄ O ₂)C ₄ H ₅ O ₂	1087.53233
C ₄ H ₅ O ₂ (HEMA) ₆ (C ₇ H ₁₄ O ₂)C ₄ H ₅ O ₂	1103.52671
H(HEMA) ₇ (C ₅ H ₆ O ₄)C ₃ H ₅	1105.50611
C ₄ H ₅ O(HEMA) ₆ (C ₇ H ₁₄ O ₂)C ₆ H ₉ O ₂	1115.56314
C ₃ H ₅ O ₃ (HEMA) ₆ (C ₇ H ₁₄ O ₂)C ₅ H ₇ O ₂	1121.53734
C ₅ H ₇ O ₂ (HEMA) ₆ (C ₇ H ₁₄ O ₂)C ₆ H ₉ O ₂	1145.57397
C ₆ H ₁₀ O ₂ (HEMA) ₆ (C ₇ H ₁₄ O ₂)C ₅ H ₇ O ₂	1146.57773
C ₆ H ₉ O ₂ (HEMA) ₆ (C ₇ H ₁₄ O ₂)C ₆ H ₉ O ₂	1159.58915
C ₆ H ₁₀ O ₂ (HEMA) ₆ (C ₇ H ₁₄ O ₂)C ₆ H ₉ O ₂	1160.59266
C ₅ H ₇ O ₂ (HEMA) ₆ (C ₇ H ₁₄ O ₂)C ₆ H ₉ O ₃	1161.56869
C ₅ H ₈ O ₃ (HEMA) ₆ (C ₇ H ₁₄ O ₂)C ₆ H ₉ O ₂	1162.57196
H(HEMA) ₇ (C ₅ H ₆ O ₄)C ₆ H ₉ O ₂	1177.52694

Table A 6: Experimental condition in AP-PECVD of the deposition performed to determine the influence of the monomer saturation ratio P_M/P_{sat} on the resulting thin films properties. The deposition rates (DR) are provided. The process is well described in previous study.^[1]

P_M/P_{sat} (%)	$F_{Ar, carrier}$ (SLM)	$F_{Ar, total}$ (SLM)	Pressure (bar)	t_{ON} (μs)	DR ($nm \cdot s^{-1}$)	Thick. incr. (μm)
35	7	20	1	15	0.21	2.1
50	10	20	1	15	0.66	6.6
80	16	20	1	15	1.12	11.2

In contrast with LA-PECVD, all samples obtained were solid and acrosopically smooth thin, irrespective of the saturation ratio. However, by naked eye observation, the saturation ratio readily suggested the difference in growth rates related to the different were readily noticeable from naked eyes observation.

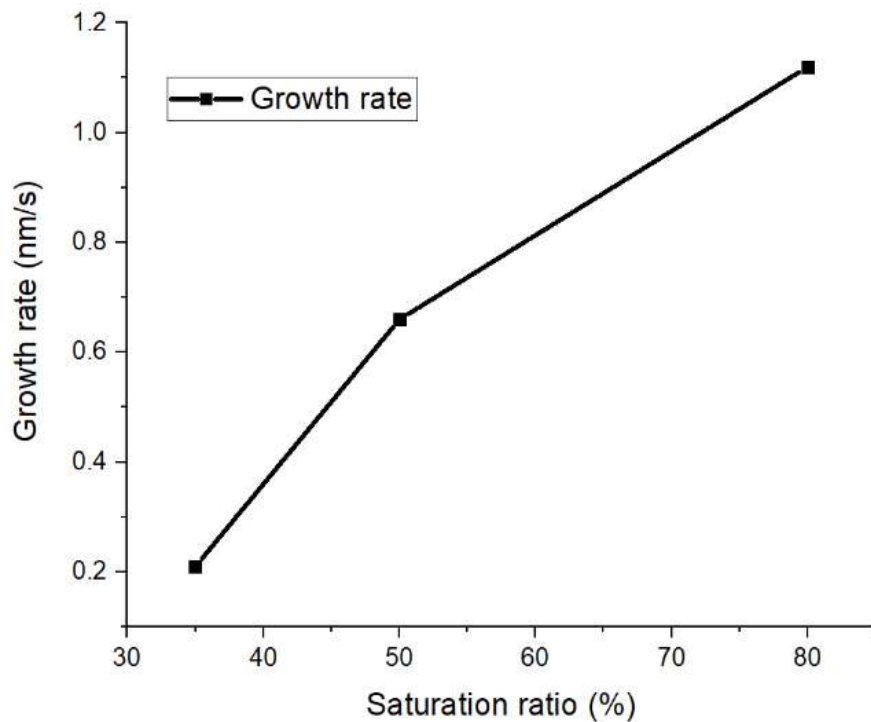


Figure A6: Growth rate of the as-deposited thin films plotted according to the monomer saturation ratio, P_M/P_{sat} , at which they were elaborated.

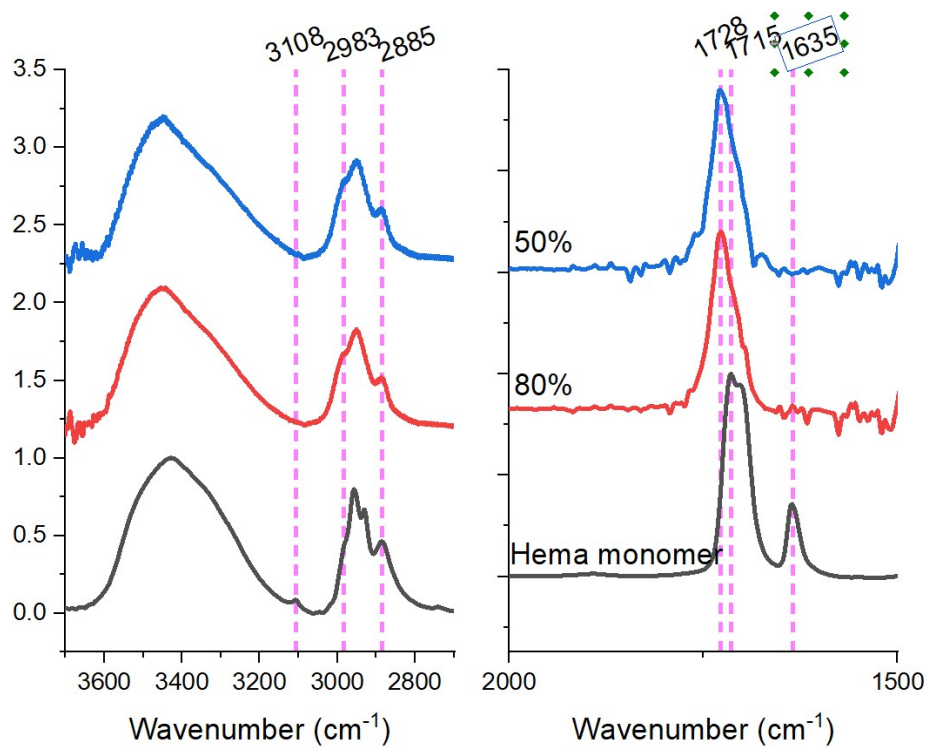


Figure A7: Fourier-transform infrared spectra (FTIR) of the 3700 - 2700 cm^{-1} and the 2000 – 1500 cm^{-1} regions, corresponding respectively to the OH and CH region as well as the C=O stretching and the C=C stretching region of HEMA monomer and AP-PECVD as-deposited thin films elaborated using various P_M/P_{sat} .

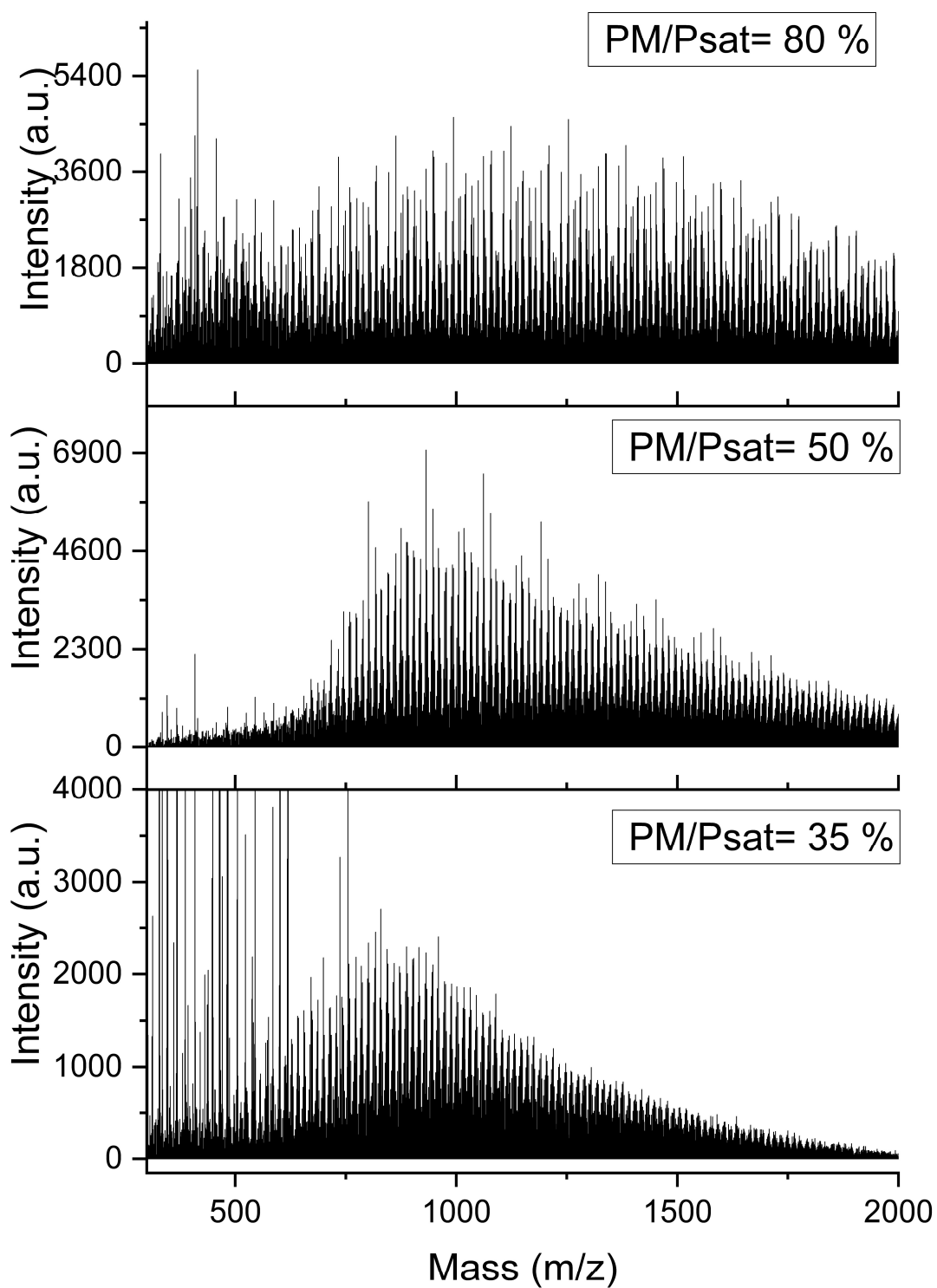


Figure A8: MALDI-HRMS spectra of AP-PECVD film at discharge frequency of 100 Hz and 35, 50 and 80% saturation ratio in the mass range $m/z = 300 - 2000$.

Table A7: List of relevant species monitored by MALDI-HRMS in AP-PECVD at discharge frequency of 100 Hz and 80% saturation ratio (Na^+ as reagent ions) with their corresponding m/z values. Only the HRMS peaks related to ionized adducts of $[\text{R}_i\text{-(HEMA)}_n\text{-R}_t + \text{Na}]^+$ are indicated. Mass assignments were carried out using PolyCalc web-based assignment tool (error mass tolerance below 3 ppm and height threshold of 5%).

$m/z = 300\text{-}2000$	
Assignment	$(m/z)_{\text{exp}}$
$\text{C}_2\text{H}_5\text{O}_2(\text{HEMA})\text{C}_6\text{H}_9\text{O}_3$	343.13635
$\text{C}_2\text{H}_5\text{O}_2(\text{HEMA})_2\text{C}_6\text{H}_9\text{O}_3$	473.19961
$\text{C}_2\text{H}_5\text{O}_2(\text{HEMA})_4\text{C}_6\text{H}_9\text{O}_3$	733.3274
$\text{C}_2\text{H}_5\text{O}_2(\text{HEMA})_5\text{C}_6\text{H}_9\text{O}_3$	863.39037
$\text{C}_2\text{H}_5\text{O}_2(\text{HEMA})_6\text{C}_6\text{H}_9\text{O}_3$	993.45377
$\text{C}_2\text{H}_5\text{O}_2(\text{HEMA})_7\text{C}_6\text{H}_9\text{O}_3$	1123.51665
$\text{C}_2\text{H}_5\text{O}_2(\text{HEMA})_8\text{C}_6\text{H}_9\text{O}_3$	1253.58013
$\text{C}_2\text{H}_5\text{O}_2(\text{HEMA})_9\text{C}_6\text{H}_9\text{O}_3$	1383.64373
$\text{C}_2\text{H}_5\text{O}_2(\text{HEMA})_{10}\text{C}_6\text{H}_9\text{O}_3$	1513.70703
$\text{C}_2\text{H}_5\text{O}_2(\text{HEMA})_{11}\text{C}_6\text{H}_9\text{O}_3$	1643.77009
$\text{C}_2\text{H}_5\text{O}_2(\text{HEMA})_{12}\text{C}_6\text{H}_9\text{O}_3$	1773.83247
$\text{C}_2\text{H}_5\text{O}_2(\text{HEMA})_{13}\text{C}_6\text{H}_9\text{O}_3$	1903.89492

$m/z = 900\text{-}1200$	
Assignment	$(m/z)_{\text{exp}}$
$\text{C}_5\text{H}_7\text{O}_2(\text{HEMA})_5\text{C}_6\text{H}_9\text{O}_3$	901.40659
$\text{C}_5\text{H}_7\text{O}_3(\text{HEMA})_5\text{C}_6\text{H}_9\text{O}_3$	903.38522
$\text{C}_4\text{H}_5\text{O}(\text{HEMA})_6\text{CH}_3\text{O}$	903.42214
$\text{OH}(\text{HEMA})_6\text{C}_4\text{H}_5\text{O}_2$	905.40093
$\text{C}_5\text{H}_7\text{O}_3(\text{HEMA})_5\text{C}_6\text{H}_9\text{O}_3$	917.40143
$\text{C}_4\text{H}_5\text{O}_2(\text{HEMA})_6\text{CH}_3\text{O}$	919.4167
$\text{C}_6\text{H}_9\text{O}_3(\text{HEMA})_5\text{C}_6\text{H}_9\text{O}_3$	931.41675
$\text{C}_5\text{H}_8\text{O}_3(\text{HEMA})_6\text{O}$	935.41203
$\text{OH}(\text{HEMA})_6\text{C}_6\text{H}_9\text{O}_3$	949.42749
$\text{C}_3\text{H}_5\text{O}_3(\text{HEMA})_6\text{C}_4\text{H}_5\text{O}$	961.42792
$\text{O}(\text{HEMA})_7\text{O}$	965.42241
$\text{C}_4\text{H}_5\text{O}_2(\text{HEMA})_6\text{C}_4\text{H}_5\text{O}_2$	973.4278
$\text{C}_3\text{H}_5\text{O}_3(\text{HEMA})_6\text{C}_4\text{H}_5\text{O}_2$	977.42224
$\text{C}_5\text{H}_7\text{O}_3(\text{HEMA})_6\text{C}_2\text{H}_5\text{O}_2$	979.43857
$\text{C}_4\text{H}_5\text{O}_2(\text{HEMA})_6\text{C}_5\text{H}_7\text{O}_2$	987.44327
$\text{C}_3\text{H}_5\text{O}_3(\text{HEMA})_6\text{C}_5\text{H}_7\text{O}_2$	991.43786
$\text{OH}(\text{HEMA})_7\text{C}_3\text{H}_5$	991.47471
$\text{C}_2\text{H}_5\text{O}_2(\text{HEMA})_6\text{C}_6\text{H}_9\text{O}_3$	993.45377
$\text{C}_5\text{H}_7\text{O}_3(\text{HEMA})_6\text{C}_4\text{H}_5\text{O}_2$	1003.43808
$\text{C}_3\text{H}_5\text{O}_3(\text{HEMA})_6\text{C}_6\text{H}_9\text{O}_2$	1005.45378
$\text{H}(\text{HEMA})_7\text{C}_4\text{H}_5\text{O}_2$	1019.46934
$\text{C}_3\text{H}_5\text{O}_3(\text{HEMA})_6\text{C}_6\text{H}_9\text{O}_3$	1021.44839
$\text{H}(\text{HEMA})_7\text{C}_3\text{H}_5\text{O}_3$	1023.46474
$\text{C}_4\text{H}_5\text{O}(\text{HEMA})_7\text{CH}_3\text{O}$	1033.48495
$\text{OH}(\text{HEMA})_7\text{C}_4\text{H}_5\text{O}_2$	1035.46416
$\text{OH}(\text{HEMA})_7\text{C}_3\text{H}_5\text{O}_3$	1039.45878
$\text{C}_6\text{H}_9\text{O}_2(\text{HEMA})_6\text{C}_6\text{H}_9\text{O}_3$	1045.48567
$\text{H}(\text{HEMA})_7\text{C}_6\text{H}_9\text{O}_2$	1047.50129
$\text{C}_4\text{H}_5\text{O}_2(\text{HEMA})_7\text{CH}_3\text{O}$	1049.47978
$\text{H}(\text{HEMA})_7\text{C}_5\text{H}_8\text{O}_3$	1050.48339
$\text{C}_6\text{H}_9\text{O}_3(\text{HEMA})_6\text{C}_6\text{H}_9\text{O}_3$	1061.47975

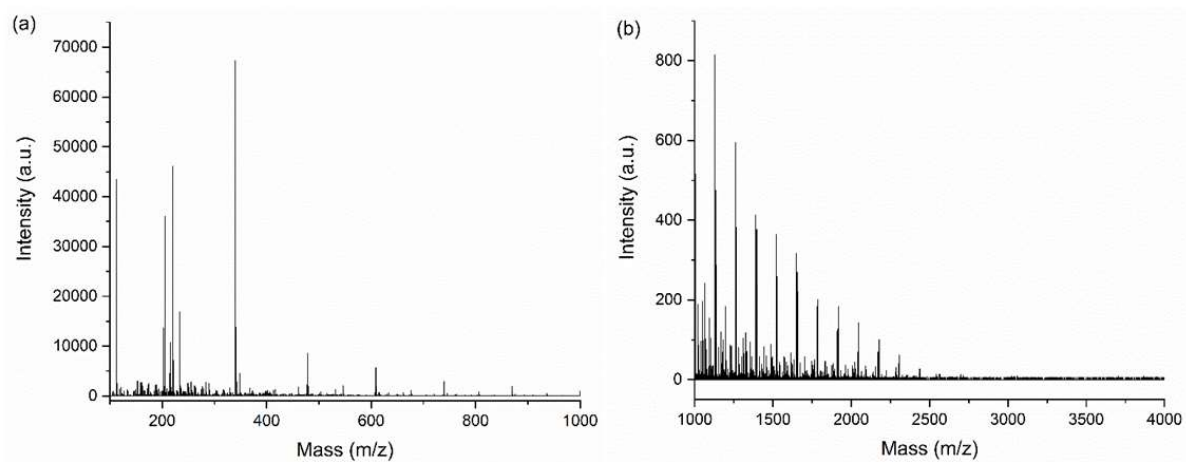
H(HEMA) ₇ C ₆ H ₉ O ₃	1063.49584
C ₅ H ₈ O ₃ (HEMA) ₇ O	1065.47492
H(HEMA) ₈ H	1065.51192
CH ₃ (HEMA) ₇ C ₆ H ₉ O ₃	1077.51154
OH(HEMA) ₇ C ₆ H ₉ O ₃	1079.49043
H(HEMA) ₈ OH	1081.50655
C ₅ H ₇ O ₃ (HEMA) ₇ C ₃ H ₅	1089.51206
C ₃ H ₅ O ₃ (HEMA) ₇ C ₄ H ₅ O	1091.49073
CH ₃ O(HEMA) ₇ C ₆ H ₉ O ₃	1093.50671
C ₃ H ₅ O ₃ (HEMA) ₇ C ₄ H ₅ O ₂	1107.48513
C ₂ H ₅ O(HEMA) ₇ C ₆ H ₉ O ₃	1107.52257
C ₅ H ₇ O ₃ (HEMA) ₇ C ₂ H ₅ O ₂	1109.50156
OH(HEMA) ₈ C ₃ H ₅	1121.53749
C ₂ H ₅ O ₂ (HEMA) ₇ C ₆ H ₉ O ₃	1123.51665
O(HEMA) ₈ C ₂ H ₅ O	1124.52036
C ₃ H ₅ O ₃ (HEMA) ₇ C ₆ H ₉ O ₂	1135.51672
C ₆ H ₁₀ O ₂ (HEMA) ₇ C ₃ H ₅ O ₃	1136.52053
H(HEMA) ₈ C ₄ H ₅ O ₂	1149.53235
C ₃ H ₅ O ₃ (HEMA) ₇ C ₆ H ₉ O ₃	1151.51143
H(HEMA) ₈ C ₃ H ₅ O ₃	1153.52775
C ₄ H ₅ O(HEMA) ₈ CH ₃ O	1163.54774
OH(HEMA) ₈ C ₄ H ₅ O ₂	1165.52714
CH ₂ (HEMA) ₈ C ₃ H ₅ O ₃	1166.53056
CH ₃ (HEMA) ₈ C ₃ H ₅ O ₃	1167.54363
OH(HEMA) ₈ C ₃ H ₅ O ₃	1169.5219
C ₄ H ₅ O ₂ (HEMA) ₈ CH ₃ O	1179.54271
H(HEMA) ₈ C ₅ H ₈ O ₃	1180.54652
C ₆ H ₉ O ₃ (HEMA) ₇ C ₆ H ₉ O ₃	1191.54268
H(HEMA) ₈ C ₆ H ₉ O ₃	1193.55907
C ₅ H ₈ O ₃ (HEMA) ₈ O	1195.53814
H(HEMA) ₉ H	1195.57514
C ₃ H ₅ O ₃ (HEMA) ₈ C ₂ H ₅ O	1197.5543

Table A8: List of relevant species monitored by MALDI-HRMS in AP-PECVD at discharge frequency of 100 Hz and 80% saturation ratio (Na^+ as reagent ions) with their corresponding m/z values. Only the HRMS peaks related to ionized adducts of $[\text{R}_i\text{-(HEMA)}_n\text{-(HEMA)}^{\pm\text{O}\pm\text{CH}}_4\text{-R}_i + \text{Na}]^+$ are indicated. Mass assignments were carried out using PolyCalc web-based assignment tool (error mass tolerance below 3 ppm and height threshold of 5%).

m/z = 900-1200	
Assignment	(m/z) _{exp}
$\text{C}_5\text{H}_7\text{O}_2(\text{HEMA})_4(\text{C}_5\text{H}_6\text{O}_4)\text{C}_6\text{H}_9\text{O}_3$	901.37015
$\text{C}_6\text{H}_{10}\text{O}_2(\text{HEMA})_4(\text{C}_5\text{H}_6\text{O}_4)\text{C}_6\text{H}_{10}\text{O}_2$	901.40659
$\text{C}_4\text{H}_5\text{O}(\text{HEMA})_5(\text{C}_5\text{H}_6\text{O}_4)\text{CH}_3\text{O}$	903.38522
$\text{C}_5\text{H}_7\text{O}_3(\text{HEMA})_4(\text{C}_7\text{H}_{14}\text{O}_2)\text{C}_3\text{H}_7\text{O}_3$	903.42214
$\text{C}_3\text{H}_5(\text{HEMA})_5(\text{C}_5\text{H}_6\text{O}_4)\text{C}_2\text{H}_5\text{O}_2$	905.40093
$\text{CH}_3(\text{HEMA})_5(\text{C}_5\text{H}_6\text{O}_4)\text{C}_3\text{H}_5\text{O}_3$	907.38014
$\text{C}_3\text{H}_5(\text{HEMA})_4(\text{C}_5\text{H}_6\text{O}_4)_2\text{C}_4\text{H}_5\text{O}$	913.3702
$\text{C}_6\text{H}_9\text{O}_2(\text{HEMA})_3(\text{C}_5\text{H}_6\text{O}_4)_2\text{C}_6\text{H}_9\text{O}_3$	915.34914
$\text{C}_6\text{H}_9\text{O}_2(\text{HEMA})_4(\text{C}_5\text{H}_6\text{O}_4)\text{C}_6\text{H}_9\text{O}_3$	915.38589
$\text{H}(\text{HEMA})_5(\text{C}_5\text{H}_6\text{O}_4)\text{C}_6\text{H}_9\text{O}_2$	917.40143
$\text{C}_4\text{H}_5\text{O}_2(\text{HEMA})_5(\text{C}_5\text{H}_6\text{O}_4)\text{CH}_3\text{O}$	919.38028
$\text{C}_3\text{H}_5(\text{HEMA})_4(\text{C}_5\text{H}_6\text{O}_4)_2\text{C}_4\text{H}_5\text{O}_2$	929.36507
$\text{C}_3\text{H}_5(\text{HEMA})_5(\text{C}_5\text{H}_6\text{O}_4)\text{C}_4\text{H}_5\text{O}_2$	929.40157
$\text{C}_6\text{H}_9\text{O}_3(\text{HEMA})_4(\text{C}_5\text{H}_6\text{O}_4)\text{C}_6\text{H}_9\text{O}_3$	931.38027
$\text{CH}_3(\text{HEMA})_5(\text{C}_5\text{H}_6\text{O}_4)\text{C}_6\text{H}_9\text{O}_2$	931.41675
$\text{H}(\text{HEMA})_5(\text{C}_5\text{H}_6\text{O}_4)\text{C}_6\text{H}_9\text{O}_3$	933.39595
$\text{H}(\text{HEMA})_6(\text{C}_5\text{H}_6\text{O}_4)\text{H}$	935.41203
$\text{C}_4\text{H}_5\text{O}(\text{HEMA})_4(\text{C}_5\text{H}_6\text{O}_4)_2\text{C}_4\text{H}_5\text{O}$	941.36468
$\text{C}_3\text{H}_5(\text{HEMA})_4(\text{C}_5\text{H}_6\text{O}_4)_2\text{C}_3\text{H}_7\text{O}_2$	943.38068
$\text{CH}_3(\text{HEMA})_5(\text{C}_5\text{H}_6\text{O}_4)\text{C}_6\text{H}_9\text{O}_3$	947.41167
$\text{H}(\text{HEMA})_6(\text{C}_5\text{H}_6\text{O}_4)\text{CH}_3$	949.42749
$\text{C}_5\text{H}_7\text{O}_3(\text{HEMA})_5(\text{C}_5\text{H}_6\text{O}_4)\text{C}_3\text{H}_5$	959.41197
$\text{C}_2\text{H}_5\text{O}(\text{HEMA})_4(\text{C}_5\text{H}_6\text{O}_4)_2\text{C}_6\text{H}_9\text{O}_2$	961.39106
$\text{C}_2\text{H}_5\text{O}(\text{HEMA})_5(\text{C}_5\text{H}_6\text{O}_4)\text{C}_6\text{H}_9\text{O}_2$	961.42792
$\text{CH}_3\text{O}(\text{HEMA})_5(\text{C}_5\text{H}_6\text{O}_4)\text{C}_6\text{H}_9\text{O}_3$	963.40659
$\text{H}(\text{HEMA})_6(\text{C}_5\text{H}_6\text{O}_4)\text{CH}_3\text{O}$	965.42241
$\text{C}_4\text{H}_5\text{O}(\text{HEMA})_4(\text{C}_5\text{H}_6\text{O}_4)_2\text{C}_5\text{H}_7\text{O}_2$	971.37565
$\text{C}_4\text{H}_5\text{O}(\text{HEMA})_5(\text{C}_5\text{H}_6\text{O}_4)\text{C}_5\text{H}_7\text{O}_2$	971.41232
$\text{C}_3\text{H}_5(\text{HEMA})_4(\text{C}_5\text{H}_6\text{O}_4)_2\text{C}_6\text{H}_9\text{O}_3$	973.39118
$\text{C}_3\text{H}_5(\text{HEMA})_5(\text{C}_5\text{H}_6\text{O}_4)\text{C}_6\text{H}_9\text{O}_3$	973.4278
$\text{H}(\text{HEMA})_5(\text{C}_5\text{H}_6\text{O}_4)_2\text{C}_3\text{H}_5$	975.40689
$\text{H}(\text{HEMA})_6(\text{C}_5\text{H}_6\text{O}_4)\text{C}_3\text{H}_5$	975.44343
$\text{C}_2\text{H}_5\text{O}(\text{HEMA})_5(\text{C}_5\text{H}_6\text{O}_4)\text{C}_6\text{H}_9\text{O}_3$	977.42224
$\text{CH}_3(\text{HEMA})_6(\text{C}_5\text{H}_6\text{O}_4)\text{CH}_3\text{O}$	979.43857
$\text{CH}_3(\text{HEMA})_5(\text{C}_5\text{H}_6\text{O}_4)_2\text{C}_3\text{H}_5$	989.4225
$\text{CH}_3(\text{HEMA})_6(\text{C}_5\text{H}_6\text{O}_4)\text{C}_3\text{H}_5$	989.45913
$\text{OH}(\text{HEMA})_6(\text{C}_5\text{H}_6\text{O}_4)\text{C}_3\text{H}_5$	991.43786
$\text{C}_3\text{H}_5\text{O}_3(\text{HEMA})_5(\text{C}_7\text{H}_{14}\text{O}_2)\text{C}_3\text{H}_7\text{O}_2$	991.47471
$\text{CH}_3(\text{HEMA})_6(\text{C}_5\text{H}_6\text{O}_4)\text{C}_2\text{H}_5\text{O}$	993.45377
$\text{C}_4\text{H}_5\text{O}(\text{HEMA})_4(\text{C}_5\text{H}_6\text{O}_4)_2\text{C}_6\text{H}_9\text{O}_3$	1001.38546
$\text{H}(\text{HEMA})_6(\text{C}_5\text{H}_6\text{O}_4)\text{C}_4\text{H}_5\text{O}$	1003.43808
$\text{C}_3\text{H}_5(\text{HEMA})_6(\text{C}_5\text{H}_6\text{O}_4)\text{CH}_3\text{O}$	1005.45378
$\text{C}_2\text{H}_5\text{O}(\text{HEMA})_6(\text{C}_5\text{H}_6\text{O}_4)\text{CH}_3\text{O}$	1009.44834
$\text{C}_3\text{H}_5(\text{HEMA})_6(\text{C}_5\text{H}_6\text{O}_4)\text{C}_2\text{H}_5\text{O}$	1019.46934
$\text{C}_2\text{H}_5\text{O}(\text{HEMA})_6(\text{C}_5\text{H}_6\text{O}_4)\text{C}_2\text{H}_5\text{O}$	1023.46474
$\text{C}_5\text{H}_7\text{O}_3(\text{HEMA})_5(\text{C}_7\text{H}_{14}\text{O}_2)\text{C}_3\text{H}_7\text{O}_3$	1033.48495

$C_3H_5(HEMA)_6(C_5H_6O_4)C_2H_5O_2$	1035.46415
$C_2H_5O_2(HEMA)_6(C_5H_6O_4)C_2H_5O$	1039.45878
$C_5H_7O_3(HEMA)_5(C_7H_{14}O_2)C_6H_9O_3$	1047.50129
$C_4H_5O_2(HEMA)_6(C_5H_6O_4)CH_3O$	1049.44333
$CH_3(HEMA)_6(C_5H_6O_4)C_6H_9O_2$	1061.47975
$H(HEMA)_6(C_5H_6O_4)C_6H_9O_3$	1063.45885
$H(HEMA)_7(C_5H_6O_4)H$	1065.47492
$C_5H_8O_3(HEMA)_6(C_7H_{14}O_2)O$	1065.51193
$CH_3(HEMA)_6(C_5H_6O_4)C_6H_9O_3$	1077.47465
$O(HEMA)_5(C_7H_{14}O_2)_2C_6H_9O_3$	1078.55312
$H(HEMA)_7(C_5H_6O_4)CH_3$	1079.49043
$C_5H_7O_3(HEMA)_6(C_5H_6O_4)C_3H_5$	1089.47493
$C_2H_5O(HEMA)_6(C_5H_6O_4)C_6H_9O_2$	1091.49073
$CH_3(HEMA)_7(C_5H_6O_4)CH_3$	1093.50671
$H(HEMA)_7(C_5H_6O_4)C_3H_5$	1105.50618
$C_2H_5O(HEMA)_6(C_5H_6O_4)C_6H_9O_3$	1107.48513
$C_3H_5O_3(HEMA)_6(C_7H_{14}O_2)C_4H_5O_2$	1107.52257
$CH_3(HEMA)_7(C_5H_6O_4)CH_3O$	1109.50156
$C_3H_5O_3(HEMA)_6(C_7H_{14}O_2)C_5H_7O_2$	1121.53749
$CH_3(HEMA)_7(C_5H_6O_4)C_2H_5O$	1123.51664
$C_3H_5(HEMA)_7(C_5H_6O_4)CH_3O$	1135.51672
$C_5H_7O_3(HEMA)_6(C_7H_{14}O_2)C_3H_5O_3$	1137.53305
$C_2H_5O(HEMA)_7(C_5H_6O_4)CH_3O$	1139.51132
$C_3H_5(HEMA)_7(C_5H_6O_4)C_2H_5O$	1149.53235
$C_3H_5O_3(HEMA)_6(C_7H_{14}O_2)C_6H_9O_3$	1151.54905
$HEMA(HEMA)_6(C_7H_{14}O_2)C_3H_5O_3$	1152.5523
$C_2H_5O(HEMA)_7(C_5H_6O_4)C_2H_5O$	1153.52775
$C_5H_7O_3(HEMA)_6(C_7H_{14}O_2)C_5H_7O_3$	1163.54774
$O(HEMA)_7(C_7H_{14}O_2)C_4H_5O_2$	1164.55193
$C_3H_5(HEMA)_7(C_5H_6O_4)C_2H_5O_2$	1165.52714
$C_2H_5O_2(HEMA)_7(C_5H_6O_4)C_2H_5O$	1169.5219
$CH_3(HEMA)_7(C_5H_6O_4)C_6H_9O_2$	1191.54268
$H(HEMA)_8(C_5H_6O_4)H$	1195.53814
$C_5H_8O_3(HEMA)_7(C_7H_{14}O_2)O$	1195.57514
$OH(HEMA)_7(C_7H_{14}O_2)C_5H_8O_3$	1196.5786
$C_3H_5O_3(HEMA)_7(C_5H_6O_4)C_2H_5O$	1197.51701

Figure A9: MALDI-HRMS spectra of the pellets of commercial poly (HEMA) reference from Sigma Aldrich average M_v 20,000 in the mass range (a) $m/z = 100 - 1000$ and (b) $m/z = 1000 - 4000$. The molecular weight was measured by GPC as M_p of $8 \text{ kg}\cdot\text{mol}^{-1}$.



References

- ⁽¹⁾ Abessolo Ondo, D.; Leturcq, R.; Boscher, N. D. Plasma-Initiated Chemical Vapor Deposition of Organosiloxane Thin Films: From the Growth Mechanisms to Ultrathin Low-k Polymer Insulating Layers. *Plasma Process. Polym.* 2020, 17 (7). <https://doi.org/10.1002/ppap.202000032>.

ANNEX B

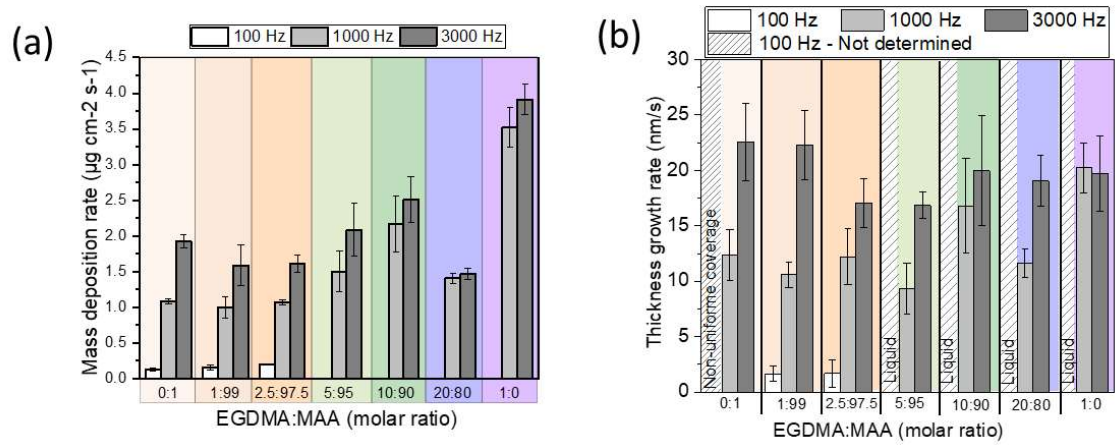


Figure B1: (a) Weight and (b) thickness growth rate for the films obtained at different plasma pulse frequencies.

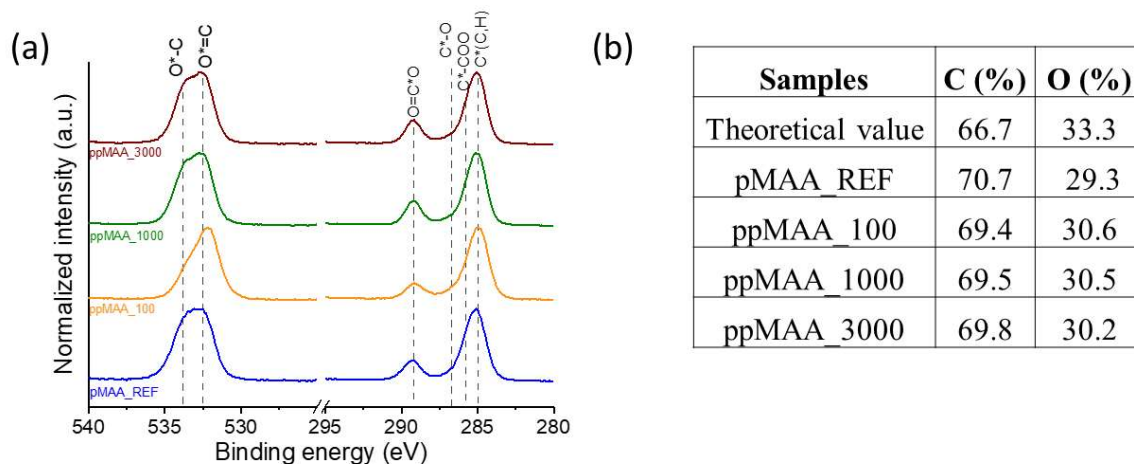


Figure B2: (a) XPS spectrum of the O 1s and C 1s core levels for the ppMAA for pulse frequencies ranging from 100-3000Hz. Commercial poly(MAA) produced by conventional polymerization (pMAA_REF, Polysciences M_w 100 $\text{kg}\cdot\text{mol}^{-1}$) is also shown for comparison. The XPS for the reference polymer powder (pMAA_REF) had the peaks assigned as follows: three peaks in C1s core level assigned as C*-(C,H) (B.E. = 285.0 eV), C*-COO (B.E. = 285.8 eV), and O=C*-O (B.E. = 289.33 eV), and two peaks in O1s core level assigned as O*=C (B.E. = 532.39 eV) and O*-C (B.E. = 533.78 eV).¹ (b) Atomic ratios of ppMAA obtained at different discharge frequencies, pMAA_REF and theoretical values. Note: In O 1 s spectra of ppMAA_100, the peak observed at 533 eV can be associated with the substrate (SiO_2).^{2,3}

Initiating/terminating fragments: $R\bullet \rightarrow R_i/R_f$

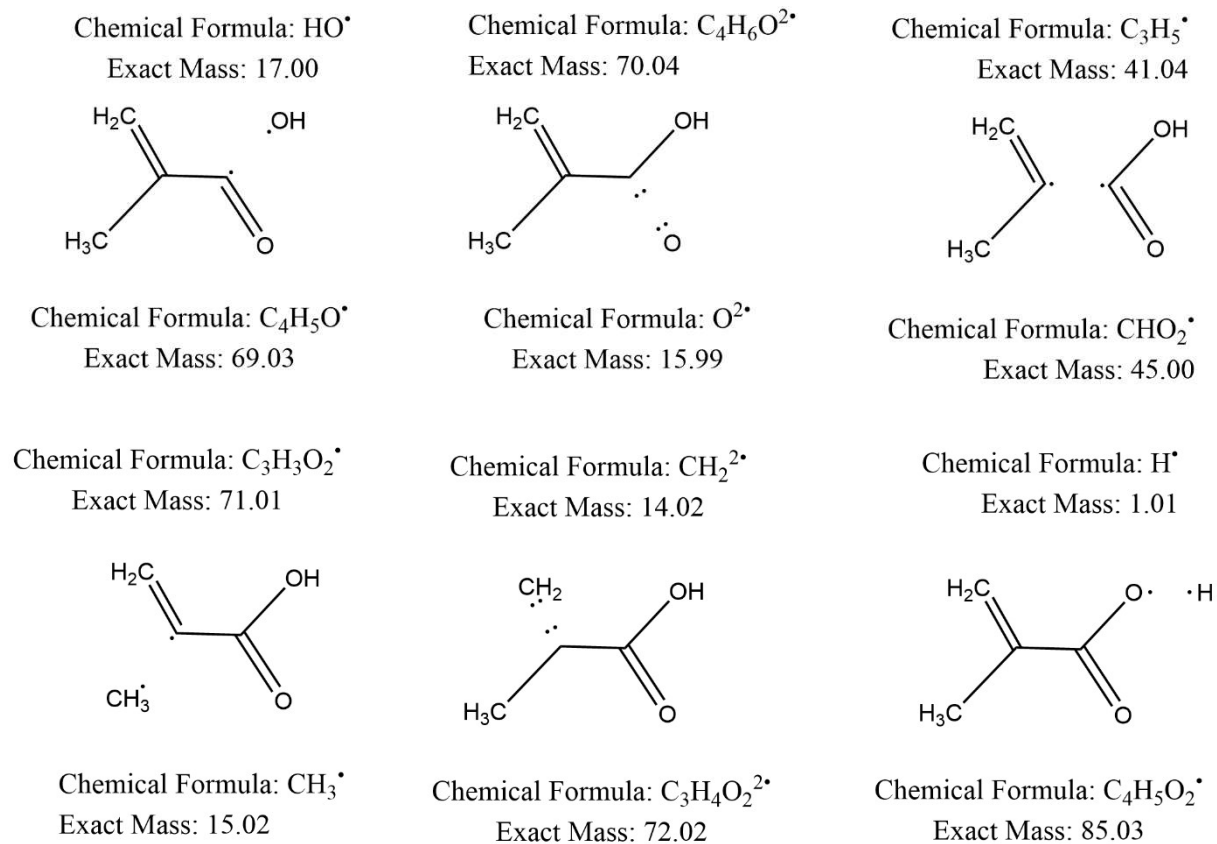


Figure B3: Proposed radical fragments originating from a single σ -bond breakdown of the MAA molecule.

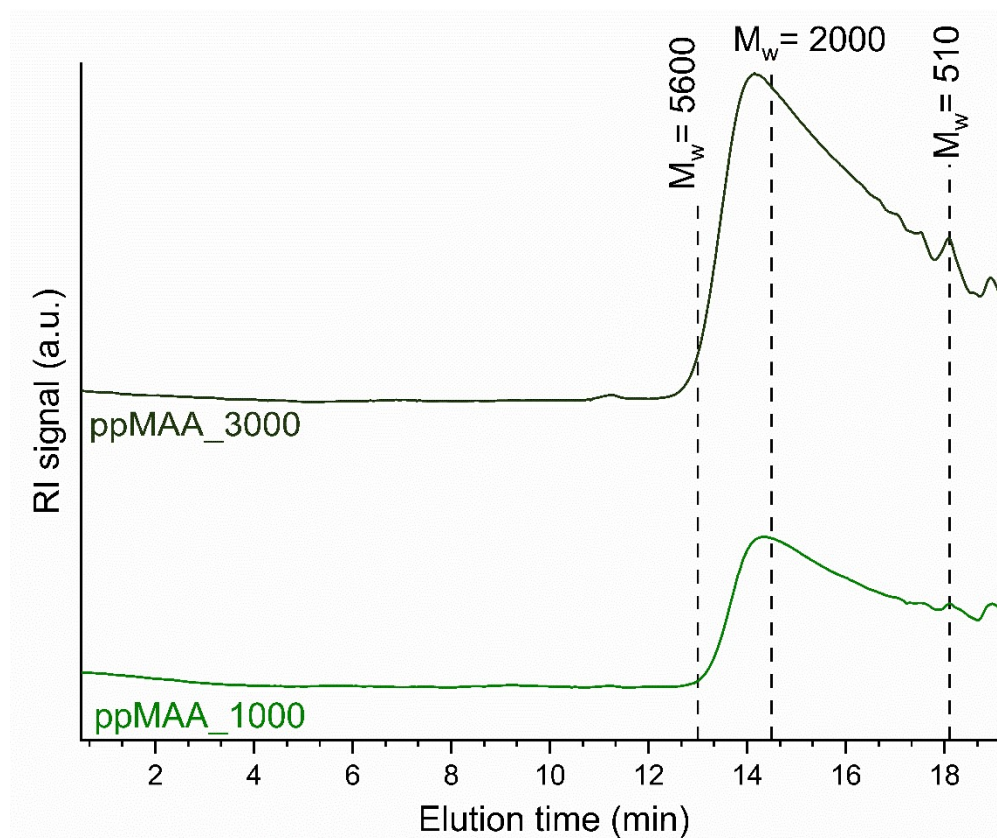


Figure B4: Representative GPC chromatogram for the ppMAA films obtained at 1000 and 3000 Hz.

Table B 1: Apparent weight average molar mass (M_w^*) and apparent number average molar mass (M_n^*) and polydispersity index (PDI) for the films studied. M_w^* and M_n^* values are extracted from the respective gaussian distribution obtained in SEC measurements in the elution time between 12 - 20 min and a polystyrene calibration. Two independent GPC measurements were performed using at least 2 different samples in each measurement.

Sample	M_n^* ($\text{g}\cdot\text{mol}^{-1}$)	M_w^* ($\text{g}\cdot\text{mol}^{-1}$)	PDI
ppMAA_1000	1200 ± 200	2150 ± 150	1.8
ppMAA_3000	1500 ± 0	2450 ± 50	1.6

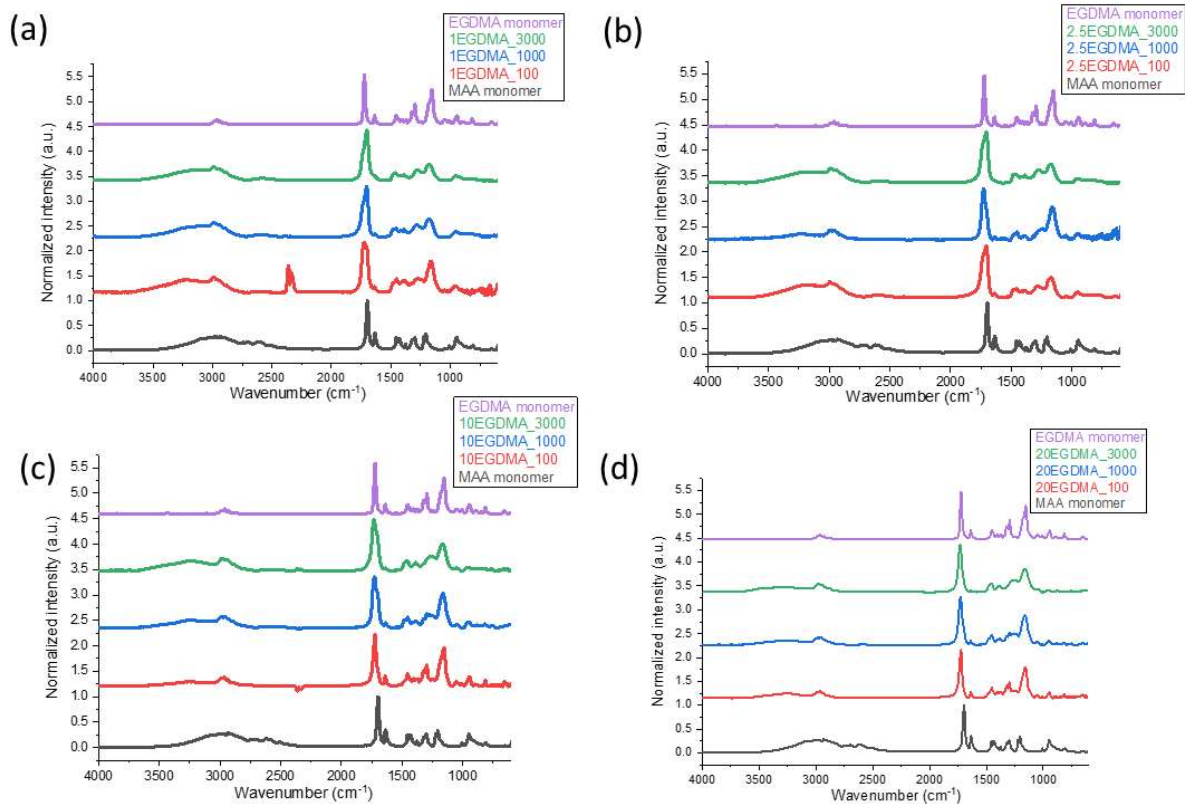


Figure B5: FTIR spectra the pp(EGDMA:MAA) copolymer films for different EGDMA:MAA molar ratios grown from 100 - 3000 Hz.

Table B2: XPS elemental composition for coatings deposited. Theoretical values are presented in brackets.

f_{pe} (Hz)	EGDMA:MAA (mol:mol)	C (1s) at%	O (1s) at%
100	0:1	69.4 (66.7)	30.6 (33.3)
	1:99	74.0 (66.7)	26.0 (33.3)
	2.5:97.5	73.0 (66.8)	27.0 (33.2)
1000	0:1	69.5 (66.7)	30.5 (33.3)
	1:99	72.3 (66.7)	27.7 (33.3)
	2.5:97.5	71.8 (66.8)	28.2 (33.2)
	5:95	71.1 (67.0)	28.9 (33.0)
	10:90	70.8 (67.2)	29.1 (32.8)
	20:80	71.3 (67.6)	28.7 (32.4)
	1:0	71.0 (71.4)	29.0 (28.6)
3000	0:1	69.8 (66.7)	30.2 (33.3)
	1:99	72.1 (66.7)	27.9 (33.3)
	2.5:97.5	71.4 (66.8)	28.6 (33.2)
	5:95	72.5 (67.0)	27.5 (33.0)
	10:90	69.7 (67.2)	30.3 (32.8)
	20:80	70.4 (67.6)	29.6 (32.4)
	1:0	69.8 (71.4)	30.2 (28.6)

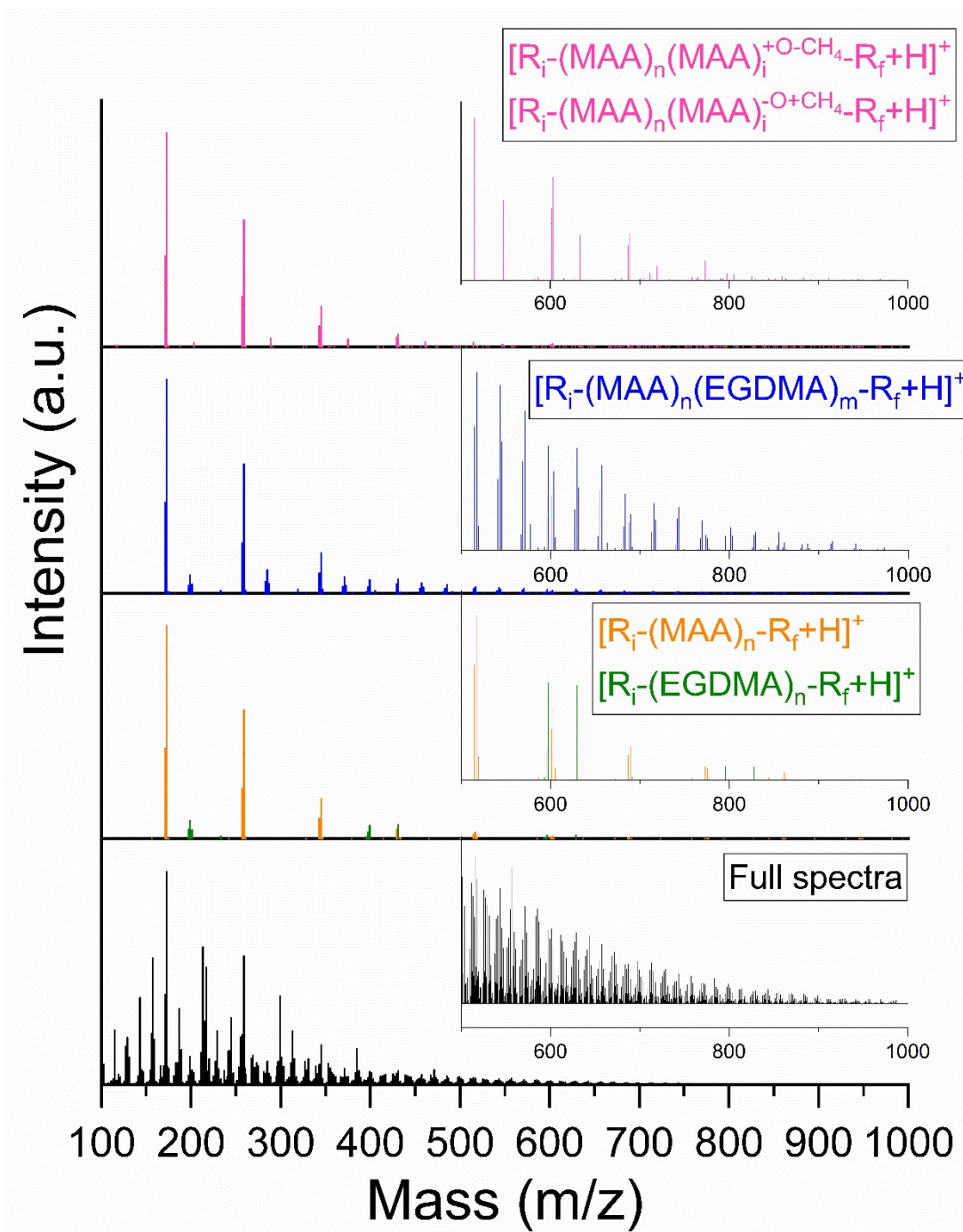


Figure B6: MALDI-HRMS spectra in the mass range $m/z = 100 - 1000$ of the pp(10EGDMA:90MAA) copolymer films for grown at 3000 Hz. The full spectra of the sample are indicated in black line. Filtration of the full spectra to the matching mass are indicated in coloured lines.

Table B3: Reactivity ratios of several (meth)acrylate monomer.

Monomer 1	Monomer 2	r_{12}	r_{21}	Reference
Methyl methacrylate	EGDMA	1.0	1.0	4
Methyl methacrylate	EGDMA	1.864	0.700	5
HEMA	EGDMA	0.811	6.548	6
MAA	Acrylic acid	2.12	0.42	7
		2.2	0.45	
		2.64	0.2	
		2.77	0.29	
MAA	Butyl methacrylate	0.75	1.2	8

Table B4: Thickness obtained for as deposited films (thickness dry state SE) and during immersion in di-ionised (DI) water (thickness swollen state) for SE and QCM-D.

Pulse frequency (Hz)	EGDMA:MAA (mol:mol)	Thickness dry state SE (nm)	Thickness swollen state SE (nm)	Thickness swollen state QCM-D (nm)
1000	5:95	78 ± 25	105 ± 28	392 ± 60
	10:90	141 ± 6	235 ± 12	400 ± 17
	20:80	107 ± 12	118 ± 18	292 ± 79
	1:0	118 ± 10	124 ± 21	325 ± 105
3000	5:95	87 ± 11	100 ± 36	360 ± 83
	10:90	67 ± 6	156 ± 6	425 ± 30
	20:80	138 ± 41	155 ± 50	397 ± 81
	1:0	111 ± 5	123 ± 22	358 ± 65

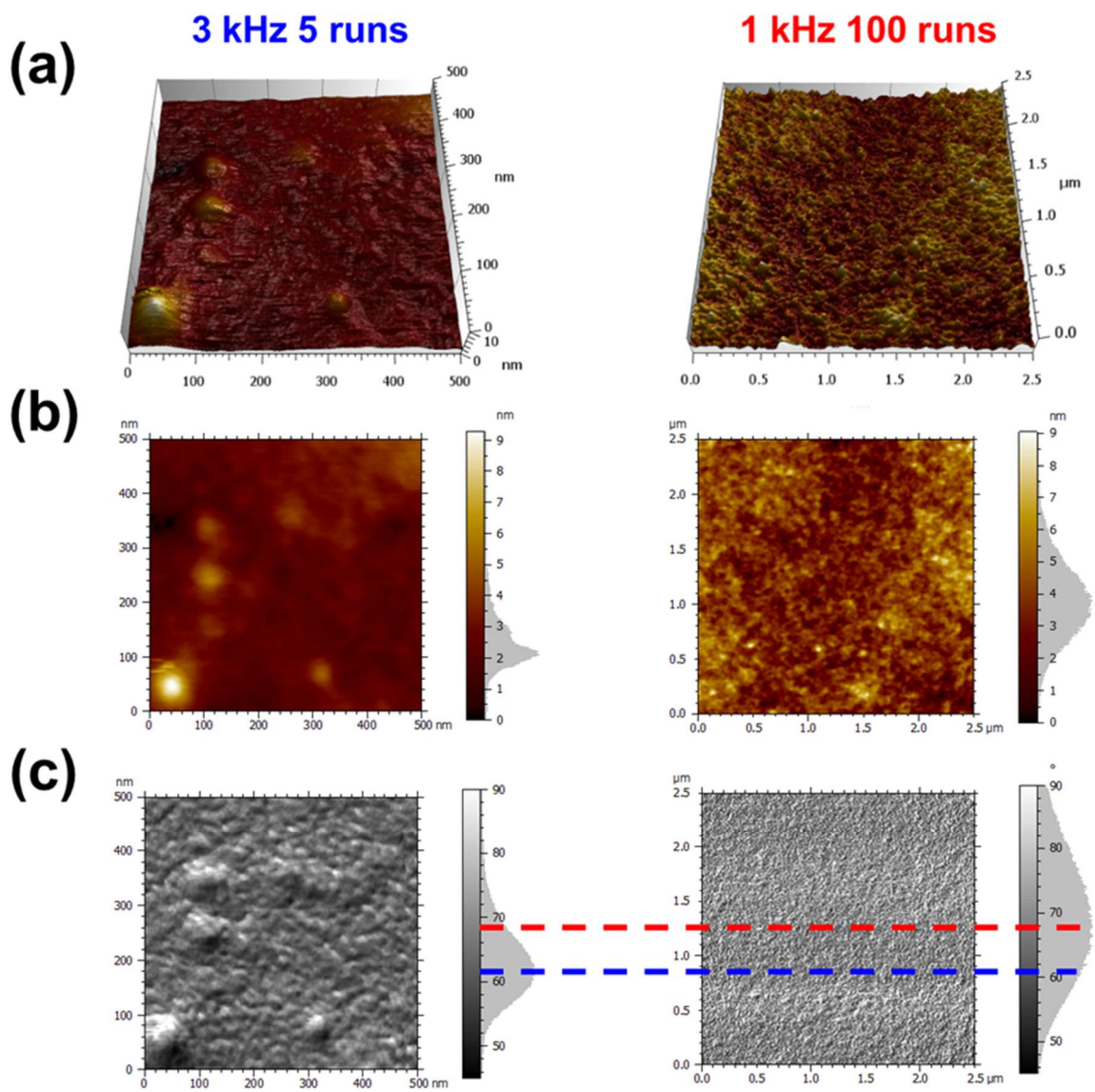


Figure B7: AFM images from: (a) 3D topographic images, (b) 2D height image; and (c) Phase images.

Table B5: Roughness parameters obtained from AFM 3D profile measurements.

Sample	S_q (nm)	S_z (nm)	S_a (nm)
1 kHz 100 runs	1.0	8.7	0.8
1 kHz 15 runs	0.3	2.7	0.3
3 kHz 100 runs	0.4	3.1	0.3
3 kHz 15 runs	0.7	5.9	0.5
3 kHz 10 runs	1.3	4.3	0.8
3 kHz 5 runs	0.9	9.3	0.6

References

- [1] Beamson, G. High Resolution XPS of Organic Polymer. *Anal. Chim. Acta* **1993**, 276, 469–470.
- [2] Hansch, W.; Nakajima, A.; Yokoyama, S. Characterization of Silicon/Oxide/Nitride Layers by x-Ray Photoelectron Spectroscopy. *Appl. Phys. Lett.* **1999**, 75 (11), 1535–1537. <https://doi.org/10.1063/1.124747>.
- [3] Tsuji, M.; Hotta, M.; Watanabe, T.; Endo, R.; Susa, M.; Hayashi, M. Factors Affecting Microscopic Basicity of Silicate Glasses from the Perspective of O1s Binding Energy. *steel Res. Int.* **2023**, 2300383. <https://doi.org/https://doi.org/10.1002/srin.202300383>.
- [4] Landin, D. T.; Macosko, C. W. Cyclization and Reduced Reactivity of Pendant Vinyls during the Copolymerization of Methyl Methacrylate and Ethylene Glycol Dimethacrylate. *Macromolecules* **1988**, 21 (3), 846–851. <https://doi.org/10.1021/ma00181a048>.
- [5] Ramelow, U. S.; Pingili, S. Synthesis of Ethylene Glycol Dimethacrylate-Methyl Methacrylate Copolymers, Determination of Their Reactivity Ratios, and a Study of Dopant and Temperature Effects on Their Conductivities. *Polymers*. 2010, pp 265–285. <https://doi.org/10.3390/polym2030265>.
- [6] Ajzenberg, N.; Ricard, A. Kinetic Study by Differential Scanning Calorimetry of the Bulk Copolymerization of 2-Hydroxyethylmethacrylate with Ethyleneglycoldimethacrylate. *J. Appl. Polym. Sci.* **2001**, 80 (8), 1220–1228. <https://doi.org/https://doi.org/10.1002/app.1207>.
- [7] Połowiński, S. Template Copolymerization of Methacrylic Acid and Acrylic Acid. *Acta Polym.* **1992**, 43 (2), 99–101. <https://doi.org/https://doi.org/10.1002/actp.1992.010430209>.
- [8] Paxton, T. R. Copolymerization Reactivity Ratios Acrylic and Methacrylic Acids with Butyl Acrylate and Butyl Methacrylate. *J. Polym. Sci. Part B Polym. Lett.* **1963**, 1 (2), 73–76. <https://doi.org/https://doi.org/10.1002/pol.1963.110010203>.

ANNEX C

2-STEP PROTOCOL FOR INSIGHTS FOR HYDRATED LAYER: TRANSCRIBED REFERENCE

Reference

Sans, J., Azevedo Gonçalves, I., & Quintana, R. (2023). Ultrathin film hydrogels with controlled swelling and viscoelastic properties deposited by nanosecond pulsed plasma induced-polymerization. *Advanced Materials Interfaces*, 11(2). <https://doi.org/10.1002/admi.202300644>

C. 1. Methodology

Quartz crystal microbalance with dissipation (QCM-D) measurements were conducted using a Q-Sense Explorer QCM-D from Biolin Scientific with a quartz sensor reaching up to 7 odd harmonics. Before each measurement, sensors (QSX 304, Q-Sense) were placed as a substrate in the AP-DBD set up for its subsequent coating under the same identical conditions reported for silicon wafer. Static measurements in air were performed to obtain the dry thickness of the hydrogels. To do so, the fundamental and overtones resonant frequencies were collected from the sensors before and after plasma deposition and compared by means of the Sauerbrey equation.

The Q-Sense Explorer was equipped with an ellipsometer flow module (coupled QCM-D/SE cell, QELM 401, Q-Sense) with temperature control allowing static and dynamic measurements on the samples submerged in liquid media.

C. 2. Results and discussion

Hence, the hydration layers derived from measurements can be attributed to real physical phenomena. To obtain more insights on the hydrated layer, a new 2-step protocol was designed

consisting in the measurement under heavy water (deuterium oxide, D₂O) and de-ionized water. To avoid concentration gradients, samples were exposed to air between each step. Figure 7c shows schematically the protocol followed and the QCM-D results obtained for ut-MAA:EGDMA-3 sample.

Despite of that, the most interesting result arise when analyzing the behavior of the samples when the chamber was exposed in air. As it can be observed in Figure 7c, the hydrogel maintains the water absorbed and the viscoelastic response (i.e. Δf and ΔD are not zero). Moreover, the resultant thickness analyses presented in Figure 7d show a slightly decrease of the thickness determined by SE (as expected) but a significant reduction of the hydrated layer. Indeed, under this specific case both SE and QCM-D results are in complete agreement with the literature showing much smaller differences, which results in a hydrated layer of ~ 7 nm.[6][30] The fact that the measured hydration layer is much higher for immersed samples could be attributed to the existence of a water layer superstructure that it is not completely bounded to the surface (i.e. hydrated layer found in proteins or polymer brushes)[30] but shows some specific order and structure (less bounded water) which also vibrates according to the QCM-D sensor.

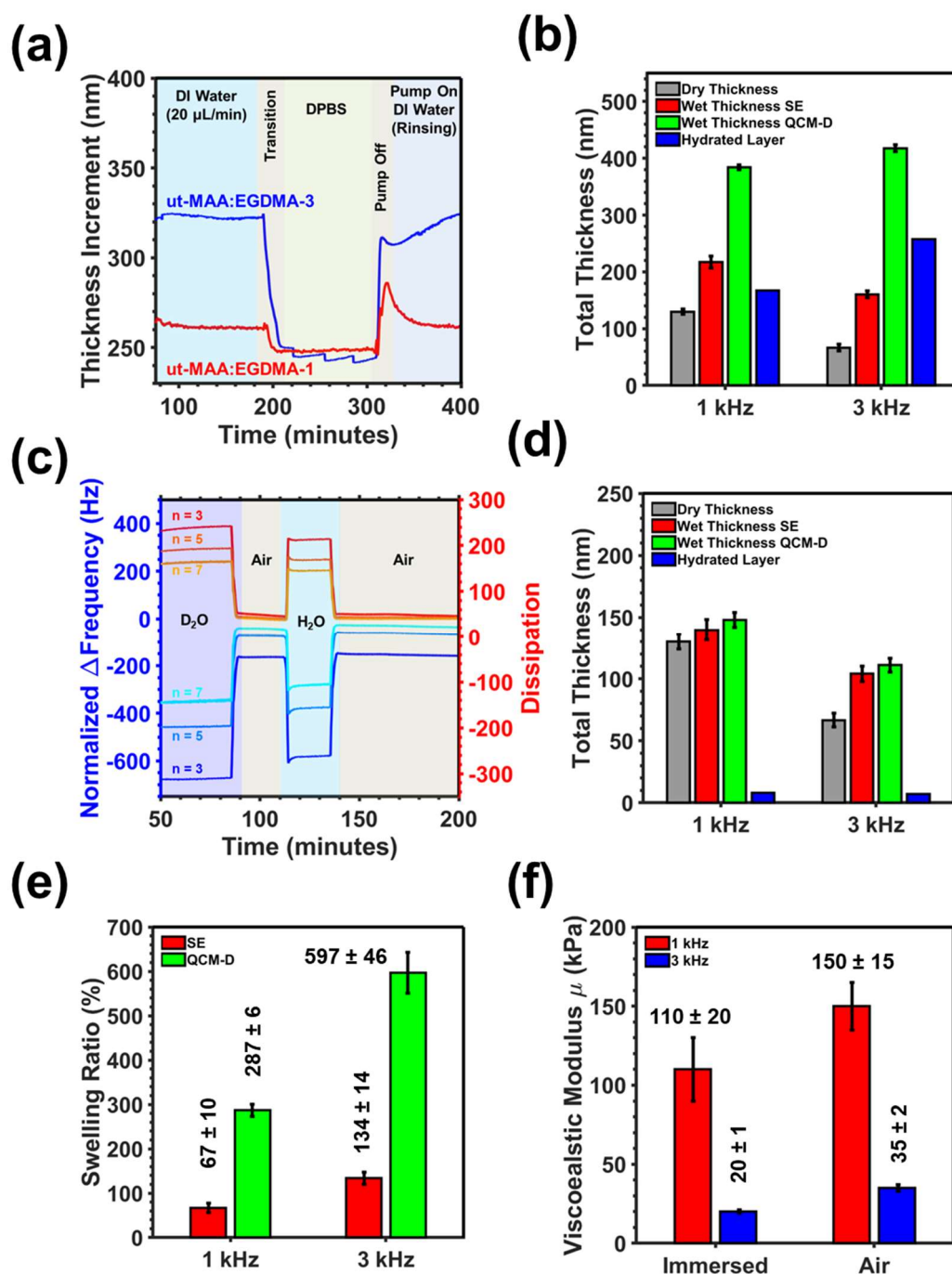


Figure C1. Quantitative results obtained for ut-MAA:EGDMA-1 and ut-MAA:EGDMA-3 by means of coupled QCM-D/SE techniques. (a) Dynamic thickness increment obtained under different media, (b) Total thickness analyses obtained for de-ionised (DI) water. The hydrated layer has been also included, (c) Raw data obtained for ut-MAA:EGDMA-3 sample following the D₂O-H₂O-Air protocol, (d) Total thickness analyses obtained for wet samples exposed to air atmosphere. Similarly, the hydrated layer has been also included, (e) Swelling ratio (in DI

water medium) determined by SE and QCM-D; and (f) Viscoelastic modulus. for the first case, the viscoelastic is maintained for both DI water and DPBS.

ANNEX D

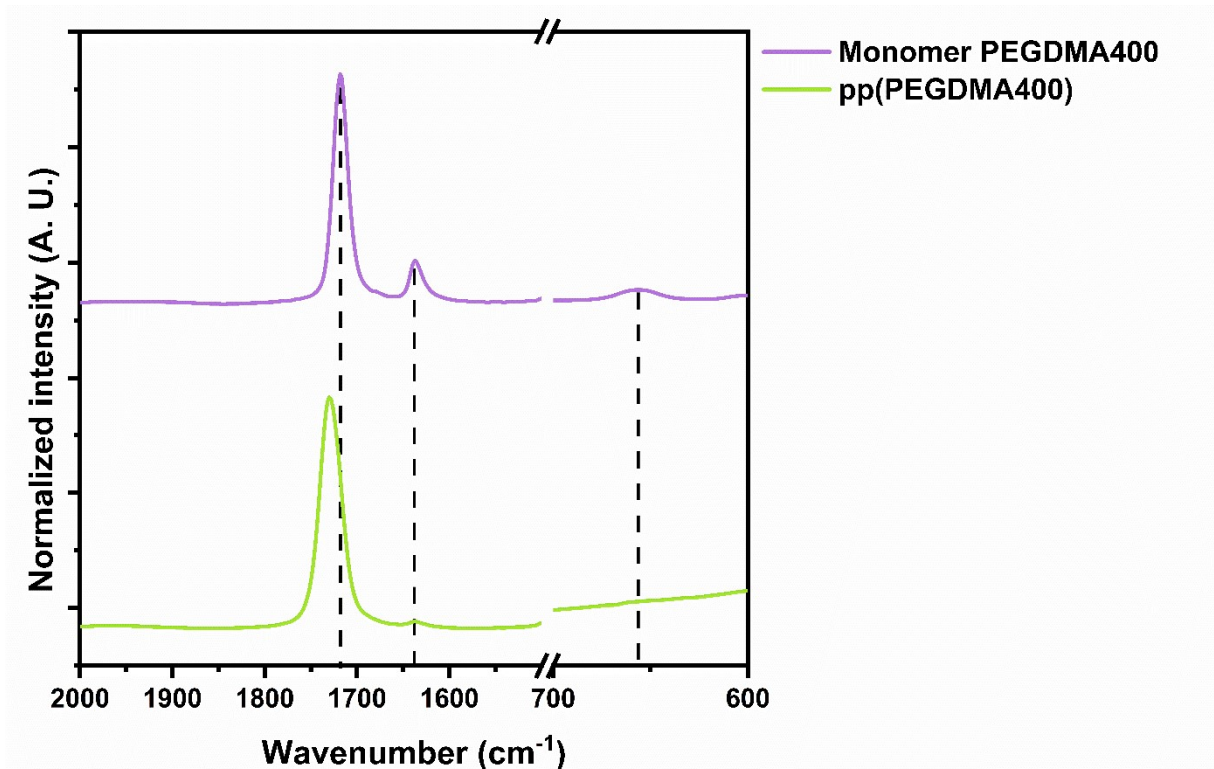


Figure D1: FTIR spectra of the plasma polymerized film grown from PEGDMA₄₀₀ deposited at 3000 Hz and monomer PEGDMA₄₀₀.

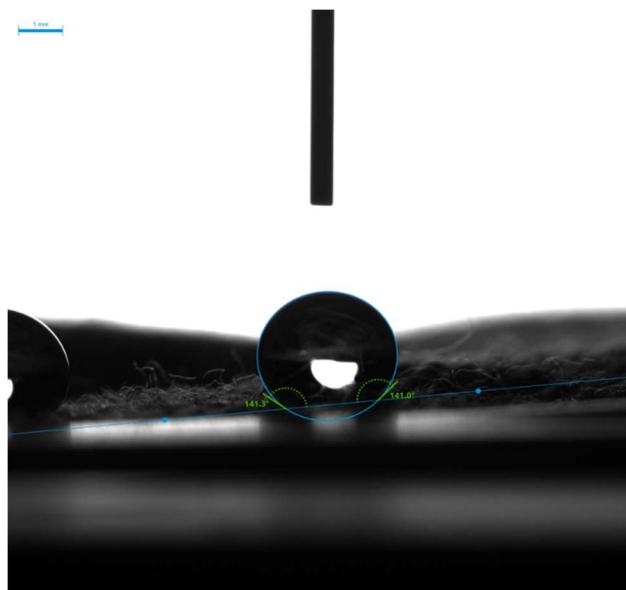


Figure D2: WCA measurements conducted to a non-coated laboratory coat after the washing tests. Note: $WCA = 140^\circ \pm 3^\circ$

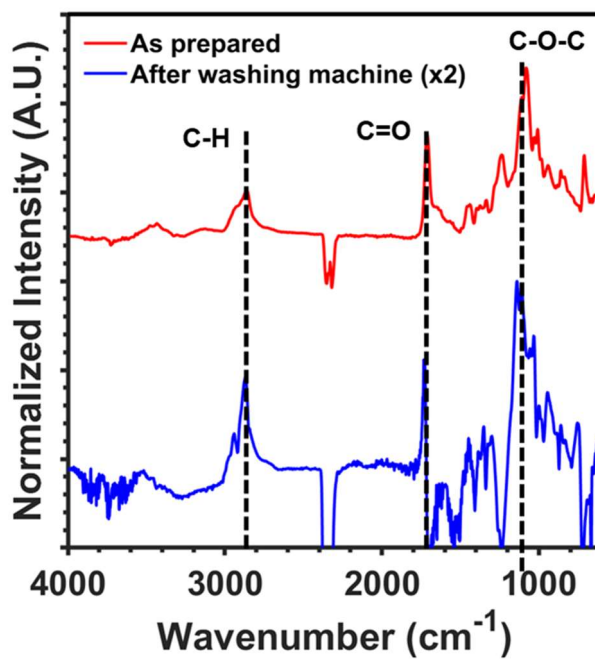


Figure D3: FTIR spectra measured before and after the stability tests.

